Characterization of Multi-Channel Denial-of-Service and Full-Scale Denial-of-Service

A Thesis Submitted in
Partial Fulfilment of the Requirements for the Degree of
Doctor of Philosophy
in
Systems, Control and Automation

by

Anindya Basu

(186102003)

Under the Supervision of

Dr. Indrani Kar

Department of Electronics and Electrical Engineering
INDIAN INSTITUTE OF TECHNOLOGY GUWAHATI
2026

Dedicated to

Sonali & Kashinath Basu

Declaration

I, Anindya Basu, hereby declare that this thesis titled "Characterization of Multi-Channel Denial-of-Service and Full-Scale Denial-of-Service" and the work presented herein are entirely my own. I further confirm that:

- This research was carried out wholly or mainly during my candidature for the PhD degree at this University.
- Any part of this thesis that has previously been submitted for a degree or qualification at this University or any other institution has been explicitly stated.
- All published work of others that I have consulted is clearly acknowledged.
- All quotations from the work of others are properly referenced. Except for such acknowledged quotations, this thesis is entirely my own work.
- All principal sources of assistance have been duly acknowledged.
- In cases where the thesis is based on collaborative work, I have clearly specified the contributions made by others and the parts undertaken by myself.

Date:
Place: North Guwahati

Anindya Basu
Roll No: 186102003

DEPARTMENT OF ELECTRONICS AND
ELECTRICAL ENGINEERING
INDIAN INSTITUTE OF TECHNOLOGY GUWAHATI

Certificate

It is certified that the work contained in this thesis entitled "Characterization of Multi-Channel Denial-of-Service and Full-scale Denial-of-Service" submitted by Anindya Basu, bearing roll No. 186102003, for the award of Doctor of Philosophy in Systems, Control and Automation is absolutely based on his own work carried out under my supervision, and this work has not been submitted elsewhere for any degree.

Dr. Indrani Kar
Thesis Supervisor
Department of Electronics and Electrical Engineering
Indian Institute of Technology Guwahati

Abstract

Cyber-Physical Systems (CPSs) are pervasive in critical infrastructures such as power grids, transportation networks, and industrial control processes. Ensuring their reliable operation is crucial, particularly in the presence of unforeseen failures and malicious external attacks. This thesis addresses the problem of resilient control for CPSs equipped with multiple sensors, where the communication channels of both sides of the control structure are susceptible to Denial-of-Service (DoS) attacks. To systematically handle such disruptions in a multi-sensor framework, the DoS are categorized into two types: Multi-Channel DoS (MCDoS) and Full-Scale DoS (FSDoS). The thesis focuses on the characterization of MCDoS and FSDoS, and proposes a resilient control strategy that guarantees system stability despite the presence of such attacks.

To begin with, a switched observer-based approach is developed to address the challenges posed by MCDoS. Following this, an Event-Triggered Mechanism (ETM) is introduced to tackle the FSDoS condition. The changing frequency of MCDoS in the absence of FSDoS is characterized while ensuring the Input-to-State Stability (ISS) of the closed-loop system. The parameters of both the switched observer and the ETM are optimally designed by solving an optimization problem formulated with Linear Matrix Inequalities (LMIs), thereby enhancing the system's resilience against the maximum allowable MCDoS changing frequency.

Secondly, a comprehensive ISS-based analysis is conducted to characterize both the frequency and duration of FSDoS, complementing the earlier characterization of MCDoS changing frequency. The parameters of the switched observer and ETM are designed using a multi-objective optimization framework involving LMIs, ensuring system resilience against the maximum allowable MCDoS changing frequency as well as the maximum frequency and duration of FSDoS. An asynchronous triggering policy is also developed to further enhance the system's resilience, particularly in scenarios where FSDoS attacks occur at different times on the Sensors-to-Controller (StC) channels and Controller-to-Actuator (CtA) channel.

Finally, the Static ETM (SETM) is replaced with a novel Dynamic ETM (DETM). The control architecture of DETM is modified to effectively handle the maximum allowable MCDoS changing frequency. A comparative analysis between SETM and DETM demonstrates that DETM requires significantly fewer triggering instants, thereby reducing the

overall control cost. Furthermore, an optimization algorithm is developed to determine the optimal parameters for both the DETM and the observer, enhancing the system's resilience against high-frequency MCDoS attacks.

Acknowledgements

I take this opportunity to express my profound gratitude and deep regard to my supervisor, Dr. Indrani Kar, Associate Professor, Department of Electronics and Electrical Engineering, IIT Guwahati, for her exemplary guidance, constant encouragement, and invaluable support throughout my Ph.D. journey. Her blessings, help, and insightful advice at every stage will remain a guiding force in my life and career.

I would like to extend my sincere gratitude to my doctoral committee members, Prof. Somanath Majhi, Dr. Srinivasan Krishnaswamy, and Dr. Hanumant Singh Shekhawat, for their valuable evaluations and constructive suggestions at different stages of this research. I am also thankful to Dr. Parijat Bhowmick and Dr. Chayan Bhawal for their kind guidance and support.

My heartfelt thanks go to the staff members of the EEE Department, Mrs. Khurshida Yasmin and Mrs. Chayanika Borah Majumdar, for maintaining the Control and Instrumentation (C&I) Laboratory and providing the necessary resources for this work.

I am deeply indebted to all my seniors from the C&I Lab for their guidance and encouragement, especially Dr. Raju Dahal, Dr. Kasturi Das, Dr. Manmohan Sharma, Dr. Sami Al-Issa, Dr. Trusna Meher, Mr. Mandar Maitra, Mr. Tamen Thapa Sarkar, Dr. Gautam Sethia, Dr. Abhijit Mazumdar, Dr. Sushanta Kundu, Dr. Uddipana Dowerah, Dr. Mriganka Biswas, and Mr. Bhim Singh. I am also grateful to my friends Bishu da, Shiv Santosh, Nitisha, and Adino for their immense help and support, and to my juniors Saikat, Souradip, Subhadeep, Athoibi, Paraj, Gangadari, Sanjeev, Malem, Deep, Yogesh, and Narendra for their love and encouragement.

I sincerely thank all my friends who made my stay at IIT Guwahati both pleasant and memorable. Special thanks go to Aritra, Surojit, Anjishnu, Anik, Arin, Sanket, and Avirup, as well as my juniors Argha, Jyotirmoy, Santanu, Partha, Tanay, Aritra, Alik, Sonal, Anit, Balaram, and Adri for their companionship and constant support in the hostel. I am especially grateful to my buddy Aritra, who stood by me through every high and low. I cherish the countless memories with Surojit, who was always there to listen whenever I needed someone, and I am equally thankful to Anik, who became a very close friend in such a short span of time. I cannot forget Suchetana and Debu, whose presence made my life at IIT Guwahati even more vibrant. From long adda sessions at Khoka tea stall to trips and adventures, the moments shared with them remain unforgettable. I

will dearly miss those evenings at Khoka with Aritra, Suchetana, Argha, Anjishnu, Debu, Srijita di, and Anwesha.

My heartfelt appreciation extends to the seniors, friends, and juniors at Tero Parbon. Subhamay sir, Araghni da, Gaurhari da, Pramit da, Atanu da, Argha da, Chandrima di, Srijita di, Sagnik, Tirupati, Tanumoy, Malay, Sayantani, Soumalya, Roop, Joyshree, Pratim, Sagarika, Sreeparna, Ayan, Arpan, Sayan, Sampad, Ruchishyo, Swastik, and Aindrila, for enriching my life with countless cultural experiences and cherished memories. I would like to acknowledge Matap and Archit for their support and friendship throughout this journey.

Above all, I owe my deepest gratitude to my family, Maa, Babai, Didu, Boromaa, Mashimani, Mesho, Mama, Mami, Boudi, Laboni, Tuli, and Raja for their unconditional love, sacrifices, and unwavering encouragement throughout this long journey. I am equally thankful to my extended family for their constant support in countless ways.

Finally, I want to thank myself, a small but necessary acknowledgement, for showing up to the lab even on the hardest days, for pushing through every frustrating mathematical mistake, every dead end when the next step seemed impossible, every stubborn coding error, and for struggling through the slow, exhausting process of writing manuscripts one sentence at a time.

Contents

List of Figures

List of Tables

List of Algorithms

List of Abbreviations

CPSs	Cyber-Physical Systems
DoS	Denial-of-Service
MCDoS	Multi-Channel Denial-of-Service
FSDoS	Full-Scale Denial-of-Service
ETM	Event-Triggered Mechanism
ISS	Input-to-State Stability
LMIs	Linear Matrix Inequalities
StC	Sensor-to-Controller
CtA	Controller-to-Actuator
SETM	Static Event-Triggered Mechanism
DETM	Dynamic Event-Triggered Mechanism
LTI	Linear Time-Invariant
NCS	Network Control Systems
MPC	Model Predictive Control
SMC	Sliding Mode Control
LKF	Lyapunov-Krasovskii Functional
LQG	Linear Quadratic Gaussian
CO	Convex Optimization
NCO	Non-Convex Optimization

List of Symbols

$\mathbb{R}$	The set of all real numbers
$\mathbb{R}_{>0}$	The set of all positive real numbers
$\mathbb{R}_{\geq 0}$	The set of all non-negative real numbers
$\mathbb{R}_{>a}$	The set of real numbers greater than a
$\mathbb{R}_{\geq a}$	The set of real numbers greater than equal to a
$\mathbb{R}^n$	The vector spaces of n real-valued tuples
$\mathbb{R}^{n\times m}$	The real-valued matrices with size $n \times m$
$\mathbb{N}$	The set of natural numbers
$\mathbb{N}_0$	$\mathbb{N} \cup \{0\}$
$\|\cdot\|$	The Eucledian norm of vector or matrix
$\|\cdot\|_{\mathcal{L}}$	The logarithmic norm of vector or matrix
$\|g_t\|_\infty$	$:= \operatorname{ess\,sup}_{s\in[0,t)} \|g(s)\|$
$\|G\|$	The length of the set of intervals G
I	Identity matrix with suitable dimension
0	Null vector or matrix with suitable dimension or a scalar number 0
$P > 0$	P is a positive definite matrix
$P \geq 0$	P is a positive semi-definite matrix
$\lambda_m(P)$	The smallest eigenvalue of the matrix P
$\lambda_M(P)$	The largest eigenvalue of the matrix P
$P^\top$	The transpose of matrix or vector P
$\mathrm{He}(P)$	$:= P + P^\top$
$\begin{bmatrix} A & B \\ * & C \end{bmatrix}$	The representation of a symmetric matrix

$\{a, b\} > c$	a and b both are greater than c
σ	Observer switching mode
$\underline{\Delta}_\sigma$	Minimum inter-execution time for σ switching mode
$\overline{\Delta}_\sigma$	Maximum inter-execution time for σ switching mode
$\underline{\Delta}$	Minimum inter-execution time over all σ
$\overline{\Delta}$	Maximum inter-execution time over all σ
$\overline{\Delta}_{\text{setm}}$	Maximum inter-execution time over all σ for SETM
$\overline{\Delta}_{\text{detm}}$	Maximum inter-execution time over all σ for DETM
t_k	k-th sampling time; it corresponds to the k-th time instant at which communication is attempted
D_{i_n}	n-th interval of DoS in i-th transmission channels
$\Omega_i(\tau, t)$	The time interval sets for each interval $[\tau, t]$ when the transmission is denied in i-th transmission channel
$\Omega(\tau, t)$	The union of FSDoS intervals over $[\tau, t]$
$\Upsilon(\tau, t)$	The relative complement of $\Omega(\tau, t)$ in $[\tau, t]$; the union of time intervals in $[\tau, t]$ over which FSDoS is absent
τ_D	Parameter whose inverse provides an upper bound on the average changing frequency of MCDoS, i.e., average number of MCDoS type changing transitions per unit time
$l(\tau, t)$	The number of MCDoS changing transitions happening in $[\tau, t)$
τ_F	Parameter whose inverse provides an upper bound on the average frequency of FSDoS off/on transitions, i.e., average number of FSDoS off/on transitions per unit time
T	Parameter whose inverse provides an upper bound on the average duration of FSDoS per unit time
$n(\tau, t)$	The number of FSDoS off/on transitions occurring in the interval $[\tau, t)$
$\eta(t)$	The internal dynamical variable of DETM
κ	The scaling parameter of DETM

Chapter 1

Introduction

1.1 Cyber-physical systems: an overview

Cyber-Physical Systems (CPSs) are advanced, interdisciplinary systems that tightly integrate embedded computing capabilities with physical processes. They are designed to incorporate computation, communication, and control functions in a seamless manner, using innovative, multi-disciplinary approaches to interact with and influence physical phenomena. This integration primarily encompasses observation, communication, and control of physical systems from a systems-level perspective [1].

Although the concept has existed since the early 1970*s*, when microprocessors first began to appear [2], the term "Cyber-Physical Systems" was formally introduced by Helen Gill at the U.S. National Science Foundation (NSF) in 2006 [3]. CPSs represent a new class of engineered systems that connect the digital and physical worlds. According to [3], these systems are distinguished by two fundamental components: (1) advanced connectivity, enabling real-time data acquisition from the physical environment and feedback from the cyber domain, and (2) intelligent data processing, analytics, and computational power that define the cyber layer.

The adoption of CPSs is driven by the goal of facilitating the implementation of complex, large-scale systems with improved adaptability, autonomy, efficiency, functionality,

reliability, safety, and user-friendliness. Research in CPSs generally falls into two major categories: theoretical foundations and practical applications [4]. Furthermore, software architecture plays a crucial role in meeting system-level business requirements [5].

Despite advancements in modelling, system design, technological development, and deployment, the field of CPSs remains relatively nascent and continues to evolve [6]. These systems have a wide range of applications across various domains, including agriculture [7, 8], energy [9–13], agricultur-based energy [14], healthcare [15–17], education [18], manufacturing [19–21], transportation [22–25], smart environments [26, 27], water distribution networks [28], and telecommunications [29].

1.2 Malicious attacks on CPSs

A malicious attack or cyber attack refers to an attempt to steal data or gain unauthorized access to network-connected computers within CPSs, typically using one or more compromised devices. Such attacks are often the preliminary step in a broader strategy aimed at breaching the security of individual or organizational networks, eventually leading to data theft or operational disruption [30, 31].

Over the past two decades, several high-profile system failures have underscored the vulnerability of CPSs to cyber threats. Notable examples include the Maroochy Shire sewage system failure in 2000, caused by a disgruntled insider who manipulated wireless pump control systems [32]; the SQL Slammer worm that affected the Davis-Besse nuclear plant in January 2003, disabling its safety monitoring system for hours [33]; the highly sophisticated Stuxnet worm attack in 2010, which targeted industrial control systems in Iran and demonstrated the potential of cyber weapons to damage physical infrastructure [34, 35]; the massive Indian grid failure in 2012, which left hundreds of millions without power and highlighted the fragility of interconnected systems [36]; and repeated power outages in Brazil, linked to vulnerabilities in grid infrastructure [37].

These incidents make it clear that robust and adaptive security mechanisms are essential for CPSs. The proliferation of low-cost sensors and communication devices, while enabling large-scale deployment, also introduces significant cyber risks due to limited security features [38]. Malicious attacks may be launched from local or international sources and have far-reaching consequences-potentially impacting the environment, economy, and even public safety. Given the critical nature of CPSs, it is imperative to develop effective detection strategies and control mechanisms to mitigate these threats and ensure secure and reliable system operation [39].

Malicious attacks are largely divided into three parts (1) deception attack [40], (2) replay attack [41], and (3) Denial-of-Service (DoS) attack [42]. By changing data packets within network transmission channels and producing inaccurate feedback, deception attacks jeopardise system stability. By capturing and retransmitting data packets, replay attacks impair system performance and interfere with CPSs' closed-loop operation. DoS attacks block data transmission and stop controller updates by interfering with communication channels between sensors and controllers and/or between controllers and actuators. The systems and control community has long anticipated the impact of deception-based attacks, particularly in the forms of false data injection attacks [43], stealth attacks [44], and covert attacks [45]. A growing body of research has also addressed the modeling, detection, and mitigation of such attacks from both theoretical and practical perspectives. The subsequent section presents a comprehensive review of the relevant literature, synthesizing existing methodologies and pinpointing research gaps that directly motivate the contributions of this thesis.

1.3 Liturature survey

DoS attacks are one of the three major attacks that have attracted a lot of attention because they can cause severe disruptions and require little prior system knowledge. This thesis focuses on resilient control design for CPSs with multiple sensors, where both sides of the communication channels are affected by DoS. Before addressing the identified

research gap, we provide a brief literature review on resilient control design, focusing first on systems with a single sensor under DoS, and then on systems with multiple sensors where only the Sensor-to-Controller (StC) communication channel is affected by DoS.

1.3.1 Resilient control for single sensor under DoS

In CPSs control over networks, adversaries commonly target the communication links, specifically, the StC and Controller-to-Actuator (CtA) channels, to introduce DoS with the aim of destabilizing the system. The foundational work by Amin et al. [46] introduced the first secure networked control system resilient to DoS attacks using a semidefinite programming-based countermeasure.

Building on this, Foroush and Martinez [47] analyzed the effects of periodic DoS on multi-input continuous Linear Time-Invariant (LTI) systems. To address the challenge of aperiodic attacks, De Persis and Tesi [48] proposed a general framework that constrains both the frequency and duration of DoS events and demonstrated Input-to-State Stability (ISS) under such conditions. Their approach was further extended to nonlinear Network Control Systems (NCS) under DoS in [49, 50].

Dolk et al. [51] adopted a hybrid systems modeling approach to design an output-based Event-Triggered Mechanism (ETM) resilient to DoS. Feng and Tesi [52–54] advanced this work with a robust control design that maximizes tolerance to DoS, proposes remote control architectures independent of actuator co-location, and incorporates variable bit-rate encoding and quantized control.

A wide variety of strategies have since emerged. Tang et al. [55] introduced event-based tracking control for mobile robots under DoS, while Yuan et al. [56] presented a hierarchical game-theoretic framework for wireless networked control systems. Sun and Yang contributed significantly through a series of works addressing asynchronous DoS in both StC and CtA channels [57], observer-based periodic ETM [58], robust Model Predictive Control (MPC) [59], and resilient remote estimation schemes [60].

Zhu et al. [61] developed a strong $\gamma_c - \gamma_{cl}$ H_∞ stable dynamic output-feedback controller for stochastic discrete-time systems under DoS. An observer-based ETM for networked linear systems facing DoS was presented by Hu et al. [62]. Chen et al. [63] proposed a distributed resilient filtering approach tailored for power systems subjected to DoS. In a related effort, Wang and Xu [64] introduced an observer-based guaranteed cost control technique for CPSs under DoS. Chen et al. [65] also developed an ETM-based quantized H_∞ controller for switched systems under DoS conditions. Wu et al. [66] designed an estimator-based resilient Sliding Mode Control (SMC) for discrete-time LTI systems under DoS, while Zhao et al. [67] presented an ETM-based SMC for uncertain switched systems compromised by DoS.

Sun et al. proposed an output-based H_∞ ETM using a Lyapunov-Krasovskii Functional (LKF) [68], and also introduced a resilient triggering strategy for LTI systems with exogenous disturbances under DoS [69]. A resilient H_∞ filtering method for ETM-based systems under DoS jamming was proposed by Hu et al. [70]. Zhang et al. [71] employed stochastic game theory to develop a Linear Quadratic Gaussian (LQG) controller for discrete LTI systems with noise under DoS attacks, and Zhao et al. [72] designed an observer-based ETM for stochastic networked control systems in the presence of DoS. Pessim and Lacerda [73] derived a state-feedback control for cyber-physical linear parameter varying systems under DoS. They also designed state-feedback control for discrete-time linear parameter-varying systems under the presence of exogenous disturbance and DoS in [74].

Liu et al. [75] integrated game theory, ETM, and the State-Action-Reward-State-Action reinforcement learning algorithm to improve the robustness of CPSs against DoS. Ma et al. proposed a dissipation-based SMC and a switched H_∞ filter for LTI systems under DoS [76, 77], and also designed a controller for a two-dimensional Fornasini-Marchesini system [78]. Zhao et al. [79] developed a periodic dynamic ETM for LTI systems with disturbances under DoS, while Qi et al. [80] proposed an energy function-based resilient switching law to address dual-ended DoS and asynchronous switching in networked systems. Li et al. [81] designed an event-based security transmission policy for discrete-time LTI systems where DoS exists in both the StC channel and CtA channel.

Further advancements include an observer-based resilient MPC design by Zhang et al. [82], an SMC for interval type−2 fuzzy nonlinear systems with immeasurable states [83], and dynamic quantization-based methods by Kato et al. for nonlinear systems affected by DoS [84]. Sathishkumar and Liu [85] designed an adaptive ETM considering actuator saturation and faults under DoS, and Zhou and Chang [86] developed a quantized $\mathfrak{L}_2-\mathfrak{L}_\infty$ filter for neural networks under DoS.

Fu et al. [87] introduced a new switching law and adaptive ETM to address asynchronous switching and DoS, and Gao et al. [88] proposed ETM-based finite-time guaranteed cost control for T-S fuzzy switched systems under DoS. Basit et al. [89] designed a distributed estimator for joint state and unknown input estimation in nonlinear systems facing stochastic disturbances and DoS. Liu et al. [90] presented a data-driven predictive control strategy for LTI systems under DoS, and Yan et al. [91] proposed a quantization-based switching algorithm for continuous-time switched systems under DoS.

Wang et al. [92] addressed the ISS problem for switched linear systems with unstabilizable modes under DoS and external disturbances. Shi et al. [93] introduced a dynamic quantization scheme that adjusts the encoder/decoder range and quantization bits to ensure system stability under DoS constraints in terms of attack duration and frequency. Wang et al. [94] also proposed an adaptive ETM-based neural network controller for discrete-time nonlinear systems under DoS. Gao et al. developed a resilient reinforcement learning method for robust optimal output regulation of partially linear systems with dynamic uncertainties and DoS [95], and later extended it to LTI systems using adaptive dynamic programming [96]. Chatterjee et al. [97] proposed a fixed-time ETM for nonlinear systems, while Gao et al. [98] designed an ETM-based adaptive control for uncertain nonlinear systems under DoS. Saif et al. [99] formulated novel Linear Matrix Inequalities (LMIs) using LKF for linear time-delay systems under DoS, and Zheng et al. [100] developed an ETM-based SMC with quantizer adjustment for linear uncertain systems. Ji et al. [101] proposed a small-gain adaptive control for switched strict-feedback systems under DoS, while Li et al. [102] introduced a variable-step predictive event-based scheme under DoS. Liu et al. [103] tackled sampled-data resilient control of stochastic

nonlinear CPSs, and Lu and Quevedo [104] co-designed optimal control and scheduling under stochastic DoS for NCS.

Coutinho et al. [105] proposed an optimal switched ETM for DoS resilience. Qu and Zhao [106] developed an ETM-based H_∞ controller for switched interval type-2 fuzzy nonlinear systems under DoS, and Zhao et al. [107] considered asynchronous DoS effects on StC and CtA channels in switched systems. Ren et al. [108] introduced a hybrid asynchronous ETM for switched CPSs under DoS. Liu and Ling [109] studied stabilization under ETM-based sampling over band-limited networks subject to DoS, and Wang et al. [110] applied adaptive event-triggered dynamic output feedback control for unmanned marine vehicles under DoS. Xie et al. [111] designed a mode-dependent ETM for switched systems with unstable subsystems under DoS duty cycles, and Shen et al. [112] developed a nonlinear MPC with dynamic sampling for CPSs under DoS.

Sharafian et al. [113] implemented fuzzy adaptive backstepping control for incommensurate fractional-order power systems under DoS, and Dong et al. [114] proposed a neural network-based asynchronous controller for uncertain Markov jump systems with dead zones. Yin et al. [115] introduced a data-driven optimal tracking control algorithm under DoS, and Wei et al. [116] developed a binary observer for FIR systems under sequential DoS, also modeling optimal attacks using covariance constraints. Fu et al. [117] presented a dynamic switched periodic ETM for LTI systems with disturbances under DoS. Wang et al. [118] designed an H_∞ controller for discrete-time hidden Markov models under DoS, while Qiu et al. [119] developed constrained MPC for switched time-varying systems under time delay and DoS.

Tian et al. [120] proposed an ETM for switched linear systems facing actuator saturation and DoS, and Tan et al. [121] addressed fault detection in T-S fuzzy systems with time-varying delays and DoS modelled via a binary Markov chain. Du et al. [122] introduced a secure ETM for load frequency control in power systems under DoS, and Zhou et al. [123] presented an asynchronous ETM handling distinct DoS effects on StC and CtA channels. Meng et al. [124] developed a secure state estimator for switched systems with disturbances and noise under DoS. Yang et al. [125] implemented a data-driven ETM

for unmanned surface vehicles under DoS, and Wang et al. [126] proposed an aperiodic data-sampling method for non-strict feedback switched systems under DoS.

An et al. [127] presented an adaptive high-gain observer-based backstepping controller under full-state DoS, while Zou et al. [128] designed a rapid exponential stabilization scheme with an update trigger to enhance DoS resilience. Roy et al. [129] addressed mismatched uncertainties and deception attacks with an adaptive finite-time ETM. Qiu et al. [130] also developed a Dynamic ETM (DETM)-based predictive controller for semi-Markov jump systems under DoS. Finally, Chen et al. [131] proposed a resilient stepped transmission strategy that adaptively adjusts sampling based on DoS status using acknowledgement feedback.

Overall, the literature presents a rich landscape of resilient control strategies against DoS attacks across diverse CPSs configurations. This progress includes both theoretical advancements in system modelling and stability analysis, as well as practical implementations in remote control, estimation, and learning-based frameworks. Although the aforementioned techniques effectively stabilize CPSs under DoS using a single sensor or communication channel, they often fail to extend to scenarios involving multiple transmission channels. In such cases, the presence of concurrent attacks on different communication paths introduces additional complexity, rendering single-channel solutions inadequate for maintaining system stability and performance.

1.3.2 Resilient control for multiple sensors under DoS

A plant equipped with multiple sensors can transmit data to the controller through multiple communication channels over a network. The advantage of using multiple transmission channels is that not all of them are likely to be compromised by DoS simultaneously. This provides the controller designer with a strategic advantage in handling DoS. Even when some channels are under attack, it is still possible to stabilize the system over an extended period by receiving sensor data through the unaffected channels.

Lu and Yang [132] were the first to examine multi-channel DoS, where they performed an ISS analysis of CPSs subject to attacks on multiple transmission channels. They modeled the compromised system as a switched controller, discarding outdated information, and applied LMI-based methods, adapted from time-varying delay analysis, to assess stability. They further characterized, for each channel independently, bounds on the frequency and duration of DoS under which the closed-loop switched system, despite containing unstable subsystems, remains stable.

In [133], they extended their earlier work by introducing a class of partial observers to tackle the combinatorial complexity that arises due to the exponential growth in the number of LMIs with increasing transmission channels. They also employed a finite-time observer design to enhance resilience against DoS by addressing the frequency and duration of attacks on each StC channel. Additionally, they proposed a disturbance rejection mechanism and refined the stability analysis method from [132] by incorporating a switching strategy that discards unreliable state estimates, thereby mitigating the impact of disturbances.

In [134], the authors further explored a decentralized ETM to balance transmission efficiency with the tolerable intensity of DoS, a problem more critical and challenging than merely determining tolerable attack levels, as addressed in their earlier work [132]. Leveraging the finite-time observer framework from [52], they developed a partial-state-observer-based ETM to further enhance transmission efficiency under multi-channel DoS conditions.

Gu et al. [135] studied an event-triggered fuzzy filtering approach for nonlinear systems with multiple sensors under DoS. They developed a novel distributed ETM model that prevented unnecessary or abrupt data from being transmitted over the network, thereby improving communication efficiency. Additionally, the filter was designed to collect more data during periods of external interference, enhancing system performance. A weighted fusion method was applied to the multi-sensor data to improve the reliability of the filtering process before making ETM decisions. The authors modeled the DoS behavior

by dividing each attack cycle into an active period and a sleeping period, treating the sleeping period as a variable while keeping the total duration of the attack cycle fixed.

Building on the DoS characterization in [132], Wu et al. [136] addressed the ISS problem for T-S fuzzy systems with multiple transmission channels under DoS. They introduced a novel data update policy formulated via LMIs and designed a switched fuzzy dynamic feedback controller that accounts for the loss of premise variables and discards outdated data. Sufficient conditions were established to ensure the stability of the T-S fuzzy system under DoS. Compared to [132], a more refined time-division mechanism was adopted to derive tighter stability conditions, including scenarios where all or none of the channels are under attack.

Ma et al. [137] addressed the security control problem for two-time-scale CPSs with multiple transmission channels under DoS. They introduced an $\varepsilon-$dependent Lyapunov function to circumvent the numerical ill-conditioning typically associated with two-time-scale systems. Furthermore, a novel $\varepsilon-$dependent composite controller was designed, along with switching laws that schedule appropriate controller gains based on the DoS attack sequences across different channels. Under this framework, the ISS of the closed-loop two-time-scale CPSs under asynchronous DoS attacks is ensured.

Li et al. [138] proposed a finite-time observer-based resilient SMC for CPSs with multiple transmission channels under DoS. They achieved improved disturbance rejection performance and introduced a switched sliding surface to mitigate the impact of unreliable state estimation channels. To enhance robustness against disturbances and network-induced uncertainties, the authors designed a switched integral-type sliding mode controller. Moreover, ETM and input saturation were simultaneously addressed by incorporating an auxiliary system into the control framework.

Gao and Yang [139] addressed the sampled-data distributed state estimation problem for systems with multiple transmission channels under DoS. The main challenge stemmed from the intricate interplay between different sampled-data schemes and attack strategies across the channels. To tackle this, they proposed a time-interval division-based method that effectively decouples these interactions. A decomposition of the system matrices

was also introduced to aid in designing distributed observers and analyzing the influence of DoS on the state estimation process. Leveraging both the interval division method and the matrix decomposition, the authors developed sampled-data distributed observers equipped with partial state resetting capabilities to maintain estimation accuracy under DoS conditions.

Zhang et al. [140] addressed a more general scenario than that considered in [136] by separately accounting for the effects of attacked and unattacked premise variables during DoS. They observed that when different transmission channels were compromised, the associated premise variables also became inaccurate, while the signals and premise variables corresponding to the unattacked channels remained reliable under each attack mode. For T-S fuzzy systems, the authors proposed a novel parallel distributed compensation controller and adopted a strategy to discard information from both attacked transmission channels and their associated premise variables. They further analyzed the stability and performance of the control system, demonstrating that it achieved exponential stability and exhibited strong disturbance rejection capability

Sun et al. [141] proposed a DETM for multi-sensor systems to ensure stability under asynchronous DoS affecting different transmission channels, while significantly reducing communication resource usage. They also derived sufficient conditions to guarantee system stability and determined the maximum attack intensity the system can tolerate under such asynchronous DoS scenarios.

Beyond resilient control design specifically for multiple transmission channels under DoS attacks, researchers have also been focusing on developing control strategies that are resilient to a combination of cyber threats, including DoS, deception, and replay attacks for a multi-sensor framework. A notable contribution in this direction is the work presented in [142].

1.3.3 Review of control frameworks relevant to this study

In this subsection, several important control architectures are reviewed, which play a key role in developing the resilient control strategies presented throughout this thesis. Among them, ETM stands out as particularly significant. Under DoS attacks, communication opportunities within a channel become limited. By scheduling transmissions in response to the presence of DoS while conserving communication resources, the designer gains a strategic advantage in constructing a resilient control framework.

Tabuada [143] addressed several critical questions regarding the real-time scheduling of ETM. His analysis ensured that execution times do not become arbitrarily close, thereby avoiding the infamous Zeno behavior, despite being implicitly defined. He also provided a detailed framework for implementing the execution rule and estimating the time intervals between consecutive executions of the control task.

Lunze and Lehmann [144] proposed a state-feedback-based approach for ETM. A key contribution of this work is the discussion on how communication frequency is affected by external disturbances.

Borgers and Heemels [145] analyzed the fundamental properties of minimum inter-event times for various ETM architectures, considering both the absence and presence of external disturbances and measurement noise. Their analysis revealed that several widely used ETMs fail to prevent Zeno behavior when even small disturbances or noise are present. Based on these findings, they emphasized the importance of explicitly incorporating the effects of external disturbances and measurement noise in the analysis of ETM-based systems.

Zhang et al. [146] presented a comprehensive overview and in-depth analysis of sampled-data-based ETM and filtering for networked systems. They demonstrated that, since data is sampled prior to applying ETM, the approach inherently ensures a positive inter-execution time, thereby avoiding Zeno behavior. Additionally, they designed compatible feedback controllers and ETM's threshold parameters jointly to enhance system performance.

Girard [147] first introduced the concept of dynamic triggering within ETM. He explicitly analyzed the system's stability under DETM and derived the minimum inter-execution time. Both his theoretical analysis and simulation results demonstrated that DETM achieves longer inter-execution times compared to conventional (static) ETM, which significantly reduces the control cost.

Liu and Yang [148] developed a novel DETM for LTI systems that guarantees asymptotic stability and $\mathcal{L}_2-$stability, by which triggering parameter and feedback gain can be co-designed. The stability conditions were established using Lyapunov-based analytical methods, with a newly constructed Lyapunov-Krasovskii functional introduced to reduce conservatism in the analysis.

Liu et al. [149] proposed a model-based DETM strategy for uncertain sampled-data linear systems operating over networks with transmission delays and communication protocols. They introduced storage variables to reformulate the overall system as a hybrid system. Using hybrid system stability theory, they then designed explicit parameters for the DETM to ensure asymptotic stability. Furthermore, for uncertain linear systems decomposable into interconnected subsystems, they developed a distributed model-based DETM. In this framework, each local network employed a local controller running a simplified model that operated independently, without relying on information from other subsystems.

In addition to ETM, the switched observer plays a crucial role in the resilient control architecture developed in this thesis. Bejarano and Pisano [150] proposed a switched observer design for switched linear systems. For scenarios where the set of unknown input distribution matrices is linearly dependent, they introduced an observer capable of achieving asymptotic state reconstruction without requiring any dwell-time constraint on the slow switching sequence. In the more general case, they assumed the presence of a minimal average dwell time across switching sequences. In both settings, they employed Lyapunov-based analysis to establish exponential convergence of the state estimation.

Tanwani et al. [151] proposed a framework for observer design and provided a detailed characterization of observability for switched linear systems with state jumps. They established a necessary and sufficient condition for global-in-time observability under known mode transitions. Additionally, while accounting for state jumps, they introduced a weaker condition for determinability, focusing on the recovery of the system's state at a specific time rather than continuously over time. The authors also demonstrated that, unlike traditional approaches, their method does not require dwell-time constraints between switchings. However, they emphasized that persistent switching is essential for the effectiveness of the proposed design.

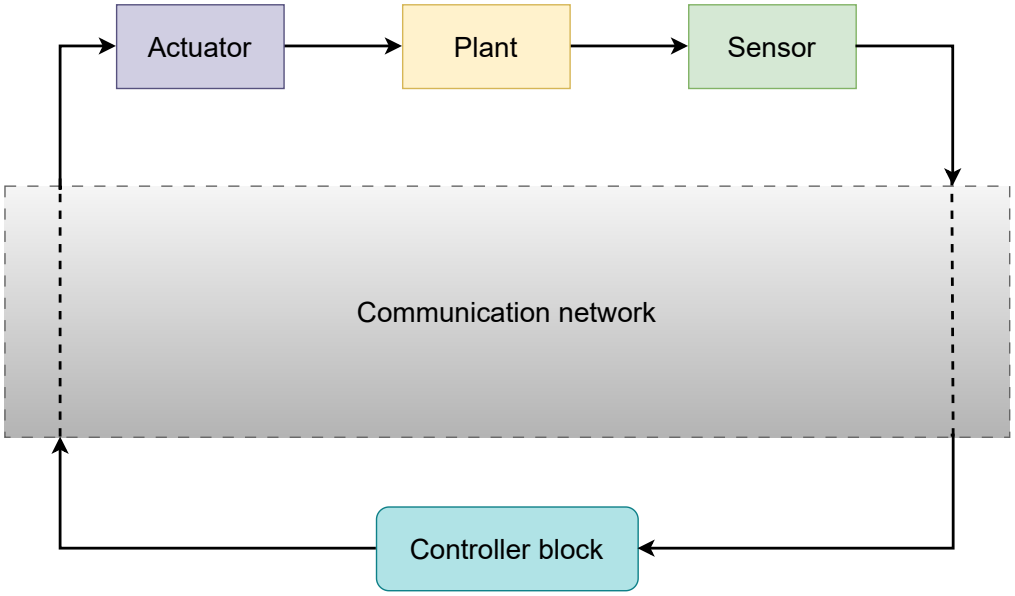

FIGURE 1.1: Block diagram of a closed-loop network control system.

1.4 Research Motivation

An NCS is a control system in which sensors, actuators, and controllers communicate over a network to regulate a process or system [152], as shown in Figure 1.1. Unlike traditional systems with direct wired connections, the loop is closed through a communication network, where signals are exchanged as information packets. Such transmissions are vulnerable to malicious attacks, such as DoS (see Figure 1.2).

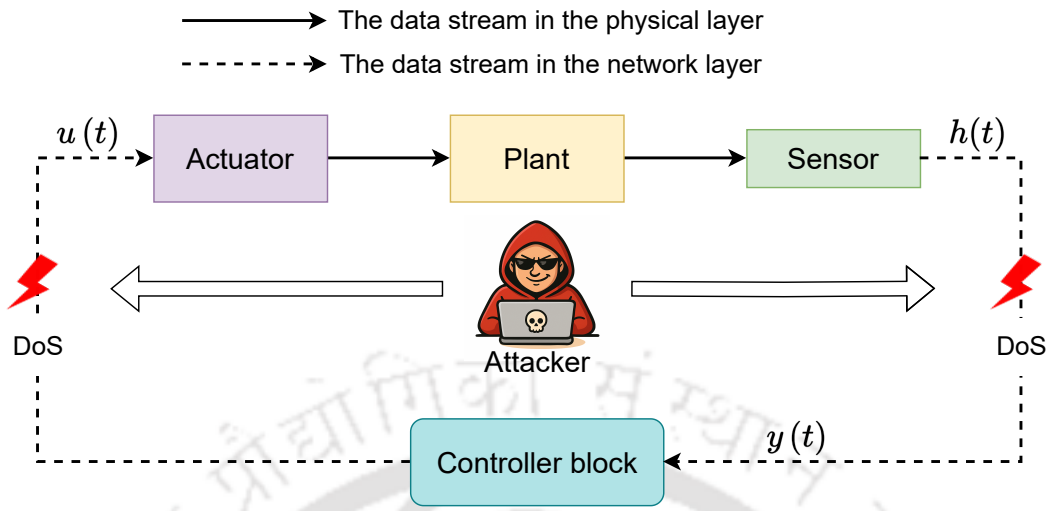

FIGURE 1.2: Block diagram of the closed-loop system for a single transmission channel under DoS.

De Persis and Tesi [48] characterized the frequency and duration of DoS under which systems can maintain ISS. Their result, followed by numerous studies [49–72, 75–131], focuses mainly on single-sensor scenarios. While effective in that case, it does not extend directly to multi-sensor settings.

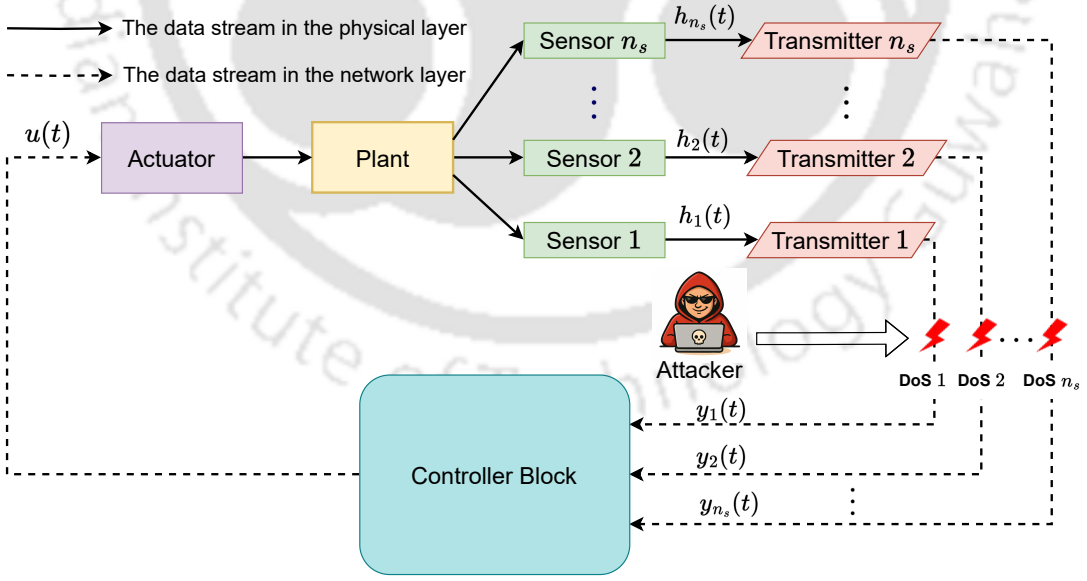

FIGURE 1.3: Block diagram of the closed-loop system for multiple transmission channels from StC under DoS.

Lu and Yang [132] addressed this by separately characterizing DoS on each StC channel. Subsequent works [133–142] adopted the same approach. However, all of them assumed

that only StC channels were affected in a multi-sensor setting (see Figure 1.3). In reality, since both sensing and actuation data share the network, DoS can also occur on CtA channels. This motivates the present work, which considers DoS on both StC and CtA channels in a multi-sensor framework.

1.5 Contributions

Since the characterization of DoS for multiple transmission channels provided in [132] considers only StC channels, it cannot be directly applied when DoS is also present in the CtA channel (see Figure 1.4). This necessitates a different characterization. To address this gap, we introduce the concepts of Multi-Channel DoS (MCDoS) and Full-Scale DoS (FSDoS).

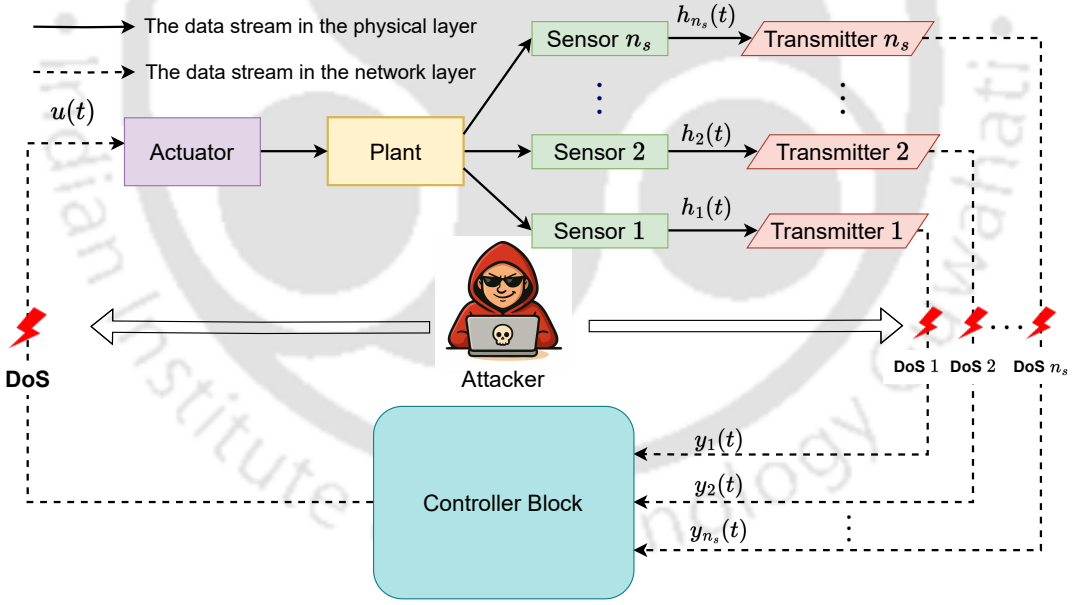

FIGURE 1.4: Block diagram of the closed-loop system for the multiple transmission channels when DoS is present in both StC and CtA channels.

MCDoS refers to scenarios where multiple transmission channels between sensors and the controller are affected by DoS, yet closed-loop stability can still be maintained. In contrast, FSDoS arises when closed-loop stability is lost due to a DoS attack on the CtA channel. FSDoS can also occur when MCDoS extends to the measurement side, affecting

enough channels to prevent the observer from estimating the states necessary for stability, rendering the system undetectable.

The primary objective of this thesis is to characterize MCDoS and FSDoS. To this end, a switched observer is first designed to mitigate MCDoS. An ETM is then developed to handle FSDoS. It is shown that the switched observer and ETM parameters can be co-designed. Specifically, an LMI-based optimization algorithm is proposed to determine the observer gain and ETM parameters to withstand the maximum MCDoS changing frequency (i.e., frequent changes in the MCDoS type). Subsequently, an LMI-based multi-objective optimization framework is developed to design these parameters for handling the maximum frequency and duration of FSDoS, along with the maximum MCDoS changing frequency.

The minimum inter-execution time for the switched observer-based ETM is derived, and a Zeno-free resilient control strategy is proposed. Furthermore, the conventional (static) ETM is replaced with a novel DETM to reduce control cost. The DETM architecture is modified to withstand the maximum MCDoS changing frequency, and the corresponding minimum inter-execution time is calculated. A Zeno-free DETM-based resilient control strategy is then implemented, with DETM parameters and observer gain jointly designed to ensure resilience against the maximum MCDoS changing frequency. Simulation results are presented throughout to validate the proposed theoretical developments.

1.6 Organization of the thesis

The remainder of this thesis unfolds as follows.

We begin in Chapter 2 by establishing the theoretical foundations required for the subsequent developments. This includes the control architecture for a single sensor operating under DoS and a concise characterization of attack frequency and duration under ISS conditions.

Building on these preliminaries, Chapter 3 focuses on the characterization of MCDoS in the absence of FSDoS. Here, a switched observer-based ETM control architecture is introduced, and ISS analysis is carried out to capture the impact of MCDoS. To counter these effects, an LMI-based optimization framework is proposed to maximize resilience against the highest permissible MCDoS changing frequency. The chapter also derives the minimum inter-execution time, ensuring Zeno-free operation, and concludes with simulation studies that demonstrate the effectiveness of the proposed strategy.

Chapter 4 builds upon the preceding analysis by addressing scenarios in which MCDoS and FSDoS occur simultaneously. While preserving the control architecture established in the previous chapter, a comprehensive joint ISS analysis is carried out to explicitly capture and characterize the behavior of FSDoS in the presence of MCDoS, jointly. On the basis of this analysis, a multi-objective LMI-based optimization framework is developed with the aim of enhancing the system's resilience against both categories of attacks. The advantages and practical significance of the proposed approach are subsequently validated and illustrated through an extensive simulation study.

The focus shifts in Chapter 5 to a novel DETM, designed to replace the ETM and further improve resilience. After presenting the DETM architecture, ISS analysis is conducted under MCDoS without FSDoS. This chapter also provides guidelines for DETM parameter selection and derives both minimum and maximum inter-execution times to guarantee Zeno-free operation. An optimization algorithm is developed to withstand the maximum MCDoS changing frequency, and simulations confirm the advantages of this new approach.

Finally, Chapter 6 concludes with the key contributions of the thesis and outlines several promising directions for future research.

Chapter 2

Preliminaries

2.1 Introduction

This chapter provides a concise yet comprehensive discussion of the scenario involving a single sensor operating under the influence of DoS. A resilient sampling-based control strategy is first presented, designed to mitigate the adverse effects of such attacks on system performance. This strategy ensures that the control loop can continue to function effectively, even when sensor measurements are intermittently unavailable due to communication interruptions. Following this, a detailed characterization of the frequency and duration of DoS attacks is developed, under which the ISS of the closed-loop system can still be guaranteed. This characterization establishes the precise conditions that define the resilience limits of the system, thereby providing a foundation for the more complex multi-channel scenarios considered in subsequent chapters.

2.2 The framework

2.2.1 Process dynamics

The process to be controlled is described by the differential equation

$$\dot{x}_p(t) = Ax_p(t) + Bu(t) + w(t) \tag{2.1}$$

where $x_p(t) \in \mathbb{R}^{n_p}$ is the state vector, $u(t) \in \mathbb{R}^{n_u}$ is the control input, A and B are the matrices with appropriate size, and $w(t) \in \mathbb{R}^{n_p}$ is an unknown input disturbance $\forall t \in \mathbb{R}_{\geq 0}$. Assume that the pair (A, B) is stabilizable. The control signal is implemented through a sample-and-hold mechanism. Denote by $\{t_k\}_{k\in\mathbb{N}_0}$ the sequence of time instants when the control action is intended to be updated, with $t_0 := 0$ by convention. Regardless of the method used to generate $\{t_k\}_{k\in\mathbb{N}_0}$, in an ideal scenario, where data transmission and reception can occur at any chosen time, the control input applied to the plant is

$$u_{\text{ideal}}(t) = -Kx_p(t_k), \tag{2.2}$$

$\forall t \in [t_k, t_{k+1})$.

2.2.2 Denial of service

DoS is referred to as a condition that may inhibit the execution of the ideal control input (2.2) at the intended time instants. In general, such disruptions can occur independently in the measurement and control channels. However, in this work, the scenario in which DoS simultaneously impairs both measurement and actuation channels is considered. Under such conditions, no data transmission, either sending or receiving, is possible during DoS intervals. To formalize this, let $\{d_n\}_{n\in\mathbb{N}}$, with $d_1 \geq 0$, denote the sequence of switching instants at which the DoS signal transitions from an inactive state (communication allowed) to an active state (communication blocked). The nth DoS interval is then defined

as

$$D_n \coloneqq d_n \cup [d_n, d_n + \tau_n), \tag{2.3}$$

where $\tau_n \in \mathbb{R}_{\geq 0}$ represents the duration during which communication remains disrupted. If $\tau_n = 0$, the nth DoS instance corresponds to an instantaneous pulse at time d_n. Given $\tau, t \in \mathbb{R}_{\geq 0}$ with $t \geq \tau$, define the sets

$$\Xi(\tau, t) \coloneqq \bigcup_{n \in \mathbb{N}} D_n \cap [\tau, t], \tag{2.4}$$

$$\Lambda(\tau, t) \coloneqq [\tau, t] \setminus \Xi(\tau, t). \tag{2.5}$$

That is, within any interval $[\tau, t]$, the set $\Xi(\tau, t)$ denotes the collection of time instants during which communication is interrupted due to DoS, while $\Lambda(\tau, t)$ identifies the instants when communication remains possible.

2.2.3 Control action

The state value available for the controller

$$x_q(t) \coloneqq \begin{cases} 0, & \text{if } t \in \Xi(0, t), \\ x_p(t), & \text{otherwise.} \end{cases} \tag{2.6}$$

In words,

$$x_q(t) = x_p(t), \tag{2.7}$$

if DoS is not present on the StC channel. The control input applied to the process can be expressed as

$$u(t) = -K x_q(t_{k(t)}) \tag{2.8}$$

where

$$k(t) := \begin{cases} -1, & \text{if } \Lambda(0,t) = \emptyset \\ \sup\{k \in \mathbb{N}_0 : t_k \in \Lambda(0,t)\}, & \text{otherwise.} \end{cases} \tag{2.9}$$

In other words, for each $t \in \mathbb{R}_{\geq 0}$, the index $k(t)$ denotes the most recent time instant at which the control input was successfully updated. When $d_0 = 0$, it follows that $k(0) = -1$, which leads to the issue of specifying the control input at the initial moment when communication is unavailable. To address this, it is assumed that $u(0) = 0$ in the case where $d_0 = 0$, and for notational consistency, $x_q(t_{-1})$ is defined as zero.

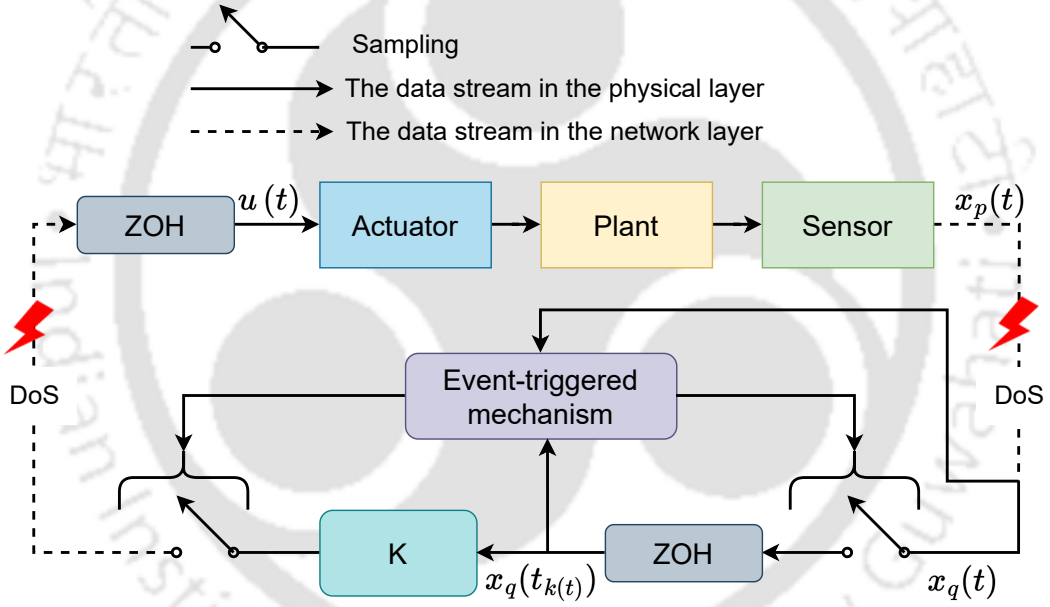

FIGURE 2.1: Block diagram of ETM-based state-feedback control for a single sensor under DoS.

2.3 Event-driven control update policy for stability

A class of control update policies that guarantee ISS in the absence of DoS is first introduced. Consider the closed-loop dynamics arising from (2.1) when the control input is defined as in (2.8). To facilitate the analysis, the system is reformulated into a more

suitable representation. In the absence of DoS, the equality in (2.7) holds. Define

$$\xi(t) \coloneqq x_p(t_{k(t)}) - x_p(t), \tag{2.10}$$

$\forall t \in \mathbb{R}_{\geq 0}$, which captures the deviation between the process state at the most recent successful control update and its current value. With this definition, the closed-loop system can be expressed as

$$\dot{x}_p(t) = (A - BK)x_p(t) + BK\xi(t) + w(t). \tag{2.11}$$

The proposed ETM is expressed by boundedness

$$\|\xi(t)\| \leq \tilde{\psi}\left(\|x_p(t)\| + \|w_t\|_\infty\right) \tag{2.12}$$

where $\tilde{\psi} \in \mathbb{R}_{\geq 0}$ is the ETM design parameter. The update rule in (2.12) is not intended for direct implementation, as it relies on the supremum norm of the disturbance w, which is typically unknown in practice. Instead, alternative control update mechanisms will be employed at a later stage to ensure that the condition in (2.12) is consistently satisfied. The full control architecture is depicted in Figure 2.1.

As established in the subsequent result, any control update strategy that ensures the error signal $\xi(t)$ satisfies the condition in (2.12) can be regarded as stabilizing, provided that the function $\tilde{\psi}$ is selected appropriately. A standard Lyapunov-based approach is adopted. For any symmetric positive definite matrix $Q \in \mathbb{R}^{n_p \times n_p}$, the corresponding Lyapunov function matrix P is defined as the unique solution to the Lyapunov equation

$$(A - BK)^\top P + P(A - BK) + Q = 0. \tag{2.13}$$

By choosing the candidate Lyapunov function $V(x(t)) = x_p^\top(t) P x_p(t)$ and evaluating its derivative along the trajectories of the closed-loop system (2.11), the bounds can be

established as

$$\lambda_m(P)\|x_p(t)\|^2 \leq V(x(t)) \leq \lambda_M(P)\|x_p(t)\|^2, \tag{2.14}$$

$$\dot{V}(x_p(t)) \leq -\lambda_m(Q)\|x_p(t)\|^2 + 2\|PBK\|\|x_p(t)\|\|e(t)\| + 2\lambda_M(P)\|x_p(t)\|\|w(t)\|. \tag{2.15}$$

These inequalities hold $\forall t \in \mathbb{R}_{\geq 0}$. It follows that, under condition (2.12), the inequality in (2.15) reduces to a Decay-type inequality, provided that the parameter $\tilde{\psi}$ is chosen to be sufficiently small.

Definition 2.1. A control update sequence $\{t_k\}_{k\in\mathbb{N}_0}$ governed by an ETM is said to exhibit the finite sampling rate property if there exists a positive constant $\underline{\Delta} \in \mathbb{R}_{>0}$ such that the inter-execution times satisfy

$$\Delta_k \coloneqq t_{k+1} - t_k \geq \underline{\Delta} \tag{2.16}$$

$\forall k \in \mathbb{N}_0$.

In this context, and throughout the remainder of the discussion, it is assumed that the network is capable of transmitting information at a rate corresponding to the lower bound $\underline{\Delta}$ on the sampling interval.

Theorem 2.2. *Let the control system described by (2.11), comprising the process dynamics (2.1) and the control law (2.8), be considered. Assume that the feedback gain matrix K is selected such that the matrix $A-BK$ is Hurwitz, i.e., all its eigenvalues have strictly negative real parts. For any symmetric positive definite matrix $Q \in \mathbb{R}^{n_p\times n_p}$, let P denote the unique positive definite solution to the Lyapunov equation given in (2.13). Define the Lyapunov candidate function as $V(x(t)) = x_p^\top(t)Px_p(t)$. Suppose a control update sequence is implemented with finite sampling frequency and satisfies inequality (2.12) $\forall t \in \mathbb{R}_{\geq 0}$, where the design parameter $\tilde{\psi}$ satisfies the condition*

$$\lambda_m(Q) - 2\tilde{\psi}\|PBK\| > 0, \tag{2.17}$$

then the closed-loop system (2.11) is ISS.

Proof. See the Appendix A.1. ■

Inequality (2.17) can be ensured by choosing $\tilde{\psi}$ to be sufficiently small, provided that $\lambda_m(Q) > 0$. Once such a $\tilde{\psi}$ is selected in accordance with (2.17), the remaining concern lies in whether sampling strategies can be devised that enforce (2.12) while operating at a finite sampling rate. As the next result shows, the minimum inter-execution time.

Lemma 2.3. *Let $\tilde{\psi}$ be chosen such that condition (2.17) holds. Then, for any initial state $x_p(0) \in \mathbb{R}^{n_p}$, the ETM defined by (2.12) produces a sequence $\{t_k\}_{k\in\mathbb{N}_0}$ that satisfies the inter-execution time condition (2.16), where the lower bound $\underline{\Delta} \in \mathbb{R}_{\geq 0}$ is given by*

$$\underline{\Delta} = \int_0^1 \frac{1}{\frac{1}{\tilde{\psi}}(\|A-BK\|+1) + (\|A-BK\|+\|BK\|+1)s + \tilde{\psi}\|BK\|s^2}\, ds. \tag{2.18}$$

Proof. See the Appendix A.2. ■

The existence of a lower bound on the inter-execution time guarantees the exclusion of Zeno behavior. This property is made possible by incorporating the disturbance term into the ETM logic in (2.12). In the absence of this disturbance-dependent term, Zeno behavior cannot be prevented. A method for eliminating the dependence on the supremum norm of the disturbance in the ETM logic, while still ensuring the avoidance of Zeno behavior, will be discussed later.

2.4 ISS guarantees under DoS-constrained networks

In the presence of DoS, the controller has access to the states $x_q(t)$ instead of $x_p(t)$. In this case, the ETM bound in (2.12) can be expressed as

$$\|x_q(t_{k(t)}) - x_q(t)\| \leq \tilde{\psi}\left(\|x_q(t)\| + \|w_t\|_\infty\right). \tag{2.19}$$

However, under DoS, (2.19) may not remain valid, whereas in the absence of DoS it coincides with (2.12). Therefore, for the stability analysis, the system states $x_p(t)$ are

considered, along with the established upper bound on $\|\zeta(t)\|$ in the presence of DoS. The notation $x_q(t)$ will be used in Section 2.5 to describe the ETM logic that does not rely on the supremum norm of disturbances.

The analysis presented in Section 2.3 assumes that condition (2.12) holds $\forall t \in \mathbb{R}_{\geq 0}$. However, in the presence of DoS, this assumption becomes problematic, as certain control update attempts may fail regardless of the chosen sampling strategy. When updates are unsuccessful and the error signal $\xi(t)$ is not reset, condition (2.12) may no longer be satisfied, potentially compromising stability due to the breakdown of the dissipation-like inequality in (2.15). This raises the question of whether the conclusions of Theorem 2.2 can be extended to incorporate the impact of DoS. The remainder of the section focuses on addressing this issue. Section 2.4.1 defines and analyzes the class of DoS signals under consideration, while Section 2.4.2 presents the main theoretical result.

2.4.1 DoS signal characterization under time constraints

The initial consideration involves identifying the extent to which a system can withstand a DoS attack without becoming unstable. It is evident that this tolerance is inherently limited, and appropriate constraints must be placed on both the frequency and the duration of DoS events.

(a) *DoS frequency:* To begin with, consider the frequency at which DoS events may occur. Let the quantity $d_{n+1} - d_n$, for each $n \in \mathbb{N}$, represent the time interval between two consecutive DoS activations. If it holds that $d_{n+1} - d_n \leq \underline{\Delta}, \forall n \in \mathbb{N}$, that is, if DoS can be triggered at a rate equal to the minimum allowable sampling rate $\underline{\Delta}$, then system stability cannot be ensured, irrespective of the chosen control update strategy. This suggests that maintaining stability necessitates that the DoS triggering frequency remains sufficiently lower than the minimum sampling rate. A standard approach to formalize this requirement is by using the concept of average dwell-time, as introduced in [153]. For any $\tau, t \in \mathbb{R}_{\geq 0}$ with $t \geq \tau$, let $n(\tau, t)$ denote the number of DoS on/off transitions within the interval $[\tau, t)$.

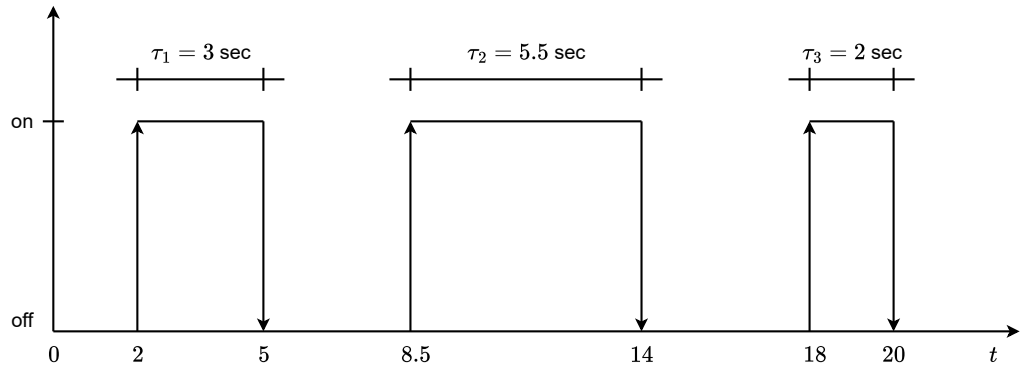

FIGURE 2.2: Illustration of a DoS signal. The transitions from the off state to the on state are denoted by $\uparrow$, whereas transitions from on to off are indicated by $\downarrow$. The off/on transitions occur at $2, 8.5$, and 18 seconds, with the corresponding DoS intervals lasting $3, 5.5$, and 2 seconds, respectively. For example, this results in $n(0,1) = 0, n(1,11) = 2$, and $n(11,20) = 1$. Similarly, $\Xi(0,1) = \emptyset$, $\Xi(1,11) = [2,5) \cup [8.5,11)$, and $\Xi(11,20) = [11,14) \cup [18,20)$.

Assumption 2.1. There exist $\varrho \in \mathbb{R}_{\geq 0}$ and $\tau_F \in \mathbb{R}_{>\underline{\Delta}}$ such that

$$n(\tau, t) \leq \varrho + \frac{t-\tau}{\tau_F} \tag{2.20}$$

$\forall t, \tau \in \mathbb{R}_{\geq 0}$ with $t \geq \tau$.

(b) *DoS duration:* Beyond limitations on the frequency of DoS, it is also essential to impose constraints on their duration, that is, the length of time during which communication remains disrupted. To illustrate this, consider a DoS sequence comprising only the single event d_1. In such a case, Assumption 2.1 is trivially satisfied for any $\varrho \geq 1$. Nevertheless, if the corresponding DoS interval is $D_1 = \mathbb{R}_{\geq 0}$, implying that communication is indefinitely blocked, then system stability cannot be preserved, regardless of the specific control update mechanism employed. In light of this, and referring to the definition of $\Xi(\tau, t)$ given in (2.4), the next assumption naturally complements Assumption 2.1 by placing restrictions on the total duration of DoS activity.

Assumption 2.2. There exist a $T \in \mathbb{R}_{>1}$ and $\zeta \in \mathbb{R}_{\geq 0}$ such that

$$|\Xi(\tau, t)| \leq \zeta + \frac{t-\tau}{T} \tag{2.21}$$

$\forall t, \tau \in \mathbb{R}_{\geq 0}$ with $t \geq \tau$.

Figure 2.2 illustrates the values of $n(\tau, t)$ and $\Xi(\tau, t)$ corresponding to a specific DoS signal pattern. Assumptions 2.1 and 2.2 define the class of DoS signals considered in the subsequent analysis of this chapter. Notably, these assumptions do not impose any restrictions regarding the attacker's knowledge of the system's dynamics, feedback gain, or the structure of the ETM. Instead, they impose constraints solely on the frequency and duration of the DoS incidents. These limitations are not only essential for ensuring that the control problem remains well-posed but are also grounded in practical considerations. In real-world scenarios, various countermeasures, such as spread spectrum techniques and high-pass filtering, can be employed to reduce the effectiveness of DoS attacks (see [154–156]). These countermeasures inherently restrict the attack's ability to consistently disrupt communication, thereby imposing practical limits on how frequently and for how long DoS conditions can persist.

2.4.2 ISS under DoS

The main result of this section can now be established. Informally, it states that any control update strategy satisfying the conditions of Lemma 2.3 ensures ISS, provided the DoS signal adheres to Assumptions 2.1 and 2.2, with sufficiently large values of τ_F and T. Although the proof involves several technical steps, the core idea is conceptually straightforward. The time domain is partitioned into segments where the condition in (2.12) is enforceable and segments where DoS activity may prevent it from holding. The closed-loop dynamics are then interpreted as a switched system alternating between stable and unstable modes. Stability is achieved when the parameters τ_F and T are chosen such that the influence of the stable mode dominates that of the unstable one over time. The result below follows accordingly.

Theorem 2.4. *Consider the control system described by (2.11), composed of the plant dynamics (2.1) and the control input (2.8), where the feedback gain matrix K is such that the matrix $A-BK$ is Hurwitz. Let $Q \in \mathbb{R}^{n_p \times n_p}$ be any symmetric positive definite matrix, and let P denote the unique solution to the Lyapunov equation $(A-BK)^\top P + P(A-BK) + Q = 0$. Define the Lyapunov function $V(x) = x_p^\top(t) P x_p(t)$. Assume that the*

control updates are triggered by the ETM in (2.12)*, where the inter-execution times are lower bounded by* $\underline{\Delta}$ *and* $\tilde{\psi}$ *satisfies condition* (2.17)*. Further, suppose the DoS sequence satisfies Assumptions 2.1 and 2.2 for arbitrary constants* ϱ *and* ζ*, and for parameters* τ_F *and* T *such that*

$$\frac{1}{T} + \frac{\underline{\Delta}}{\tau_F} < \frac{\omega_1}{\omega_1 + \omega_2} \tag{2.22}$$

holds, where

$$\omega_1 := \frac{\lambda_m(Q) - 2\tilde{\psi}\|PBK\|}{2\lambda_M(P)} \tag{2.23}$$

and

$$\omega_2 := \frac{4\|PBK\|}{\lambda_m(P)}. \tag{2.24}$$

Then, the closed-loop system (2.11) *is ISS.*

Proof. See the Appendix A.3. ■

Theorem 2.4 provides a formal characterization of the allowable frequency and duration of DoS for which the closed-loop system retains its ISS property. Specifically, the upper bound constraints on the admissible frequency and duration of DoS are introduced in (2.20) and (2.21), as stated in Assumptions 2.1 and 2.2, respectively. Theorem 2.4 determines the admissible values of these bounds by deriving explicit conditions in (2.22). When the actual DoS frequency and duration remain strictly within the limits established by Theorem 2.4, the system is guaranteed to preserve ISS. Conversely, if the DoS characteristics exceed these bounds, either in terms of occurrence frequency or attack duration, the stability of the system can no longer be assured.

2.5 Disturbance-free triggering scheme

The ETM logic in (2.19) depends on the supremum norm of the disturbance w, which is unknown to the designer. Without this term, a minimum inter-execution time $\underline{\Delta}$ cannot be guaranteed, leading to possible Zeno behavior. To prevent this, a lower bound $\underline{\Delta}$ is imposed so that the $(k+1)$th event cannot occur before $t_k + \underline{\Delta}$. The disturbance-free ETM logic is

$$t_{k+1} = \begin{cases} t_k + \underline{\Delta}, & \text{if } \varpi_k < t_k + \underline{\Delta}, \\ \varpi_k, & \text{otherwise}, \end{cases} \tag{2.25}$$

where

$$\varpi_k \coloneqq \inf \left\{ t > t_k : \|x_q(t_k) - x_q(t)\| \geq \tilde{\psi} \|x_q(t)\| \right\}. \tag{2.26}$$

This ensures that inter-sampling times remain no shorter than $\underline{\Delta}$.

2.6 Chapter summary

In this chapter, a preliminary framework for resilient control of a single-sensor system under DoS was presented. The discussion began with the design of an ETM-based state-feedback control strategy. The ISS of the resulting closed-loop system was then analyzed in the absence of DoS to establish a baseline of performance. Subsequently, the impact of DoS attacks was incorporated into the analysis, and explicit constraints on the upper bounds of both the attack frequency and duration were introduced. Finally, the admissible values for these bounds were derived, identifying the range of conditions under which the system remains stable despite the presence of DoS.

The insights gained from this single-sensor DoS analysis have had a profound influence on the development of the work presented in this thesis. The techniques, results, and interpretations established here serve as a foundational reference point that resonates

throughout the subsequent chapters. In numerous instances within the multi-sensor analysis, the single-sensor framework re-emerges, either directly guiding the derivations or inspiring methodological adaptations. Indeed, the single-sensor study provides not only valuable theoretical grounding but also a significant source of motivation for extending the resilient control design to more complex, multi-sensor settings.

Chapter 3

Characterization of multi-channel denial-of-service

3.1 Introduction

MCDoS refers to a scenario in which multiple transmission channels from the StC side are subjected to DoS attacks, yet the system retains the capability to maintain closed-loop stability. Such attacks occur exclusively between the sensors and the controller, thereby compromising only the measurement data. Under MCDoS conditions, stability can still be preserved by reconstructing or estimating the corrupted measurement data corresponding to the affected transmission channels. In contrast, FSDoS arises when DoS affects multiple StC transmission channels to the extent that certain unstable states become unobservable. In other words, the presence of FSDoS on the measurement side causes the system to lose detectability. FSDoS can also manifest when the CtA transmission channel is subjected to DoS attacks. While resilient control strategies can be devised to counter FSDoS, the primary emphasis of this chapter is on the systematic characterization of MCDoS.

3.2 Problem formulation

The central objective of this chapter is the detailed characterization of MCDoS. As established in the formal definition provided in Section 3.1, a system subject to MCDoS can remain stabilizable. Therefore, imposing restrictions on the total duration of MCDoS is unnecessary. However, frequent changes in the type of MCDoS can compromise stability, thereby making it essential to impose an upper bound on its changing frequency. In this chapter, an explicit bound on the allowable MCDoS changing frequency is derived. To facilitate this, a switched observer is employed to counteract the effects of MCDoS, while an ETM is introduced to address potential FSDoS effects. A rigorous ISS analysis is then presented under conditions where FSDoS is absent, but MCDoS changing frequency remains the key destabilizing factor. Subsequently, the switched observer gains and ETM parameters are determined through an optimization framework formulated using LMIs, ensuring system resilience against the worst-case MCDoS changing rate. Furthermore, the minimum inter-execution time is analytically computed and embedded into the resilient control logic to preclude Zeno behavior, thereby guaranteeing the feasibility of the proposed control strategy in practical implementations.

3.3 The framework

3.3.1 System description

The dynamic system under consideration is described by (2.1), while the output of the ith sensor is given by

$$h_i(t) = C_i x_p(t), \tag{3.1}$$

where $h_i(t) \in \mathbb{R}^{n_{h_i}}$, $i \in \{1, 2, \ldots, n_s\}$, and n_s denotes the total number of transmission channels or sensors. In (2.1) and (3.1), the matrices A and B correspond to the system

dynamics and input matrices, respectively, while C_i represents the output matrix associated with the ith sensor, all having appropriate dimensions. It is assumed that the pair (A, B) is controllable and the pair $(A, \{C_1, C_2, \ldots, C_{n_s}\})$ is observable. The analysis in this work is carried out under the assumption that the system described by (2.1) and (3.1) is fully observable. In cases where full observability does not hold, the system can be decomposed into observable and unobservable subsystems, as discussed in [133]. The sequence of time instants at which control updates are intended to occur is denoted by $\{t_k\}_{k\in\mathbb{N}_0}$, where $t_0 \coloneqq 0$. In the ideal scenario, when data transmission and reception can occur at any desired instant and the state $x_p(t)$ is entirely measurable, the control input is applied according to (2.2) $\forall t \in [t_k, t_{k+1})$.

3.3.2 Multi-channel DoS and full-scale DoS

When multiple transmission channels from the StC path are subjected to DoS, yet the closed-loop stability of the overall system can still be preserved, the phenomenon is referred to as MCDoS. In contrast, FSDoS arises when the closed-loop stability is compromised due to either (i) a DoS affecting the transmission line from the controller to the plant actuator, or (ii) an MCDoS persisting over a sufficient subset of measurement-side channels such that the system loses detectability. The subsequent analysis of FSDoS in a later chapter will explicitly distinguish between its impact on the StC channels and on the CtA channel. For the present discussion, FSDoS is assumed to occur synchronously between the sensors and the controller, as well as between the controller and the actuator. Let n_s denote the total number of transmission channels. For the ith transmission channel, let $\{d_{i_a}\}_{a\in\mathbb{N}}$ represent the sequence of DoS on/off transition instants, where $d_{i_1} \geq 0$ indicates the time at which the DoS switches from zero (transmission allowed) to one (transmission blocked). The ath DoS interval in the ith channel is expressed as

$$D_{i_a} \coloneqq d_{i_a} \cup [d_{i_a}, d_{i_a} + \tau_{i_a}), \tag{3.2}$$

where $\tau_{i_a} \in \mathbb{R}_{\geq 0}$ denotes the duration of communication blockage. When $\tau_{i_a} = 0$, the DoS reduces to a single impulsive event at d_{i_a}. Given $t, \tau \in \mathbb{R}_{\geq 0}$ with $\tau \leq t$, the cumulative

set of DoS intervals for the ith channel over the observation window $[\tau, t]$ is defined as

$$\Omega_i(\tau, t) \coloneqq \bigcup_{a \in \mathbb{N}} D_{i_a} \cap [\tau, t]. \tag{3.3}$$

In other words, $\Omega_i(\tau, t)$ denotes the union of all time segments within $[\tau, t]$ during which transmission in the ith channel is blocked. Extending this definition across all channels, the sets

$$\Omega(\tau, t) \coloneqq \bigcap_{i \in \{1,\dots,n_s\}} \Omega_i(\tau, t), \tag{3.4}$$

$$\Upsilon(\tau, t) \coloneqq [\tau, t] \setminus \Omega(\tau, t), \tag{3.5}$$

respectively, capture the intervals when FSDoS is active and when it is absent over the given time horizon. Notably, MCDoS conditions can only occur during the intervals represented by $\Upsilon(\tau, t)$.

3.4 Control architecture

After the occurrence of a DoS on the measurement side, the available output data can be described as

$$y_i(t) \coloneqq \begin{cases} 0, & \text{if } t \in \Omega_i(0, t), \\ h_i(t), & \text{otherwise,} \end{cases} \tag{3.6}$$

where $h_i(t)$ and Ω_i are mentioned in (3.1) and (3.3), respectively. To address MCDoS conditions, a switched Luenberger-based observer is employed, formulated as

$$\dot{x}_e(t) = Ax_e(t) + Bu(t) + L_\sigma(\hat{y}_\sigma(t) - C_\sigma x_e(t)), \tag{3.7}$$

where

$$\sigma \coloneqq \begin{cases} \min\{i : \|y_i(t)\| > v\}, & \text{if } \|y_{\sigma^-}(t)\| \leq v \\ \sigma^-, & \text{otherwise,} \end{cases} \tag{3.8}$$

$$\hat{y}_i(t) \coloneqq y_i(t_{k(t)}), \quad \forall t \in [t_k, t_{k+1}), \tag{3.9}$$

$$k(t) \coloneqq \begin{cases} -1, & \text{if } \Upsilon(0,t) = \emptyset \\ \sup\{k \in \mathbb{N}_0 : t_k \in \Upsilon(0,t)\}, & \text{otherwise.} \end{cases} \tag{3.10}$$

For notational consistency, let $y_i(t_{-1}) \coloneqq 0$. Here, σ serves as the switching index, where $\sigma(\cdot) : \mathbb{R}_{\geq 0} \to \{1, 2, \cdots, n_s\}$ is a piecewise constant function. The set $\overline{\mathbb{S}}_\sigma \subset \mathbb{R}_{\geq 0}$ is defined as the collection of time instants at which $\sigma(\cdot)$ is discontinuous, that is, $\overline{\mathbb{S}}_\sigma \coloneqq \tau \in \mathbb{R}_{\geq 0} : \sigma(\tau^-) \neq \sigma(\tau^+)$ [150]. The notation $\sigma(t_k^+)$ represents the value of σ within the interval $[t_{k(t)}, t_{k(t)+1})$, which is denoted simply as σ for brevity. The pair $(A, \{C_1, C_2, \cdots, C_{n_s}\})$ is assumed to be completely observable, ensuring that the channel index and the switching index coincide. Over the time span $[t_{k(t)-1}, t_{k(t)})$, the symbol σ^- refers to the active channel index before switching, while $y_{\sigma^-}(t)$ denotes the corresponding channel output. At $t_k = 0$, $\sigma = 0$ because $0 \in \Omega(0,t)$. The control input applied to the process is therefore given by

$$u(t) = \begin{cases} 0, & \text{if } \Upsilon(0,t) = \emptyset \\ -K\hat{x}_e(t), & \text{otherwise,} \end{cases} \tag{3.11}$$

$\forall t \in \mathbb{R}_{\geq 0}$, where

$$\hat{x}_e(t) = x_e(t_{k(t)}), \quad \forall t \in [t_k, t_{k+1}). \tag{3.12}$$

The state error of the process output available to the observer is defined as

$$\xi_\sigma(t) \coloneqq \hat{y}_\sigma(t) - y_\sigma(t), \tag{3.13}$$

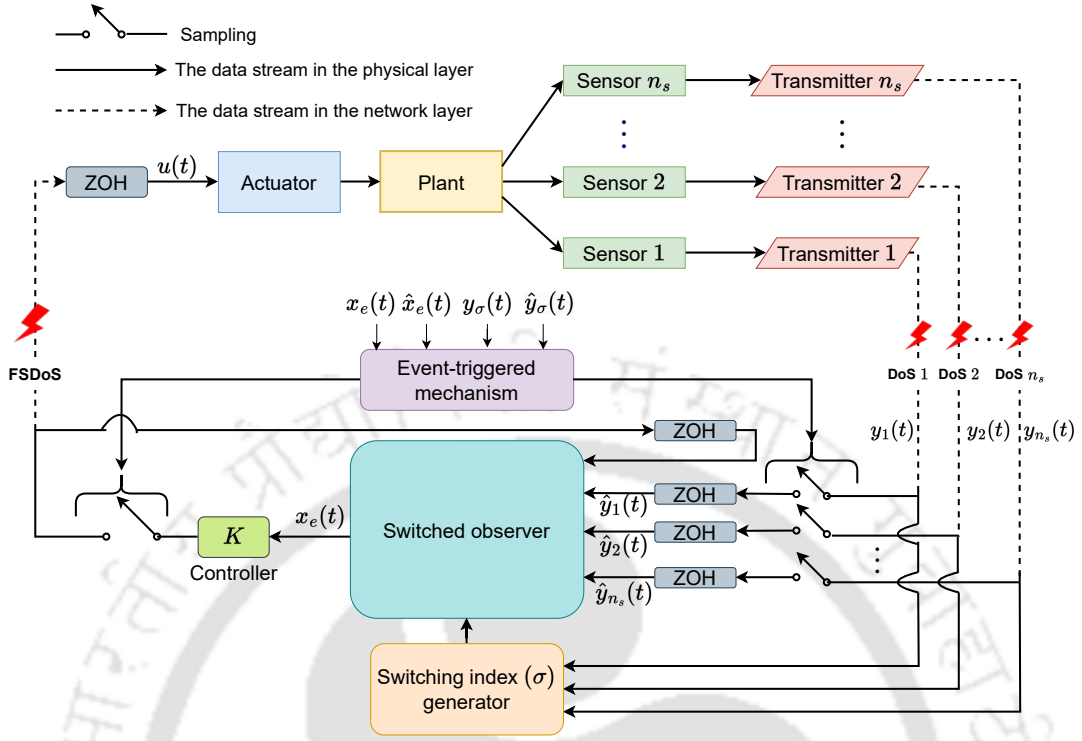

FIGURE 3.1: Block diagram of the system with switched observer-based ETM architecture for multiple transmission channels under DoS.

while the observer's state error is expressed as

$$\xi_e(t) := \hat{x}_e(t) - x_e(t). \tag{3.14}$$

The combined switched observer-based control system is therefore represented by

$$\begin{aligned} \dot{x}_p(t) &= (A - BK)x_p(t) + BK\tilde{x}(t) - BK\xi_e(t) + w(t), \\ \dot{\tilde{x}}(t) &= (A - L_\sigma C_\sigma)\tilde{x}(t) - L_\sigma \xi_\sigma(t) + w(t), \end{aligned} \tag{3.15}$$

where

$$\tilde{x}(t) := x_p(t) - x_e(t). \tag{3.16}$$

The ETM is governed by the boundedness condition

$$\xi_\sigma^\top(t)\xi_\sigma(t) + \xi_e^\top(t)\xi_e(t) \leq \psi_1 \left(y_\sigma^\top(t) y_\sigma(t) + \|w_t\|_\infty^2 \right) + \psi_2 x_e^\top(t) x_e(t), \tag{3.17}$$

where $\psi_1, \psi_2 \in \mathbb{R}_{>0}$. Whenever (3.17) is violated, the $(k+1)$th task execution is triggered. Since (3.17) involves the supremum norm of the disturbance w, this condition is not applied directly as the control update rule. Instead, alternative triggering conditions are adopted to ensure that (3.17) remains satisfied under all circumstances. The following result outlines the selection of ψ_1 and ψ_2 to guarantee that the closed-loop system (3.15) achieves ISS under the ETM defined in (3.17). The overall control architecture is depicted in Figure 3.1. For the stability analysis, a standard Lyapunov framework is utilized. The candidate Lyapunov function is

$$V_\sigma(x_p(t), \tilde{x}(t)) = x_p^\top(t) P_{p_\sigma} x_p(t) + \tilde{x}^\top(t) P_{e_\sigma} \tilde{x}(t), \tag{3.18}$$

where P_{p_σ} and P_{e_σ} are positive-definite matrices of appropriate dimensions.

Remark 3.1. It is considered that when a transmission channel is subjected to DoS, observers receive no data. For this reason, a small positive threshold υ is added in (3.8). For the ideal case, υ is equal to zero. But in practice, noise can be present in the channel. So, estimating the value of υ is a practical problem depending on the noise intensity in the channel. It is believed that the value of υ should be kept low. The transmission channel can also receive data below the threshold value in steady-state regulatory scenarios without experiencing DoS. Since the system is already in a steady-state condition, it won't violate (3.17). Therefore, $k(t)$ will not be updated, and the observer gain still contains the previous value. The reader may be curious about the significance of the observer gain during the FSDoS. The $k(t)$ value does not update during the FSDoS, allowing the observer to hold onto the previous value. For the same reason, the value of C_σ does not change during FSDoS. It holds the previous value.

3.5 Stability analysis of switched observer-based ETM under MCDoS

3.5.1 Assumption: time-constrained MCDoS

The MCDoS is a phenomenon where DoS can be present in any (multiple) transmission channels, and still, the closed-loop stability of the system can be preserved. The term "changing of MCDoS" refers to a DoS that suddenly appears or disappears in a single transmission channel without hampering the stability of the closed-loop system. The changing frequency of MCDoS has to be limited. Let $E_l, \forall l \in \mathbb{N}$ indicates the time between lth and $(l+1)$th changing of MCDoS. If $E_l \leq \underline{\Delta}$ for any $l \in \mathbb{N}$ (MCDoS changing occurs at the same pace as minimum feasible sampling rate $\underline{\Delta}$), the controller can't process estimated data from the observer, and that leads towards the instability. It is self-evident that the frequency at which MCDoS changes must be modest enough compared to the minimum sampling rate to achieve stability. Let $l(\tau, t)$ indicate the number of MCDoS changing transitions happening on the interval $[\tau, t)$ given $t, \tau \in \mathbb{R}_{\geq 0}$ with $t \geq \tau$.

Assumption 3.1. (*MCDoS frequency:*) There exist $\varkappa \in \mathbb{R}_{\geq 0}$ and $\tau_D \in \mathbb{R}_{>\underline{\Delta}}$ such that

$$l(\tau, t) \leq \varkappa + \frac{t-\tau}{\tau_D}, \tag{3.19}$$

$\forall \tau, t \in \mathbb{R}_{\geq 0}$ with $t \geq \tau$.

Remark 3.2. Assumption 3.1 specifies the variation frequency of MCDoS. In particular, the condition in (3.19) limits MCDoS exclusively in terms of its changing frequency. It should be emphasized that the occurrence of FSDoS is not regarded as a change in MCDoS. For example, in Figure 3.2, the value is $l(0, 1) = 3$, where the on/off transition of FSDoS at $t = 0.3$s is not considered a change in MCDoS. Likewise, $l(2.7, 3.1) = 0$ because only an FSDoS transition occurs at $t = 3$s, without any alteration in MCDoS during the interval $[2.7, 3.1)$

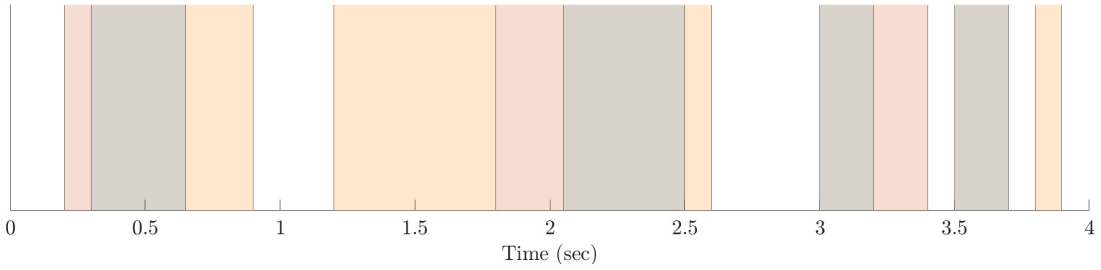

FIGURE 3.2: Example of MCDoS and FSDoS signals. Two data transmission channels exist between the sensors and the switched observer. Grey-shaded regions indicate FSDoS intervals, orange-shaded regions denote MCDoS type 1 (only channel 2 affected by DoS), and yellow-shaded regions denote MCDoS type 2 (only channel 1 affected by DoS). The durations of MCDoS type 1 are $[0.2, 0.3)$, $[1.8, 2.05)$, and $[3.2, 3.4)$, while the durations of MCDoS type 2 are $[0.65, 0.9)$, $[1.2, 1.8)$, $[2.5, 2.6)$, and $[3.8, 3.9)$. The FSDoS intervals over $[0, 4]$ are given by $\Omega(0, 4) = [0.3, 0.65) \cup [2.05, 2.5) \cup [3, 3.2) \cup [3.5, 3.7)$.

The switching of the observer is directly linked to MCDoS transitions. Whenever MCDoS changes, the observer also switches to accommodate the new MCDoS. Therefore, by defining the changing frequency of MCDoS, the switching frequency of the observer is inherently characterized. Additionally, the proposed switched observer in (3.7) mitigates the impact of MCDoS frequency changes on the overall system. For example, in Figure 3.2, while the actual MCDoS changes result in $l(0, 1) = 3$, the proposed switched observer technique yields $l(0, 1) = 2$. This occurs because, at $t = 0.9, \mathrm{s}$, when MCDoS transitions from type 2 to a no-attack condition, the switched observer does not treat it as an MCDoS frequency change.

Unlike Assumption 2 in [132], which imposes frequency constraints on individual DoS channels, Assumption 3.1 characterizes the overall changing frequency of MCDoS across all channels. This assumption is derived from the concept of average dwell time [153].

3.5.2 Control objectives

The primary goal is to design a sampling logic with a finite sampling rate that ensures resilience against both MCDoS and FSDoS while maintaining the characterization of MCDoS. The following definitions are introduced in alignment with these objectives.

Definition 3.3. [157] Let (3.15) be the overall system that results from (2.1), (3.1) and (3.7) with a control input (3.11). If a K_∞ function γ and a KL function β exist for each $w \in \mathcal{L}_\infty(\mathbb{R}_{\geq 0})$ and $x(t_0) \in \mathbb{R}^{2n_p}$, such that

$$\|x(t)\| \leq \beta(\|x(t_0)\|, t) + \gamma(\|w_t\|_\infty), \tag{3.20}$$

where

$$x(t) \coloneqq \begin{bmatrix} x_p^\top(t) & \tilde{x}^\top(t) \end{bmatrix}^\top, \tag{3.21}$$

$\forall t \in \mathbb{R}_{\geq t_0}$, then the system (3.20) is said to be ISS. Throughout this article, t_0 is considered to be zero.

Definition 3.4. [143] The sampling interval $\{t_k\}_{k \in \mathbb{N}_0}$, fulfills (2.16), $\forall k \in \mathbb{N}_0$. $\underline{\Delta}$ is the lower bound of the sampling rate. From this point on, the possibility is that the network can transmit data at the sampling rate affected by $\underline{\Delta}$.

3.5.3 ISS under MCDoS

In this subsection, a switched observer-based ETM update strategy is presented that guarantees ISS in the absence of FSDoS. The conclusions form the basis for the developments in the following section. The feedback process is now influenced by the ETM-based control update technique, as the terms $\xi_\sigma(t)$ and $\xi_e(t)$ enter the dynamics as disturbances. Therefore, it follows intuitively that stability is not compromised when control update mechanisms are adopted that keep $\xi_\sigma(t)$ and $\xi_e(t)$ sufficiently small in a realistic sense. The ensuing result demonstrates that if ψ_1 and ψ_2 are carefully chosen, any control update approach (3.17) that confines $\xi_\sigma(t)$ and $\xi_e(t)$ within a small neighbourhood will satisfy the stability criterion. Standard Lyapunov arguments are employed to illustrate the proposed control architecture. Next, using the resultant system with controller and observer in

(3.15), V_σ from (3.18) is computed to obtain

$$\frac{d}{dt}V_\sigma(x_p(t),\tilde{x}(t),\xi_\sigma(t),\xi_e(t)) = x_p^\top(t)\mathrm{He}(P_{p_\sigma}(A-BK))x_p(t) + 2x_p^\top(t)P_{p_\sigma}BK\tilde{x}(t)$$
$$+ \tilde{x}^\top(t)\mathrm{He}(P_{e_\sigma}(A-L_\sigma C_\sigma))\tilde{x}(t) - 2x_p^\top(t)P_{p_\sigma}BK\xi_e(t) - 2\tilde{x}^\top(t)P_{e_\sigma}L_\sigma\xi_\sigma(t)$$
$$+ 2x_s^\top(t)P_{p_\sigma}w(t) + 2\tilde{x}^\top(t)P_{e_\sigma}w(t). \tag{3.22}$$

Applying Young's inequality yields

$$\frac{d}{dt}V_\sigma(x_p(t),\tilde{x}(t),\xi_\sigma(t),\xi_e(t)) \le x_p^\top(t)\left[\mathrm{He}(P_{p_\sigma}(A-BK)) + P_{p_\sigma}BKK^\top B^\top P_{p_\sigma}\right]x_p(t)$$
$$+ 2x_p^\top(t)P_{p_\sigma}BK\tilde{x}(t) + \tilde{x}^\top(t)\left[\mathrm{He}(P_{e_\sigma}(A-L_\sigma C_\sigma)) + P_{e_\sigma}L_\sigma L_\sigma^\top P_{e_\sigma}\right]\tilde{x}(t) + \xi_\sigma^\top(t)\xi_\sigma(t)$$
$$+ \xi_e^\top(t)\xi_e(t) + \frac{1}{\varepsilon_{1_\sigma}}x_p^\top(t)P_{p_\sigma}^2x_p(t) + \frac{1}{\varepsilon_{2_\sigma}}\tilde{x}^\top(t)P_{e_\sigma}^2\tilde{x}(t) + (\varepsilon_{1_\sigma}+\varepsilon_{2_\sigma})w^\top(t)w(t), \tag{3.23}$$

where ε_{1_σ} and $\varepsilon_{2_\sigma} > 0$. From (3.17),

$$\xi_\sigma^\top(t)\xi_\sigma(t) + \xi_e^\top(t)\xi_e(t) \le x_p^\top(t)(\psi_1 C_\sigma^\top C_\sigma + \psi_2 I)x_p(t) - 2\psi_2 x_p^\top(t)\tilde{x}(t) + \psi_2\tilde{x}^\top(t)\tilde{x}(t)$$
$$+ \psi_1\|w_t\|_\infty^2. \tag{3.24}$$

can be written. Using (3.24) in (3.23) leads to

$$\frac{d}{dt}V_\sigma(x(t)) \le -x^\top(t)\Gamma_{1_\sigma}x(t) + (\varepsilon_{1_\sigma}+\varepsilon_{2_\sigma}+\psi_1)d^2(t), \tag{3.25}$$

where

$$\Gamma_{1_\sigma} := \begin{bmatrix}\Theta_{11_\sigma} & \Theta_{12_\sigma}\\ * & \Theta_{22_\sigma}\end{bmatrix}, \tag{3.26}$$

$$d(t) := \sup\{\|w(t)\|, \|w_t\|_\infty\}, \tag{3.27}$$

$\Theta_{11_\sigma} := -\mathrm{He}(P_{p_\sigma}(A-BK)) - P_{p_\sigma}BKK^\top B^\top P_{p_\sigma} - \psi_1 C_\sigma^\top C_\sigma - \psi_2 I - \frac{1}{\varepsilon_{1_\sigma}}P_{p_\sigma}^2$, $\Theta_{12_\sigma} := -P_{p_\sigma}BK + \psi_2 I$, and $\Theta_{22_\sigma} := -\mathrm{He}(P_{e_\sigma}(A-L_\sigma C_\sigma)) - P_{e_\sigma}L_\sigma L_\sigma^\top P_{e_\sigma} - \psi_2 I - \frac{1}{\varepsilon_{2_\sigma}}P_{e_\sigma}^2$. Now the following results hold.

Theorem 3.5. *Consider the control system* (3.15) *with process dynamics given by* (2.1),

(3.1), *and the control law* (3.11), *where the gain matrix* K *is such that* $A - BK$ *is Hurwitz. Let restricted sampling rate with* ψ_1 *and* ψ_2, *which satisfies ETM* (3.17), *and let the switched observer* (3.7) *use observer gains* L_σ. *Suppose there exist positive definite matrices* $P_{p_\sigma}, P_{e_\sigma} > 0$, *positive scalars* $\psi_1, \psi_2, \varepsilon_{1_\sigma}, \varepsilon_{2_\sigma} \in \mathbb{R}_{>0}$, *and matrix* $H_\sigma \in \mathbb{R}^{n_p \times n_{h_\sigma}}$, *such that the following LMIs*

$$\Gamma_{2_\sigma} \coloneqq \begin{bmatrix} \Theta_{1_\sigma} & P_{p_\sigma} & P_{p_\sigma}BK & \Theta_{12_\sigma} & 0 & 0 \\ * & \varepsilon_{1_\sigma} I & 0 & 0 & 0 & 0 \\ * & * & I & 0 & 0 & 0 \\ * & * & * & \Theta_{2_\sigma} & P_{e_\sigma} & H_\sigma \\ * & * & * & * & \varepsilon_{2_\sigma} I & 0 \\ * & * & * & * & * & I \end{bmatrix} > 0, \tag{3.28}$$

hold $\forall \sigma \in 1, \cdots, n_s$, *where the terms are defined as*

$$\Theta_{1_\sigma} \coloneqq -He(P_{p_\sigma}(A - BK)) - \psi_1 C_\sigma^\top C_\sigma - \psi_2 I, \tag{3.29}$$

$$\Theta_{2_\sigma} \coloneqq -He(P_{e_\sigma} A) + He(H_\sigma C_\sigma) - \psi_2 I, \tag{3.30}$$

$$H_\sigma \coloneqq P_{e_\sigma} L_\sigma, \tag{3.31}$$

and the MCDoS satisfies Assumption 3.1, with arbitrary parameters $\varkappa$ *and* τ_D *such that the frequency and duration conditions*

$$\tau_D > \max\left\{\underline{\Delta}, \max_{\forall \sigma \in \{1,\cdots,n_s\}} \frac{\max\{\lambda_M(P_{p_\sigma}), \lambda_M(P_{e_\sigma})\}}{\lambda_m(\Gamma_{2_\sigma})} \ln\left\{\frac{\max\{\lambda_M(P_{p_\sigma}), \lambda_M(P_{e_\sigma})\}}{\min\{\lambda_m(P_{p_\sigma}), \lambda_m(P_{e_\sigma})\}}\right\}\right\} \tag{3.32}$$

and

$$\varkappa \leq 1 - \frac{\underline{\Delta}}{\tau_D}, \tag{3.33}$$

hold. Then, the closed-loop system (3.15) *is ISS.*

Proof. The idea here is to partition the time axis into intervals according to the observer-switching technique, as explained in Section 3.4. The characterization of these intervals is indispensable to the Lyapunov-based analysis. The interval $[\tau, t]$ is the disjoint union of $\mathcal{O}_\sigma(\tau,t)_{,\sigma\in\{1,\cdots,n_s\}}$ for any $\tau, t \in \mathbb{R}_{\geq 0}$, with $\tau \leq t$. The union of sub-intervals of $[\tau, t]$ occurs when the system is operated in the σth switching mode. In particular, there are two non-negative and positive real number sequences $\{m_{\sigma_f}\}_{\sigma\in\{1,\cdots,n_s\},f\in\mathbb{N}} \in \bar{\mathbb{S}}_\sigma$, $\{v_{\sigma_f}\}_{\sigma\in\{1,\cdots,n_s\},f\in\mathbb{N}}$ such that

$$\mathcal{O}_\sigma(\tau,t) \coloneqq \bigcup_{f\in\mathbb{N}} \mathcal{M}_{\sigma_f} \bigcap [\tau,t], \tag{3.34}$$

where

$$\mathcal{M}_{\sigma_f} \coloneqq \{m_{\sigma_f}\} \cup [m_{\sigma_f}, m_{\sigma_f} + v_{\sigma_f}), \tag{3.35}$$

$m_{0_0} \coloneqq 0$, and $m_{\sigma_f} + v_{\sigma_f} \in \bar{\mathbb{S}}_\sigma$. The times at which switching occurs are defined by

$$\iota_g \coloneqq \begin{cases} \text{Undefined}, & \text{if } \bar{\mathbb{S}}_\sigma \setminus [0, \iota_{g-1}] = \emptyset, \\ \inf\left\{\bar{\mathbb{S}}_\sigma \setminus [0,\iota_{g-1}]\right\}, & \text{otherwise}, \end{cases} \tag{3.36}$$

$\forall g \in \mathbb{N}$, where $\iota_0 \coloneqq 0$. From Definition 3.4 (which is discussed later in Subsection 3.5.2), we can write,

$$\iota_{g+1} - \iota_g \geq \Delta_k \geq \underline{\Delta}. \tag{3.37}$$

Employing the Schur complement and substitution approach [158] in (3.26) yields (3.28), making (3.26) and (3.28) equivalent. Hence, $\Gamma_{1_\sigma} > 0$, and the smallest eigenvalues of Γ_{1_σ} and Γ_{2_σ} are greater than zero. Thus, equation (3.25) can now be rewritten as

$$\frac{d}{dt}V_\sigma(x(t)) \leq -\zeta_{1_\sigma}\|x(t)\|^2 + (\varepsilon_{1_\sigma} + \varepsilon_{2_\sigma} + \psi_1)d^2(t), \tag{3.38}$$

where $x(t)$ and $d(t)$ are mentioned in (3.21) and (3.27), respectively, and

$$\zeta_{1_\sigma} \coloneqq \lambda_m(\Gamma_{2_\sigma}), \tag{3.39}$$

which is also the smallest eigenvalue of Γ_{1_σ} as $\Gamma_{2_\sigma}(>0)$ is the LMIs of $\Gamma_{1_\sigma}(>0)$. Furthermore, Lyapunov function in (3.18) can be recast as

$$\underline{\alpha}_{p_\sigma}\left\|x_p(t)\right\|^2+\underline{\alpha}_{e_\sigma}\left\|\tilde{x}(t)\right\|^2\leq V_\sigma(x_p(t),\tilde{x}(t))\leq\overline{\alpha}_{p_\sigma}\left\|x_p(t)\right\|^2+\overline{\alpha}_{e_\sigma}\left\|\tilde{x}(t)\right\|^2, \tag{3.40}$$

where

$$\underline{\alpha}_{p_\sigma}\coloneqq\lambda_m(P_{p_\sigma}),\ \ \overline{\alpha}_{p_\sigma}\coloneqq\lambda_M(P_{p_\sigma}), \tag{3.41}$$

$$\underline{\alpha}_{e_\sigma}\coloneqq\lambda_m(P_{e_\sigma}),\ \ \overline{\alpha}_{e_\sigma}\coloneqq\lambda_M(P_{e_\sigma}). \tag{3.42}$$

Equation (3.38) implies

$$\frac{d}{dt}V_\sigma(x(t))\leq-\omega_{1_\sigma}V_\sigma(x(t))+(\varepsilon_{1_\sigma}+\varepsilon_{2_\sigma}+\psi_1)d^2(t), \tag{3.43}$$

where

$$\omega_{1_\sigma}\coloneqq\frac{\zeta_{1_\sigma}}{\max\{\overline{\alpha}_{p_\sigma},\overline{\alpha}_{e_\sigma}\}}. \tag{3.44}$$

Note that $\forall t\in\mathbb{R}_{>0},\|d_t\|_\infty=\|w_t\|_\infty$. Let

$$g(t)\coloneqq\begin{cases}0, & \text{if } \overline{\mathbb{S}}_\sigma\cap[0,t]=\emptyset,\\ \sup\left\{g\in\mathbb{N}:\iota_g\in\overline{\mathbb{S}}_\sigma\cap[0,t]\right\}, & \text{otherwise.}\end{cases} \tag{3.45}$$

Hence, from the comparison lemma,

$$V_\sigma(x(t))\leq e^{-\omega_{1_\sigma}\left(t-\iota_{g(t)}\right)}V_\sigma(x(\iota^+_{g(t)}))+\nu_{1_\sigma}\|w_t\|^2_\infty, \tag{3.46}$$

is obtained in the interval $[\iota_{g(t)},t]$, where

$$\nu_{1_\sigma}\coloneqq\frac{\varepsilon_{1_\sigma}+\varepsilon_{2_\sigma}+\psi_1}{\omega_{1_\sigma}}. \tag{3.47}$$

From (3.46), it follows that

$$\|x(t)\|^2 \leq \frac{\overline{\alpha}_{\sigma(\iota^+_{g(t)})}}{\underline{\alpha}_\sigma} e^{-\omega_{1_\sigma}(t-\iota_{g(t)})} \|x(\iota^+_{g(t)})\|^2 + \frac{\nu_{1_\sigma}}{\underline{\alpha}_\sigma} \|w_t\|^2_\infty, \tag{3.48}$$

where

$$\underline{\alpha}_\sigma := \min\{\underline{\alpha}_{p_\sigma}, \underline{\alpha}_{e_\sigma}\}, \tag{3.49}$$

and

$$\overline{\alpha}_\sigma := \max\{\overline{\alpha}_{p_\sigma}, \overline{\alpha}_{e_\sigma}\}. \tag{3.50}$$

Similarly, for the time interval $[\iota_{g(t)-1}, \iota_{g(t)}]$,

$$\left\|x(\iota^-_{g(t)})\right\|^2 \leq \frac{\overline{\alpha}_{\sigma(\iota^+_{g(t)-1})}}{\underline{\alpha}_{\sigma(\iota^+_{g(t)-1})}} e^{-\omega_{1_{\sigma(\iota^+_{g(t)-1})}}(\iota_{g(t)}-\iota_{g(t)-1})} \left\|x(\iota^+_{g(t)-1})\right\|^2 + \frac{\nu_{1_{\sigma(\iota^+_{g(t)-1})}}}{\underline{\alpha}_{\sigma(\iota^+_{g(t)-1})}} \|w_t\|^2_\infty \tag{3.51}$$

satisfies. Considering $\|x(\iota^- g(t))\| \simeq \|x(\iota^+ g(t))\| \simeq \left\|x(\iota_{g(t)})\right\|$ and substituting the value of $\left\|x(\iota_{g(t)})\right\|$ into (3.48), the inequality

$$\begin{aligned}\|x(t)\|^2 \leq{}& \frac{\overline{\alpha}_{\sigma(\iota^+_{g(t)})}\overline{\alpha}_{\sigma(\iota^+_{g(t)-1})}}{\underline{\alpha}_{\sigma(\iota^+_{g(t)})}\underline{\alpha}_{\sigma(\iota^+_{g(t)-1})}} e^{-\left\{\omega_{1_{\sigma(\iota^+_{g(t)})}}(t-\iota_{g(t)})+\omega_{1_{\sigma(\iota^+_{g(t)-1})}}(\iota_{g(t)}-\iota_{g(t)-1})\right\}} \left\|x(\iota_{g(t)-1})\right\|^2 \\ &+ \left[\frac{\nu_{1_{\sigma(\iota^+_{g(t)})}}}{\underline{\alpha}_{\sigma(\iota^+_{g(t)})}} + \frac{\nu_{1_{\sigma(\iota^+_{g(t)-1})}}\overline{\alpha}_{\sigma(\iota^+_{g(t)})}}{\underline{\alpha}_{\sigma(\iota^+_{g(t)-1})}\underline{\alpha}_{\sigma(\iota^+_{g(t)})}} e^{-\omega_{1_{\sigma(\iota^+_{g(t)})}}(t-\iota_{g(t)})}\right] \|w_t\|^2_\infty\end{aligned} \tag{3.52}$$

is obtained for the interval $\left[\iota_{g(t)-1}, t\right]$. It is important to note that $\iota_{g(t)}$ denotes the most recent recognized time instant when the observer changes its switching mode. Consequently, $\sigma(\iota^+_{g(t)}) = \sigma(t^+_{k(t)}) = \sigma$. By following the iterative process, the subsequent lemma is obtained.

Lemma 3.6. *If* (3.43) *holds* $\forall\sigma \in 1,\cdots,n_s$ *and* $\omega_{1_\sigma},\varepsilon_{1_\sigma},\varepsilon_{2_\sigma},\psi_1,\psi_2 \in \mathbb{R}> 0$, *then* $\forall t \in \mathbb{R}_{\geq 0}$, *the upper bound of* $\|x(t)\|$

$$\|x(t)\|^2 \leq \frac{\overline{\alpha}_{\sigma(\iota^+_{g(t)})}\cdots\overline{\alpha}_{\sigma(\iota^+_0)}}{\underline{\alpha}_{\sigma(\iota^+_{g(t)})}\cdots\underline{\alpha}_{\sigma(\iota^+_0)}} e^{-\left(\sum_{i=1}^{n_s}\omega_{1_i}|\mathcal{O}_i(\iota_0,t)|\right)}\|x(\iota_0)\|^2 + \left[\frac{\nu_{1_{\sigma(\iota^+_{g(t)})}}}{\underline{\alpha}_{\sigma(\iota^+_{g(t)})}} + \sum_{\substack{l\in\mathbb{N};\\ 0\leq\iota_{g(t)-l}\leq t}} \left\{\frac{\nu_{1_{\sigma(\iota^+_{g(t)-l})}}}{\underline{\alpha}_{\sigma(\iota^+_{g(t)})}} \prod_{\substack{j\in\mathbb{N}_0;\\ \iota_{g(t)-l}<\iota_{g(t)-j}\leq t}} \left(\frac{\overline{\alpha}_{\sigma(\iota^+_{g(t)-j})}}{\underline{\alpha}_{\sigma(\iota^+_{g(t)-(j+1)})}}\right) e^{-\left(\sum_{i=1}^{n_s}\omega_{1_i}|\mathcal{O}_i(\iota_{g(t)-(l-1)},t)|\right)}\right\}\right]\|w_t\|^2_\infty, \tag{3.53}$$

is satisfied, where $\underline{\alpha}_\sigma$ *and* $\overline{\alpha}_\sigma$ *are mentioned in* (3.49) *and* (3.50), *respectively and* $\iota_0 = 0$.

Proof of Lemma 3.6: An induction argument is employed. First, the inequality is shown to hold when $\overline{\mathbb{S}}_\sigma = \emptyset$. This corresponds to the case where the system operates in a single observer mode, since $g(t) = 0$. In this case, (3.53) directly reduces to (3.48). Next, assume that (3.53) holds for the interval $[\iota_{g(t)-p}, t]$ where $p \in \mathbb{N}$ and $p < g(t)$. By hypothesis, and since $\|x(t)\|$ is continuous, we have

$$\|x(t)\|^2 \leq \frac{\overline{\alpha}_{\sigma(\iota^+_{g(t)})}\cdots\overline{\alpha}_{\sigma(\iota^+_{g(t)-p})}}{\underline{\alpha}_{\sigma(\iota^+_{g(t)})}\cdots\underline{\alpha}_{\sigma(\iota^+_{g(t)-p})}} e^{-\left(\sum_{j=1}^{n_s}\omega_{1_j}|\mathcal{O}_j\left(\iota_{g(t)-p},t\right)|\right)}\|x(\iota_{g(t)-p})\|^2 + \left[\frac{\nu_{1_{\sigma(\iota^+_{g(t)})}}}{\underline{\alpha}_{\sigma(\iota^+_{g(t)})}}\right.$$
$$\left. + \sum_{\substack{l\in\mathbb{N};\\ \iota_{g(t)-p}\leq\iota_{g(t)-l}\leq t}} \left\{\frac{\nu_{1_{\sigma(\iota^+_{g(t)-l})}}}{\underline{\alpha}_{\sigma(\iota^+_{g(t)})}} \prod_{\substack{q\in\mathbb{N}_0;\\ \iota_{g(t)-l}<\iota_{g(t)-q}\leq t}} \left(\frac{\overline{\alpha}_{\sigma(\iota^+_{g(t)-q})}}{\underline{\alpha}_{\sigma(\iota^+_{g(t)-(q+1)})}}\right) e^{-\left(\sum_{j=1}^{n_s}\omega_{1_j}|\mathcal{O}_j(\iota_{g(t)-(l-1)},t)|\right)}\right\}\right]$$
$$\|w_t\|^2_\infty. \tag{3.54}$$

Similar to (3.54), in the switching interval $[\iota_{g(t)-(p+1)}, \iota_{g(t)-p}]$,

$$\|x(\iota_{g(t)-p})\|^2 \leq \frac{\overline{\alpha}_{\sigma(\iota^+_{g(t)-(p+1)})}}{\underline{\alpha}_{\sigma(\iota^+_{g(t)-(p+1)})}} e^{-\omega_{1_{\sigma(\iota^+_{g(t)-(p+1)})}}\left(\iota_{g(t)-p}-\iota_{g(t)-(p+1)}\right)}\|x(\iota_{g(t)-(p+1)})\|^2 + \frac{\nu_{1_{\sigma(\iota^+_{g(t)-(p+1)})}}}{\underline{\alpha}_{\sigma(\iota^+_{g(t)-(p+1)})}}$$
$$\|w_t\|^2_\infty. \tag{3.55}$$

Thus, using the inequality (3.55), in (3.54) for the time interval $[\iota_{g(t)-(p+1)}, t]$, the upper bound of $\|x(t)\|$

$$\|x(t)\|^2 \leq \frac{\overline{\alpha}_{\sigma(\iota^+_{g(t)})}\cdots\overline{\alpha}_{\sigma(\iota^+_{g(t)-p})}\overline{\alpha}_{\sigma(\iota^+_{g(t)-(p+1)})}}{\underline{\alpha}_{\sigma(\iota^+_{g(t)})}\cdots\underline{\alpha}_{\sigma(\iota^+_{g(t)-p})}\underline{\alpha}_{\sigma(\iota^+_{g(t)-(p+1)})}}$$
$$e^{-\left\{\sum_{j=1}^{n_s}\omega_{1_j}|\mathcal{O}_j(\iota_{g(t)-p},t)|+\omega_{1_{\sigma(\iota^+_{g(t)-(p+1)})}}(\iota_{g(t)-p}-\iota_{g(t)-(p+1)})\right\}}\|x(\iota_{g(t)-(p+1)})\|^2 + \left[\frac{\nu_{1_{\sigma(\iota^+_{g(t)})}}}{\underline{\alpha}_{\sigma(\iota^+_{g(t)})}}\right.$$
$$+\frac{\nu_{1_{\sigma(\iota^+_{g(t)-(p+1)})}}\overline{\alpha}_{\sigma(\iota^+_{g(t)})}\cdots\overline{\alpha}_{\sigma(\iota^+_{g(t)-p})}}{\underline{\alpha}_{\sigma(\iota^+_{g(t)})}\cdots\underline{\alpha}_{\sigma(\iota^+_{g(t)-(p+1)})}}e^{-\left(\sum_{j=1}^{n_s}\omega_{1_j}|\mathcal{O}_j(\iota_{g(t)-p},t)|\right)}+\sum_{\substack{l\in\mathbb{N};\\ \iota_{g(t)-p}\leq\iota_{g(t)-l}\leq t}}$$
$$\left.\left\{\frac{\nu_{1_{\sigma(\iota^+_{g(t)-l})}}}{\underline{\alpha}_{\sigma(\iota^+_{g(t)})}}\prod_{\substack{q\in\mathbb{N}_0;\\ \iota_{g(t)-l}<\iota_{g(t)-q}\leq t}}\left(\frac{\overline{\alpha}_{\sigma(\iota^+_{g(t)-q})}}{\underline{\alpha}_{\sigma(\iota^+_{g(t)-(q+1)})}}\right)e^{-\left(\sum_{j=1}^{n_s}\omega_{1_j}|\mathcal{O}_j(\iota_{g(t)-(l-1)},t)|\right)}\right\}\right]\|w_t\|^2_\infty$$
$$\leq\frac{\overline{\alpha}_{\sigma(\iota^+_{g(t)})}\cdots\overline{\alpha}_{\sigma(\iota^+_{g(t)-(p+1)})}}{\underline{\alpha}_{\sigma(\iota^+_{g(t)})}\cdots\underline{\alpha}_{\sigma(\iota^+_{g(t)-(p+1)})}}e^{-\left(\sum_{j=1}^{n_s}\omega_{1_j}|\mathcal{O}_j(\iota_{g(t)-(p+1)},t)|\right)}\|x(\iota_{g(t)-(p+1)})\|^2+\left[\frac{\nu_{1_{\sigma(\iota^+_{g(t)})}}}{\underline{\alpha}_{\sigma(\iota^+_{g(t)})}}+\right.$$
$$\left.\sum_{\substack{l\in\mathbb{N};\\ \iota_{g(t)-(p+1)}\leq\iota_{g(t)-l}\leq t}}\left\{\frac{\nu_{1_{\sigma(\iota^+_{g(t)-l})}}}{\underline{\alpha}_{\sigma(\iota^+_{g(t)})}}\prod_{\substack{q\in\mathbb{N}_0;\\ \iota_{g(t)-l}<\iota_{g(t)-q}\leq t}}\left(\frac{\overline{\alpha}_{\sigma(\iota^+_{g(t)-q})}}{\underline{\alpha}_{\sigma(\iota^+_{g(t)-(q+1)})}}\right)e^{-\left(\sum_{j=1}^{n_s}\omega_{1_j}|\mathcal{O}_j(\iota_{g(t)-(l-1)},t)|\right)}\right\}\right]$$
$$\|w_t\|^2_\infty \tag{3.56}$$

remains true. Thus, (3.56) holds true for the time interval $[\iota_{g(t)-(p+1)}, t]$, which concludes the proof of Lemma 3.6. ■

Lemma 3.7. *Under the Assumption 3.1 the sequence of (3.53)*

$$\prod_{\substack{p\in\mathbb{N}_0;\\ 0\leq\iota_{g(t)-p}\leq t}}\left(\frac{\overline{\alpha}_{\sigma(\iota^+_{g(t)-p})}}{\underline{\alpha}_{\sigma(\iota^+_{g(t)-p})}}\right)e^{-\left(\sum_{j=1}^{n_s}\omega_{1_j}|\mathcal{O}_j(\iota_{g(t)-p},t)|\right)} \tag{3.57}$$

is convergent in nature.

Proof of Lemma 3.7 : Let's take the exponential term of (3.57)

$$\prod_{\substack{p\in\mathbb{N}_0;\\ 0\le\iota_{g(t)-p}\le t}} e^{-\left(\sum_{j=1}^{n_s}\omega_{1_j}|O_j(\iota_{g(t)-p},t)|\right)}$$

$$= \prod_{\substack{p\in\mathbb{N}_0;\\ 0\le\iota_{g(t)-p}\le t}} e^{-\left\{\omega_{1_{\sigma(\iota^+_{g(t)})}}(t-\iota_{g(t)})+\omega_{1_{\sigma(\iota^+_{g(t)-1})}}(\iota_{g(t)}-\iota_{g(t)-1})+\cdots+\omega_{1_{\sigma(\iota^+_{g(t)-p})}}(\iota_{g(t)-(p+1)}-\iota_{g(t)-p})\right\}}. \quad (3.58)$$

Assumption 3.1 yields,

$$\iota_1-\iota_0\ge\tau_D l(\iota_0,\iota_1)-\tau_D\varkappa=\tau_D-\tau_D\varkappa, \quad (3.59)$$

where just one time switching is altered in $[\iota_0,\iota_1)$ interval, causing $l(\iota_0,\iota_1)=1$. From (3.33), it follows that (3.59) avoids Zeno behaviour when compared with (3.37). Similarly,

$$\iota_2-\iota_1\ge\tau_D,\cdots,\iota_{g(t)}-\iota_{g(t)-1}\ge\tau_D, \quad (3.60)$$

persists and so on by omitting the term $\varkappa$ because it is already taken in the first interval. Hence

$$\prod_{\substack{p\in\mathbb{N}_0;\\ 0\le\iota_{g(t)-p}\le t}} e^{-\left\{\omega_{1_{\sigma(\iota^+_{g(t)})}}(t-\iota_{g(t)})+\omega_{1_{\sigma(\iota^+_{g(t)-1})}}(\iota_{g(t)}-\iota_{g(t)-1})+\cdots+\omega_{1_{\sigma(\iota^+_{g(t)-p})}}(\iota_{g(t)-(p+1)}-\iota_{g(t)-p})\right\}}$$

$$\le e^{\omega_{1_{\sigma(\iota^+_0)}}\tau_D\varkappa}\prod_{\substack{p\in\mathbb{N}_0;\\ 0\le\iota_{g(t)-p}\le t}} e^{-\left\{\omega_{1_{\sigma(\iota^+_{g(t)})}}+\omega_{1_{\sigma(\iota^+_{g(t)-1})}}+\cdots+\omega_{1_{\sigma(\iota^+_{g(t)-p})}}\right\}\tau_D}. \quad (3.61)$$

By using (3.61) from (3.57),

$$\begin{aligned}
&\prod_{\substack{p\in\mathbb{N}_0;\\ 0\le\iota_{g(t)-p}\le t}} \frac{\overline{\alpha}_{\sigma(\iota^+_{g(t)-p})}}{\underline{\alpha}_{\sigma(\iota^+_{g(t)-p})}} e^{-\left\{\sum_{j=1}^{n_s}\omega_{1_j}|\mathcal{O}_j(\iota_{g(t)-p},t)|\right\}} \\
&\le e^{\omega_{1_{\sigma(\iota^+_0)}}\tau_D\varkappa} \prod_{\substack{p\in\mathbb{N}_0;\\ 0\le\iota_{g(t)-p}\le t}} \frac{\overline{\alpha}_{\sigma(\iota^+_{g(t)-p})}}{\underline{\alpha}_{\sigma(\iota^+_{g(t)-p})}} e^{-\left(\sum_{\substack{z\in\mathbb{N}_0;\\ \iota_{g(t)-p}\le\iota_{g(t)-z}\le t}} \omega_{1_{\sigma(\iota^+_{g(t)-z})}}\tau_D\right)} \\
&\le e^{\omega_1\tau_D\varkappa} \prod_{\substack{p\in\mathbb{N}_0;\\ 0\le\iota_{g(t)-p}\le t}} \frac{\overline{\alpha}_{\sigma(\iota^+_{g(t)-p})}}{\underline{\alpha}_{\sigma(\iota^+_{g(t)-p})}} e^{-\left(\sum_{\substack{z\in\mathbb{N}_0;\\ \iota_{g(t)-p}\le\iota_{g(t)-z}\le t}} \omega_{1_{\sigma(\iota^+_{g(t)-z})}}\tau_D\right)},
\end{aligned} \tag{3.62}$$

stands, where

$$\omega_1 := \max_{\forall\sigma\in\{1,\cdots,n_s\}}\{\omega_{1_\sigma}\}. \tag{3.63}$$

p^{th} term of (3.62) is

$$F_p = e^{\omega_1\tau_D\varkappa}\frac{\overline{\alpha}_{\sigma(\iota^+_{g(t)})}\cdots\overline{\alpha}_{\sigma(\iota^+_{g(t)-(p-1)})}}{\underline{\alpha}_{\sigma(\iota^+_{g(t)})}\cdots\underline{\alpha}_{\sigma(\iota^+_{g(t)-(p-1)})}} e^{-\left\{\omega_{1_{\sigma(\iota^+_{g(t)})}}+\omega_{1_{\sigma(\iota^+_{g(t)-1})}}+\cdots+\omega_{1_{\sigma(\iota^+_{g(t)-(p-1)})}}\right\}\tau_D}. \tag{3.64}$$

$(p+1)^{\text{th}}$ term of the series is

$$F_{p+1} = e^{\omega_1\tau_D\varkappa}\frac{\overline{\alpha}_{\sigma(\iota^+_{g(t)})}\cdots\overline{\alpha}_{\sigma(\iota^+_{g(t)-p})}}{\underline{\alpha}_{\sigma(\iota^+_{g(t)})}\cdots\underline{\alpha}_{\sigma(\iota^+_{g(t)-p})}} e^{-\left\{\omega_{1_{\sigma(\iota^+_{g(t)})}}+\omega_{1_{\sigma(\iota^+_{g(t)-1})}}+\cdots+\omega_{1_{\sigma(\iota^+_{g(t)-p})}}\right\}\tau_D}.$$

Hence,

$$\frac{F_{p+1}}{F_p} = \frac{\overline{\alpha}_{\sigma(\iota^+_{g(t)-p})}}{\underline{\alpha}_{\sigma(\iota^+_{g(t)-p})}} e^{-\omega_{1_{\sigma(\iota^+_{g(t)-p})}}\tau_D}. \tag{3.65}$$

From (3.32),

$$\lim_{p\to\infty}\left|\frac{\overline{\alpha}_{\sigma(\iota^+_{g(t)-p})}}{\underline{\alpha}_{\sigma(\iota^+_{g(t)-p})}} e^{-\omega_{1_{\sigma(\iota^+_{g(t)-p})}}\tau_D}\right| < 1 \tag{3.66}$$

is valid. Therefore, (3.57) is convergent in nature. Note that $p \leq g(t)$. Hence, $p \to \infty \Rightarrow g(t) \to \infty$. From (3.45), $g(t)$ is directly proportional to t, which implies that $t \to \infty$. □

Lemma 3.8. *Under the Assumption 3.1 the sum*

$$\sum_{\substack{l\in\mathbb{N};\\ 0\leq \iota_{g(t)-l}\leq t}} \left\{ \frac{\nu_{1_{\sigma(\iota^{+}_{g(t)-l})}}}{\underline{\alpha}_{\sigma(\iota^{+}_{g(t)})}} \prod_{\substack{q\in\mathbb{N}_0;\\ \iota_{g(t)-l}<\iota_{g(t)-q}\leq t}} \left(\frac{\overline{\alpha}_{\sigma(\iota^{+}_{g(t)-q})}}{\underline{\alpha}_{\sigma(\iota^{+}_{g(t)-(q+1)})}} \right) e^{-\left(\sum_{j=1}^{n_s} \omega_{1_j} |\mathcal{O}_j(\iota_{g(t)-(l-1)},t)|\right)} \right\} \tag{3.67}$$

is bounded from above.

Proof of Lemma 3.8 :Let's take the exponential term of (3.67)

$$\begin{aligned} &\sum_{\substack{l\in\mathbb{N};\\ 0\leq \iota_{g(t)-l}\leq t}} e^{-\left(\sum_{j=1}^{n_s} \omega_{1_j} |\mathcal{O}_i(\iota_{g(t)-(l-1)},t)|\right)} \\ &= \sum_{\substack{l\in\mathbb{N};\\ 0\leq \iota_{g(t)-l}\leq t}} e^{-\left\{ \omega_{1_{\sigma\left(\iota^{+}_{g(t)}\right)}} (t-\iota_{g(t)}) + \omega_{1_{\sigma\left(\iota^{+}_{g(t)-1}\right)}} \left(\iota_{g(t)}-\iota_{g(t)-1}\right) + \cdots + \omega_{1_{\sigma\left(\iota^{+}_{g(t)-(l-1)}\right)}} \left(\iota_{g(t)-(l-2)}-\iota_{g(t)-(l-1)}\right) \right\}}. \end{aligned} \tag{3.68}$$

Applying (3.59) and (3.60),

$$\begin{aligned} &\sum_{\substack{l\in\mathbb{N};\\ 0\leq \iota_{g(t)-l}\leq t}} e^{-\left\{ \omega_{1_{\sigma(\iota^{+}_{g(t)})}} (t-\iota_{g(t)}) + \omega_{1_{\sigma(\iota^{+}_{g(t)-1})}} (\iota_{g(t)}-\iota_{g(t)-1}) + \cdots + \omega_{1_{\sigma(\iota^{+}_{g(t)-(l-1)})}} (\iota_{g(t)-(l-2)}-\iota_{g(t)-(l-1)}) \right\}} \\ &\leq e^{\omega_{1_{\sigma(\iota^{+}_{1})}} \tau_D \varkappa} \sum_{\substack{l\in\mathbb{N};\\ 0\leq \iota_{g(t)-l}\leq t}} e^{-\left\{ \omega_{1_{\sigma(\iota^{+}_{g(t)})}} + \omega_{1_{\sigma(\iota^{+}_{g(t)-1})}} + \cdots + \omega_{1_{\sigma(\iota^{+}_{g(t)-(l-1)})}} \right\} \tau_D} \\ &\leq e^{\omega_1 \tau_D \varkappa} \sum_{\substack{l\in\mathbb{N};\\ 0\leq \iota_{g(t)-l}\leq t}} e^{-\left\{ \omega_{1_{\sigma(\iota^{+}_{g(t)})}} + \omega_{1_{\sigma(\iota^{+}_{g(t)-1})}} + \cdots + \omega_{1_{\sigma(\iota^{+}_{g(t)-(l-1)})}} \right\} \tau_D}. \end{aligned} \tag{3.69}$$

hold. This implies

$$\begin{aligned}
&\sum_{\substack{l\in\mathbb{N};\\ 0\le\iota_{g(t)-l}\le t}}\left\{\frac{\nu_{1_{\sigma(\iota^+_{g(t)-l})}}}{\underline{\alpha}_{\sigma(\iota^+_{g(t)})}}\prod_{\substack{q\in\mathbb{N}_0;\\ \iota_{g(t)-l}<\iota_{g(t)-q}\le t}}\left(\frac{\overline{\alpha}_{\sigma(\iota^+_{g(t)-q})}}{\underline{\alpha}_{\sigma(\iota^+_{g(t)-(q+1)})}}\right)e^{-\left(\sum_{j=1}^{n_s}\omega_{1_j}|\mathcal{O}_j(\iota_{g(t)-(l-1)},t)|\right)}\right\}\\
&\le e^{\omega_1\tau_D\varkappa}\sum_{\substack{l\in\mathbb{N};\\ 0\le\iota_{g(t)-l}\le t}}\left\{\frac{\nu_{1_{\sigma(\iota^+_{g(t)-l})}}}{\underline{\alpha}_{\sigma(\iota^+_{g(t)})}}\prod_{\substack{q\in\mathbb{N}_0;\\ \iota_{g(t)-l}<\iota_{g(t)-q}\le t}}\left(\frac{\overline{\alpha}_{\sigma(\iota^+_{g(t)-q})}}{\underline{\alpha}_{\sigma(\iota^+_{g(t)-(q+1)})}}\right)\right.\\
&\left.e^{-\left(\sum_{\substack{q\in\mathbb{N}_0;\\ \iota_{g(t)-l}<\iota_{g(t)-q}\le t}}{\omega_1}_{\sigma(\iota^+_{g(t)-q})}\tau_D\right)}\right\}\\
&= e^{\omega_1\tau_D\varkappa}\sum_{\substack{l\in\mathbb{N};\\ 0\le\iota_{g(t)-l}\le t}}\left\{\frac{\left(\varepsilon_{1_{\sigma(\iota^+_{g(t)-l})}}+\varepsilon_{2_{\sigma(\iota^+_{g(t)-l})}}+\psi_1\right)\overline{\alpha}_{\sigma(\iota^+_{g(t)-l})}}{\zeta_{1_{\sigma(\iota^+_{g(t)-l})}}\underline{\alpha}_{\sigma(\iota^+_{g(t)})}}\right.\\
&\left.\prod_{\substack{q\in\mathbb{N}_0;\\ \iota_{g(t)-l}<\iota_{g(t)-q}\le t}}\left(\frac{\overline{\alpha}_{\sigma(\iota^+_{g(t)-q})}}{\underline{\alpha}_{\sigma(\iota^+_{g(t)-(q+1)})}}\right)e^{-\left(\sum_{\substack{q\in\mathbb{N}_0;\\ \iota_{g(t)-l}<\iota_{g(t)-q}\le t}}{\omega_1}_{\sigma(\iota^+_{g(t)-q})}\tau_D\right)}\right\}\\
&\le \frac{\varepsilon_1+\varepsilon_2+\psi_1}{\zeta_1}e^{\omega_1\tau_D\varkappa}\sum_{\substack{l\in\mathbb{N};\\ 0\le\iota_{g(t)-l}\le t}}\left\{\frac{\overline{\alpha}_{\sigma(\iota^+_{g(t)-l})}}{\underline{\alpha}_{\sigma(\iota^+_{g(t)})}}\prod_{\substack{q\in\mathbb{N}_0;\\ \iota_{g(t)-l}<\iota_{g(t)-q}\le t}}\left(\frac{\overline{\alpha}_{\sigma(\iota^+_{g(t)-q})}}{\underline{\alpha}_{\sigma(\iota^+_{g(t)-(q+1)})}}\right)\right.\\
&\left.e^{-\left(\sum_{\substack{q\in\mathbb{N}_0;\\ \iota_{g(t)-l}<\iota_{g(t)-q}\le t}}{\omega_1}_{\sigma(\iota^+_{g(t)-q})}\tau_D\right)}\right\},
\end{aligned}\tag{3.70}$$

where $\varepsilon_1 \coloneqq \max_{\forall\sigma\in\{1,2,\cdots,n_s\}}\varepsilon_{1_\sigma}$, $\varepsilon_2 \coloneqq \max_{\forall\sigma\in\{1,2,\cdots,n_s\}}\varepsilon_{2_\sigma}$, and $\zeta_1 \coloneqq \min_{\forall\sigma\in\{1,2,\cdots,n_s\}}\zeta_{1_\sigma}$. A ratio test is employed to prove that the sum term in (3.70) is convergent. pth term of the series is

$$Z_p \coloneqq \frac{\overline{\alpha}_{\sigma(\iota^+_{g(t)})}\cdots\overline{\alpha}_{\sigma(\iota^+_{g(t)-p})}}{\underline{\alpha}_{\sigma(\iota^+_{g(t)})}\cdots\underline{\alpha}_{\sigma(\iota^+_{g(t)-p})}}e^{-\left\{{\omega_1}_{\sigma(\iota^+_{g(t)})}+{\omega_1}_{\sigma(\iota^+_{g(t)-1})}+\cdots+{\omega_1}_{\sigma(\iota^+_{g(t)-(p-1)})}\right\}\tau_D}.\tag{3.71}$$

Recall that to compute Z_{p+1} is substituted in place of all occurrences of p in Z_p, then

$$Z_{p+1} = \frac{\overline{\alpha}_{\sigma(\iota^+_{g(t)})} \cdots \overline{\alpha}_{\sigma(\iota^+_{g(t)-(p+1)})}}{\underline{\alpha}_{\sigma(\iota^+_{g(t)})} \cdots \underline{\alpha}_{\sigma(\iota^+_{g(t)-(p+1)})}} e^{-\left\{ \omega_{1_{\sigma(\iota^+_{g(t)})}} + \omega_{1_{\sigma(\iota^+_{g(t)-1})}} + \cdots + \omega_{1_{\sigma(\iota^+_{g(t)-p})}} \right\} \tau_D} \tag{3.72}$$

satisfies. Now,

$$\frac{Z_{p+1}}{Z_p} = \frac{\overline{\alpha}_{\sigma(\iota^+_{g(t)-(p+1)})}}{\underline{\alpha}_{\sigma(\iota^+_{g(t)-(p+1)})}} e^{-\omega_{1_{\sigma(\iota^+_{g(t)-p})}} \tau_D} \tag{3.73}$$

holds. From (3.32),

$$\lim_{p\to\infty} \left| \frac{\overline{\alpha}_{\sigma(\iota^+_{g(t)-(p+1)})}}{\underline{\alpha}_{\sigma(\iota^+_{g(t)-(p+1)})}} e^{-\omega_{1_{\sigma(\iota^+_{g(t)-p})}} \tau_D} \right| < 1 \tag{3.74}$$

persists, which proves that the sum term of (3.70) is convergent. And every convergent series has an upper bound. Hence, the sum (3.67) is bounded from above. Let's denote the bound G_1. ■

Since $c^2 + d^2 \leq (c+d)^2$ for any pair of positive reals c and d, it follows that

$$\|x(t)\| \leq \sqrt{\frac{\overline{\alpha}_{\sigma(\iota_0^+)} \cdots \overline{\alpha}_{\sigma(\iota^+_{g(t)})}}{\underline{\alpha}_{\sigma(\iota_0^+)} \cdots \underline{\alpha}_{\sigma(\iota^+_{g(t)})}}} e^{-\frac{1}{2}\left(\sum_{j=1}^{n_s} \omega_{1_j} |\mathcal{O}_j(\iota_0,t)|\right)} \|x(\iota_0)\| + \sqrt{\frac{(\varepsilon_1+\varepsilon_2+\psi_1)\overline{\alpha}}{\zeta_1 \underline{\alpha}} + G_1}$$

$$\|w_t\|_\infty, \tag{3.75}$$

where $\overline{\alpha} \coloneqq \max_{\forall\sigma\in\{1,\cdots,n_s\}}\{\overline{\alpha}_\sigma\}$ and $\underline{\alpha} \coloneqq \min_{\forall\sigma\in\{1,\cdots,n_s\}}\{\underline{\alpha}_\sigma\}$. Therefore, comparing (3.53) with (3.20), (3.15) is ISS. ■

Remark 3.9. The sources of the parameters ε_{1_σ} and ε_{2_σ} are explicitly stated in the proof of Theorem 3.5. These parameters are associated with disturbance, and their values can be determined by solving the LMIs in (3.28). The primary result of Theorem 3.5 is the lower bound of τ_D. A lower τ_D allows the system to tolerate a higher MCDoS changing frequency. Therefore, the next section focuses on minimizing τ_D.

3.5.4 Minimum inter-execution time

Avoiding Zeno behaviour is an important phenomenon in the ETM mechanism. To avoid it, we have to set up a minimum inter-execution time first.

Lemma 3.10. *Let $\psi_1, \psi_2 \in \mathbb{R}_{\geq 0}$. Then for any initial condition $x(0) \in \mathbb{R}^{2n_p}$, and $\forall t \in \Upsilon(0,t)$, the sequence $(t_k)_{k\in\mathbb{N}_0}$ defined by ETM (3.17) satisfies (2.16) with*

$$\underline{\Delta} = \min_{\forall \sigma \in \{1,\cdots,n_s\}} \underline{\Delta}_\sigma, \tag{3.76}$$

where $\underline{\Delta}_\sigma \in \mathbb{R}_{>0}$ is given by

$$\underline{\Delta}_\sigma = \int_0^1 \frac{1}{\mathcal{I}_\sigma(s)}\, ds, \tag{3.77}$$

where

$$\mathcal{I}_\sigma(s) \coloneqq \frac{1}{\sqrt{\psi}} \left(\|\mathcal{G}_\sigma\| + \|C_\sigma\|\right) + \left(\|\mathcal{G}_\sigma\| + \|\mathcal{H}_\sigma\| + \|C_\sigma\|\right) s + \sqrt{\psi}\|\mathcal{H}_\sigma\| s^2, \tag{3.78}$$

$$\psi \coloneqq \min\{\psi_1, \psi_2\}, \tag{3.79}$$

$$\mathcal{G}_\sigma \coloneqq \begin{bmatrix} C_\sigma A C_\sigma^\dagger & -C_\sigma BK \\ L_\sigma & A - BK - L_\sigma C_\sigma \end{bmatrix}, \tag{3.80}$$

$$\mathcal{H}_\sigma \coloneqq \begin{bmatrix} 0 & -C_\sigma BK \\ L_\sigma & -BK \end{bmatrix}, \tag{3.81}$$

and $C_\sigma^\dagger$ is the right pseudo-inverse of C_σ.

Proof. From (3.15), it follows

$$\begin{aligned} \dot{x}_p(t) &= Ax_p(t) - BKx_e(t) - BK\xi_e(t) + w(t) \\ \dot{x}_e(t) &= (A - BK - L_\sigma C_\sigma)x_e(t) + L_\sigma C_\sigma x_p(t) + L_\sigma \xi_\sigma(t) - BK\xi_e(t). \end{aligned} \tag{3.82}$$

Hence,

$$\dot{x}_\sigma(t) = \mathcal{G}_\sigma x_\sigma(t) + \mathcal{H}_\sigma e_\sigma(t) + \begin{bmatrix} C_\sigma^\top & 0 \end{bmatrix}^\top w(t), \tag{3.83}$$

where

$$x_\sigma(t) \coloneqq \begin{bmatrix} y_\sigma^\top(t) & x_e^\top(t) \end{bmatrix}^\top \tag{3.84}$$

and

$$e_\sigma(t) \coloneqq \begin{bmatrix} \xi_\sigma^\top(t) & \xi_e^\top(t) \end{bmatrix}^\top, \tag{3.85}$$

as it follows from (3.82). From (3.83), it is stated that

$$\|\dot{x}_\sigma(t)\| \leq \|\mathcal{G}_\sigma\|\|x_\sigma(t)\| + \|\mathcal{H}_\sigma\|\|e_\sigma(t)\| + \|C_\sigma\|\|w_t\|_\infty. \tag{3.86}$$

If

$$\|e_\sigma(t)\| \leq \sqrt{\psi}\sqrt{\|x_\sigma(t)\|^2 + \|w_t\|_\infty^2}, \tag{3.87}$$

then (3.17) is true where ψ is mentioned in (3.79). Thus, it obeys a lower bound on the inter-execution time given by the time it takes for the function

$$\phi_{1_\sigma}(t) \coloneqq \frac{\|e_\sigma(t)\|}{\sqrt{\|x_\sigma(t)\|^2 + \|w_t\|_\infty^2}} \tag{3.88}$$

to go from 0 to $\sqrt{\psi}$. Hence

$$\dot{\phi}_{1_\sigma}(t) = \frac{e_\sigma^\top(t)\dot{e}_\sigma(t)}{\|e_\sigma(t)\|\sqrt{\|x_\sigma(t)\|^2 + \|w_t\|_\infty^2}} - \frac{\|e_\sigma(t)\|x_\sigma^\top(t)\dot{x}_\sigma(t)}{(\|x_\sigma(t)\|^2 + \|w_t\|_\infty^2)^{\frac{3}{2}}} \tag{3.89}$$

persists. By observing that

$$\dot{e}_\sigma(t) = -\dot{x}_\sigma(t) \tag{3.90}$$

and the bound of $\|\dot{x}_\sigma(t)\|$ in (3.86), it follows that

$$\begin{aligned}
\dot{\phi}_{1_\sigma}(t) &\leq \frac{1}{\sqrt{\|x_\sigma(t)\|^2+\|w_t\|_\infty^2}}\left(\|\mathcal{G}_\sigma\|\|x_\sigma(t)\|+\|\mathcal{H}_\sigma\|\|e_\sigma(t)\|+\|C_\sigma\|\|w_t\|_\infty\right)\\
&+\frac{\|e_\sigma(t)\|}{(\|x_\sigma(t)\|^2+\|w_t\|_\infty^2)^{\frac{3}{2}}}\left(\|\mathcal{G}_\sigma\|\|x_\sigma(t)\|^2+\|\mathcal{H}_\sigma\|\|x_\sigma(t)\|\|e_\sigma(t)\|+\|C_\sigma\|\|x_\sigma(t)\|\|w_t\|_\infty\right)\\
&\leq \|\mathcal{G}_\sigma\|\frac{\|x_\sigma(t)\|}{\sqrt{\|x_\sigma(t)\|^2+\|w_t\|_\infty^2}}+\|\mathcal{H}_\sigma\|\phi_{1_\sigma}(t)+\|C_\sigma\|\frac{\|w_t\|_\infty}{\sqrt{\|x_\sigma(t)\|^2+\|w_t\|_\infty^2}}\\
&+\|\mathcal{G}_\sigma\|\frac{\|x_\sigma(t)\|^2}{\|x_\sigma(t)\|^2+\|w_t\|_\infty^2}\phi_{1_\sigma}(t)+\|\mathcal{H}_\sigma\|\frac{\|x_\sigma(t)\|}{\sqrt{\|x_\sigma(t)\|^2+\|w_t\|_\infty^2}}\phi_{1_\sigma}^2(t)\\
&+\|C_\sigma\|\frac{\|x_\sigma(t)\|}{\sqrt{\|x_\sigma(t)\|^2+\|w_t\|_\infty^2}}\frac{\|w_t\|_\infty}{\sqrt{\|x_\sigma(t)\|^2+\|w_t\|_\infty^2}}\phi_{1_\sigma}(t).
\end{aligned} \tag{3.91}$$

Note that $\left\{\|x_\sigma(t)\|/\sqrt{\|x_\sigma(t)\|^2+\|w_t\|_\infty^2}, \|w_t\|_\infty/\sqrt{\|x_\sigma(t)\|^2+\|w_t\|_\infty^2}\right\} \leq 1$ due to $\{\|x_\sigma(t)\|, \|w_t\|_\infty\} \geq 0$. Hence, it can be written that

$$\dot{\phi}_{1_\sigma}(t) \leq \|\mathcal{G}_\sigma\|+\|C_\sigma\|+\left(\|\mathcal{G}_\sigma\|+\|\mathcal{H}_\sigma\|+\|C_\sigma\|\right)\phi_{1_\sigma}(t)+\|\mathcal{H}_\sigma\|\phi_{1_\sigma}^2(t). \tag{3.92}$$

Thus, the comparison lemma for differential inequalities yields

$$\int_{t_k}^{t_{k+1}} dt \geq \int_0^{\sqrt{\psi}} \frac{1}{\|\mathcal{G}_\sigma\|+\|C_\sigma\|+\left(\|\mathcal{G}_\sigma\|+\|\mathcal{H}_\sigma\|+\|C_\sigma\|\right)\phi_{1_\sigma}+\|\mathcal{H}_\sigma\|\phi_{1_\sigma}^2} d\phi_\sigma. \tag{3.93}$$

Replacing ϕ_{1_σ} with $s \coloneqq \phi_{1_\sigma}/\sqrt{\psi}$, the result of (3.77) is reached. ■

3.6 Optimization problems

The problem addressed in this work has two main objectives: the characterization of MCDoS and the design of control parameters such that the system remains resilient against the maximum MCDoS changing frequency. The first objective is already fulfilled in Section 3.5. This section provides a comprehensive algorithm to minimize τ_D. Since τ_D is lower bounded by the right-hand side of (3.32), the lower bound can be taken as the cost function, which in turn ensures that τ_D can be chosen sufficiently small. The

objective function is thus defined by

$$J_{\text{mcdos}} = \max_{\forall\sigma\in\{1,\cdots,n_s\}} \frac{\max\{\overline{\alpha}_{p_\sigma}, \overline{\alpha}_{e_\sigma}\}}{\zeta_{1_\sigma}} \ln\left\{\frac{\max\{\overline{\alpha}_{p_\sigma}, \overline{\alpha}_{e_\sigma}\}}{\min\{\underline{\alpha}_{p_\sigma}, \underline{\alpha}_{e_\sigma}\}}\right\}, \tag{3.94}$$

where $\underline{\alpha}_{p_\sigma}$ and $\overline{\alpha}_{p_\sigma}$ are mentioned in (3.41), $\underline{\alpha}_{e_\sigma}$ and $\overline{\alpha}_{e_\sigma}$ are mentioned in (3.42), and ζ_{1_σ} is mentioned in (3.39). Therefore, the optimization problem is to minimize J_{mcdos} subject to $\underline{\alpha}_{p_\sigma} I \leq P_{p_\sigma} \leq \overline{\alpha}_{p_\sigma} I, \underline{\alpha}_{e_\sigma} I \leq P_{e_\sigma} \leq \overline{\alpha}_{e_\sigma} I, \Gamma_{2_\sigma} \geq \zeta_{1_\sigma} I, \{\psi_1, \psi_2, \varepsilon_{1_\sigma}, \varepsilon_{2_\sigma}\} > 0$ and $H_\sigma \in \mathbb{R}^{n_p \times n_{h_\sigma}}$. In this case, the cost function is non-convex, and the constraints have LMIs. This Non-Convex Optimization (NCO) finds the optimal value of J_{mcdos} by solving LMIs present in constraints. However, no optimization tool is available to solve both NCO and LMIs. To address this issue, J_{mcdos} is minimized using a two-step procedure in which the NCO problem is converted into Convex Optimization (CO) problems. The minimization of J_{mcdos} is achieved by minimizing $\left(\max\{\overline{\alpha}_{p_\sigma}, \overline{\alpha}_{e_\sigma}\} / \min\left\{\underline{\alpha}_{p_\sigma}, \underline{\alpha}_{e_\sigma}\right\}\right)$ and maximizing ζ_{1_σ}.

Step 1 Now, it can be written that

$$\frac{\max\{\overline{\alpha}_{p_\sigma}, \overline{\alpha}_{e_\sigma}\}}{\min\{\underline{\alpha}_{p_\sigma}, \underline{\alpha}_{e_\sigma}\}} \geq 1. \tag{3.95}$$

Hence, from (3.95)

$$J_\sigma \coloneqq \max\{\overline{\alpha}_{p_\sigma}, \overline{\alpha}_{e_\sigma}\} - \min\{\underline{\alpha}_{p_\sigma}, \underline{\alpha}_{e_\sigma}\} \geq 0 \tag{3.96}$$

persists. Minimizing J_σ allows by minimizing $\max\{\overline{\alpha}_{p_\sigma}, \overline{\alpha}_{e_\sigma}\}$ and maximizing of $\min\{\underline{\alpha}_{p_\sigma}, \underline{\alpha}_{e_\sigma}\}$. If (3.95) can be minimized, the same outcome occurs. Therefore, minimize J_σ subject to $\underline{\alpha}_{p_\sigma} I \leq P_{p_\sigma} \leq \overline{\alpha}_{p_\sigma} I, \underline{\alpha}_{e_\sigma} I \leq P_{e_\sigma} \leq \overline{\alpha}_{e_\sigma} I, \Gamma_{2_\sigma} \geq qI, \{\psi_1, \psi_2, \varepsilon_{1_\sigma}, \varepsilon_{2_\sigma}\} > 0$, and $H_\sigma \in \mathbb{R}^{n_p \times n_{h_\sigma}}$ is the first CO problem.

Step 2 From (3.96), it can be written that

$$J_\sigma = \max\left\{\overline{\alpha}_{p_\sigma} - \underline{\alpha}_{p_\sigma}, \overline{\alpha}_{p_\sigma} - \underline{\alpha}_{e_\sigma}, \overline{\alpha}_{e_\sigma} - \underline{\alpha}_{p_\sigma}, \overline{\alpha}_{e_\sigma} - \underline{\alpha}_{e_\sigma}\right\}. \tag{3.97}$$

From (3.97), it follows that $\overline{\alpha}_{p_\sigma} - \underline{\alpha}_{p_\sigma}$, $\overline{\alpha}_{p_\sigma} - \underline{\alpha}_{e_\sigma}$, $\overline{\alpha}_{e_\sigma} - \underline{\alpha}_{p_\sigma}$, and $\overline{\alpha}_{e_\sigma} - \underline{\alpha}_{e_\sigma}$ are bounded above by J_σ. The value of J_σ is then utilized in the subsequent optimization steps. The second objective function is

$$J \coloneqq \min_{\forall \sigma \in \{1,\cdots,n_s\}} \zeta_{1_\sigma}. \tag{3.98}$$

The next task is to maximize J. All values of $\zeta_{1_\sigma}, \forall \sigma \in \{1,\cdots,n_s\}$ can be maximized by maximizing the minimum value of ζ_{1_σ}. Hence, maximize J subject to $\Gamma_{2_\sigma} \geq \zeta_{1_\sigma}, \underline{\alpha}_{p_\sigma} I \leq P_{p_\sigma} \leq \overline{\alpha}_{p_\sigma} I, \underline{\alpha}_{e_\sigma} I \leq P_{e_\sigma} \leq \overline{\alpha}_{e_\sigma} I, \{\overline{\alpha}_{p_\sigma} - \underline{\alpha}_{p_\sigma}, \overline{\alpha}_{p_\sigma} - \underline{\alpha}_{e_\sigma}, \overline{\alpha}_{e_\sigma} - \underline{\alpha}_{p_\sigma}, \overline{\alpha}_{e_\sigma} - \underline{\alpha}_{e_\sigma}\} \leq J_\sigma, \{\psi_1, \psi_2, \varepsilon_{1_\sigma}, \varepsilon_{2_\sigma}\} > 0$, and $H_\sigma \in \mathbb{R}^{n_p \times n_{h_\sigma}}$ is the second CO problem.

Please note that due to this relaxation scheme, the solution obtained may sometimes be sub-optimal rather than optimal. The parameter q in Step 1 should be chosen to be very small and positive, as the optimization procedure is highly sensitive to q. Selecting a sufficiently small q tends to yield better optimization results.

3.7 Resilient control logic

The ETM in (3.17) cannot be directly implemented due to its dependency on the supremum norm of the disturbance w. The term involving the supremum norm of the disturbance in the event-based control logic in (3.17) can be avoided by omitting the disturbance term. By doing so, the following

$$\xi_\sigma^\top(t)\xi_\sigma(t) + \xi_e^\top(t)\xi_e(t) = \psi_1 y_\sigma^\top(t) y_\sigma(t) + \psi_2 x_e^\top(t) x_e(t) \tag{3.99}$$

is obtained from (3.17). However, omitting the disturbance does not prevent Zeno behaviour; therefore, a lower bound on the sampling rate must be imposed a priori. The lower bound of the sampling rate ($\underline{\Delta}$) is calculated in Lemma 3.10. Let

$$\varpi_{1_{\sigma_k}} \coloneqq \inf\left\{t \in \mathbb{R}_{>t_k} : \xi_\sigma^\top(t^-)\xi_\sigma(t^-) + \xi_e^\top(t^-)\xi_e(t^-) \geq \psi_1 y_\sigma^\top(t) y_\sigma(t) + \psi_2 x_e^\top(t) x_e(t)\right\} \tag{3.100}$$

$\forall k \in \mathbb{N}_0$ and $\forall \sigma \in \{1, \cdots, n_s\}$.

Proposition 3.11. *Let $\underline{\Delta}$ be the positive constant which follows (3.76) and (3.77) as in Lemma 3.10. Then the sequence $\{t_k\}_{k\in\mathbb{N}_0}$ for ETM is formally defined by*

$$t_{k+1} = \begin{cases} t_k + \underline{\Delta}, & \text{if } \varpi_{1_{\sigma_k}} \leq t_k + \underline{\Delta}, \\ \varpi_{1_{\sigma_k}}, & \text{otherwise.} \end{cases} \tag{3.101}$$

Proof. The inter-sampling related to (3.101) is equivalent to $\varpi_{1_{\sigma_k}} - t_k$ or $\underline{\Delta}$. By (3.101), $t_{k+1} = \varpi_{1_{\sigma_k}}$ only if $\varpi_{1_{\sigma_k}} \geq t_k + \underline{\Delta}$. Otherwise, the control update occurs at a minimum feasible time of $\underline{\Delta}$. With this resilient control logic, we are avoiding the Zeno behaviour. ■

3.8 Simulation results

3.8.1 Example 1

A process dynamic is employed to control the speed of a DC motor with two transmission channels [159], as follows

$$\begin{aligned} \dot{x}_{p_1}(t) &= -\frac{b}{J}x_{p_1}(t) + \frac{K_t}{J}x_{p_2}(t), \\ \dot{x}_{p_2}(t) &= -\frac{K_b}{L_a}x_{p_1}(t) - \frac{R_a}{L_a}x_{p_2}(t) + \frac{1}{L_a}u(t), \end{aligned} \tag{3.102}$$

where $x_{p_1}(t)$, $x_{p_2}(t)$, $u(t)$ are rotor shaft speed (rad/sec), armature current (amp), applied armature voltage (volts), respectively. The remaining parameters are explained in the table below. Both the states $x_{p_1}(t)$ and $x_{p_2}(t)$ are measurable, and data is transferred by two different channels. Under MCDoS type 1, channel 2 (value of x_{p_2}) is compromised and for the case of MCDoS type 2, channel 1 (value of x_{p_1}) is compromised. Output matrices are

$$C_1 = \begin{bmatrix} 1 & 0 \end{bmatrix} \tag{3.103}$$

TABLE 3.1: Parameters of DC motor [159]

Parameters	Values
Friction coefficient (b)	0.1 N-m/rad/sec
Mechanical inertia (J)	0.01 Kg.m^2
Motor torque constant (K_t)	0.01 N.m/A
Back emf constant (K_b)	0.01 V/rad/sec
Armature inductance (L_a)	0.5 H
Armature resistance (R_a)	1Ω

and

$$C_2 = \begin{bmatrix} 0 & 1 \end{bmatrix} \tag{3.104}$$

in the presence of MCDoS type 1 and type 2 attack respectively where $\sigma \in \{1, 2\}$. However, to properly illustrate the effectiveness of the proposed result, a model error of $2.01 \begin{bmatrix} 2.5 & 0.1 \\ 0.5 & 0.9 \end{bmatrix}$ is added to make the system unstable and introduce disturbances. Therefore, the unstable dynamics with disturbance are

$$\begin{aligned} \dot{x}_{p_1}(t) &= -4.975x_{p_1}(t) + 1.201x_{p_2}(t) + w_1(t), \\ \dot{x}_{p_2}(t) &= 0.985x_{p_1}(t) - 0.191x_{p_2}(t) + 2u(t) + w_2(t), \end{aligned} \tag{3.105}$$

$w_1(t)$ and $w_2(t)$ are the pseudo-random values drawn from the standard normal distribution, which are present in the system as disturbances. Pole placement gain $K = \begin{bmatrix} 0.466584096586178 & 0.3245 \end{bmatrix}$, by choosing closed loop pole position $-0.825, -4.99$. The resilient control logic proposed in (3.101) is implemented, following the two-step optimization procedure described in Section 3.6. In step 1 of the optimization, with $q = 10^{-4}$, the results are $J_1 = 2.072969001001672 \times 10^{-5}$ and $J_2 = 1.57773794029481 \times 10^{-12}$. Using

the values of J_1 and J_2 in step 2 of the optimization yields

$$P_{p_1} = \begin{bmatrix} 0.008871426116479 & -0.000006792623163 \\ -0.000006792623163 & 0.008855769458504 \end{bmatrix},$$

$$P_{p_2} = \begin{bmatrix} 0.515299931286159 & 0 \\ 0 & 0.515299931286159 \end{bmatrix},$$

$$P_{e_1} = \begin{bmatrix} 0.00886179364292 & -0.00001020655305 \\ -0.00001020655305 & 0.008865402613122 \end{bmatrix},$$

$$P_{e_2} = \begin{bmatrix} 0.515299931286159 & 0 \\ 0 & 0.515299931286159 \end{bmatrix},$$

$$L_1 = \begin{bmatrix} 37.251369637553793 \\ 1.620197932761986 \end{bmatrix}, L_2 = \begin{bmatrix} 1.79111472236966 \\ 1.400277128925236 \end{bmatrix}, \psi_1 = 0.001000001510214, \psi_2$$

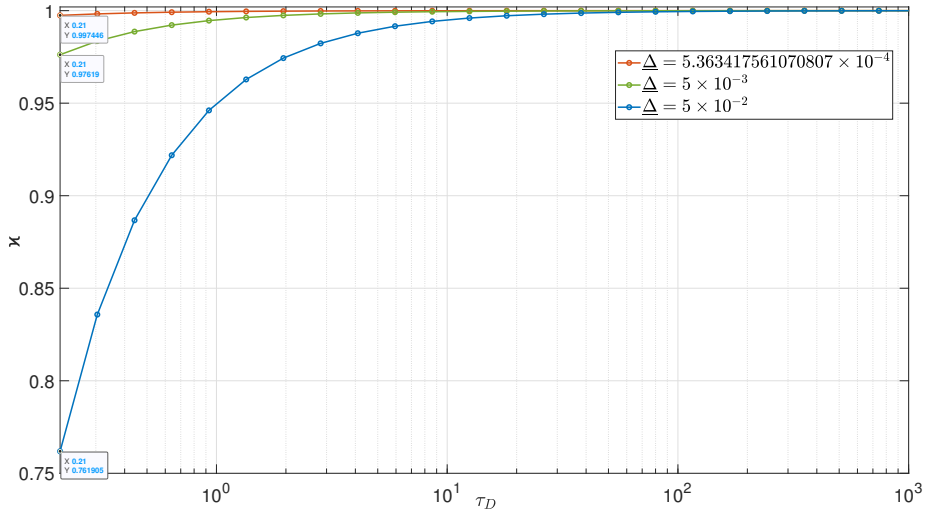

FIGURE 3.3: Maximum allowable values of $\varkappa$ versus choice of τ_D for $\underline{\Delta} = 5.363417561 \times 10^{-4}, 5 \times 10^{-3}$, and 5×10^{-2}.

$= 0.001000000011216, \varepsilon_{1_1} = 8248.8013238, \varepsilon_{2_1} = 10567.4457871, \varepsilon_{1_2} = 5961.78662263, \varepsilon_{2_2}$ $= 5960.39779048, \zeta_{1_1} = 1.00164915432705 \times 10^{-4}$, and $\zeta_{1_2} = 0.090178765464519$. Hence $\tau_D > 0.207197584758976$. In order to minimize τ_D, the controller and observer parameters ψ_1, ψ_2, L_1, and L_2 are designed by solving LMIs. Hence ψ_1, ψ_2, L_1, and L_2 are optimal values. From Lemma 3.10, we get $\underline{\Delta} = 5.363417561070807 \times 10^{-4}$. The maximum allowable value of $\varkappa$ is 0.997445991637585 considering $\tau_D = 0.21$, as shown in Figure 3.3.

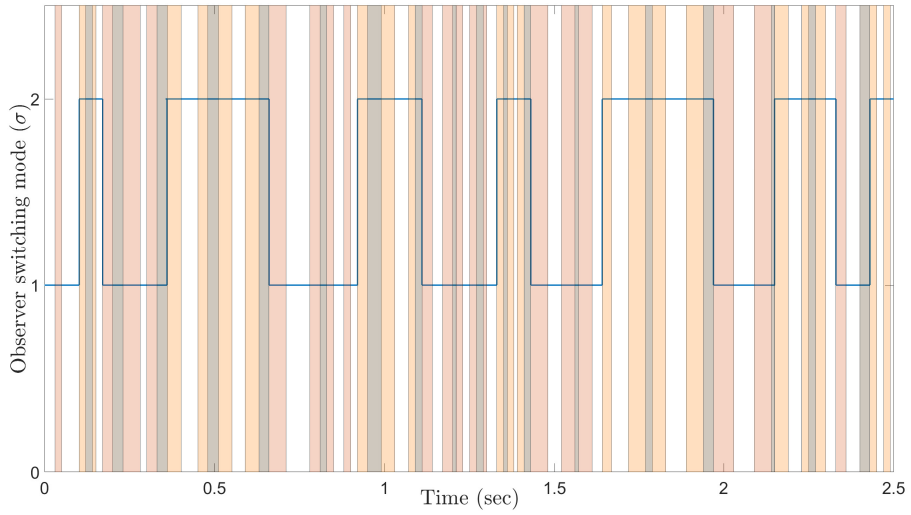

FIGURE 3.4: Real-time plot of the switched observer responding to an MCDoS frequency variation by adjusting its switching mode σ according to the detected MCDoS type, illustrating the characterization of MCDoS. The relation $l(0, 2.5) \approx 13$ indicates that the observer switches modes 13 times within the $0 - 2.5$ s interval. Grey stripes indicate FSDoS, orange stripes indicate DoS affecting only channel 2 (MCDoS type 1), and yellow stripes indicate DoS affecting only channel 1 (MCDoS type 2).

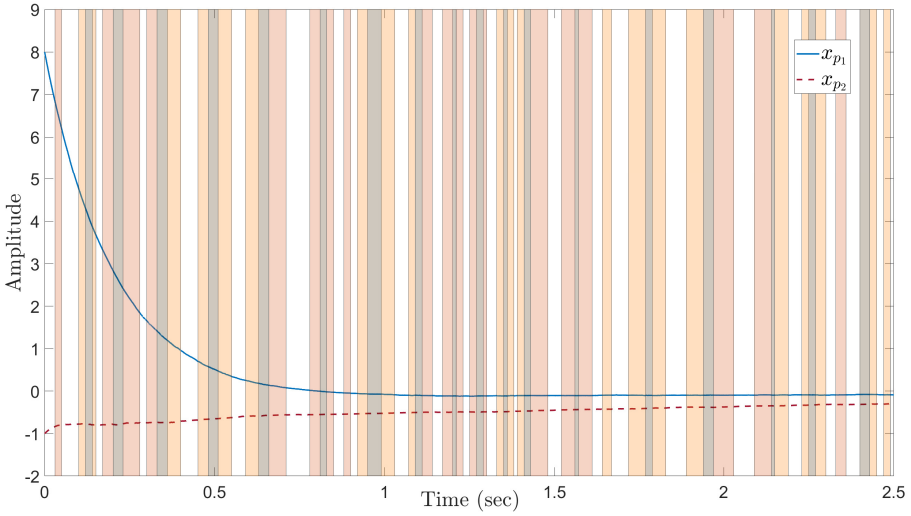

FIGURE 3.5: Plant state response illustrating the characterization of MCDoS where the initial condition is $x_p(0) = (8, -1)$. Here, grey stripes represent FSDoS, orange stripes represent only channel 2 is affected by DoS (MCDoS type 1), and yellow stripes represent only channel 1 is affected by DoS (MCDoS type 2).

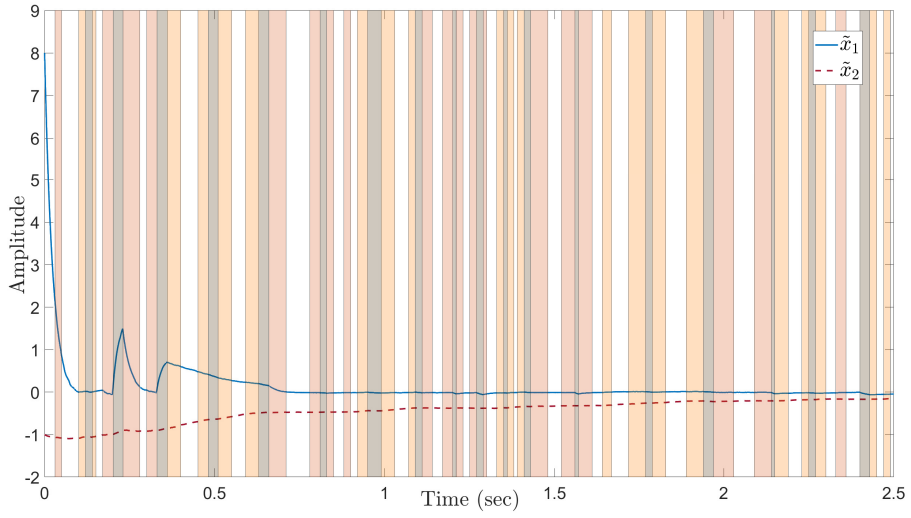

FIGURE 3.6: Switched-observer error ($\tilde{x}(t) = x_p(t) - x_e(t)$) response illustrating the characterization of MCDoS with initial conditions $x_p(0) = (8, -1)$ and $x_e(0) = (0, 0)$. Grey stripes indicate FSDoS periods, orange stripes denote MCDoS type 1 (DoS affecting only channel 2), and yellow stripes denote MCDoS type 2 (DoS affecting only channel 1).

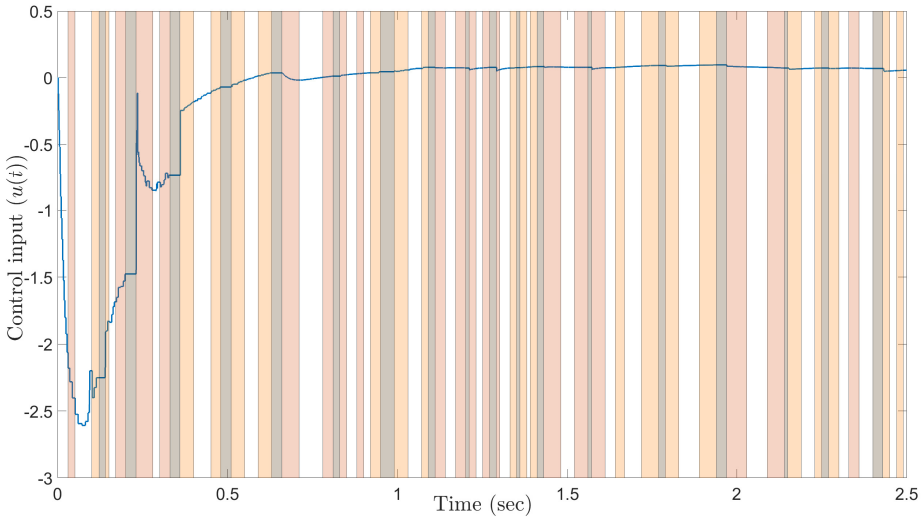

FIGURE 3.7: Control input ($u(t)$) response illustrating the characterization of MCDoS. Here, grey stripes represent FSDoS, orange stripes represent only channel 2 is affected by DoS (MCDoS type 1), and yellow stripes represent only channel 1 is affected by DoS (MCDoS type 2).

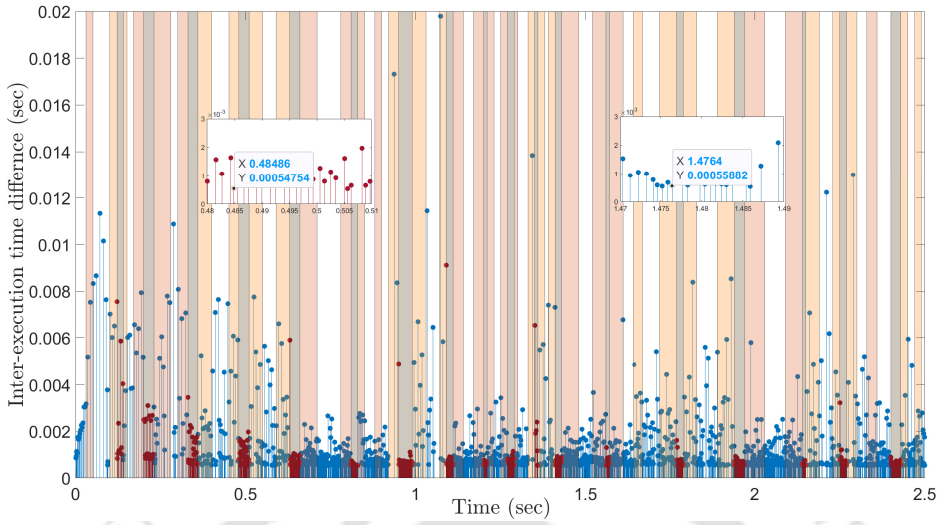

FIGURE 3.8: Data updates instants for ETM illustrating the characterization of MC-DoS, where blue sticks are successful data updates and red sticks are failed attempts because of the presence of FSDoS. Here, grey stripes represent FSDoS, orange stripes represent only channel 2 is affected by DoS (MCDoS type 1), and yellow stripes represent only channel 1 is affected by DoS (MCDoS type 2).

So, the maximum allowable changing frequency is $l(0, 0.5) \approx 3.4, l(0, 1) \approx 5.8, l(0, 1.5) \approx 8.1, l(0, 2) \approx 10.5, l(0, 2.5) \approx 13$ and so on. The switched observer switching mode (σ) is shown in Figure 3.4, where $t = 0.1$s, 0.17s, 0.36s, 0.66s, 0.92s, 1.11s, 1.33s, 1.43s, 1.64s, 1.97s, 2.15s, 2.33s, and 2.43s observer detects it MCDoS frequency changing phenomenon and changes its switching mode. From Figure 3.4, it is also noticeable that the observer does not change its switching mode when FSDoS condition (grey stripes) and the no DoS condition (white stripes) occur. The responses of the states of the plant ($x_p(t)$), observer error ($\tilde{x}(t)$), control law ($u(t)$) and control law triggering instants (t_k) for ETM are shown in Figures 3.5, 3.6, 3.7 and 3.8, respectively. It follows intuitively from (3.33) that the maximum allowable value of $\varkappa$ depends on both τ_D and $\underline{\Delta}$. Figure 3.3 illustrates how the permissible range of $\varkappa$ varies across different values of τ_D and $\underline{\Delta}$. Additionally, the value of τ_D is influenced by the extent of model error present in the system.

3.8.2 Example 2

An unstable process dynamics of higher order with disturbances is considered as

$$\begin{aligned}
\dot{x}_{p_1}(t) &= -0.15x_{p_1}(t) - 0.35x_{p_2}(t) + 0.3x_{p_3}(t) + w_1(t),\\
\dot{x}_{p_2}(t) &= 0.25x_{p_1}(t) - 0.75x_{p_2}(t) - 0.25x_{p_3}(t) + w_2(t),\\
\dot{x}_{p_3}(t) &= 0.61x_{p_1}(t) - 0.6x_{p_2}(t) - 0.4x_{p_3}(t) + u(t) + w_3(t),
\end{aligned} \tag{3.106}$$

where $x_{p_1}(t), x_{p_2}(t)$, and $x_{p_3}(t)$ are the states of the system, $u(t)$ is the control input, and $w_1(t), w_2(t)$ are the pseudo-random values drawn from the standard normal distribution, which are present in the system as disturbances. The states $x_{p_1}(t)$ and $x_{p_3}(t)$ are measurable, and data are transmitted through two separate transmission channels. Under MCDoS type 1, channel 2 (value of x_{p_3}) is compromised, and for the case of MCDoS type 2, channel 1 (value of x_{p_1}) is compromised. Output matrices are $C_1 = \begin{bmatrix}1 & 0 & 0\end{bmatrix}$ and $C_2 = \begin{bmatrix}0 & 0 & 1\end{bmatrix}$ in the presence of MCDoS type 1 and type 2 attacks respectively, where $\sigma \in \{1, 2\}$. Pole placement gain $K = \begin{bmatrix}1.189020979020984 & -1.105174825174828 & 1.1\end{bmatrix}$, by choosing closed loop pole position -0.6,-0.7,-1.1. The resilient control logic proposed in (3.101) is implemented as in Example 1, following the two-step optimization procedure described in Section 3.6. In step 1 of the optimization, with $q = 10^{-4}$, the results are $J_1 = 0.003782721702803$ and $J_2 = 0.00305197940286$. Using the values of J_1 and J_2 in step 2 of the optimization yields

$$P_{p_1} = \begin{bmatrix}
0.006122103639167 & -0.001241051243291 & -0.000234907142443\\
-0.001241051243291 & 0.00417981115399 & 0.000009884716369\\
-0.000234907142443 & 0.000009884716369 & 0.002983260269758
\end{bmatrix},$$

$$P_{p_2} = \begin{bmatrix}
0.004221587108664 & -0.000453974645277 & 0.000341275671779\\
-0.000453974645277 & 0.003219551691718 & 0.000557165492793\\
0.000341275671779 & 0.000557165492793 & 0.001598587543883
\end{bmatrix},$$

$$P_{e_1} = \begin{bmatrix} 0.00468177510411 & 0.000372181312444 & -0.001804820483412 \\ 0.000372181312444 & 0.006512096167909 & 0.000133572574704 \\ -0.001804820483412 & 0.000133572574704 & 0.004923531256519 \end{bmatrix},$$

$$P_{e_2} = \begin{bmatrix} 0.003228256626336 & -0.00055929684728 & -0.001375432886353 \\ -0.00055929684728 & 0.003320598239907 & -0.000333480225865 \\ -0.001375432886353 & -0.000333480225865 & 0.002663747720527 \end{bmatrix},$$

$$L_1 = \begin{bmatrix} 160.221694583746 \\ 2.56434000558495 \\ 66.3088904577563 \end{bmatrix}, L_2 = \begin{bmatrix} 153.02609857041 \\ 61.610088476346 \\ 326.841965823136 \end{bmatrix}, \psi_1 = 0.001000000001376, \psi_2 =$$

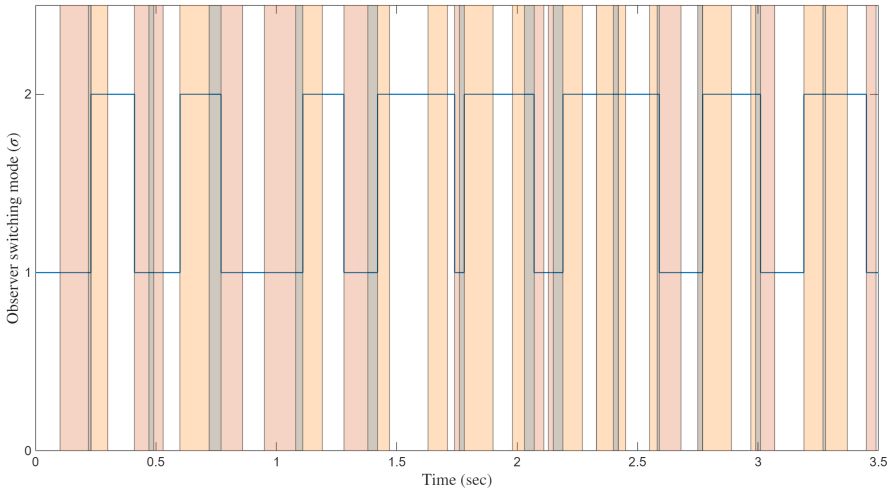

FIGURE 3.9: Real-time plot of the switched observer for higher order system responding to an MCDoS frequency variation by adjusting its switching mode σ according to the detected MCDoS type, illustrating the characterization of MCDoS. The relation $l(0, 3.5) = 16$ indicates that the observer switches modes 16 times within the $0 - 3.5$s interval. Grey stripes indicate FSDoS, orange stripes indicate DoS affecting only channel 2 (MCDoS type 1), and yellow stripes indicate DoS affecting only channel 1 (MCDoS type 2).

$0.001000000000196, \varepsilon_{1_1} = 2949.583566, \varepsilon_{1_2} = 2940.33361103, \varepsilon_{2_1} = 2729.01407403, \varepsilon_{2_2} = 2767.17748726, \zeta_{1_1} = 1.000110674915 \times 10^{-4}$, and $\zeta_{1_2} = 1.000061679092 \times 10^{-4}$. Hence $\tau_D > 55.5195865424358$. From Lemma 3.10, it is calculated that $\underline{\Delta} = 5.92572252565179 \times 10^{-5}$. The maximum allowable value of $\varkappa$ is 0.999717822736874 considering $\tau_D = 55.52$. So, the maximum allowable DoS frequency over the interval $0 - 3.5$s is $l(0, 3.5) = 1.0628$.

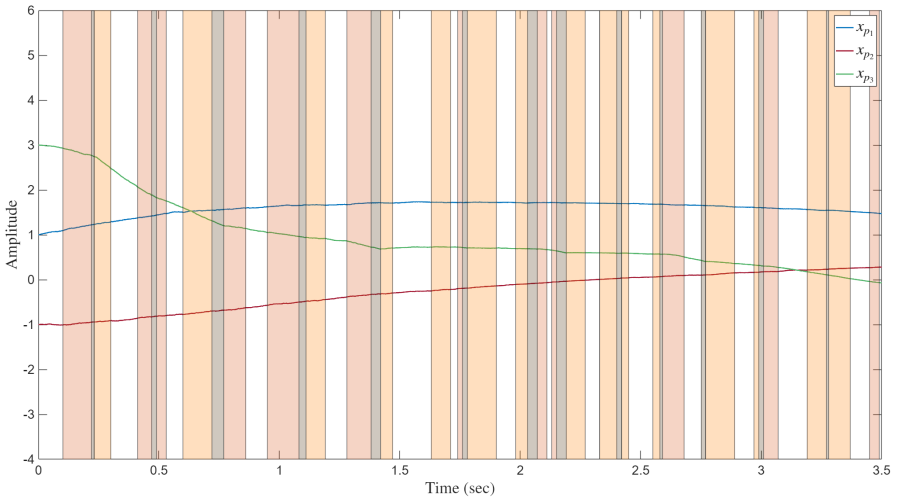

FIGURE 3.10: Plant state response for higher order system illustrating the characterization of MCDoS for higher order where the initial condition is $x_p(0) = (1, -1, 3)$. Here, grey stripes represent FSDoS, orange stripes represent only channel 2 is affected by DoS (MCDoS type 1), and yellow stripes represent only channel 1 is affected by DoS (MCDoS type 2).

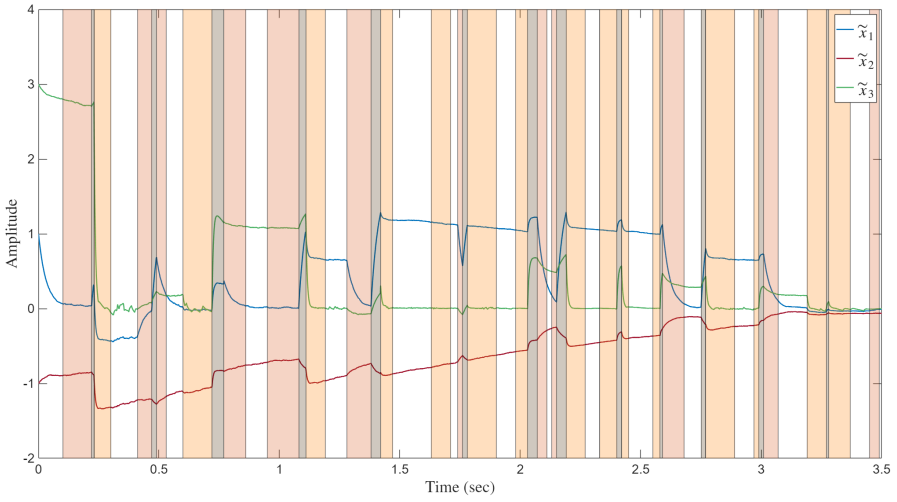

FIGURE 3.11: Switched-observer error ($\tilde{x}(t) = x_p(t) - x_e(t)$) response for higher order system illustrating the characterization of MCDoS with initial conditions $x_p(0) = (1, -1, 3)$ and $x_e(0) = (0, 0, 0)$. Grey stripes indicate FSDoS periods, orange stripes denote MCDoS type 1 (DoS affecting only channel 2), and yellow stripes denote MCDoS type 2 (DoS affecting only channel 1).

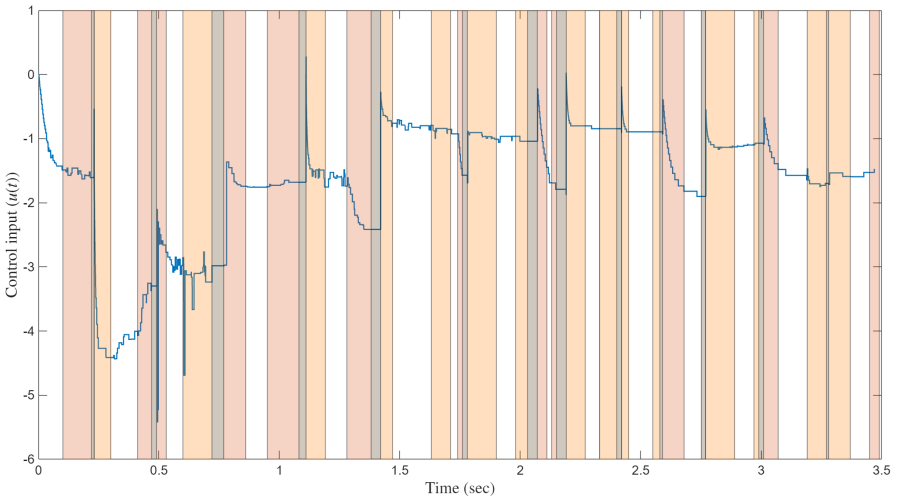

FIGURE 3.12: Control input ($u(t)$) response for higher order system illustrating the characterization of MCDoS. Here, grey stripes represent FSDoS, orange stripes represent only channel 2 is affected by DoS (MCDoS type 1), and yellow stripes represent only channel 1 is affected by DoS (MCDoS type 2).

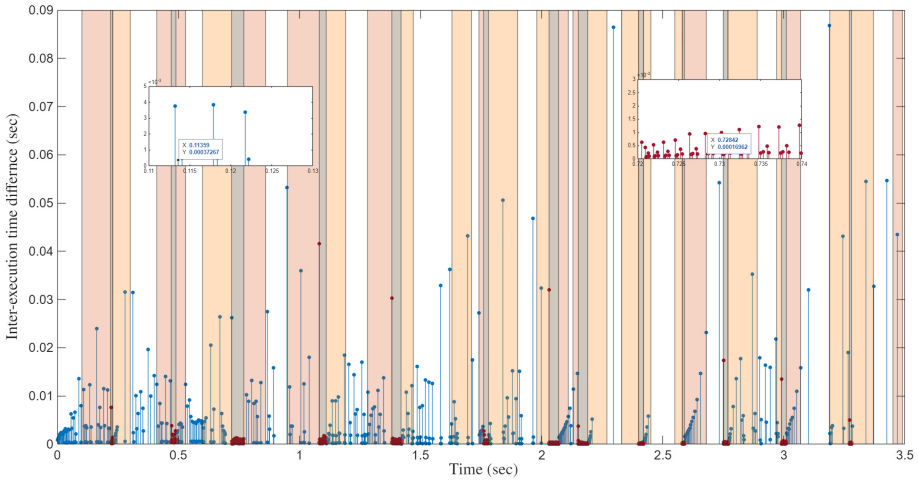

FIGURE 3.13: Data updates instants for ETM for higher order system illustrating the characterization of MCDoS, where blue sticks are successful data updates and red sticks are failed attempts because of the presence of FSDoS. Here, grey stripes represent FSDoS, orange stripes represent only channel 2 is affected by DoS (MCDoS type 1), and yellow stripes represent only channel 1 is affected by DoS (MCDoS type 2).

This value is conservative; in practice, the system can tolerate a significantly higher level of MCDoS. To evaluate the system's resiliency, MCDoS is injected at a rate of $l(0, 3.5) = 16$. This indicates that within the interval $0 - 3.5$s, the observer detects the MCDoS variation 16 times and correspondingly adjusts its switching mode. The resulting switching behavior is illustrated in Figure 3.9. Next, the plant response, observer error dynamics, control action, and ETM inter-execution time instants are presented in Figure 3.10, 3.11, 3.12, and 3.13, respectively. The simulation results of the higher-order system indicate that the theoretical bounds on admissible MCDoS values are conservative. This becomes particularly evident in the resiliency test, which demonstrates that the system can tolerate higher MCDoS levels than predicted.

3.9 Chapter summary

This chapter presented a detailed and comprehensive characterization of the varying frequency of MCDoS occurrences. The discussion began with the introduction of an initial assumption that served to bound the rate at which the MCDoS frequency changed. This assumption was not left as a mere premise; rather, it was subsequently verified and analytically derived, providing it with a firm theoretical foundation. Building upon this characterization, an optimal switched-observer-based control strategy was developed to ensure that the system remained resilient even under the most adverse conditions corresponding to the maximum possible MCDoS frequency variations. In addition, the minimum inter-execution time was computed for scenarios where FSDoS was absent, ensuring efficient event-triggered operation without unnecessary communication overhead. In preparation for FSDoS scenarios, an ETM was formulated. By incorporating the previously computed minimum inter-execution time into the ETM framework, a resilient control logic was designed, explicitly constructed to eliminate the possibility of Zeno behaviour while maintaining stability and performance.

It should be noted that while this chapter primarily focused on MCDoS frequency characterization and its associated control design, the formal and in-depth characterization of

FSDoS is beyond its scope and is intended to be systematically explored and rigorously addressed in the subsequent chapter.

Chapter 4

Characterization of full-scale denial-of-service

4.1 Introduction

While the previous chapter concentrated on the characterization of MCDoS, the present chapter is devoted to a thorough characterization of FSDoS. FSDoS arises in situations where a DoS simultaneously targets multiple transmission channels on the measurement side, thereby rendering the system undetectable, or when it disrupts the CtA communication, consequently jeopardizing closed-loop stability. In the case of MCDoS, the analysis required the imposition of constraints solely on the rate at which its frequency could change. By contrast, FSDoS presents a more severe threat, as it demands restrictions on both its frequency and duration. This additional requirement stems from the fact that extended periods of FSDoS can gradually drive the system toward instability, posing significant risks to overall system performance. Therefore, the careful regulation of FSDoS characteristics becomes not merely advisable but essential for ensuring robust and resilient operation.

4.2 Problem formulation

The notable contribution of this chapter lies in the characterization of FSDoS while accounting for the previously characterized MCDoS. Serving as a direct continuation of the preceding chapter, where the changing frequency of MCDoS was formally analyzed, this chapter builds upon that foundation while preserving the same core control architecture. A rigorous ISS-based analysis is carried out to jointly characterize the frequency and duration of FSDoS alongside the changing frequency of MCDoS.

Through the formulation and solution of an LMI-based multi-objective optimization problem, optimal values for the switched observer gain and ETM parameters are obtained. These parameters are selected to guarantee system resilience against the maximum admissible MCDoS changing frequency as well as the highest tolerable FSDoS frequency and duration. While the previous chapter's optimization strategy was aimed solely at addressing the maximum MCDoS changing frequency, the current work extends the scope to simultaneously optimize resilience against both MCDoS and FSDoS.

Furthermore, an asynchronous triggering mechanism is developed to handle FSDoS events occurring at different times on the StC channels and CtA channel. While an ETM-based approach for asynchronous DoS attack in a single-sensor context was first introduced in [57], the present work marks the first consideration of asynchronous DoS within a multi-sensor framework.

4.3 Stability analysis under full scale denial-of-service

The analysis in Section 3.5 is based on the feasibility of satisfying condition (3.17), $\forall t \in \mathbb{R}_{\geq 0}$. As stated in Lemma 3.10, this condition is always achievable in the absence of FSDoS. However, when FSDoS is present, the analysis becomes more complex, as certain control update attempts may fail regardless of the sampling strategy used. If $\xi_\sigma(t)$ and $\xi_e(t)$ are not reset, (3.17) may be violated, and stability may be lost since (3.25) no longer

has to fulfil a dissipation-like inequality. As a result, it's logical to wonder how Theorem 3.5's results might be expanded to account for the presence of FSDoS. This question will be addressed in the remainder of this section. The type of FSDoS signals under study is introduced and discussed in Section 4.3.1. Section 4.3.2 contains the major result.

4.3.1 Assumptions: time-constrained FSDoS

The first question to be addressed is establishing the maximum quantity of FSDoS that a system can withstand before becoming unstable. In this regard, it is clear that such a figure is not arbitrary and that appropriate limits on FSDoS frequency and duration must be enforced. De Persis and Tesi restricted the DoS frequency and duration for the single sensor in [48] by using the concept of dwell time [153]. The assumptions from [48] are used here to restrict the frequency and duration of FSDoS.

(a) *FSDoS frequency :* Let $\{e_n\}_{n\in\mathbb{N}}$ denote the sequence of FSDoS on/off transition instants, where $e_1 \geq 0$ represents the time when FSDoS switches from zero (transmission allowed in at least one channel) to one (transmission completely blocked in all channels). The nth FSDoS interval is defined as

$$E_n := e_n \cup [e_n, e_n + \tau_n), \tag{4.1}$$

where τ_n denotes the duration of complete communication blockage across all channels. Consequently, the time interval during which FSDoS is active is expressed as

$$\Omega(\tau, t) = \bigcup_{n\in\mathbb{N}} E_n \cap [\tau, t]. \tag{4.2}$$

The representation of $\Omega(\tau, t)$ in (4.2) is equivalent to that in (3.4). The union of the FSDoS sequence form is introduced in (4.2) to emphasize the FSDoS frequency n. Let $e_{n+1} - e_n, n \in \mathbb{N}$, denote the time elapsed between two consecutive FSDoS activations. It is evident that if $e_{n+1} - e_n \leq \underline{\Delta}, \forall n \in \mathbb{N}$, meaning FSDoS can occur as frequently as the minimum feasible sampling interval $\underline{\Delta}$, then stability can be lost regardless of the control

update strategy employed. Let $n(\tau, t)$ denote the number of FSDoS on/off transitions that occur within the interval $[\tau, t)$, where $t, \tau \in \mathbb{R}_{\geq 0}$ and $t \geq \tau$.

Assumption 4.1. [48] There exist $\varrho \in \mathbb{R}_{\geq 0}$ and $\tau_F \in \mathbb{R}_{>\underline{\Delta}}$ such that

$$n(\tau, t) \leq \varrho + \frac{t - \tau}{\tau_F}, \tag{4.3}$$

$\forall t, \tau \in \mathbb{R}_{\geq 0}$ with $t \geq \tau$.

(b) *FSDoS duration :* Along with the FSDoS frequency, the FSDoS duration, or the length of the intervals during which communication is disrupted, must be limited. Consider an FSDoS sequence with the singleton $\{e_1\}$ to illustrate what it means. With $\varrho \geq 1$, Assumption 4.1 is obviously met. However, regardless of the control update policy used, stability is lost if $E_1 = \mathbb{R}_{\geq 0}$ (communication is never feasible). Remembering the definition of $\Omega(\tau, t)$ in (4.2), the assumption that follows is a natural complement to Assumption 4.1 in terms of FSDoS duration.

Assumption 4.2. [48] There exist a $T \in \mathbb{R}_{>1}$ and $\zeta \in \mathbb{R}_{\geq 0}$ such that

$$|\Omega(\tau, t)| \leq \zeta + \frac{t - \tau}{T}, \tag{4.4}$$

$\forall t, \tau \in \mathbb{R}_{\geq 0}$ with $t \geq \tau$.

Remark 4.1. To characterize the frequency and duration of FSDoS, the assumptions on DoS frequency and duration for a single-sensor setting, as proposed in Chapter 2, are adopted. Although the bounds for τ_F and T align closely with those commonly used in the existing literature, establishing suitable bounds for τ_F and T becomes considerably more intricate when MCDoS, characterized by τ_D and $\varkappa$, is also present. The additional complexity introduced by the interaction between FSDoS and MCDoS is systematically addressed in the subsequent subsection.

4.3.2 ISS under FSDoS

Any control update policy that satisfies the conditions of Lemma 3.10 ensures ISS for any FSDoS signal, provided that the associated MCDoS changing frequency and the assumptions 3.1, 4.1, and 4.2 are satisfied with sufficiently large values of τ_D, τ_F, and T. Although the detailed proof of this result is technically involved, the underlying approach is conceptually straightforward. The time axis is partitioned into intervals during which condition (3.17) is upheld, and intervals during which it may be violated due to the presence of FSDoS. The feedback dynamics are then examined as a switched system alternating between stable and potentially unstable modes. Appropriate values for $\tau_D, \varkappa, \tau_F$, and T are selected to ensure that stable behaviour dominates over time. The following result formalizes this reasoning.

Theorem 4.2. *Consider the control system (3.15) with process dynamics given by (2.1), (3.1), and the control law (3.11), where the gain matrix K is such that $A - BK$ is Hurwitz. Let restricted sampling rate with ψ_1 and ψ_2, which satisfies SETM (3.17), and let the switched observer (3.7) use observer gains L_σ, which persuades the LMIs mentioned in (3.28). Consider any MCDoS changing frequency and FSDoS sequence that meets Assumptions 3.1, 4.1, and 4.2 and has arbitrary $\varkappa, \zeta$, and η, with τ_D, τ_F, and T such that (3.32), (3.33), and*

$$\frac{1}{T} + \frac{\Delta}{\tau_F} < \min_{\forall \sigma \in \{1,\cdots,n_s\}} \frac{\omega_{1_\sigma}}{\omega_{1_\sigma} + \omega_{2_\sigma}} \tag{4.5}$$

satisfy, where

$$\omega_{2_\sigma} := \frac{\lambda_M(\Gamma_{3_\sigma}) + \|\Gamma_{4_\sigma}\|}{\min\{\lambda_m(P_{p_\sigma}), \lambda_m(P_{e_\sigma})\}}, \tag{4.6}$$

$$\Gamma_{3_\sigma} \coloneqq \begin{bmatrix} 2\gamma_{2_\sigma} - \gamma_{1_\sigma} & \gamma_{3_\sigma} \\ \gamma_{3_\sigma} & -\gamma_{1_\sigma} \end{bmatrix}, \tag{4.7}$$

$$\Gamma_{4_\sigma} \coloneqq \begin{bmatrix} \Xi_{11_\sigma} & \Xi_{12_\sigma} \\ \Xi_{21_\sigma} & \Xi_{22_\sigma} \end{bmatrix}, \tag{4.8}$$

$\Xi_{11_\sigma} \coloneqq \gamma_{2_\sigma}\{(1+\sqrt{2})\sqrt{\psi_1}\|C_\sigma\| + (1+\sqrt{2})\sqrt{\psi_2}+2\}, \Xi_{12_\sigma} \coloneqq \gamma_{2_\sigma}\{(1+\sqrt{2})\sqrt{\psi_2}+2\}, \Xi_{21_\sigma} \coloneqq \gamma_{3_\sigma}[\{(1+\sqrt{2})\sqrt{\psi_1}+2\}\|C_\sigma\|+(1+\sqrt{2})\sqrt{\psi_2}], \Xi_{22_\sigma} \coloneqq \gamma_{3_\sigma}(1+\sqrt{2})\sqrt{\psi_2}, \gamma_{1_\sigma} \coloneqq \lambda_m(-\Gamma_{5_\sigma}), \gamma_{2_\sigma} \coloneqq \|P_{p_\sigma}BK\|, \gamma_{3_\sigma} \coloneqq \|H_\sigma\|,$

$$\Gamma_{5_\sigma} \coloneqq \begin{bmatrix} He(P_{p_\sigma}(A-BK)) & P_{p_\sigma} & P_{p_\sigma}BK & 0 \\ P_{p_\sigma} & -\varepsilon_{1_\sigma} I & 0 & 0 \\ K^\top B^\top P_{p_\sigma} & 0 & He(P_{e_\sigma}A) - He(H_\sigma C_\sigma) & P_{e_\sigma} \\ 0 & 0 & P_{e_\sigma} & -\varepsilon_{2_\sigma} I \end{bmatrix}, \tag{4.9}$$

and ω_{1_σ} and H_σ are mentioned in (3.44) and (3.31), respectively. Then, the control system (3.15) is ISS.

Proof. In practice, control updates occur at a finite sampling rate, which influences the overall duration of FSDoS. If a sensor attempts to transmit data but receives no acknowledgement due to FSDoS, it will continue retrying until communication is successful. However, due to the limited transmission rate, even when communication becomes possible, there will be a delay between the end of FSDoS and the initiation of transmission. This delay lengthens the FSDoS interval, which impacts the proof of Theorem 4.2. Lemma 4.3 takes those delays into account.

Lemma 4.3. *[49] The interval $[\tau, t]$ is the disjoint union of $\overline{\Omega}(\tau,t)$ and $\overline{\Upsilon}(\tau,t)$, where $\overline{\Omega}(\tau,t)$ (respectively, $\overline{\Upsilon}(\tau,t)$) is the union of sub-intervals of $[\tau,t]$ over which (3.17) need not hold (respectively, holds) for any, $t,\tau \in \mathbb{R}_{\geq 0}$, with $0 \leq \tau \leq t$. There are two sequences*

of positive and non-negative real integers $\{\varphi_m\}_{m\in\mathbb{N}}$, $\{v_m\}_{m\in\mathbb{N}}$ *such that*

$$\overline{\Omega}(\tau,t) \coloneqq \bigcup_{m\in\mathbb{N}} W_m \cap [\tau,t] \tag{4.10}$$

$$\overline{\Upsilon}(\tau,t) \coloneqq \bigcup_{m\in\mathbb{N}} Y_{m-1} \cap [\tau,t] \tag{4.11}$$

where $\forall m \in \mathbb{N}$,

$$W_m \coloneqq \{\varphi_m\} \cup [\varphi_m, \varphi_m + v_m), \tag{4.12}$$

$$Y_m \coloneqq \{\varphi_m + v_m\} \cup [\varphi_m + v_m, \varphi_{m+1}), \tag{4.13}$$

and $\varphi_0 = v_0 \coloneqq 0$.

Proof of Lemma 4.3: The corresponding lemma in the Appendix A, originally formulated for DoS under a single-sensor setting, is extended here to address FSDoS. The detailed proof is provided in Lemma A.1. □

Lemma 4.3 already outlines the time interval decomposition technique, distinguishing between periods where condition (3.17) can be satisfied and those where it may not hold due to the presence of FSDoS. The interval $Y_m, m \in \mathbb{N}$, where (3.17) holds. Consider the intervals $W_m, m \in \mathbb{N}$, across which the inequality (3.17) may not hold. In W_m, certain intermediary procedures are required to derive a constraint on the development of $V(x(t))$. First, we have to prove that each $m \in \mathbb{N}$

$$\begin{aligned}\|\xi_\sigma(t)\| \leq& \left(\frac{1+\sqrt{2}}{2}\sqrt{\psi_1}+1\right)\|y_\sigma(\varphi_m)\| + \frac{1+\sqrt{2}}{2}\sqrt{\psi_2}\|x_e(\varphi_m)\| + \|y_\sigma(t)\| \\ &+ \frac{1+\sqrt{2}}{2}\sqrt{\psi_1}\|w_{\varphi_m}\|_\infty \end{aligned} \tag{4.14}$$

$$\begin{aligned}\|\xi_e(t)\| \leq& \frac{1+\sqrt{2}}{2}\sqrt{\psi_1}\|y_\sigma(\varphi_m)\| + \left(\frac{1+\sqrt{2}}{2}\sqrt{\psi_2}+1\right)\|x_e(\varphi_m)\| + \|x_e(t)\| \\ &+ \frac{1+\sqrt{2}}{2}\sqrt{\psi_1}\|w_{\varphi_m}\|_\infty \end{aligned} \tag{4.15}$$

$\forall t \in W_m$. From (3.17), we can write

$$\|\xi_\sigma(\varphi_m)\|^2 + \|\xi_e(\varphi_m)\|^2 \leq \psi_1\|y_\sigma(\varphi_m)\|^2 + \psi_2\|x_e(\varphi_m)\|^2 + \psi_1\|w_{\varphi_m}\|_\infty^2. \tag{4.16}$$

From (4.16), it can be written that

$$2\|\xi_\sigma(\varphi_m)\|^2 + 2\|\xi_e(\varphi_m)\|^2 \leq 2\psi_1\|y_\sigma(\varphi_m)\|^2 + 2\psi_2\|x_e(\varphi_m)\|^2 + 2\psi_1\|w_{\varphi_m}\|_\infty^2. \tag{4.17}$$

From (4.17),

$$\begin{aligned}\|\xi_\sigma(\varphi_m)\|^2 + \|\xi_e(\varphi_m)\|^2 + 2\|\xi_\sigma(\varphi_m)\|\|\xi_e(\varphi_m)\| \leq 2\{\psi_1\|y_\sigma(\varphi_m)\|^2 + \psi_2\|x_e(\varphi_m)\|^2 \\ + \psi_1\|w_{\varphi_m}\|_\infty^2 + 2\sqrt{\psi_1}\|y_\sigma(\varphi_m)\|\sqrt{\psi_2}\|x_e(\varphi_m)\| + 2\sqrt{\psi_2}\|x_e(\varphi_m)\|\sqrt{\psi_1}\|w_{\varphi_m}\|_\infty \\ + 2\sqrt{\psi_1}\|w_{\varphi_m}\|_\infty\sqrt{\psi_1}\|y_\sigma(\varphi_m)\|\}.\end{aligned} \tag{4.18}$$

persists. Hence,

$$\|\xi_\sigma(\varphi_m)\| + \|\xi_e(\varphi_m)\| \leq \sqrt{2\psi_1}(\|y_\sigma(\varphi_m)\| + \|w_{\varphi_m}\|_\infty) + \sqrt{2\psi_2}\|x_e(\varphi_m)\|. \tag{4.19}$$

From (4.16),

$$\begin{aligned}\|\xi_\sigma(\varphi_m)\|^2 + \|\xi_e(\varphi_m)\|^2 - 2\|\xi_\sigma(\varphi_m)\|\|\xi_e(\varphi_m)\| \leq \psi_1\|y_\sigma(\varphi_m)\|^2 + \psi_2\|x_e(\varphi_m)\|^2 \\ + \psi_1\|w_{\varphi_m}\|_\infty^2 + 2\sqrt{\psi_1}\|y_\sigma(\varphi_m)\|\sqrt{\psi_2}\|x_e(\varphi_m)\| + 2\sqrt{\psi_2}\|x_e(\varphi_m)\|\sqrt{\psi_1}\|w_{\varphi_m}\|_\infty \\ + 2\sqrt{\psi_1}\|w_{\varphi_m}\|_\infty\sqrt{\psi_1}\|y_\sigma(\varphi_m)\|.\end{aligned} \tag{4.20}$$

can be reached. Therefore,

$$\|\xi_\sigma(\varphi_m)\| - \|\xi_e(\varphi_m)\| \leq \sqrt{\psi_1}\,(\|y_\sigma(\varphi_m)\| + \|w_{\varphi_m}\|_\infty) + \sqrt{\psi_2}\|x_e(\varphi_m)\| \tag{4.21}$$

and

$$\|\xi_e(\varphi_m)\| - \|\xi_\sigma(\varphi_m)\| \leq \sqrt{\psi_1}\,(\|y_\sigma(\varphi_m)\| + \|w_{\varphi_m}\|_\infty) + \sqrt{\psi_2}\|x_e(\varphi_m)\|. \tag{4.22}$$

hold true. Addition of (4.19) and (4.21) yields

$$\|\xi_\sigma(\varphi_m)\| \leq \frac{1+\sqrt{2}}{2}\sqrt{\psi_1}(\|y_\sigma(\varphi_m)\| + \|w_{\varphi_m}\|_\infty) + \frac{1+\sqrt{2}}{2}\sqrt{\psi_2}\|x_e(\varphi_m)\| \tag{4.23}$$

and addition of (4.19) and (4.22) delivers

$$\|\xi_e(\varphi_m)\| \leq \frac{1+\sqrt{2}}{2}\sqrt{\psi_1}(\|y_\sigma(\varphi_m)\| + \|w_{\varphi_m}\|_\infty) + \frac{1+\sqrt{2}}{2}\sqrt{\psi_2}\|x_e(\varphi_m)\|. \tag{4.24}$$

Hence from (4.23),

$$\|y_\sigma(t_{k(\varphi_m)}) - y_\sigma(\varphi_m)\| \leq \frac{1+\sqrt{2}}{2}\sqrt{\psi_1}(\|y_\sigma(\varphi_m)\| + \|w_{\varphi_m}\|_\infty) + \frac{1+\sqrt{2}}{2}\sqrt{\psi_2}\|x_e(\varphi_m)\| \tag{4.25}$$

holds and (4.14) follows by applying the triangular inequality. From (4.24), it can be reached

$$\|x_e(t_{k(\varphi_m)}) - x_e(\varphi_m)\| \leq \frac{1+\sqrt{2}}{2}\sqrt{\psi_1}(\|y_\sigma(\varphi_m)\| + \|w_{\varphi_m}\|_\infty) + \frac{1+\sqrt{2}}{2}\sqrt{\psi_2}\|x_e(\varphi_m)\| \tag{4.26}$$

and (4.15) persists by applying triangular inequality. From (3.22), it follows that

$$\begin{aligned}\frac{d}{dt}V_\sigma(x(t), e_\sigma(t)) &\leq x^\top(t)\Gamma_{6_\sigma}x(t) - 2x_p^\top(t)P_{p_\sigma}BK\xi_e(t) - 2\tilde{x}^\top(t)P_{e_\sigma}L_\sigma\xi_\sigma(t) \\ &+ (\varepsilon_{1_\sigma} + \varepsilon_{2_\sigma})w^\top(t)w(t),\end{aligned} \tag{4.27}$$

where

$$\Gamma_{6_\sigma} := \begin{bmatrix} \mathrm{He}(P_{p_\sigma}(A - BK)) + \frac{P_{p_\sigma}^2}{\varepsilon_{1_\sigma}} & P_{p_\sigma}BK \\ * & \mathrm{He}(P_{e_\sigma}(A - L_\sigma C_\sigma)) + \frac{P_{e_\sigma}^2}{\varepsilon_{2_\sigma}} \end{bmatrix}, \tag{4.28}$$

ε_{1_σ} and ε_{2_σ} are mentioned in (3.23). Γ_{5_σ} in (4.9) is the LMI of Γ_{6_σ}. If Γ_{2_σ} is positive definite then Γ_{5_σ} and Γ_{6_σ} are negative definite. The lowest eigen value of $-\Gamma_{5_\sigma}$ and $-\Gamma_{6_\sigma}$

are also equal because Γ_{5_σ} is the LMI of Γ_{6_σ}. Hence,

$$\frac{d}{dt}V_\sigma(x(t),e_\sigma(t)) \leq -\gamma_{1_\sigma}\|x(t)\|^2 + 2\gamma_{2_\sigma}\|x_p(t)\|\|\xi_e(t)\| + 2\gamma_{3_\sigma}\|\tilde{x}(t)\|\|\xi_\sigma(t)\| + (\varepsilon_{1_\sigma}+\varepsilon_{2_\sigma})\|w(t)\|^2, \tag{4.29}$$

where $\gamma_{1_\sigma}, \gamma_{2_\sigma}$, and γ_{3_σ} are mentioned in (4.7). From (4.14) and (4.15), it follows that

$$\|\xi_\sigma(t)\| \leq \left\{\left(\frac{1+\sqrt{2}}{2}\sqrt{\psi_1}+1\right)\|C_\sigma\| + \frac{1+\sqrt{2}}{2}\sqrt{\psi_2}\right\}\|x_p(\varphi_m)\| + \frac{1+\sqrt{2}}{2}\sqrt{\psi_2}\|\tilde{x}(\varphi_m)\| + \|C_\sigma\|\|x_p(t)\| + \frac{1+\sqrt{2}}{2}\sqrt{\psi_1}\|w_{\varphi_m}\|_\infty \tag{4.30}$$

and

$$\|\xi_e(t)\| \leq \left(\frac{1+\sqrt{2}}{2}\sqrt{\psi_1}\|C_\sigma\| + \frac{1+\sqrt{2}}{2}\sqrt{\psi_2}+1\right)\|x_p(\varphi_m)\| + \left(\frac{1+\sqrt{2}}{2}\sqrt{\psi_2}+1\right)\|\tilde{x}(\varphi_m)\| + \|x_p(t)\| + \|\tilde{x}(t)\| + \frac{1+\sqrt{2}}{2}\sqrt{\psi_1}\|w_{\varphi_m}\|_\infty, \tag{4.31}$$

respectively, by using (3.16) and $y_\sigma(t) = C_\sigma x_p(t)$. Using (4.30) and (4.31) in (4.29) yields

$$\frac{d}{dt}V_\sigma(x_p(t),\tilde{x}(t),x_p(\varphi_m),\tilde{x}(\varphi_m),f(t)) \leq (2\gamma_{2_\sigma}-\gamma_{1_\sigma})\|x_p(t)\|^2 - \gamma_{1_\sigma}\|\tilde{x}(t)\|^2 + 2\gamma_{3_\sigma}\|C_\sigma\|\|x_p(t)\|\|\tilde{x}(t)\| + \gamma_{2_\sigma}\{(1+\sqrt{2})\sqrt{\psi_1}\|C_\sigma\| + (1+\sqrt{2})\sqrt{\psi_2}+2\}\|x_p(t)\|\|x_p(\varphi_m)\| + \gamma_{2_\sigma}\{(1+\sqrt{2})\sqrt{\psi_2}+2\}\|x_p(t)\|\|\tilde{x}(\varphi_m)\| + \gamma_{3_\sigma}[\{(1+\sqrt{2})\sqrt{\psi_1}+2\}\|C_\sigma\| + (1+\sqrt{2})\sqrt{\psi_2}]\|\tilde{x}(t)\|\|x_p(\varphi_m)\| + \gamma_{3_\sigma}(1+\sqrt{2})\sqrt{\psi_2}\|\tilde{x}(t)\|\|\tilde{x}(\varphi_m)\| + \gamma_{2_\sigma}(1+\sqrt{2})\sqrt{\psi_1}\|x_p(t)\|\|w_{\varphi_m}\|_\infty + \gamma_{3_\sigma}(1+\sqrt{2})\sqrt{\psi_1}\|\tilde{x}(t)\|\|w_{\varphi_m}\|_\infty + (\varepsilon_{1_\sigma}+\varepsilon_{2_\sigma})\|w(t)\|^2, \tag{4.32}$$

where $d(t)$ is mentioned in (3.27). By using Young's inequality,

$$\gamma_{2_\sigma}(1+\sqrt{2})\sqrt{\psi_1}\|x_p(t)\|\|w_{\varphi_m}\|_\infty \leq \gamma_{2_\sigma}\frac{1+\sqrt{2}}{2\varepsilon_{3_\sigma}}\sqrt{\psi_1}\|x_p(t)\|^2 + \frac{\varepsilon_{3_\sigma}}{2}\|w_{\varphi_m}\|_\infty^2 \tag{4.33}$$

and

$$\gamma_{3_\sigma}(1+\sqrt{2})\sqrt{\psi_1}\|\tilde{x}(t)\|\|w_{\varphi_m}\|_\infty \leq \gamma_{3_\sigma}\frac{1+\sqrt{2}}{2\varepsilon_{4_\sigma}}\sqrt{\psi_1}\|\tilde{x}(t)\|^2 + \frac{\varepsilon_{4_\sigma}}{2}\|w_{\varphi_m}\|^2(t) \tag{4.34}$$

stand. If ε_{3_σ} and ε_{4_σ} are chosen to be sufficiently large, the terms $\gamma_{2_\sigma}(1+\sqrt{2})/(2\varepsilon_{3_\sigma})\sqrt{\psi_1}$ $\|x_p(t)\|^2$ and $\gamma_{3_\sigma}(1+\sqrt{2})/(2\varepsilon_{4_\sigma})\sqrt{\psi}\|\tilde{x}(t)\|^2$ become negligible. Substituting (4.33) and (4.34) into (4.32) yields

$$\frac{d}{dt}V_\sigma(X_f(t)) \leq X_f^\top(t)\Gamma_{3_\sigma}X_f(t) + X_f^\top(t)\Gamma_{4_\sigma}X_f(\varphi_m) + \nu_{2_\sigma}d^2(t), \tag{4.35}$$

where Γ_{3_σ} and Γ_{4_σ} are mentioned in (4.7) and (4.8),

$$X_f(t) \coloneqq \begin{bmatrix} \|x_p(t)\| & \|\tilde{x}(t)\| \end{bmatrix}^\top, \tag{4.36}$$

and

$$\nu_{2_\sigma} \coloneqq \varepsilon_{1_\sigma} + \varepsilon_{2_\sigma} + \frac{\varepsilon_{3_\sigma}}{2} + \frac{\varepsilon_{4_\sigma}}{2}. \tag{4.37}$$

Hence,

$$\frac{d}{dt}V_\sigma(x(t)) \leq \omega_{2_\sigma}\max\{V_\sigma(x(t)), V_\sigma(x(\varphi_m)\} + \nu_{2_\sigma}f^2(t), \tag{4.38}$$

where ω_{2_σ} is mentioned in (4.6). Thus, standard comparison results of differential inequalities yields

$$V_\sigma(x(t)) \leq e^{\omega_{2_\sigma}(t-\varphi_m)}V_\sigma(x(\varphi_m)) + \nu_{3_\sigma}e^{\omega_{2_\sigma}(t-\varphi_m)}\|w_t\|_\infty^2, \tag{4.39}$$

where $\nu_{3_\sigma} \coloneqq \nu_{2_\sigma}/\omega_{2_\sigma}, \forall t \in W_m$. Consider the interval Y_m where (3.17) holds true by construction and contains q_m jump points. $g(t)$ is total number of jump points, so $q_m \leq g(t)$. In W_m, the starting point φ_m may not be a jump point, but the ending point $\varphi_m + v_m$ may be a jump point where the mode of the observer is going to change. From (3.46), it follows that

$$V_\sigma(x(\varphi_{m(t)})) \leq e^{-\omega_{1_\sigma}(\varphi_{m(t)}-\iota_{g(t)})}V_\sigma(x(\iota_{g(t)})) + \nu_{1_\sigma}\|w_t\|_\infty^2 \tag{4.40}$$

$\forall t \in [\varphi_{m(t)}, \iota_{g(t)}]$ where

$$m(t) := \begin{cases} 0, & \text{if } t < \varphi_1 \\ \sup\{m \in \mathbb{N} : \varphi_m \leq t\}, & \text{otherwise.} \end{cases} \tag{4.41}$$

The sum of all the jump points in Y_m equals to $g(t)$. Hence, from Figure 4.1, it follows that

$$\sum_{s=1}^{m(t)} q_{m(t)-s} = g(t). \tag{4.42}$$

sing the upper bound of $V_\sigma(x(\varphi_{m(t)}))$ in (4.39),

$$V_\sigma(x(t)) \leq e^{-\omega_{1_\sigma}|\overline{\Upsilon}(\iota_{g(t)},t)|} e^{\omega_{2_\sigma}|\overline{\Omega}(\iota_{g(t)},t)|} V_\sigma(x(\iota_{g(t)})) + (\nu_{1_\sigma} + \nu_{3_\sigma}) e^{\omega_{2_\sigma}(t-\varphi_{m(t)})} \|w_t\|_\infty^2 \tag{4.43}$$

satisfies, $\forall t \in [\iota_{g(t)}, \varphi_{m(t)} + v_{m(t)})$. Using (3.40),

$$\|x(t)\|^2 \leq \frac{\overline{\alpha}_{\sigma(\iota^+_{g(t)})}}{\underline{\alpha}_{\sigma(\iota^+_{g(t)})}} e^{-\omega_{1_\sigma}|\overline{\Upsilon}(\iota_{g(t)},t)|} e^{\omega_{2_\sigma}|\overline{\Omega}(\iota_{g(t)},t)|} \|x(\iota_{g(t)})\|^2 + \frac{\nu_{1_\sigma} + \nu_{3_\sigma}}{\underline{\alpha}_{\sigma(\iota^+_{g(t)})}} e^{\omega_{2_\sigma}(t-\varphi_{m(t)})} \|w_t\|_\infty^2 \tag{4.44}$$

persists, $\forall t \in [\iota_{g(t)}, \varphi_{m(t)} + v_{m(t)})$. The results in (3.51) and (4.44), combined with an iterative process, lead to the following conclusions in Lemma 4.4.

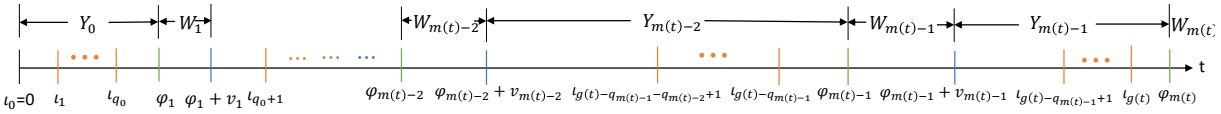

FIGURE 4.1: Time axis from 0 to t where red lines represent jump points, green lines represent the starting points of the interval $W_m, m \in \mathbb{N}$ where (3.17) may not hold, and blue lines represent the ending point of the interval $W_m, m \in \mathbb{N}$. Green lines are not jump points, but some blue lines may be jump points. This blue line and the next red line will be considered a single point in that scenario. For example, if $\varphi_1 + v_1$ is a jump point then $\varphi_1 + v_1 = \iota_{q_0+1}$.

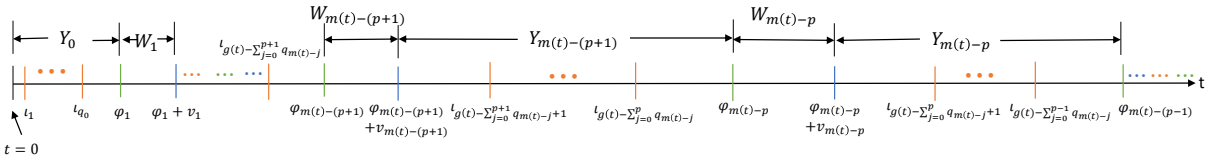

FIGURE 4.2: Time axis from 0 to t where $W_{m(t)-(p+1)}, Y_{m(t)-(p+1)}, W_{m(t)-p}$, and $Y_{m(t)-p}$ sections are highlighted and red lines represent jump points, green lines represent the starting points of the interval $W_m, m \in \mathbb{N}$ where (3.17) may not hold, and blue lines represent the ending point of the interval $W_m, m \in \mathbb{N}$.

Lemma 4.4. *For all $t \in [0, \varphi_{m(t)} + v_{m(t)})$, it follows that*

$$\|x(t)\|^2 \leq \frac{\overline{\alpha}_{\sigma(\iota_0^+)} \cdots \overline{\alpha}_{\sigma(\iota_{g(t)}^+)}}{\underline{\alpha}_{\sigma(\iota_0^+)} \cdots \underline{\alpha}_{\sigma(\iota_{g(t)}^+)}} e^{-\sum_{i=1}^{n_s} \omega_{1_i} |(\mathcal{O}_i \cap \overline{\Upsilon})(\iota_0, t)|} e^{\sum_{i=1}^{n_s} \omega_{2_i} |(\mathcal{O}_i \cap \overline{\Omega})(\iota_0, t)|} \|x(\iota_0)\|^2 + \frac{1}{\underline{\alpha}_{\sigma(\iota_{g(t)}^+)}}$$
$$\left[\sum_{\substack{l \in \mathbb{N}; \\ 0 \leq \iota_{g(t)-l} < \iota_{g(t)}}} \left\{ \nu_{1_{\sigma(\iota_{g(t)-l}^+)}} \prod_{\substack{j \in \mathbb{N}_0; \\ \iota_{g(t)-l} < \iota_{g(t)-j} \leq \iota_{g(t)}}} \left(\frac{\overline{\alpha}_{\sigma(\iota_{g(t)-j}^+)}}{\underline{\alpha}_{\sigma(\iota_{g(t)-(j+1)}^+)}} \right) e^{-(\sum_{i=1}^{n_s} \omega_{1_i} |(\mathcal{O}_i \cap \overline{\Upsilon})(\iota_{g(t)-(l-1)}, t)|)} \right.\right.$$
$$\left. e^{(\sum_{i=1}^{n_s} \omega_{2_i} |(\mathcal{O}_i \cap \overline{\Omega})(\iota_{g(t)-l}, t)|)} \right\} + \sum_{\substack{k \in \mathbb{N}_0; \\ q := \sum_{s=0}^{k} q_{m(t)-s} \leq g(t)}} \left\{ \left(\nu_{1_{\sigma(\iota_{g(t)-q}^+)}} + \nu_{3_{\sigma(\iota_{g(t)-q}^+)}} \right) \prod_{\substack{j \in \mathbb{N}_0; \\ \iota_{g(t)-q} < \iota_{g(t)-j} \leq \iota_{g(t)}}} \right.$$
$$\left.\left. \left(\frac{\overline{\alpha}_{\sigma(\iota_{g(t)-j}^+)}}{\underline{\alpha}_{\sigma(\iota_{g(t)-(j+1)}^+)}} \right) e^{-(\sum_{i=1}^{n_s} \omega_{1_i} |(\mathcal{O}_i \cap \overline{\Upsilon})(\iota_{g(t)-(q-1)}, t)|)} e^{(\sum_{i=1}^{n_s} \omega_{2_i} |(\mathcal{O}_i \cap \overline{\Omega})(\iota_{g(t)-q}, t)|)} \right\} \right] \|w_t\|_\infty^2, \quad (4.45)$$

by considering $q_{m(t)} = 0$ (because $Y_{m(t)}$ does not exist in Figure 4.1) and $|(\mathcal{O}_i \cap \overline{\Upsilon})(\iota_{g(t)+1}, t)| = 0$ (because $t < \iota_{g(t)+1}$ in Figure 4.1).

Proof of Lemma 4.4: Consider the interval Y_m where (3.17) holds true, and it contains q_m jump points (time instants when observer switching takes place). Lets consider $Y_{m(t)-1}$ interval which contains $q_{m(t)-1}$ jump points and last jump point is $\iota_{g(t)}$ shown in Figure

4.1. Therefore, from (3.51), it follows that

$$\|x(\iota_{g(t)})\|^2 \leq \frac{\overline{\alpha}_{\sigma(\iota^+_{g(t)-1})}\cdots\overline{\alpha}_{\sigma(\iota^+_{g(t)-q_{m(t)-1}+1})}}{\underline{\alpha}_{\sigma(\iota^+_{g(t)-1})}\cdots\underline{\alpha}_{\sigma(\iota^+_{g(t)-q_{m(t)-1}+1})}} e^{-\left(\sum_{i=1}^{n_s}\omega_{1_i}|\mathcal{O}_i(\iota_{g(t)-q_{m(t)-1}+1},\iota_{g(t)})|\right)}$$

$$\|x(\iota_{g(t)-q_{m(t)-1}+1})\|^2 + \left[\frac{\nu_{1_{\sigma(\iota^+_{g(t)-1})}}}{\underline{\alpha}_{\sigma(\iota^+_{g(t)-1})}} + \sum_{\substack{l\in\mathbb{N}\setminus 1;\\ \iota_{g(t)-q_{m(t)-1}+1}\leq\iota_{g(t)-l}<\iota_{g(t)}}}\left\{\frac{\nu_{1_{\sigma(\iota^+_{g(t)-l})}}}{\underline{\alpha}_{\sigma(\iota^+_{g(t)-1})}}\prod_{\substack{j\in\mathbb{N};\\ \iota_{g(t)-l}<\iota_{g(t)-j}<\iota_{g(t)}}}\left(\frac{\overline{\alpha}_{\sigma(\iota^+_{g(t)-j})}}{\underline{\alpha}_{\sigma(\iota^+_{g(t)-(j+1)})}}\right)e^{-\left(\sum_{i=1}^{n_s}\omega_{1_i}|\mathcal{O}_i(\iota_{g(t)-(l-1)},\iota_{g(t)})|\right)}\right\}\right]\|w_t\|^2_\infty. \tag{4.46}$$

Using the inequality of (4.46), in (4.44),

$$\|x(t)\|^2 \leq \frac{\overline{\alpha}_{\sigma(\iota^+_{g(t)})}\cdots\overline{\alpha}_{\sigma(\iota^+_{g(t)-q_{m(t)-1}+1})}}{\underline{\alpha}_{\sigma(\iota^+_{g(t)})}\cdots\underline{\alpha}_{\sigma(\iota^+_{g(t)-q_{m(t)-1}+1})}} e^{-\left(\sum_{i=1}^{n_s}\omega_{1_i}|(\mathcal{O}_i\cap\overline{\Upsilon})(\iota_{g(t)-q_{m(t)-1}+1},t)|\right)}$$

$$e^{\left(\sum_{i=1}^{n_s}\omega_{2_i}|(\mathcal{O}_i\cap\overline{\Omega})(\iota_{g(t)-q_{m(t)-1}+1},t)|\right)}\|x(\iota_{g(t)-q_{m(t)-1}+1})\|^2 + \frac{1}{\underline{\alpha}_{\sigma(\iota^+_{g(t)})}}\left[\left(\nu_{1_{\sigma(\iota^+_{g(t)})}}+\nu_{3_{\sigma(\iota^+_{g(t)})}}\right)\right.$$

$$e^{\omega_{2_{\sigma(\iota^+_{g(t)})}}(t-\varphi_{m(t)})} + \sum_{\substack{l\in\mathbb{N};\\ \iota_{g(t)-q_{m(t)-1}+1}\leq\iota_{g(t)-l}<\iota_{g(t)}}}\left\{\nu_{1_{\sigma(\iota^+_{g(t)-l})}}\prod_{\substack{j\in\mathbb{N}_0;\\ \iota_{g(t)-l}<\iota_{g(t)-j}\leq\iota_{g(t)}}}\left(\frac{\overline{\alpha}_{\sigma(\iota^+_{g(t)-j})}}{\underline{\alpha}_{\sigma(\iota^+_{g(t)-(j+1)})}}\right)\right.$$

$$\left.\left.e^{-\left(\sum_{i=1}^{n_s}\omega_{1_i}|(\mathcal{O}_i\cap\overline{\Upsilon})(\iota_{g(t)-(l-1)},t)|\right)}e^{\left(\sum_{i=1}^{n_s}\omega_{2_i}|(\mathcal{O}_i\cap\overline{\Omega})(\iota_{g(t)-(l-1)},t)|\right)}\right\}\right]\|w_t\|^2_\infty, \tag{4.47}$$

persist $\forall t \in \mathbb{R}_{\geq\iota_{g(t)-q_{m(t)-1}+1}}$ and for $|\overline{\Omega}(\iota_{g(t)-q_{m(t)-1}+1},\iota_{g(t)})| = 0$. From (4.43), it can be written that

$$V_{\sigma(\iota^+_{g(t)-q_{m(t)-1}})}(x(\varphi_{m(t)-1}+v_{m(t)-1})) \leq e^{-\left(\omega_{1_{\sigma(\iota^+_{g(t)-q_{m(t)-1}})}}|\overline{\Upsilon}(\iota_{g(t)-q_{m(t)-1}},\varphi_{m(t)-1}+v_{m(t)-1})|\right)}$$

$$e^{\left(\omega_{2_{\sigma(\iota^+_{g(t)-q_{m(t)-1}})}}|\overline{\Omega}(\iota_{g(t)-q_{m(t)-1}},\varphi_{m(t)-1}+v_{m(t)-1})|\right)}V_{\sigma(\iota^+_{g(t)-q_{m(t)-1}})}(x(\iota_{g(t)-q_{m(t)-1}}))$$

$$+\left(\nu_{1_{\sigma(\iota^+_{g(t)-q_{m(t)-1}})}}+\nu_{3_{\sigma(\iota^+_{g(t)-q_{m(t)-1}})}}\right)e^{\omega_{2_{\sigma(\iota^+_{g(t)-q_{m(t)-1}})}}v_{m(t)-1}}\|w_t\|^2_\infty. \tag{4.48}$$

Thus, (4.40) yields

$$V_{\sigma(\iota^+_{g(t)-q_{m(t)-1}})}(x(\iota_{g(t)-q_{m(t)-1}+1})) \leq e^{-\omega_{1_{\sigma(\iota^+_{g(t)-q_{m(t)-1}})}}\left(\iota_{g(t)-q_{m(t)-1}+1}-(\varphi_{m(t)-1}+v_{m(t)-1})\right)}$$
$$V_{\sigma(\iota^+_{g(t)-q_{m(t)-1}})}\left(x(\varphi_{m(t)-1}+v_{m(t)-1})\right)+\nu_{1_{\sigma(\iota^+_{g(t)-q_{m(t)-1}})}}\|w_t\|^2_\infty. \tag{4.49}$$

Using the inequality of (4.48) in (4.49), it follows that

$$V_{\sigma(\iota^+_{g(t)-q_{m(t)-1}})}(x(\iota_{g(t)-q_{m(t)-1}+1})) \leq e^{-\left(\omega_{1_{\sigma(\iota^+_{g(t)-q_{m(t)-1}})}}|\overline{\Upsilon}(\iota_{g(t)-q_{m(t)-1}},\iota_{g(t)-q_{m(t)-1}+1})|\right)}$$
$$e^{\left(\omega_{2_{\sigma(\iota^+_{g(t)-q_{m(t)-1}})}}|\overline{\Omega}(\iota_{g(t)-q_{m(t)-1}},\iota_{g(t)-q_{m(t)-1}+1})|\right)}V_{\sigma(\iota^+_{g(t)-q_{m(t)-1}})}(x(\iota_{g(t)-q_{m(t)-1}}))$$
$$+\left[\nu_{1_{\sigma(\iota^+_{g(t)-q_{m(t)-1}})}}e^{-\left(\omega_{1_{\sigma(\iota^+_{g(t)-q_{m(t)-1}})}}|\overline{\Upsilon}(\iota_{g(t)-q_{m(t)-1}},\varphi_{m(t)-1}+v_{m(t)-1})|\right)}\right.$$
$$e^{\left(\omega_{2_{\sigma(\iota^+_{g(t)-q_{m(t)-1}})}}|\overline{\Omega}(\iota_{g(t)-q_{m(t)-1}},\varphi_{m(t)-1}+v_{m(t)-1})|\right)}+\left(\nu_{1_{\sigma(\iota^+_{g(t)-q_{m(t)-1}})}}+\nu_{3_{\sigma(\iota^+_{g(t)-q_{m(t)-1}})}}\right)$$
$$\left.e^{\omega_{2_{\sigma(\iota^+_{g(t)-q_{m(t)-1}})}}v_{m(t)-1}}\right]\|w_t\|^2_\infty. \tag{4.50}$$

Hence,

$$\|x(\iota_{g(t)-q_{m(t)-1}+1})\|^2 \leq \frac{\overline{\alpha}_{\sigma(\iota^+_{g(t)-q_{m(t)-1}})}}{\underline{\alpha}_{\sigma(\iota^+_{g(t)-q_{m(t)-1}})}}e^{-\left(\omega_{1_{\sigma(\iota^+_{g(t)-q_{m(t)-1}})}}|\overline{\Upsilon}(\iota_{g(t)-q_{m(t)-1}},\iota_{g(t)-q_{m(t)-1}+1})|\right)}$$
$$e^{\left(\omega_{2_{\sigma(\iota^+_{g(t)-q_{m(t)-1}})}}|\overline{\Omega}(\iota_{g(t)-q_{m(t)-1}},\iota_{g(t)-q_{m(t)-1}+1})|\right)}\|x(\iota_{g(t)-q_{m(t)-1}})\|^2+\frac{1}{\underline{\alpha}_{\sigma(\iota^+_{g(t)-q_{m(t)-1}})}}$$
$$\left[\nu_{1_{\sigma(\iota^+_{g(t)-q_{m(t)-1}})}}e^{-\left(\omega_{1_{\sigma(\iota^+_{g(t)-q_{m(t)-1}})}}|\overline{\Upsilon}(\iota_{g(t)-q_{m(t)-1}},\varphi_{m(t)-1}+v_{m(t)-1})|\right)}\right.$$

$$e^{\left(\omega_{2_{\sigma(\iota^+_{g(t)-q_{m(t)-1}})}}|\overline{\Omega}(\iota_{g(t)-q_{m(t)-1}},\varphi_{m(t)-1}+v_{m(t)-1})|\right)}+\left(\nu_{1_{\sigma(\iota^+_{g(t)-q_{m(t)-1}})}}+\nu_{3_{\sigma(\iota^+_{g(t)-q_{m(t)-1}})}}\right)$$
$$e^{\omega_{2_{\sigma(\iota^+_{g(t)-q_{m(t)-1}})}}v_{m(t)-1}}\Big]\|w_t\|^2_\infty. \tag{4.51}$$

satisfies. Using the inequality of (4.51) in (4.47),

$$\|x(t)\|^2\leq\frac{\overline{\alpha}_{\sigma(\iota^+_{g(t)})}\cdots\overline{\alpha}_{\sigma(\iota^+_{g(t)-q_{m(t)-1}})}}{\underline{\alpha}_{\sigma(\iota^+_{g(t)})}\cdots\underline{\alpha}_{\sigma(\iota^+_{g(t)-q_{m(t)-1}})}}e^{-\left(\sum_{i=1}^{n_s}\omega_{1_i}|(\mathcal{O}_i\cap\overline{\Upsilon})(\iota_{g(t)-q_{m(t)-1}},t)|\right)}$$
$$e^{\left(\sum_{i=1}^{n_s}\omega_{2_i}|(\mathcal{O}_i\cap\overline{\Omega})(\iota_{g(t)-q_{m(t)-1}},t)|\right)}\|x(\iota_{g(t)-q_{m(t)-1}})\|^2+\frac{1}{\underline{\alpha}_\sigma}\Big[(\nu_{1_\sigma}+\nu_{3_\sigma})e^{\omega_{2\sigma}(t-\varphi_{m(t)})}$$
$$+\sum_{\substack{l\in\mathbb{N};\\ \iota_{g(t)-q_{m(t)-1}+1}\leq\iota_{g(t)-l}<\iota_{g(t)}}}\left\{\nu_{1_{\sigma(\iota^+_{g(t)-l})}}\prod_{\substack{j\in\mathbb{N}_0;\\ \iota_{g(t)-l}<\iota_{g(t)-j}\leq\iota_{g(t)}}}\left(\frac{\overline{\alpha}_{\sigma(\iota^+_{g(t)-j})}}{\underline{\alpha}_{\sigma(\iota^+_{g(t)-(j+1)})}}\right)\right.$$
$$\left.e^{-\left(\sum_{i=1}^{n_s}\omega_{1_i}|(\mathcal{O}_i\cap\overline{\Upsilon})(\iota_{g(t)-(l-1)},t)|\right)}e^{\left(\sum_{i=1}^{n_s}\omega_{2_i}|(\mathcal{O}_i\cap\overline{\Omega})(\iota_{g(t)-(l-1)},t)|\right)}\right\}$$
$$+\frac{\overline{\alpha}_{\sigma(\iota^+_{g(t)})}\cdots\overline{\alpha}_{\sigma(\iota^+_{g(t)-q_{m(t)-1}+1})}}{\underline{\alpha}_{\sigma(\iota^+_{g(t)-1})}\cdots\underline{\alpha}_{\sigma(\iota^+_{g(t)-q_{m(t)-1}+1})}\underline{\alpha}_{\sigma(\iota^+_{g(t)-q_{m(t)-1}})}}e^{-\left(\sum_{i=1}^{n_s}\omega_{1_i}|(\mathcal{O}_i\cap\overline{\Upsilon})(\iota_{g(t)-q_{m(t)-1}+1},t)|\right)}$$
$$e^{\left(\sum_{i=1}^{n_s}\omega_{2_i}|(\mathcal{O}_i\cap\overline{\Omega})(\iota_{g(t)-q_{m(t)-1}+1},t)|\right)}\left\{\nu_{1_{\sigma(\iota^+_{g(t)-q_{m(t)-1}})}}\right.$$
$$e^{-\left(\omega_{1_{\sigma(\iota^+_{g(t)-q_{m(t)-1}})}}|\overline{\Upsilon}(\iota_{g(t)-q_{m(t)-1}},\varphi_{m(t)-1}+v_{m(t)-1})|\right)}$$
$$e^{\left(\omega_{2_{\sigma(\iota^+_{g(t)-q_{m(t)-1}})}}|\overline{\Omega}(\iota_{g(t)-q_{m(t)-1}},\varphi_{m(t)-1}+v_{m(t)-1})|\right)}+\left(\nu_{1_{\sigma(\iota^+_{g(t)-q_{m(t)-1}})}}+\nu_{3_{\sigma(\iota^+_{g(t)-q_{m(t)-1}})}}\right)$$
$$\left.e^{\omega_{2_{\sigma(\iota^+_{g(t)-q_{m(t)-1}})}}v_{m(t)-1}}\right\}\Big]\|w_t\|^2_\infty \tag{4.52}$$

follows. From (4.52), the boundedness inequality

$$\|x(t)\|^2\leq\frac{\overline{\alpha}_{\sigma(\iota^+_{g(t)})}\cdots\overline{\alpha}_{\sigma(\iota^+_{g(t)-q_{m(t)-1}})}}{\underline{\alpha}_{\sigma(\iota^+_{g(t)})}\cdots\underline{\alpha}_{\sigma(\iota^+_{g(t)-q_{m(t)-1}})}}e^{-\left(\sum_{i=1}^{n_s}\omega_{1_i}|(\mathcal{O}_i\cap\overline{\Upsilon})(\iota_{g(t)-q_{m(t)-1}},t)|\right)}$$

$$e^{\left(\sum_{i=1}^{n_s}\omega_{2_i}|(\mathcal{O}_i\cap\overline{\Omega})(\iota_{g(t)-q_{m(t)-1}},t)|\right)}\|x(\iota_{g(t)-q_{m(t)-1}})\|^2+\frac{1}{\underline{\alpha}_\sigma}\Big[(\nu_{1_\sigma}+\nu_{3_\sigma})e^{\omega_{2\sigma}(t-\varphi_{m(t)})}$$
$$+\sum_{\substack{l\in\mathbb{N};\\ \iota_{g(t)-q_{m(t)-1}}\leq\iota_{g(t)-l}<\iota_{g(t)}}}\left\{\nu_{1_{\sigma(\iota^+_{g(t)-l})}}\prod_{\substack{j\in\mathbb{N}_0;\\ \iota_{g(t)-l}<\iota_{g(t)-j}\leq\iota_{g(t)}}}\left(\frac{\overline{\alpha}_{\sigma(\iota^+_{g(t)-j})}}{\underline{\alpha}_{\sigma(\iota^+_{g(t)-(j+1)})}}\right)\right.$$
$$\left.e^{-\left(\sum_{i=1}^{n_s}\omega_{1_i}|(\mathcal{O}_i\cap\overline{\Upsilon})(\iota_{g(t)-(l-1)},t)|\right)}e^{\left(\sum_{i=1}^{n_s}\omega_{2_i}|(\mathcal{O}_i\cap\overline{\Omega})(\iota_{g(t)-l},t)|\right)}\right\}+\left(\nu_{1_{\sigma(\iota^+_{g(t)-q_{m(t)-1}})}}\right.$$
$$\left.+\nu_{3_{\sigma(\iota^+_{g(t)-q_{m(t)-1}})}}\right)\frac{\overline{\alpha}_{\sigma(\iota^+_{g(t)})}\cdots\overline{\alpha}_{\sigma(\iota^+_{g(t)-q_{m(t)-1}+1})}}{\underline{\alpha}_{\sigma(\iota^+_{g(t)-1})}\cdots\underline{\alpha}_{\sigma(\iota^+_{g(t)-q_{m(t)-1}+1})}\underline{\alpha}_{\sigma(\iota^+_{g(t)-q_{m(t)-1}})}}$$
$$\left.e^{-\left(\sum_{i=1}^{n_s}\omega_{1_i}|(\mathcal{O}_i\cap\overline{\Upsilon})(\iota_{g(t)-q_{m(t)-1}+1},t)|\right)}e^{\left(\sum_{i=1}^{n_s}\omega_{2_i}|(\mathcal{O}_i\cap\overline{\Omega})(\iota_{g(t)-q_{m(t)-1}},t)|\right)}\right\}\Big]\|w_t\|^2_\infty \tag{4.53}$$

holds, by avoiding $\exp\left\{-\left(\omega_{1_{\sigma(\iota^+_{g(t)-q_{m(t)-1}})}}|\overline{\Upsilon}(\iota_{g(t)-q_{m(t)-1}},\varphi_{m(t)-1}+v_{m(t)-1})|\right)\right\}$ term because $exp\{-(a+b)\}\leq\exp\{-a\},\forall\{a,b\}\in\mathbb{R}_{\geq0}$. Rewrite (4.53),

$$\|x(t)\|^2\leq\frac{\overline{\alpha}_{\sigma(\iota^+_{g(t)})}\cdots\overline{\alpha}_{\sigma(\iota^+_{g(t)-q_{m(t)-1}})}}{\underline{\alpha}_{\sigma(\iota^+_{g(t)})}\cdots\underline{\alpha}_{\sigma(\iota^+_{g(t)-q_{m(t)-1}})}}e^{-\left(\sum_{i=1}^{n_s}\omega_{1_i}|(\mathcal{O}_i\cap\overline{\Upsilon})(\iota_{g(t)-q_{m(t)-1}},t)|\right)}$$
$$e^{\left(\sum_{i=1}^{n_s}\omega_{2_i}|(\mathcal{O}_i\cap\overline{\Omega})(\iota_{g(t)-q_{m(t)-1}},t)|\right)}\|x(\iota_{g(t)-q_{m(t)-1}})\|^2+\frac{1}{\underline{\alpha}_{\sigma(\iota^+_{g(t)})}}\left[\sum_{\substack{l\in\mathbb{N};\\ \iota_{g(t)-q_{m(t)-1}}\leq\iota_{g(t)-l}<\iota_{g(t)}}}\right.$$
$$\left\{\nu_{1_{\sigma(\iota^+_{g(t)-l})}}\prod_{\substack{j\in\mathbb{N}_0;\\ \iota_{g(t)-l}<\iota_{g(t)-j}\leq\iota_{g(t)}}}\left(\frac{\overline{\alpha}_{\sigma(\iota^+_{g(t)-j})}}{\underline{\alpha}_{\sigma(\iota^+_{g(t)-(j+1)})}}\right)e^{-\left(\sum_{i=1}^{n_s}\omega_{1_i}|(\mathcal{O}_i\cap\overline{\Upsilon})(\iota_{g(t)-(l-1)},t)|\right)}\right.$$
$$\left.e^{\left(\sum_{i=1}^{n_s}\omega_{2_i}|(\mathcal{O}_i\cap\overline{\Omega})(\iota_{g(t)-l},t)|\right)}\right\}+\sum_{\substack{k\in\mathbb{N}_0;\\ q:=\sum_{s=0}^{k}q_{m(t)-s}\leq q_{m(t)}+q_{m(t)-1}}}\left\{\left(\nu_{1_{\sigma(\iota^+_{g(t)-q})}}+\nu_{3_{\sigma(\iota^+_{g(t)-q})}}\right)\right.$$
$$\prod_{\substack{j\in\mathbb{N}_0;\\ \iota_{g(t)-q}<\iota_{g(t)-j}\leq\iota_{g(t)}}}\left(\frac{\overline{\alpha}_{\sigma(\iota^+_{g(t)-j})}}{\underline{\alpha}_{\sigma(\iota^+_{g(t)-(j+1)})}}\right)e^{-(\sum_{i=1}^{n_s}\omega_{1_i}|(\mathcal{O}_i\cap\overline{\Upsilon})(\iota_{g(t)-(q-1)},t)|)}$$
$$\left.\left.e^{(\sum_{i=1}^{n_s}\omega_{2_i}|(\mathcal{O}_i\cap\overline{\Omega})(\iota_{g(t)-q},t)|)}\right\}\right]\|w_t\|_\infty. \tag{4.54}$$

persists. Consider $Y_{m(t)-p}$ interval where $q_{m(t)-p}$ jump points are present (see in Figure 4.2). Since $x(t)$ is continuous, it can be written from (4.45) that

$$\|x(t)\|^2 \leq \frac{\overline{\alpha}_{\sigma(\iota^+_{g(t)})}\cdots\overline{\alpha}_{\sigma(\iota^+_{g(t)-\sum_{j=0}^{p}q_{m(t)-j}})}}{\underline{\alpha}_{\sigma(\iota^+_{g(t)})}\cdots\underline{\alpha}_{\sigma(\iota^+_{g(t)-\sum_{j=0}^{p}q_{m(t)-j}})}} e^{-\left(\sum_{i=1}^{n_s}\omega_{1_i}|(\mathcal{O}_i\cap\overline{\Upsilon})(\iota_{g(t)-\sum_{j=0}^{p}q_{m(t)-j}},t)|\right)}$$
$$e^{\left(\sum_{i=1}^{n_s}\omega_{2_i}|(\mathcal{O}_i\cap\overline{\Omega})(\iota_{g(t)-\sum_{j=0}^{p}q_{m(t)-j}},t)|\right)}\|x(\iota_{g(t)-\sum_{j=0}^{p}q_{m(t)-j}})\|^2+\frac{1}{\underline{\alpha}_{\sigma(\iota^+_{g(t)})}}$$
$$\Bigg[\sum_{\substack{l\in\mathbb{N};\\ \iota_{g(t)-\sum_{j=0}^{p}q_{m(t)-j}}\leq\iota_{g(t)-l}<\iota_{g(t)}}}\Bigg\{\nu_{1_{\sigma(\iota^+_{g(t)-l})}}\prod_{\substack{j\in\mathbb{N}_0;\\ \iota_{g(t)-l}<\iota_{g(t)-j}\leq\iota_{g(t)}}}\left(\frac{\overline{\alpha}_{\sigma(\iota^+_{g(t)-j})}}{\underline{\alpha}_{\sigma(\iota^+_{g(t)-(j+1)})}}\right)$$
$$e^{-\left(\sum_{i=1}^{n_s}\omega_{1_i}|(\mathcal{O}_i\cap\overline{\Upsilon})(\iota_{g(t)-(l-1)},t)|\right)}e^{\left(\sum_{i=1}^{n_s}\omega_{2_i}|(\mathcal{O}_i\cap\overline{\Omega})(\iota_{g(t)-l},t)|\right)}\Bigg\}+\sum_{\substack{k\in\mathbb{N}_0;\\ q:=\sum_{s=0}^{k}q_{m(t)-s}\leq\sum_{j=0}^{p}q_{m(t)-j}}}$$
$$\Bigg\{\left(\nu_{1_{\sigma(\iota^+_{g(t)-q})}}+\nu_{3_{\sigma(\iota^+_{g(t)-q})}}\right)\prod_{\substack{j\in\mathbb{N}_0;\\ \iota_{g(t)-q}<\iota_{g(t)-j}\leq\iota_{g(t)}}}\left(\frac{\overline{\alpha}_{\sigma(\iota^+_{g(t)-j})}}{\underline{\alpha}_{\sigma(\iota^+_{g(t)-(j+1)})}}\right)$$
$$e^{-(\sum_{i=1}^{n_s}\omega_{1_i}|(\mathcal{O}_i\cap\overline{\Upsilon})(\iota_{g(t)-(q-1)},t)|)}e^{(\sum_{i=1}^{n_s}\omega_{2_i}|(\mathcal{O}_i\cap\overline{\Omega})(\iota_{g(t)-q},t)|)}\Bigg\}\Bigg]\|w_t\|_\infty, \tag{4.55}$$

$\forall t\in\mathbb{R}_{\geq\iota_{g(t)-\sum_{j=0}^{p}q_{m(t)-j}}}$. $Y_{m(t)-(p+1)}$ contains $q_{m(t)-(p+1)}$ jump points. The jump points are $\iota_{g(t)-\sum_{j=0}^{p+1}q_{m(t)-j}+1}$ to $\iota_{g(t)-\sum_{j=0}^{p}q_{m(t)-j}}$. And the last jump points of $Y_{m(t)-(p+2)}$ is $\iota_{g(t)-\sum_{j=0}^{p+1}q_{m(t)-j}}$ (see in Figure 4.2). Hence from (4.46), it can be written that

$$\|x(\iota_{g(t)-\sum_{j=0}^{p}q_{m(t)-j}})\|^2 \leq \frac{\overline{\alpha}_{\sigma(\iota^+_{g(t)-\sum_{j=0}^{p}q_{m(t)-j}{}^{-1}})}\cdots\overline{\alpha}_{\sigma(\iota^+_{g(t)-\sum_{j=0}^{p+1}q_{m(t)-j}{}^{+1}})}}{\underline{\alpha}_{\sigma(\iota^+_{g(t)-\sum_{j=0}^{p}q_{m(t)-j}{}^{-1}})}\cdots\underline{\alpha}_{\sigma(\iota^+_{g(t)-\sum_{j=0}^{p+1}q_{m(t)-j}{}^{+1}})}}$$
$$e^{-\left(\sum_{i=1}^{n_s}\omega_{1_i}|\mathcal{O}_i(\iota_{g(t)-\sum_{j=0}^{p+1}q_{m(t)-j}{}^{+1}},\iota_{g(t)-\sum_{j=0}^{p}q_{m(t)-j}})|\right)}\|x(\iota_{g(t)-\sum_{j=0}^{p+1}q_{m(t)-j}+1})\|^2$$

$$+\left[\sum_{\substack{l\in\mathbb{N};\\ \iota_{g(t)-\sum_{j=0}^{p+1}q_{m(t)-j}+1}\leq\iota_{g(t)-l}<\iota_{g(t)-\sum_{j=0}^{p}q_{m(t)-j}}}}\left\{\frac{\nu_{1_{\sigma(\iota^{+}_{g(t)-l})}}}{\underline{\alpha}_{\sigma(\iota^{+}_{g(t)-\sum_{j=0}^{p}q_{m(t)-j}-1})}}\right.\right.$$

$$\left.\left.\prod_{\substack{j\in\mathbb{N};\\ \iota_{g(t)-l}<\iota_{g(t)-j}<\iota_{g(t)-\sum_{j=0}^{p}q_{m(t)-j}}}}\left(\frac{\overline{\alpha}_{\sigma(\iota^{+}_{g(t)-j})}}{\underline{\alpha}_{\sigma(\iota^{+}_{g(t)-(j+1)})}}\right)e^{-\left(\sum_{i=1}^{n_s}\omega_{1_i}|\mathcal{O}_i(\iota_{g(t)-(l-1)},\iota_{g(t)-\sum_{j=0}^{p}q_{m(t)-j}})|\right)}\right\}\right]$$

$$\|w_t\|^2_\infty. \tag{4.56}$$

Thus, (4.51) yields

$$\|x(\iota_{g(t)-\sum_{j=0}^{p+1}q_{m(t)-j}+1})\|^2\leq\frac{\overline{\alpha}_{\sigma(\iota^{+}_{g(t)-\sum_{j=0}^{p+1}q_{m(t)-j}})}}{\underline{\alpha}_{\sigma(\iota^{+}_{g(t)-\sum_{j=0}^{p+1}q_{m(t)-j}})}}$$

$$e^{-\left(\omega_{1_{\sigma(\iota^{+}_{g(t)-\sum_{j=0}^{p+1}q_{m(t)-j}})}}|\overline{\Upsilon}(\iota_{g(t)-\sum_{j=0}^{p+1}q_{m(t)-j}},\iota_{g(t)-\sum_{j=0}^{p+1}q_{m(t)-j}+1})|\right)}$$

$$e^{\left(\omega_{2_{\sigma(\iota^{+}_{g(t)-\sum_{j=0}^{p+1}q_{m(t)-j}})}}|\overline{\Omega}(\iota_{g(t)-\sum_{j=0}^{p+1}q_{m(t)-j}},\iota_{g(t)-\sum_{j=0}^{p+1}q_{m(t)-j}+1})|\right)}\|x(\iota_{g(t)-\sum_{j=0}^{p+1}q_{m(t)-j}})\|^2$$

$$+\frac{1}{\underline{\alpha}_{\sigma(\iota^{+}_{g(t)-\sum_{j=0}^{p+1}q_{m(t)-j}})}}\left[\nu_{1_{\sigma(\iota^{+}_{g(t)-\sum_{j=0}^{p+1}q_{m(t)-j}})}}\right.$$

$$e^{-\left(\omega_{1_{\sigma(\iota^{+}_{g(t)-\sum_{j=0}^{p+1}q_{m(t)-j}})}}|\overline{\Upsilon}(\iota_{g(t)-\sum_{j=0}^{p+1}q_{m(t)-j}},\varphi_{m(t)-(p+1)}+v_{m(t)-(p+1)})|\right)}$$

$$e^{\left(\omega_{2_{\sigma(\iota^{+}_{g(t)-\sum_{j=0}^{p+1}q_{m(t)-j}})}}|\overline{\Omega}(\iota_{g(t)-\sum_{j=0}^{p+1}q_{m(t)-j}},\varphi_{m(t)-(p+1)}+v_{m(t)-(p+1)})|\right)}$$

$$\left.+\left(\nu_{1_{\sigma(\iota^{+}_{g(t)-\sum_{j=0}^{p+1}q_{m(t)-j}})}}+\nu_{3_{\sigma(\iota^{+}_{g(t)-\sum_{j=0}^{p+1}q_{m(t)-j}})}}\right)e^{\omega_{2_{\sigma(\iota^{+}_{g(t)-\sum_{j=0}^{p+1}q_{m(t)-j}})}}v_{m(t)-(p+1)}}\right]\|w_t\|^2_\infty. \tag{4.57}$$

Using the inequality of (4.57), in (4.56), the boundedness inequality

$$\|x(\iota_{g(t)-\sum_{j=0}^{p} q_{m(t)-j}})\|^2 \leq \frac{\overline{\alpha}_{\sigma(\iota^+_{g(t)-\sum_{j=0}^{p} q_{m(t)-j}-1})} \cdots \overline{\alpha}_{\sigma(\iota^+_{g(t)-\sum_{j=0}^{p+1} q_{m(t)-j}})}}{\underline{\alpha}_{\sigma(\iota^+_{g(t)-\sum_{j=0}^{p} q_{m(t)-j}-1})} \cdots \underline{\alpha}_{\sigma(\iota^+_{g(t)-\sum_{j=0}^{p+1} q_{m(t)-j}})}}$$

$$e^{-\left(\sum_{i=1}^{n_s} \omega_{1_i} |\mathcal{O}_i(\iota_{g(t)-\sum_{j=0}^{p+1} q_{m(t)-j}}, \iota_{g(t)-\sum_{j=0}^{p} q_{m(t)-j}})|\right)} \|x(\iota_{g(t)-\sum_{j=0}^{p+1} q_{m(t)-j}})\|^2$$

$$+ \left[\sum_{\substack{l\in\mathbb{N}; \\ \iota_{g(t)-\sum_{j=0}^{p+1} q_{m(t)-j}+1} \leq \iota_{g(t)-l} < \iota_{g(t)-\sum_{j=0}^{p} q_{m(t)-j}}}} \left\{ \frac{\nu_{1_{\sigma(\iota^+_{g(t)-l})}}}{\underline{\alpha}_{\sigma(\iota^+_{g(t)-\sum_{j=0}^{p} q_{m(t)-j}-1})}} \right.\right.$$

$$\left.\left. \prod_{\substack{j\in\mathbb{N}; \\ \iota_{g(t)-l} < \iota_{g(t)-j} < \iota_{g(t)-\sum_{j=0}^{p} q_{m(t)-j}}}} \left(\frac{\overline{\alpha}_{\sigma(\iota^+_{g(t)-j})}}{\underline{\alpha}_{\sigma(\iota^+_{g(t)-(j+1)})}} \right) e^{-\left(\sum_{i=1}^{n_s} \omega_{1_i} |\mathcal{O}_i(\iota_{g(t)-(l-1)}, \iota_{g(t)-\sum_{j=0}^{p} q_{m(t)-j}})|\right)} \right\} \right.$$

$$+ \frac{\overline{\alpha}_{\sigma(\iota^+_{g(t)-\sum_{j=0}^{p} q_{m(t)-j}-1})} \cdots \overline{\alpha}_{\sigma(\iota^+_{g(t)-\sum_{j=0}^{p+1} q_{m(t)-j}+1})}}{\underline{\alpha}_{\sigma(\iota^+_{g(t)-\sum_{j=0}^{p} q_{m(t)-j}-1})} \cdots \underline{\alpha}_{\sigma(\iota^+_{g(t)-\sum_{j=0}^{p+1} q_{m(t)-j}+1})} \underline{\alpha}_{\sigma(\iota^+_{g(t)-\sum_{j=0}^{p+1} q_{m(t)-j}})}}$$

$$e^{-\left(\sum_{i=1}^{n_s} \omega_{1_i} |\mathcal{O}_i(\iota_{g(t)-\sum_{j=0}^{p+1} q_{m(t)-j}+1}, \iota_{g(t)-\sum_{j=0}^{p} q_{m(t)-j}})|\right)} \left\{ \nu_{1_{\sigma(\iota^+_{g(t)-\sum_{j=0}^{p+1} q_{m(t)-j}})}} \right.$$

$$e^{-\left(\omega_{1_{\sigma(\iota^+_{g(t)-\sum_{j=0}^{p+1} q_{m(t)-j}})}} |\overline{\Upsilon}(\iota_{g(t)-\sum_{j=0}^{p+1} q_{m(t)-j}}, \varphi_{m(t)-(p+1)}+v_{m(t)-(p+1)})|\right)}$$

$$e^{\left(\omega_{2_{\sigma(\iota^+_{g(t)-\sum_{j=0}^{p+1} q_{m(t)-j}})}} |\overline{\Omega}(\iota_{g(t)-\sum_{j=0}^{p+1} q_{m(t)-j}}, \varphi_{m(t)-(p+1)}+v_{m(t)-(p+1)})|\right)} + \left(\nu_{1_{\sigma(\iota^+_{g(t)-\sum_{j=0}^{p+1} q_{m(t)-j}})}} \right.$$

$$\left.\left. \left. + \nu_{3_{\sigma(\iota^+_{g(t)-\sum_{j=0}^{p+1} q_{m(t)-j}})}} \right) e^{\omega_{2_{\sigma(\iota^+_{g(t)-\sum_{j=0}^{p+1} q_{m(t)-j}})}} v_{m(t)-(p+1)}} \right\} \right] \|w_t\|^2_\infty \tag{4.58}$$

is reached. By resizing (4.58),

$$\|x(\iota_{g(t)-\sum_{j=0}^{p} q_{m(t)-j}})\|^2 \leq \frac{\overline{\alpha}_{\sigma(\iota^+_{g(t)-\sum_{j=0}^{p} q_{m(t)-j}-1})} \cdots \overline{\alpha}_{\sigma(\iota^+_{g(t)-\sum_{j=0}^{p+1} q_{m(t)-j}})}}{\underline{\alpha}_{\sigma(\iota^+_{g(t)-\sum_{j=0}^{p} q_{m(t)-j}-1})} \cdots \underline{\alpha}_{\sigma(\iota^+_{g(t)-\sum_{j=0}^{p+1} q_{m(t)-j}})}}$$

$$e^{-\left(\sum_{i=1}^{n_s} \omega_{1_i} |\mathcal{O}_i(\iota_{g(t)-\sum_{j=0}^{p+1} q_{m(t)-j}}, \iota_{g(t)-\sum_{j=0}^{p} q_{m(t)-j}})|\right)} \|x(\iota_{g(t)-\sum_{j=0}^{p+1} q_{m(t)-j}})\|^2$$

$$+ \frac{1}{\underline{\alpha}_{\sigma(\iota^+_{g(t)-\sum_{j=0}^{p} q_{m(t)-j}-1})}} \left[\sum_{\substack{l\in\mathbb{N}; \\ \iota_{g(t)-\sum_{j=0}^{p+1} q_{m(t)-j}} \leq \iota_{g(t)-l} < \iota_{g(t)-\sum_{j=0}^{p} q_{m(t)-j}}}} \left\{ \nu_{1_{\sigma(\iota^+_{g(t)-l})}} \right.\right.$$

$$\prod_{\substack{j\in\mathbb{N}; \\ \iota_{g(t)-l} < \iota_{g(t)-j} < \iota_{g(t)-\sum_{j=0}^{p} q_{m(t)-j}}}} \left(\frac{\overline{\alpha}_{\sigma(\iota^+_{g(t)-j})}}{\underline{\alpha}_{\sigma(\iota^+_{g(t)-(j+1)})}} \right) e^{-\left(\sum_{i=1}^{n_s} \omega_{1_i} |\mathcal{O}_i(\iota_{g(t)-(l-1)}, \iota_{g(t)-\sum_{j=0}^{p} q_{m(t)-j}})|\right)}$$

$$e^{\left(\omega_{2_{\sigma(\iota^+_{g(t)-\sum_{j=0}^{p+1} q_{m(t)-j}})}} |\bar{\Omega}(\iota_{g(t)-\sum_{j=0}^{p+1} q_{m(t)-j}}, \varphi_{m(t)-(p+1)} + v_{m(t)-(p+1)})|\right)} + \left(\nu_{1_{\sigma(\iota^+_{g(t)-\sum_{j=0}^{p+1} q_{m(t)-j}})}} \right.$$

$$\left. + \nu_{3_{\sigma(\iota^+_{g(t)-\sum_{j=0}^{p+1} q_{m(t)-j}})}} \right) \frac{\overline{\alpha}_{\sigma(\iota^+_{g(t)-\sum_{j=0}^{p} q_{m(t)-j}-1})} \cdots \overline{\alpha}_{\sigma(\iota^+_{g(t)-\sum_{j=0}^{p+1} q_{m(t)-j}+1})}}{\underline{\alpha}_{\sigma(\iota^+_{g(t)-\sum_{j=0}^{p} q_{m(t)-j}-2})} \cdots \underline{\alpha}_{\sigma(\iota^+_{g(t)-\sum_{j=0}^{p+1} q_{m(t)-j}})}}$$

$$\left. e^{\omega_{2_{\sigma(\iota^+_{g(t)-\sum_{j=0}^{p+1} q_{m(t)-j}})}} v_{m(t)-(p+1)}} \right\} \Bigg] \|w_t\|^2_\infty, \tag{4.59}$$

follows by avoiding $e^{-\left(\omega_{1_{\sigma(\iota^+_{g(t)-\sum_{j=0}^{p+1} q_{m(t)-j}})}} |\bar{\Upsilon}(\iota_{g(t)-\sum_{j=0}^{p+1} q_{m(t)-j}}, \varphi_{m(t)-(p+1)} + v_{m(t)-(p+1)})|\right)}$ term because $e^{-(a+b)} \leq e^{-a}, \forall\{a,b\} \in \mathbb{R}_{\geq 0}$. Therefore using the inequality (4.59) in (4.55), it

follows that

$$\|x(t)\|^2 \leq \frac{\overline{\alpha}_{\sigma(\iota^+_{g(t)})} \cdots \overline{\alpha}_{\sigma(\iota^+_{g(t)-\sum_{j=0}^{p+1} q_{m(t)-j}})}}{\underline{\alpha}_{\sigma(\iota^+_{g(t)})} \cdots \underline{\alpha}_{\sigma(\iota^+_{g(t)-\sum_{j=0}^{p+1} q_{m(t)-j}})}} e^{-\left(\sum_{i=1}^{n_s} \omega_{1_i} |(\mathcal{O}_i \cap \overline{\Upsilon})(\iota_{g(t)-\sum_{j=0}^{p+1} q_{m(t)-j}}, t)|\right)}$$

$$e^{\left(\sum_{i=1}^{n_s} \omega_{2_i} |(\mathcal{O}_i \cap \overline{\Omega})(\iota_{g(t)-\sum_{j=0}^{p+1} q_{m(t)-j}}, t)|\right)} \|x\big(\iota_{g(t)-\sum_{j=0}^{p+1} q_{m(t)-j}}\big)\|^2 + \frac{1}{\underline{\alpha}_{\sigma(\iota^+_{g(t)})}}$$

$$\Bigg[\sum_{\substack{l \in \mathbb{N}; \\ \iota_{g(t)-\sum_{j=0}^{p} q_{m(t)-j}} \leq \iota_{g(t)-l} < \iota_{g(t)}}} \Bigg\{ \nu_{1_{\sigma(\iota^+_{g(t)-l})}} \prod_{\substack{j \in \mathbb{N}_0; \\ \iota_{g(t)-l} < \iota_{g(t)-j} \leq \iota_{g(t)}}} \left(\frac{\overline{\alpha}_{\sigma(\iota^+_{g(t)-j})}}{\underline{\alpha}_{\sigma(\iota^+_{g(t)-(j+1)})}} \right)$$

$$e^{-\left(\sum_{i=1}^{n_s} \omega_{1_i} |(\mathcal{O}_i \cap \overline{\Upsilon})(\iota_{g(t)-(l-1)}, t)|\right)} e^{\left(\sum_{i=1}^{n_s} \omega_{2_i} |(\mathcal{O}_i \cap \overline{\Omega})(\iota_{g(t)-l}, t)|\right)} \Bigg\} + \sum_{\substack{k \in \mathbb{N}_0; \\ q := \sum_{s=0}^{k} q_{m(t)-s} \leq \sum_{j=0}^{p} q_{m(t)-j}}}$$

$$\Bigg\{ \left(\nu_{1_{\sigma(\iota^+_{g(t)-q})}} + \nu_{3_{\sigma(\iota^+_{g(t)-q})}} \right) \prod_{\substack{j \in \mathbb{N}_0; \\ \iota_{g(t)-q} < \iota_{g(t)-j} \leq \iota_{g(t)}}} \left(\frac{\overline{\alpha}_{\sigma(\iota^+_{g(t)-j})}}{\underline{\alpha}_{\sigma(\iota^+_{g(t)-(j+1)})}} \right) e^{-\left(\sum_{i=1}^{n_s} \omega_{1_i} |(\mathcal{O}_i \cap \overline{\Upsilon})(\iota_{g(t)-(q-1)}, t)|\right)}$$

$$e^{\left(\sum_{i=1}^{n_s} \omega_{2_i} |(\mathcal{O}_i \cap \overline{\Omega})(\iota_{g(t)-q}, t)|\right)} \Bigg\} + \frac{\overline{\alpha}_{\sigma(\iota^+_{g(t)})} \cdots \overline{\alpha}_{\sigma(\iota^+_{g(t)-\sum_{j=0}^{p} q_{m(t)-j}})}}{\underline{\alpha}_{\sigma(\iota^+_{g(t)-1})} \cdots \underline{\alpha}_{\sigma(\iota^+_{g(t)-\sum_{j=0}^{p} q_{m(t)-j}-1})}}$$

$$e^{-\left(\sum_{i=1}^{n_s} \omega_{1_i} |(\mathcal{O}_i \cap \overline{\Upsilon})(\iota_{g(t)-\sum_{j=0}^{p} q_{m(t)-j}}, t)|\right)} e^{\left(\sum_{i=1}^{n_s} \omega_{2_i} |(\mathcal{O}_i \cap \overline{\Omega})(\iota_{g(t)-\sum_{j=0}^{p} q_{m(t)-j}}, t)|\right)}$$

$$\Bigg[\sum_{\substack{l \in \mathbb{N}; \\ \iota_{g(t)-\sum_{j=0}^{p+1} q_{m(t)-j}} \leq \iota_{g(t)-l} < \iota_{g(t)-\sum_{j=0}^{p} q_{m(t)-j}}}} \Bigg\{ \nu_{1_{\sigma(\iota^+_{g(t)-l})}} \prod_{\substack{j \in \mathbb{N}; \\ \iota_{g(t)-l} < \iota_{g(t)-j} < \iota_{g(t)-\sum_{j=0}^{p} q_{m(t)-j}}}}$$

$$\left(\frac{\overline{\alpha}_{\sigma(\iota^+_{g(t)-j})}}{\underline{\alpha}_{\sigma(\iota^+_{g(t)-(j+1)})}} \right) e^{-\left(\sum_{i=1}^{n_s} \omega_{1_i} |\mathcal{O}_i(\iota_{g(t)-(l-1)}, \iota_{g(t)-\sum_{j=0}^{p} q_{m(t)-j}})|\right)} \Bigg\}$$

$$e^{\left(\omega_{2_{\sigma(\iota^+_{g(t)-\sum_{j=0}^{p+1} q_{m(t)-j}})}} |\bar{\Omega}(\iota_{g(t)-\sum_{j=0}^{p+1} q_{m(t)-j}}, \varphi_{m(t)-(p+1)} + v_{m(t)-(p+1)})|\right)} + \left(\nu_{1_{\sigma(\iota^+_{g(t)-\sum_{j=0}^{p+1} q_{m(t)-j}})}} \right.$$

$$\left. + \nu_{3_{\sigma(\iota^+_{g(t)-\sum_{j=0}^{p+1} q_{m(t)-j}})}} \right) \frac{\overline{\alpha}_{\sigma(\iota^+_{g(t)-\sum_{j=0}^{p} q_{m(t)-j}-1})} \cdots \overline{\alpha}_{\sigma(\iota^+_{g(t)-\sum_{j=0}^{p+1} q_{m(t)-j}+1})}}{\underline{\alpha}_{\sigma(\iota^+_{g(t)-\sum_{j=0}^{p} q_{m(t)-j}-2})} \cdots \underline{\alpha}_{\sigma(\iota^+_{g(t)-\sum_{j=0}^{p+1} q_{m(t)-j}})}}$$

$$e^{\omega_{2_{\sigma(\iota^+_{g(t)-\sum_{j=0}^{p+1} q_{m(t)-j}})}} v_{m(t)-(p+1)}}\Bigg]\Bigg] \|w_t\|^2_\infty. \tag{4.60}$$

Resizing (4.60),

$$\|x(t)\|^2 \leq \frac{\overline{\alpha}_{\sigma(\iota^+_{g(t)})} \cdots \overline{\alpha}_{\sigma(\iota^+_{g(t)-\sum_{j=0}^{p+1} q_{m(t)-j}})}}{\underline{\alpha}_{\sigma(\iota^+_{g(t)})} \cdots \underline{\alpha}_{\sigma(\iota^+_{g(t)-\sum_{j=0}^{p+1} q_{m(t)-j}})}} e^{-\left(\sum_{i=1}^{n_s} \omega_{1_i} |(\mathcal{O}_i \cap \overline{\Upsilon})(\iota_{g(t)-\sum_{j=0}^{p+1} q_{m(t)-j}}, t)|\right)}$$
$$e^{\left(\sum_{i=1}^{n_s} \omega_{2_i} |(\mathcal{O}_i \cap \overline{\Omega})(\iota_{g(t)-\sum_{j=0}^{p+1} q_{m(t)-j}}, t)|\right)} \|x(\iota_{g(t)-\sum_{j=0}^{p+1} q_{m(t)-j}})\|^2 + \frac{1}{\underline{\alpha}_{\sigma(\iota^+_{g(t)})}}$$
$$\Bigg[\sum_{\substack{l \in \mathbb{N}; \\ \iota_{g(t)-\sum_{j=0}^{p+1} q_{m(t)-j}} \leq \iota_{g(t)-l} < \iota_{g(t)}}} \Bigg\{ \nu_{1_{\sigma(\iota^+_{g(t)-l})}} \prod_{\substack{j \in \mathbb{N}_0; \\ \iota_{g(t)-l} < \iota_{g(t)-j} \leq \iota_{g(t)}}} \left(\frac{\overline{\alpha}_{\sigma(\iota^+_{g(t)-j})}}{\underline{\alpha}_{\sigma(\iota^+_{g(t)-(j+1)})}} \right)$$
$$e^{-\left(\sum_{i=1}^{n_s} \omega_{1_i} |(\mathcal{O}_i \cap \overline{\Upsilon})(\iota_{g(t)-(l-1)}, t)|\right)} e^{\left(\sum_{i=1}^{n_s} \omega_{2_i} |(\mathcal{O}_i \cap \overline{\Omega})(\iota_{g(t)-l}, t)|\right)} \Bigg\} + \sum_{\substack{k \in \mathbb{N}_0; \\ q := \sum_{s=0}^{k} q_{m(t)-s} \leq \sum_{j=0}^{p+1} q_{m(t)-j}}}$$
$$\Bigg\{ \left(\nu_{1_{\sigma(\iota^+_{g(t)-q})}} + \nu_{3_{\sigma(\iota^+_{g(t)-q})}} \right) \prod_{\substack{j \in \mathbb{N}_0; \\ \iota_{g(t)-q} < \iota_{g(t)-j} \leq \iota_{g(t)}}} \left(\frac{\overline{\alpha}_{\sigma(\iota^+_{g(t)-j})}}{\underline{\alpha}_{\sigma(\iota^+_{g(t)-(j+1)})}} \right)$$
$$e^{-\left(\sum_{i=1}^{n_s} \omega_{1_i} |(\mathcal{O}_i \cap \overline{\Upsilon})(\iota_{g(t)-(q-1)}, t)|\right)} e^{\left(\sum_{i=1}^{n_s} \omega_{2_i} |(\mathcal{O}_i \cap \overline{\Omega})(\iota_{g(t)-q}, t)|\right)} \Bigg\} \Bigg] \|w_t\|_\infty \tag{4.61}$$

follows, $\forall t \in \mathbb{R}_{\geq \iota_{g(t)-\sum_{j=0}^{p+1} q_{m(t)-j}}}$, which concludes the proof. ■

To ensure that the overall system is input-to-state stable (ISS), the term associated with the disturbance norm $\|w_t\|_\infty$ must be bounded, and the term associated with the initial state norm $\|x(\iota_0)\|$ must exhibit convergent behaviour in (4.45). The satisfaction of these conditions guarantees that the effect of external disturbances remains bounded while the influence of the initial state diminishes over time. The following two lemmas, namely Lemmas 4.5 and 4.6, formally establish these properties by providing sufficient conditions for boundedness and convergence, respectively.

Lemma 4.5. *Under Assumptions 3.1, 4.1, and 4.2 and condition (3.32) and (3.33) in Lemma 3.7, the sum*

$$\frac{1}{\underline{\alpha}_{\sigma(\iota^+_{g(t)})}} \sum_{\substack{k\in\mathbb{N}_0;\\ q:=\sum_{s=0}^{k} q_{m(t)-s}\le g(t)}} \left(\nu_{1_{\sigma(\iota^+_{g(t)-q})}} + \nu_{3_{\sigma(\iota^+_{g(t)-q})}}\right) \prod_{\substack{j\in\mathbb{N}_0;\\ \iota_{g(t)-q}<\iota_{g(t)-j}\le\iota_{g(t)}}} \left(\frac{\overline{\alpha}_{\sigma(\iota^+_{g(t)-j})}}{\underline{\alpha}_{\sigma(\iota^+_{g(t)-(j+1)})}}\right) e^{-(\sum_{i=1}^{n_s}\omega_{1_i}|(\mathcal{O}_i\cap\overline{\Upsilon})(\iota_{g(t)-(q-1)},t)|)} e^{(\sum_{i=1}^{n_s}\omega_{2_i}|(\mathcal{O}_i\cap\overline{\Omega})(\iota_{g(t)-q},t)|)} \tag{4.62}$$

is bounded from above.

Proof of Lemma 4.5 : Let's take the exponential term of (4.62),

$$\begin{aligned}
&\sum_{\substack{k\in\mathbb{N}_0;\\ q\le g(t)}} e^{-(\sum_{i=1}^{n_s}\omega_{1_i}|(\mathcal{O}_i\cap\overline{\Upsilon})(\iota_{g(t)-(q-1)},t)|)} e^{(\sum_{i=1}^{n_s}\omega_{2_i}|(\mathcal{O}_i\cap\overline{\Omega})(\iota_{g(t)-q},t)|)} \\
&= \sum_{\substack{k\in\mathbb{N}_0;\\ q\le g(t)}} e^{-\left\{\omega_{1_{\sigma(\iota^+_{g(t)})}}|\overline{\Upsilon}(\iota_{g(t)},t)|+\omega_{1_{\sigma(\iota^+_{g(t)-1})}}|\overline{\Upsilon}(\iota_{g(t)-1},\iota_{g(t)})|+\cdots+\omega_{1_{\sigma(\iota^+_{g(t)-(q-1)})}}|\overline{\Upsilon}(\iota_{g(t)-(q-1)},\iota_{g(t)-(q-2)})|\right\}} \\
&\quad e^{\left\{\omega_{2_{\sigma(\iota^+_{g(t)})}}|\overline{\Omega}(\varphi_{m(t)},t)|+\omega_{2_{\sigma(\iota^+_{g(t)-q_{m(t)-1}})}}|\overline{\Omega}(\varphi_{m(t)-1},\iota_{g(t)-q_{m(t)-1}+1}|)+\cdots+\omega_{2_{\sigma(\iota^+_{g(t)-q})}}|\overline{\Omega}(\varphi_{m(t)-k},\iota_{g(t)-(q-1)})|\right\}}.
\end{aligned} \tag{4.63}$$

Note that

$$|\overline{\Omega}(\tau,t)| \le |\Omega(\tau,t)| + (1+n(\tau,t))\underline{\Delta} \tag{4.64}$$

$\forall t,\tau\in\mathbb{R}_{\ge 0}$ with $t>\tau$. In words, $|\overline{\Omega}(\tau,t)|$ can be upper bounded by the total length of DoS over $[\tau,t]$ plus the maximum actuation delay $\underline{\Delta}$, which may occur once at the beginning of the interval $[\tau,t]$ (as a result of a previous FSDoS) plus $n(\tau,t)$ times, where $n(\tau,t)$ represents the number of off/on transitions of FSDoS occurring over $[\tau,t)$. From Assumption 4.1 and 4.2, it follows that

$$|\overline{\Omega}(\tau,t)| \le \zeta + \frac{t-\tau}{T} + \left(1+\varrho\frac{t-\tau}{\tau_f}\right)\underline{\Delta} =: \zeta_* + \frac{t-\tau}{T_*}, \tag{4.65}$$

considering $\zeta_* := \zeta + (1+\varrho)\underline{\Delta}$ and $T_* := T\tau_F/(T\underline{\Delta} + \tau_F)$. With this in mind, the sum term in (4.63) can now be analyzed. From the above inequality,

$$|\overline{\Omega}(\varphi_{m(t)}, t)| \leq \zeta_* + \frac{t - \varphi_{m(t)}}{T_*} \tag{4.66}$$

holds, $\forall t \in \mathbb{R}_{\geq \varphi_{m(t)}}, m \in \mathbb{N}$. Similarly, $|\overline{\Omega}(\varphi_{m(t)-1}, \iota_{g(t)-(q_{m(t)-1}-1)})| \leq (\iota_{g(t)-(q_{m(t)-1}-1)} - \varphi_{m(t)-1})/T_*$ and $|\overline{\Omega}(\varphi_{m(t)-k}, \iota_{g(t)-(q-1)})| \leq (\iota_{g(t)-(q-1)} - \varphi_{m(t)-k})/T_*$ satisfy. Consider next $|\overline{\Upsilon}(\iota_{g(t)-(q-1)}, \iota_{g(t)-(q-2)})|$. The constant term ζ_* is avoided in the rest of the intervals. Hence, it follows

$$|\overline{\Upsilon}(\iota_{g(t)}, t)| = t - \iota_{g(t)} - |\overline{\Omega}(\varphi_{m(t)}, t)| \tag{4.67}$$

$\forall t \in \mathbb{R}_{\varphi_{m(t)}}$, where $\varphi_{m(t)} > \iota_{g(t)}$. Similarly, $|\overline{\Upsilon}(\iota_{g(t)-1}, \iota_{g(t)})| = \iota_{g(t)} - \iota_{g(t)-1} - |\overline{\Omega}(\iota_{g(t)-1}, \iota_{g(t)})| = \iota_{g(t)} - \iota_{g(t)-1}, |\overline{\Upsilon}(\iota_{g(t)-q_{m(t)-1}}, \iota_{g(t)-q_{m(t)-1}+1})| = \iota_{g(t)-q_{m(t)-1}+1} - \iota_{g(t)-q_{m(t)-1}} - |\overline{\Omega}(\varphi_{m(t)-1}, \iota_{g(t)-q_{m(t)-1}+1})|$, and $|\overline{\Upsilon}(\iota_{g(t)-(q-1)}, \iota_{g(t)-(q-2)})| = \iota_{g(t)-(q-2)} - \varphi_{m(t)-k} - |\overline{\Omega}(\varphi_{m(t)-k}, \iota_{g(t)-(q-1)})|$. Hence, from (4.63),

$$\begin{aligned}
&\sum_{\substack{k\in\mathbb{N}_0;\\ q\leq g(t)}} \exp\left\{\begin{array}{l} -\left[\sum_{i=1}^{n_s} \omega_{1_i}|\mathcal{O}_i(\varphi_{m(t)-k},t)| - \left\{\left(\omega_{1_{\sigma(\iota^+_{g(t)})}} + \omega_{2_{\sigma(\iota^+_{g(t)})}}\right)|\overline{\Omega}(\varphi_{m(t)},t)|\right.\right. \\ + \left(\omega_{1_{\sigma(\iota^+_{g(t)-q_{m(t)-1}})}} + \omega_{2_{\sigma(\iota^+_{g(t)-q_{m(t)-1}})}}\right)|\overline{\Omega}(\varphi_{m(t)-1},\iota_{g(t)-(q_{m(t)-1}-1)})| \\ \left.\left. + \cdots + \left(\omega_{1_{\sigma(\iota^+_{g(t)-q})}} + \omega_{2_{\sigma(\iota^+_{g(t)-q})}}\right)|\overline{\Omega}(\varphi_{m(t)-k},\iota_{g(t)-(q-1)})|\right\}\right] \end{array}\right\} \\
&\leq \exp\left\{\left(\omega_{1_{\sigma(\iota^+_{g(t)})}} + \omega_{2_{\sigma(\iota^+_{g(t)})}}\right)\zeta_*\right\} \\
&\sum_{\substack{k\in\mathbb{N}_0;\\ q\leq g(t)}} \exp\left\{\begin{array}{l} -\left[\sum_{i=1}^{n_s} \omega_{1_i}|\mathcal{O}_i(\varphi_{m(t)-k},t)| - \frac{1}{T_*}\left\{\left(\omega_{1_{\sigma(\iota^+_{g(t)})}} + \omega_{2_{\sigma(\iota^+_{g(t)})}}\right)\left(t-\varphi_{m(t)}\right)\right.\right. \\ + \left(\omega_{1_{\sigma(\iota^+_{g(t)-q_{m(t)-1}})}} + \omega_{2_{\sigma(\iota^+_{g(t)-q_{m(t)-1}})}}\right)\left(\iota_{g(t)-(q_{m(t)-1}-1)}-\varphi_{m(t)-1}\right) \\ \left.\left. + \cdots + \left(\omega_{1_{\sigma(\iota^+_{g(t)-q})}} + \omega_{2_{\sigma(\iota^+_{g(t)-q})}}\right)\left(\iota_{g(t)-(q-1)}-\varphi_{m(t)-k}\right)\right] \end{array}\right\}
\end{aligned} \tag{4.68}$$

persists. Moreover, Assumption 3.1 and Assumption 4.1 yields

$$t - \varphi_{m(t)} \geq \tau_F n(\varphi_{m(t)}, t) - \tau_F \varrho = \tau_F - \tau_F \varrho \tag{4.69}$$

where $n(\varphi_{m(t)}, t) = 1$ because only one FSDoS on transition is present in $[\varphi_{m(t)}, t)$ interval and $l(\varphi_{m(t)}, t) = 0$ because $[\varphi_{m(t)}, t)$ is operated in a single switching mode considering that $t < \varphi_{m(t)} + \upsilon_{m(t)}$. Similarly, $\iota_{g(t)-(q_{m(t)-1}-1)} - \varphi_{m(t)-1} \geq \tau_F, \iota_{g(t)-(q-1)} - \varphi_{m(t)-k} \geq \tau_F$ and so on, are obtained by avoiding the constant term ϱ in the remaining cases. Again, Assumption 3.1 and Assumption 4.1 yields

$$\varphi_{m(t)} - \iota_{g(t)} \geq \tau_D l(\iota_{g(t)}, \varphi_{m(t)}) - \tau_D \varkappa = \tau_D - \tau_D \varkappa \tag{4.70}$$

where $l(\iota_{g(t)}, \varphi_{m(t)}) = 1$ because only one time switching is changed in $[\iota_{g(t)}, \varphi_{m(t)})$ interval and $n(\iota_{g(t)}, \varphi_{m(t)}) = 0$ because there is no FSDoS present in the interval $[\iota_{g(t)}, \varphi_{m(t)})$. Similarly, $\iota_{g(t)} - \iota_{g(t)-1} \geq \tau_D, \varphi_{m(t)-1} - \iota_{g(t)-(q_{m(t)-1})} \geq \tau_D, \iota_{g(t)-q} - \iota_{g(t)-(q+1)} \geq \tau_D$ and so on, are obtained by avoiding the constant term ν in the remaining cases. Hence,

$$\begin{aligned}
&\sum_{\substack{k\in\mathbb{N}_0;\\ q\leq g(t)}} \exp\left\{ \begin{array}{c} -\left[\sum_{i=1}^{n_s} \omega_{1_i} |\mathcal{O}_i(\varphi_{m(t)-k}, t)| - \frac{1}{T_*}\left\{ \left(\omega_{1_{\sigma(\iota^+_{g(t)})}} + \omega_{2_{\sigma(\iota^+_{g(t)})}}\right)(t-\varphi_{m(t)}) \right.\right. \\ + \left(\omega_{1_{\sigma(\iota^+_{g(t)-q_{m(t)-1}})}} + \omega_{2_{\sigma(\iota^+_{g(t)-q_{m(t)-1}})}}\right)(\iota_{g(t)-(q_{m(t)-1}-1)} - \varphi_{m(t)-1}) \\ \left.\left. + \cdots + \left(\omega_{1_{\sigma(\iota^+_{g(t)-q})}} + \omega_{2_{\sigma(\iota^+_{g(t)-q})}}\right)\left(\iota_{g(t)-(q-1)} - \varphi_{m(t)-k}\right)\right\}\right] \end{array} \right\} \\
&= \sum_{\substack{k\in\mathbb{N}_0;\\ q\leq g(t)}} \exp\left\{ \begin{array}{c} -\left[\omega_{1_{\sigma(\iota^+_{g(t)})}}\left(t - \iota_{g(t)}\right) + \omega_{1_{\sigma(\iota^+_{g(t)-1})}}\left(\iota_{g(t)} - \iota_{g(t)-1}\right) + \cdots + \omega_{1_{\sigma(\iota^+_{g(t)-q_{m(t)-1}})}} \right. \\ \left(\iota_{g(t)-(q_{m(t)-1}-1)} - \iota_{g(t)-q_{m(t)-1}}\right) + \cdots + \omega_{1_{\sigma(\iota^+_{g(t)-q})}}\left(\iota_{g(t)-(q-1)} - \varphi_{m(t)-k}\right) \\ -\frac{1}{T_*}\left\{ \left(\omega_{1_{\sigma(\iota^+_{g(t)})}} + \omega_{2_{\sigma(\iota^+_{g(t)})}}\right)(t-\varphi_{m(t)}) + \left(\omega_{1_{\sigma(\iota^+_{g(t)-q_{m(t)-1}})}} \right.\right. \\ \left.\left. + \omega_{2_{\sigma(\iota^+_{g(t)-q_{m(t)-1}})}}\right)\left(\iota_{g(t)-(q_{m(t)-1}-1)} - \varphi_{m(t)-1}\right) + \cdots \right. \\ \left.\left. + \left(\omega_{1_{\sigma(\iota^+_{g(t)-q})}} + \omega_{2_{\sigma(\iota^+_{g(t)-q})}}\right)\left(\iota_{g(t)-(q-1)} - \varphi_{m(t)-k}\right)\right\}\right] \end{array} \right\} \\
&\leq \exp\left\{\omega_{1_{\sigma(\iota^+_{g(t)})}} \tau_D \varkappa\right\} \sum_{\substack{k\in\mathbb{N}_0;\\ q\leq g(t)}} \exp\left\{ -\left(\omega_{1_{\sigma(\iota^+_{g(t)})}} + \cdots + \omega_{1_{\sigma(\iota^+_{g(t)-q})}}\right)\tau_D \right\}
\end{aligned}$$

$$\exp\left\{\begin{array}{l} -\left[\left(\omega_{1_{\sigma(\iota^+_{g(t)})}}-\frac{\omega_{1_{\sigma(\iota^+_{g(t)})}}+\omega_{2_{\sigma(\iota^+_{g(t)})}}}{T_*}\right)(t-\varphi_{m(t)})+\left(\omega_{1_{\sigma(\iota^+_{g(t)-q_{m(t)-1}})}}\right.\right. \\ \left.\left.-\frac{\omega_{1_{\sigma(\iota^+_{g(t)-q_{m(t)-1}})}}+\omega_{2_{\sigma(\iota^+_{g(t)-q_{m(t)-1}})}}}{T_*}\right)\left(\iota_{g(t)-(q_{m(t)-1}-1)}-\varphi_{m(t)-1}\right)+\cdots+ \\ \left(\omega_{1_{\sigma(\iota^+_{g(t)-q})}}-\frac{\omega_{1_{\sigma(\iota^+_{g(t)-q})}}+\omega_{1_{\sigma(\iota^+_{g(t)-q})}}}{T_*}\right)\left(\iota_{g(t)-(q-1)}-\varphi_{m(t)-k}\right)\Bigg] \end{array}\right\}$$

$$\leq \exp\left\{\omega_{1_{\sigma(\iota^+_{g(t)})}}\tau_D\varkappa\right\}\sum_{\substack{k\in\mathbb{N}_0;\\ q\leq g(t)}}\exp\left\{-\left(\omega_{1_{\sigma(\iota^+_{g(t)})}}+\cdots+\omega_{1_{\sigma(\iota^+_{g(t)-q})}}\right)\tau_D\right\}$$

$$\exp\left\{\begin{array}{l} -\Bigg[\beta_{\sigma(\iota^+_{g(t)})}\left(t-\varphi_{m(t)}\right)+\beta_{\sigma(\iota^+_{g(t)-q_{m(t)-1}})}\left(\iota_{g(t)-(q_{m(t)-1}-1)}-\varphi_{m(t)-1}\right) \\ +\cdots+\beta_{\sigma(\iota^+_{g(t)-q})}\left(\iota_{g(t)-(q-1)}-\varphi_{m(t)-k}\right)\Bigg] \end{array}\right\} \tag{4.71}$$

hold, where $\beta_{\sigma(\iota^+_{g(t)-q})} := \omega_{1_{\sigma(\iota^+_{g(t)-q})}} - (\omega_{1_{\sigma(\iota^+_{g(t)-q})}} + \omega_{2_{\sigma(\iota^+_{g(t)-q})}})/T_*$ and so on. Under the condition of (4.5), $\beta_\sigma > 0$ persists. Equation (4.71) is bounded from above by

$$\exp\left\{\omega_{1_{\sigma(\iota^+_{g(t)})}}\tau_D\varkappa\right\}\sum_{\substack{k\in\mathbb{N}_0;\\ q\leq g(t)}}\exp\left\{-\left(\omega_{1_{\sigma(\iota^+_{g(t)})}}+\cdots+\omega_{1_{\sigma(\iota^+_{g(t)-q})}}\right)\tau_D\right\}$$
$$\exp\left\{\beta_{\sigma(\iota^+_{g(t)})}\tau_F\varrho\right\}\exp\left\{-\left(\beta_{\sigma(\iota^+_{g(t)})}+\beta_{\sigma(\iota^+_{g(t)-q_{m(t)-1}})}+\cdots+\beta_{\sigma(\iota^+_{g(t)-q})}\right)\tau_F\right\}, \tag{4.72}$$

using (4.69) and so on. Hence equation (4.62) is bounded from above by

$$\frac{1}{\underline{\alpha}_{\sigma(\iota^+_{g(t)})}}e^{\left(\omega_{1_{\sigma(\iota^+_{g(t)})}}+\omega_{2_{\sigma(\iota^+_{g(t)})}}\right)\zeta_*}e^{\omega_{1_{\sigma(\iota^+_{g(t)})}}\tau_D\varkappa}e^{\beta_{\sigma(\iota^+_{g(t)})}\tau_F\varrho}\sum_{\substack{k\in\mathbb{N}_0;\\ q\leq g(t)}}\left[\left(\nu_{1_{\sigma(\iota^+_{g(t)-q})}}+\nu_{3_{\sigma(\iota^+_{g(t)-q})}}\right)\right.$$
$$\prod_{\substack{j\in\mathbb{N}_0;\\ \iota_{g(t)-q}<\iota_{g(t)-j}\leq\iota_{g(t)}}}\left(\frac{\overline{\alpha}_{\sigma(\iota^+_{g(t)-j})}}{\underline{\alpha}_{\sigma(\iota^+_{g(t)-(j+1)})}}\right)e^{-\sum_{j=0}^{q}\omega_{1_{\sigma(\iota^+_{g(t)-j})}}\tau_D}$$
$$\left.e^{-\left(\beta_{\sigma(\iota^+_{g(t)})}+\beta_{\sigma(\iota^+_{g(t)-q_{m(t)-1}})}+\cdots+\beta_{\sigma(\iota^+_{g(t)-q})}\right)\tau_F}\right]$$

$$\leq \overline{\nu} e^{\left(\omega_{1_{\sigma(\iota^+_{g(t)})}} + \omega_{2_{\sigma(\iota^+_{g(t)})}}\right)\zeta_*} e^{\omega_{1_{\sigma(\iota^+_{g(t)})}}\tau_D \varkappa} e^{\beta_{\sigma(\iota^+_{g(t)})}\tau_F \varrho} \sum_{\substack{k\in\mathbb{N}_0;\\ q\leq g(t)}} \left[\frac{1}{\underline{\alpha}_{\sigma(\iota^+_{g(t)-q})}} \prod_{\substack{j\in\mathbb{N}_0;\\ \iota_{g(t)-q}<\iota_{g(t)-j}\leq\iota_{g(t)}}} \left(\frac{\overline{\alpha}_{\sigma(\iota^+_{g(t)-j})}}{\underline{\alpha}_{\sigma(\iota^+_{g(t)-j})}}\right) e^{-\sum_{j=0}^{q}\omega_{1_{\sigma(\iota_{g(t)-j})}}\tau_D} e^{-\left(\beta_{\sigma(\iota^+_{g(t)})}+\beta_{\sigma(\iota^+_{g(t)-q_{m(t)-1}})}+\cdots+\beta_{\sigma(\iota^+_{g(t)-q})}\right)\tau_F} \right]$$

$$\leq \frac{\overline{\nu}}{\underline{\alpha}} e^{\left(\omega_{1_{\sigma(\iota^+_{g(t)})}} + \omega_{2_{\sigma(\iota^+_{g(t)})}}\right)\zeta_*} e^{\omega_{1_{\sigma(\iota^+_{g(t)})}}\tau_D \varkappa} e^{\beta_{\sigma(\iota^+_{g(t)})}\tau_F \varrho} \sum_{\substack{k\in\mathbb{N}_0;\\ q:=\sum_{s=0}^{k} q_{m(t)-s}\leq g(t)}} \left[\prod_{\substack{j\in\mathbb{N}_0;\\ \iota_{g(t)-q}<\iota_{g(t)-j}\leq\iota_{g(t)}}} \left(\frac{\overline{\alpha}_{\sigma(\iota^+_{g(t)-j})}}{\underline{\alpha}_{\sigma(\iota^+_{g(t)-j})}}\right) e^{-\sum_{j=0}^{q}\omega_{1_{\sigma(\iota^+_{g(t)-j})}}\tau_D} e^{-\left(\beta_{\sigma(\iota^+_{g(t)})}+\beta_{\sigma(\iota^+_{g(t)-q_{m(t)-1}})}+\cdots+\beta_{\sigma(\iota^+_{g(t)-q})}\right)\tau_F} \right], \tag{4.73}$$

where $\overline{\nu} := \max_{\forall\sigma\in\{1,\cdots,n_s\}} (\nu_{1_\sigma} + \nu_{3_\sigma})$. If the sum term of (4.73)'s RHS can be proved to be convergent, then (4.62) is bounded from above. A ratio test is used to prove the convergence of the sum term in (4.73). Consider $qp := \sum_{s=0}^{p} q_{m(t)-s}$ and $qp' := \sum_{s=0}^{p+1} q_{m(t)-s}$. The pth sum term of that series is

$$a_p := \prod_{\substack{j\in\mathbb{N}_0;\\ \iota_{g(t)-qp}<\iota_{g(t)-j}\leq\iota_{g(t)}}} \left(\frac{\overline{\alpha}_{\sigma(\iota^+_{g(t)-j})}}{\underline{\alpha}_{\sigma(\iota^+_{g(t)-j})}}\right) e^{-\sum_{j=0}^{qp}\omega_{1_{\sigma(\iota_{g(t)-j})}}\tau_D} e^{-\left(\beta_{\sigma(\iota^+_{g(t)})}+\beta_{\sigma(\iota^+_{g(t)-q_{m(t)-1}})}+\cdots+\beta_{\sigma(\iota^+_{g(t)-qp})}\right)\tau_F}. \tag{4.74}$$

Recall that to compute a_{p+1} it is sufficient to substitute $p+1$ for all instances of p in a_p

$$a_{p+1} := \prod_{\substack{j\in\mathbb{N}_0;\\ \iota_{g(t)-qp'}<\iota_{g(t)-j}\leq\iota_{g(t)}}} \left(\frac{\overline{\alpha}_{\sigma(\iota^+_{g(t)-j})}}{\underline{\alpha}_{\sigma(\iota^+_{g(t)-j})}}\right) e^{-\sum_{j=0}^{qp'}\omega_{1_{\sigma(\iota_{g(t)-j})}}\tau_D} e^{-\left(\beta_{\sigma(\iota^+_{g(t)})}+\beta_{\sigma(\iota^+_{g(t)-q_{m(t)-1}})}+\cdots+\beta_{\sigma(\iota^+_{g(t)-qp'})}\right)\tau_F}. \tag{4.75}$$

Now,

$$\frac{a_{p+1}}{a_p} = \frac{\overline{\alpha}_{\sigma(\iota^+_{g(t)-qp})} \cdots \overline{\alpha}_{\sigma(\iota^+_{g(t)-(qp'-1)})}}{\underline{\alpha}_{\sigma(\iota^+_{g(t)-qp})} \cdots \underline{\alpha}_{\sigma(\iota^+_{g(t)-(qp'-1)})}} e^{-\left(\omega_{1_{\sigma(\iota^+_{g(t)-(qp+1)})}} + \cdots + \omega_{1_{\sigma(\iota^+_{g(t)-qp'})}}\right)\tau_D} e^{-\beta_{\sigma(\iota^+_{g(t)-qp'})}\tau_F}$$
$$= \frac{\overline{\alpha}_{\sigma(\iota^+_{g(t)-qp})}}{\underline{\alpha}_{\sigma(\iota^+_{g(t)-qp})}} e^{-\omega_{1_{\sigma(\iota^+_{g(t)-(qp+1)})}}\tau_D} \cdots \frac{\overline{\alpha}_{\sigma(\iota^+_{g(t)-(qp'-1)})}}{\underline{\alpha}_{\sigma(\iota^+_{g(t)-(qp'-1)})}} e^{-\omega_{1_{\sigma(\iota^+_{g(t)-qp'})}}\tau_D} e^{-\beta_{\sigma(\iota^+_{g(t)-qp'})}\tau_F}. \quad (4.76)$$

satisfies. Hence, (3.32) yields

$$\lim_{p\to\infty} \left| \frac{\overline{\alpha}_{\sigma(\iota^+_{g(t)-qp})}}{\underline{\alpha}_{\sigma(\iota^+_{g(t)-qp})}} e^{-\omega_{1_{\sigma(\iota^+_{g(t)-(qp+1)})}}\tau_D} \cdots \frac{\overline{\alpha}_{\sigma(\iota^+_{g(t)-(qp'-1)})}}{\underline{\alpha}_{\sigma(\iota^+_{g(t)-(qp'-1)})}} e^{-\omega_{1_{\sigma(\iota^+_{g(t)-qp'})}}\tau_D} e^{-\beta_{\sigma(\iota^+_{g(t)-qp'})}\tau_F} \right|$$
$$\leq \lim_{p\to\infty} \left| \frac{\overline{\alpha}_{\sigma(\iota^+_{g(t)-qp})}}{\underline{\alpha}_{\sigma(\iota^+_{g(t)-qp})}} e^{-\omega_{1_{\sigma(\iota^+_{g(t)-(qp+1)})}}\tau_D} \right| \cdots \left| \frac{\overline{\alpha}_{\sigma(\iota^+_{g(t)-(qp'-1)})}}{\underline{\alpha}_{\sigma(\iota^+_{g(t)-(qp'-1)})}} e^{-\omega_{1_{\sigma(\iota^+_{g(t)-qp'})}}\tau_D} \right| \left| e^{-\beta_{\sigma(\iota^+_{g(t)-qp'})}\tau_F} \right|$$
$$< 1, \quad (4.77)$$

because from (4.5), it can be said that $\beta_{\sigma(\iota^+_{g(t)-qp'})} > 0$ and from Assumption 4.1, $\tau_F > \underline{\Delta}$. If $e^{-\beta_{\sigma(\iota^+_{g(t)-qp'})}\tau_F} < 1$ then equation (4.5) and Assumption 4.1 are true. Therefore, the upper bound of the sum term of (4.73) is convergent. So it is bounded from above. Hence, (4.62) is also bounded from above. Consider the upper bound is G_2. ■

In the same way as in Lemma 4.5, it can be shown that

$$\frac{1}{\underline{\alpha}_{\sigma(\iota^+_{g(t)})}} \sum_{\substack{l\in\mathbb{N};\\ 0\leq\iota_{g(t)-l}<\iota_{g(t)}}} \left\{ \nu_{1_{\sigma(\iota^+_{g(t)-l})}} \prod_{\substack{j\in\mathbb{N}_0;\\ \iota_{g(t)-l}<\iota_{g(t)-j}\leq\iota_{g(t)}}} \left(\frac{\overline{\alpha}_{\sigma(\iota^+_{g(t)-j})}}{\underline{\alpha}_{\sigma(\iota^+_{g(t)-(j+1)})}} \right) \right.$$
$$\left. e^{-(\sum_{i=1}^{n_s} \omega_{1_i} |(\mathcal{O}_i \cap \overline{\Upsilon})(\iota_{g(t)-(l-1)},t)|)} e^{(\sum_{i=1}^{n_s} \omega_{2_i} |(\mathcal{O}_i \cap \overline{\Omega})(\iota_{g(t)-l},t)|)} \right\} \quad (4.78)$$

is bounded from above. Let's take the upper bound as G_3.

Lemma 4.6. *Under the Assumption 3.1, 4.1, and 4.2, the first term of* (4.45)

$$\prod_{\substack{f\in\mathbb{N}_0;\\ 0\leq\iota_{g(t)-f}\leq t}} \left(\frac{\overline{\alpha}_{\sigma(\iota^+_{g(t)-f})}}{\underline{\alpha}_{\sigma(\iota^+_{g(t)-f})}} \right) e^{-\sum_{i=1}^{n_s} \omega_{1_i} |(\mathcal{O}_i \cap \overline{\Upsilon})(\iota_0,t)|} e^{\sum_{i=1}^{n_s} \omega_{2_i} |(\mathcal{O}_i \cap \overline{\Omega})(\iota_0,t)|} \quad (4.79)$$

is convergent in nature.

Proof of Lemma 4.6 : Using (4.63)−(4.73), upper bound of (4.79) is

$$e^{\left(\omega_{1_{\sigma(\iota^+_{g(t)})}}+\omega_{2_{\sigma(\iota^+_{g(t)})}}\right)\zeta_*}\, e^{\omega_{1_{\sigma(\iota^+_{g(t)})}}\tau_D\varkappa}\, e^{\beta_{\sigma(\iota^+_{g(t)})}\tau_F\varrho} \prod_{\substack{f\in\mathbb{N}_0;\\ 0\le\iota_{g(t)-f}\le t}} \left(\frac{\overline{\alpha}_{\sigma(\iota^+_{g(t)-f})}}{\underline{\alpha}_{\sigma(\iota^+_{g(t)-f})}}\right) e^{-\sum_{j=0}^{f}\omega_{1_{\sigma(\iota^+_{g(t)-j})}}\tau_D}$$
$$e^{-\sum\limits_{\substack{k\in\mathbb{N}_0;\\ q:=\sum_{s=0}^{k}q_{m(t)-s}\le f}}\beta_{\sigma(\iota^+_{g(t)-q})}\tau_F}. \tag{4.80}$$

If it can be shown that (4.80) is convergent, then from the direct comparison test, (4.79) is also convergent. A ratio test is employed to prove that (4.80) is convergent. pth term of (4.80) by avoiding constants are

$$b_p := \prod_{\substack{f\in\mathbb{N}_0;\\ \iota_{g(t)-p}<\iota_{g(t)-f}\le t}} \left(\frac{\overline{\alpha}_{\sigma(\iota^+_{g(t)-f})}}{\underline{\alpha}_{\sigma(\iota^+_{g(t)-f})}}\right) e^{-\sum_{j=0}^{f}\omega_{1_{\sigma(\iota^+_{g(t)-j})}}\tau_D}\, e^{-\sum_{\substack{k\in\mathbb{N}_0;\\ q\le f}}\beta_{\sigma(\iota^+_{g(t)-q})}\tau_F}. \tag{4.81}$$

Hence,

$$b_{p+1} := \prod_{\substack{f\in\mathbb{N}_0;\\ \iota_{g(t)-(p+1)}<\iota_{g(t)-f}\le t}} \left(\frac{\overline{\alpha}_{\sigma(\iota^+_{g(t)-f})}}{\underline{\alpha}_{\sigma(\iota^+_{g(t)-f})}}\right) e^{-\sum_{j=0}^{f}\omega_{1_{\sigma(\iota^+_{g(t)-j})}}\tau_D}\, e^{-\sum_{\substack{k\in\mathbb{N}_0;\\ q\le f}}\beta_{\sigma(\iota^+_{g(t)-q})}\tau_F}. \tag{4.82}$$

First, consider FSDoS does not exist in the interval $[\iota_{g(t)-p}, \iota_{g(t)-(p-1)}]$. Therefore,

$$\frac{b_{p+1}}{b_p} = \frac{\overline{\alpha}_{\sigma(\iota^+_{g(t)-p})}}{\underline{\alpha}_{\sigma(\iota^+_{g(t)-p})}} e^{-\omega_{1_{\sigma(\iota^+_{g(t)-p})}}\tau_D}. \tag{4.83}$$

Hence (3.32) yields,

$$\lim_{p\to\infty}\left|\frac{\overline{\alpha}_{\sigma(\iota^+_{g(t)-p})}}{\underline{\alpha}_{\sigma(\iota^+_{g(t)-p})}} e^{-\omega_{1_{\sigma(\iota^+_{g(t)-p})}}\tau_D}\right| < 1. \tag{4.84}$$

Now consider FSDoS exists in the interval $[\iota_{g(t)-p}, \iota_{g(t)-(p-1)}]$. Therefore,

$$\frac{b_{p+1}}{b_p} = \frac{\overline{\alpha}_{\sigma(\iota^+_{g(t)-p})}}{\underline{\alpha}_{\sigma(\iota^+_{g(t)-p})}} e^{-\omega_{1_{\sigma(\iota^+_{g(t)-p})}}\tau_D} e^{-\beta_{\sigma(\iota^+_{g(t)-p})}\tau_F}. \tag{4.85}$$

Hence,

$$\lim_{p\to\infty}\left|\frac{\overline{\alpha}_{\sigma(\iota^+_{g(t)-p})}}{\underline{\alpha}_{\sigma(\iota^+_{g(t)-p})}}e^{-\omega_{1_{\sigma(\iota^+_{g(t)-p})}}\tau_D}e^{-\beta_{\sigma(\iota^+_{g(t)-p})}\tau_F}\right|$$
$$\leq \lim_{p\to\infty}\left\{\left|\frac{\overline{\alpha}_{\sigma(\iota^+_{g(t)-p})}}{\underline{\alpha}_{\sigma(\iota^+_{g(t)-p})}}e^{-\omega_{1_{\sigma(\iota^+_{g(t)-p})}}\tau_D}\right|\left|e^{-\beta_{\sigma(\iota^+_{g(t)-p})}\tau_F}\right|\right\}<1 \tag{4.86}$$

$\forall\beta_\sigma\in\mathbb{R}_{>0},\tau_F\in\mathbb{R}_{\geq\underline{\Delta}}$, which concludes that (4.79) is convergent in nature. ■

Hence, from (4.45), it follows that

$$\|x(t)\|\leq\sqrt{\frac{\overline{\alpha}_{\sigma(\iota_0^+)}\cdots\overline{\alpha}_{\sigma(\iota^+_{g(t)})}}{\underline{\alpha}_{\sigma(\iota_0^+)}\cdots\underline{\alpha}_{\sigma(\iota^+_{g(t)})}}}e^{-\frac{1}{2}\sum_{i=1}^{n_s}\omega_{1_i}|(\mathcal{O}_i\cap\overline{\Upsilon})(\iota_0,t)|}e^{\frac{1}{2}\sum_{i=1}^{n_s}\omega_{2_i}|(\mathcal{O}_i\cap\overline{\Omega})(\iota_0,t)|}\|x(\iota_0)\|$$
$$+\sqrt{G_2+G_3}\|w_t\|_\infty, \tag{4.87}$$

$\forall t\in[0,\varphi_{m(t)}+v_{m(t)})$. Therefore, (4.87) is ISS. ■

4.4 Multi-objective optimization problem

The bounds of changing frequency of MCDoS parameters are expressed in (3.32) and (3.33). The bound of the frequency and duration of FSDoS parameters is expressed in (4.5). This section's motivation is to find the optimal parameters so that the system is resilient against the maximum changing frequency of MCDoS as well as the maximum frequency and duration of FSDoS. To do so, we have to optimize two cost functions, which makes it a multi-objective optimization problem. The lower bound of τ_D in (3.32) is taken as the first cost function, denoted by J_{mcdos} in (3.94). The upper bound of $1/T+\underline{\Delta}/\tau_F$ in (4.5) is taken as the second cost function, given by

$$J_{\text{fsdos}}:=\min_{\forall\sigma\in\{1,\cdots,n_s\}}\frac{\omega_{1_\sigma}}{\omega_{1_\sigma}+\omega_{2_\sigma}} \tag{4.88}$$

where ω_{1_σ} and ω_{2_σ} are defined in (3.44) and (4.6), respectively. To allow maximum MCDoS changing frequency in the system, J_{mcdos} must be minimized subject to $\underline{\alpha}_{p_\sigma}I\leq P_{p_\sigma}\leq\overline{\alpha}_{p_\sigma}I,\underline{\alpha}_{e_\sigma}I\leq P_{e_\sigma}\leq\overline{\alpha}_{e_\sigma}I,\Gamma_{2_\sigma}\geq\zeta_{1_\sigma}I,\{\psi_1,\psi_2,\varepsilon_{1_\sigma},\varepsilon_{2_\sigma}\}>0$ and $H_\sigma\in\mathbb{R}^{n_p\times n_{h_\sigma}}$.

To allow maximum FSDoS frequency and duration, J_{fsdos} must be maximized subject to $\underline{\alpha}_{p_\sigma} I \leq P_{p_\sigma} \leq \overline{\alpha}_{p_\sigma} I, \underline{\alpha}_{e_\sigma} I \leq P_{e_\sigma} \leq \overline{\alpha}_{e_\sigma} I, \Gamma_{2_\sigma} \geq \zeta_{1_\sigma} I, \Gamma_{3_\sigma} \leq \zeta_{2_\sigma} I, \zeta_{3_\sigma} = \|\gamma_{4_\sigma}\|, \Gamma_{5_\sigma} \leq -\gamma_{1_\sigma} I, \|P_{p_\sigma} BK\| \leq \gamma_{2_\sigma}, \|H_\sigma\| \leq \gamma_{3_\sigma}$, and $\{\psi_1, \psi_2, \varepsilon_{1_\sigma}, \varepsilon_{2_\sigma}\} > 0$ where

$$\zeta_{2_\sigma} \coloneqq \lambda_M(\Gamma_{3_\sigma}) \tag{4.89}$$

and

$$\zeta_{3_\sigma} \coloneqq \|\Gamma_{4_\sigma}\|. \tag{4.90}$$

J_{mcdos} and J_{fsdos} both are non-convex cost function. However, there is no optimization tool available that can handle non-convex cost functions and LMIs together. In the previous chapter, Section 3.6, J_{mcdos} was minimized using 2−steps procedure. These 2−steps optimize the cost function mentioned in (3.94) to allow maximum MCDoS changing frequency in the system.

Now, the focus shifts to maximizing J_{fsdos} in (4.88) to make the system resilient against maximum FSDoS frequency and duration. To achieve this, ω_{1_σ} must be maximized and ω_{2_σ} minimized. From (3.44) and (3.39), it is evident that ω_{1_σ} is linearly proportional to ζ_{1_σ}. Thus, maximizing ζ_{1_σ} leads to maximizing ω_{1_σ}. Step 2 already maximized ζ_{1_σ}. The remaining task is to minimize ω_{2_σ}. The term ω_{2_σ} directly depends on Γ_{3_σ} and Γ_{4_σ}. The matrix Γ_{4_σ} is not symmetrical and cannot be expressed in LMI form, whereas Γ_{3_σ} is in LMI form. Since Γ_{3_σ} and Γ_{4_σ} depend on the same parameters, optimizing one will optimize the other. By optimizing Γ_{3_σ}, both Γ_{4_σ} and ω_{2_σ} can be optimized.

Step 3 So, the final cost function is

$$J_{\text{final}} \coloneqq \max_{\forall \sigma \in \{1,\cdots,n_s\}} \zeta_{2_\sigma}. \tag{4.91}$$

J_{final} is the maximum of $\zeta_{2_\sigma}, \forall \sigma \in \{1, \cdots, n_s\}$. Minimizing the maximum value of all ζ_{2_σ} ensures that all ζ_{2_σ} are minimized. Minimize J_{final} subject to $\Gamma_{2_\sigma} \geq JI, \Gamma_{3_\sigma} \geq \zeta_{2_\sigma} I, \underline{\alpha}_{p_\sigma} I \leq P_{p_\sigma} \leq \overline{\alpha}_{p_\sigma} I$, $\underline{\alpha}_{e_\sigma} I \leq P_{e_\sigma} \leq \overline{\alpha}_{e_\sigma} I, \Gamma_{5_\sigma} \leq -\gamma_{1_\sigma} I, \|P_{p_\sigma} BK\| \leq \gamma_{2_\sigma}, H_\sigma \leq \gamma_{3_\sigma} \begin{bmatrix} 1 & 1 \end{bmatrix}^\top, \{\overline{\alpha}_{p_\sigma} -$

$\underline{\alpha}_{p_\sigma}, \overline{\alpha}_{p_\sigma} - \underline{\alpha}_{e_\sigma}, \overline{\alpha}_{e_\sigma} - \underline{\alpha}_{p_\sigma}, \overline{\alpha}_{e_\sigma} - \underline{\alpha}_{e_\sigma}\} \leq J_\sigma$, and $\{\psi_1, \psi_2, \varepsilon_{1_\sigma}, \varepsilon_{2_\sigma}\} > 0$ is the third CO problem.

The whole optimization technique is presented in Algorithm 4.1. Thus, 3−step optimization techniques are sensitive to choosing the variable q in the first CO problem in Step 1 in the previous chapter Section 3.6. The value of q should be kept small (< 1) and positive. Choosing $q \approx 0$ may enhance the system's resilience against a high MCDoS changing frequency, but may also reduce its resilience against lower frequency and shorter duration FSDoS. The value of q should be chosen wisely to effectively handle both MCDoS and FSDoS.

4.5 Asynchronous triggering policy

Throughout this report, we have assumed that the presence of FSDoS on the StC channels and CtA channel is synchronous. However, the CtA channel and StC channels can be interrupted asynchronously. In this scenario, Ω described in (3.4) is now Ω_m, which means FSDoS is present on the StC channel. And the FSDoS present in CtA channel is described as Ω_c. Now, the FSDoS present in the system is described as

$$\Omega(\tau, t) \coloneqq \Omega_m(\tau, t) \cup \Omega_c(\tau, t), \tag{4.92}$$

$\forall t \geq \tau$. In this scenario, the control input $u(t)$ can also be updated when Ω_m is present but Ω_c is not present by using the estimated state values $x_e(t)$ from the switched observer (3.7), which operates based on the plant output $\hat{y}_\sigma(t)$ updated when Ω_m was not present in the system, with the value of σ updated according to (3.8). When the actuator sends the data receiving acknowledgement to the controller $\xi_e(t)$ in (3.14) turns to 0 when t_k instants. However, $\xi_\sigma(t)$ in (3.13) is not reset because of the presence of Ω_m. Similarly, in the presence of Ω_c when Ω_m is not present $\hat{y}_\sigma(t)$ receives data at t_k instants which helps the switched observer to estimate states ($x_e(t)$) accurately but control input ($u(t)$) does not receive the updated data. In this scenario, $\xi_\sigma(t)$ turns to 0 at t_k instants but

Algorithm 4.1 Optimization of the design parameter to make the system resilient against maximum MCDoS changing frequency as well as maximum frequency and duration of FSDoS

1: Assign the value of q.
2: Start a for loop for $\sigma = 1$ to n_s.
3: Begin CVX with CVX solver Sedumi.
4: Consider variables $P_{p_\sigma}, P_{e_\sigma}, \underline{\alpha}_{p_\sigma}, \overline{\alpha}_{p_\sigma}, \underline{\alpha}_{e_\sigma}, \overline{\alpha}_{e_\sigma} \psi_1, \psi_2, \varepsilon_{1_\sigma}, \varepsilon_{2_\sigma}$, and H_σ.
5: Compute Γ_{2_σ} from (3.28).
6: Performe Step 1 LP.
7: End CVX.
8: Store the value of J_σ.
9: End for loop.
10: Begin CVX with CVX solver Sedumi.
11: Consider variables $P_{p_\sigma}, P_{e_\sigma}, \underline{\alpha}_{p_\sigma}, \overline{\alpha}_{p_\sigma}, \underline{\alpha}_{e_\sigma}, \overline{\alpha}_{e_\sigma} \psi_1, \psi_2, \varepsilon_{1_\sigma}, \varepsilon_{2_\sigma}, H_\sigma$, and $\zeta_{1_\sigma}, \forall \sigma \in \{1, 2, \cdots, n_s\}$.
12: Compute Γ_{2_σ}, from (3.28) $\forall \sigma \in \{1, 2, \cdots, n_s\}$.
13: Perform Step 2 LP by using the values of $J_\sigma, \forall \sigma \in \{1, 2, \cdots, n_s\}$.
14: End CVX.
15: Store the value of J.
16: Begin CVX with CVX solver Sedumi.
17: Consider variables $P_{p_\sigma}, P_{e_\sigma}, \underline{\alpha}_{p_\sigma}, \overline{\alpha}_{p_\sigma}, \underline{\alpha}_{e_\sigma}, \overline{\alpha}_{e_\sigma} \psi_1, \psi_2, \varepsilon_{1_\sigma}, \varepsilon_{2_\sigma}, \gamma_{1_\sigma}, \gamma_{2_\sigma}, \gamma_{3_\sigma}, \zeta_{2_\sigma}$, and H_σ, $\forall \sigma \in \{1, 2, \cdots, n_s\}$.
18: Compute $\Gamma_{2_\sigma}, \Gamma_{3_\sigma}$, and Γ_{5_σ}, from (3.28), (4.7), and (4.9), respectively, $\forall \sigma \in \{1, 2, \cdots, n_s\}$.
19: Perform Step 3 LP by using the values of $J_\sigma, \forall \sigma \in \{1, 2, \cdots, n_s\}$ from Step 1 and J from Step 2.
20: End CVX.
21: Store the values of $P_{p_\sigma}, P_{e_\sigma}, \Gamma_{2_\sigma}, \Gamma_{3_\sigma}, \Gamma_{5_\sigma}, \psi_1, \psi_2, \varepsilon_{1_\sigma}, \varepsilon_{2_\sigma}, \gamma_{1_\sigma}, \gamma_{2_\sigma}, \gamma_{3_\sigma}, \zeta_{2_\sigma}$, and $H_\sigma, \forall \sigma \in \{1, 2, \cdots, n_s\}$.
22: Compute L_σ from (3.31), $\forall \sigma \in \{1, 2, \cdots, n_s\}$ which is $P_{e_\sigma}^{-1} H_\sigma$.
23: Compute ζ_{1_σ}, from (3.39), $\forall \sigma \in \{1, 2, \cdots, n_s\}$.

$\xi_e(t)$ stands tall. Triggering instants t_{k+1} follow the same ETM proposed in (3.101). If an FSDoS attack occurs on both sides, update attempts will fail. When Ω_m is present and Ω_c is absent, only CtA updates are possible. Conversely, when Ω_c is present and Ω_m is absent, only StC updates can take place.

4.6 Simulation results

A simulation example is presented in this section to demonstrate the use of the suggested optimal switched observer-based ETM. The same dynamics as in (3.105) are used, where $x_{p_1}(t), x_{p_2}(t), u(t)$ represent rotor shaft speed (rad/sec), armature current (amp), and applied armature voltage (volts), respectively, and $w_1(t)$ and $w_2(t)$ denote disturbances, which are pseudo-random values from the standard normal distribution. Sensors are available for both states $x_{p_1}(t)$ and $x_{p_2}(t)$, with data transmitted through two separate channels. Under MCDoS type 1, channel 2 (value of x_{p_2}) is affected, while in the case of MCDoS type 2, channel 1 (value of x_{p_1}) is affected. The output matrices of the state-space model are C_1 and C_2, as mentioned in (3.103) and (3.104), respectively, corresponding to the occurrence of MCDoS type 1 and type 2 attacks, with $\sigma \in 1, 2$. The controller gain is $K = \begin{bmatrix} 0.9533 & 0.242 \end{bmatrix}$, obtained by placing the closed-loop poles $(A - BK)$ of system (3.105) at -0.95 and -4.7. The ETM proposed in (3.101) is implemented, and the 3−step optimization procedure in Section 4.4 is followed. In step 1, optimization with $q = 0.005$ yields $J_1 = 0.00406346840082$ and $J_2 = 2.65898414397725 \times 10^{-14}$. Using the values of J_1 and J_2 in step 2 yields $J = 0.004999804673468$. Finally, in step 3, optimization using J_1, J_2, and J produces

$$P_{p_1} = \begin{bmatrix} 0.011731990170481 & -0.001789973978992 \\ -0.001789973978992 & 0.009809557321526 \end{bmatrix},$$

$$P_{p_2} = \begin{bmatrix} 0.010456538125746 & 0 \\ 0 & 0.010456538125746 \end{bmatrix},$$

$$P_{e_1} = \begin{bmatrix} 0.010388261755008 & -0.001995401823611 \\ -0.001995401823611 & 0.011153285737363 \end{bmatrix},$$

$$P_{e_2} = \begin{bmatrix} 0.010456538125746 & 0 \\ 0 & 0.010456538125746 \end{bmatrix},$$

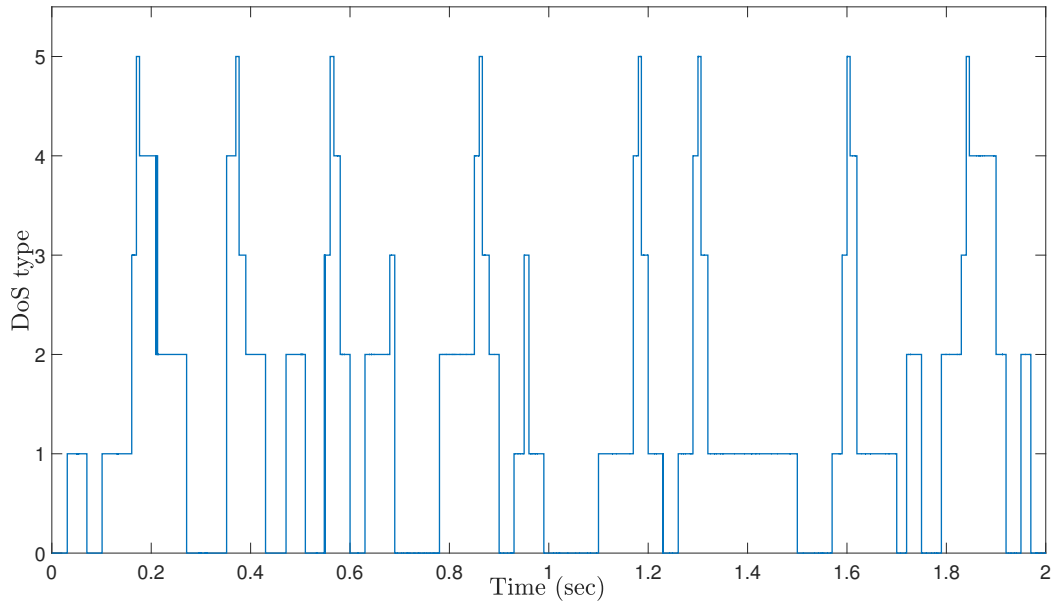

FIGURE 4.3: Different DoS types illustrating characterization of FSDoS. DoS type 0 means no DoS is present, DoS type 1 means MCDoS type 1 (only channel 2 is affected by DoS), DoS type 2 means MCDoS type 2 (only channel 1 is affected by DoS), DoS type 3 means FSDoS present only in the measurement side (Ω_m), DoS type 4 means FSDoS present only in controller side (Ω_c), and DoS type 5 means FSDoS present both the side of the system ($\Omega_m \cap \Omega_c$).

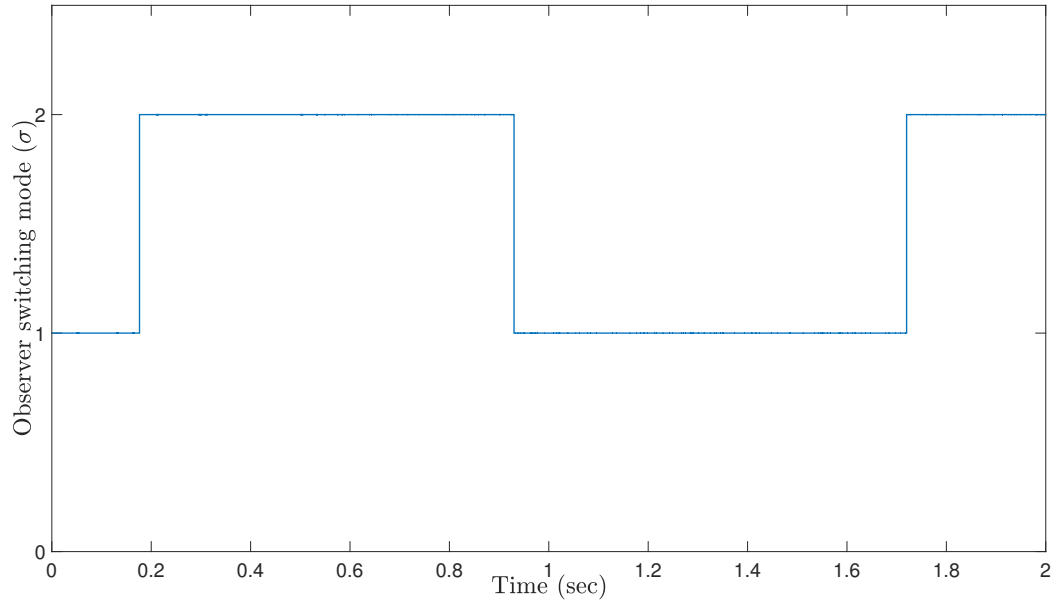

FIGURE 4.4: Real-time plot showing the observer interpreting the phenomenon as an MCDoS frequency variation based on the DoS type in Figure 4.3, and switching its mode σ accordingly illustrating characterization of FSDoS. The behavior follows $l(0,1) \approx 2$ and $l(0,2) \approx 3$, indicating that the observer switches modes three times within the interval from 0 to 2 seconds.

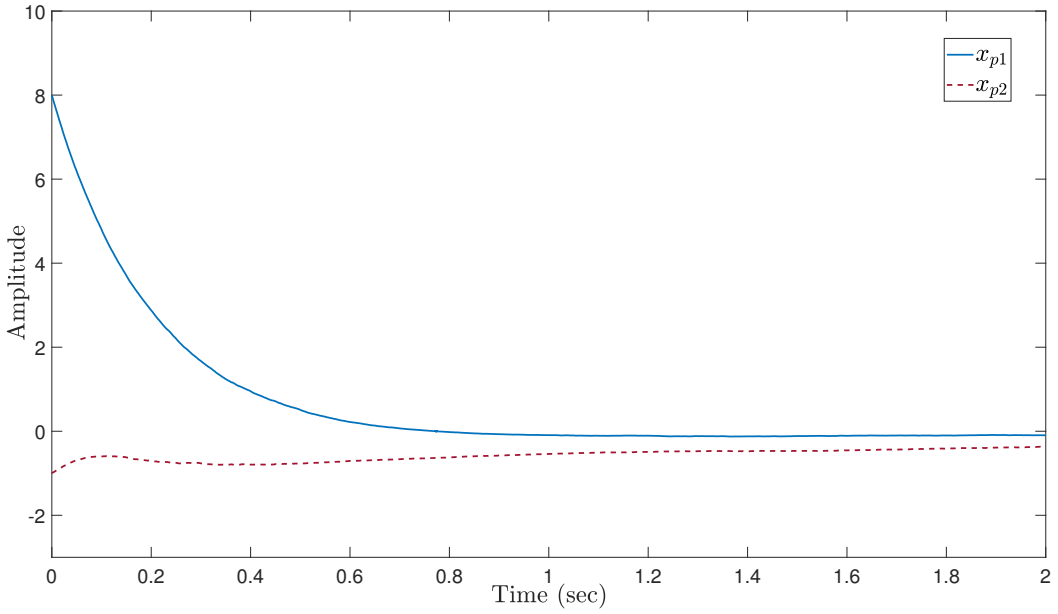

FIGURE 4.5: Plant state response for switched observer-based ETM illustrating characterization of FSDoS where the initial condition is $x_p(0) = (8, -1)$.

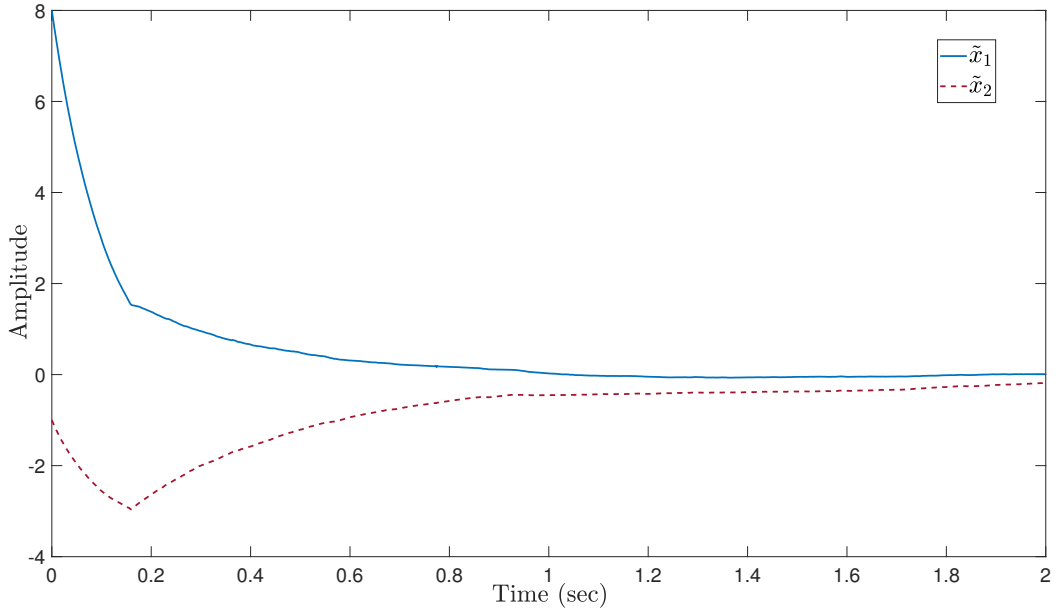

FIGURE 4.6: Observer error ($\tilde{x}(t) = x_p(t) - x_e(t)$) response of switched observer illustrating characterization of FSDoS where the initial condition is $x_p(0) = (8, -1)$ and $x_e(0) = (0, 0)$.

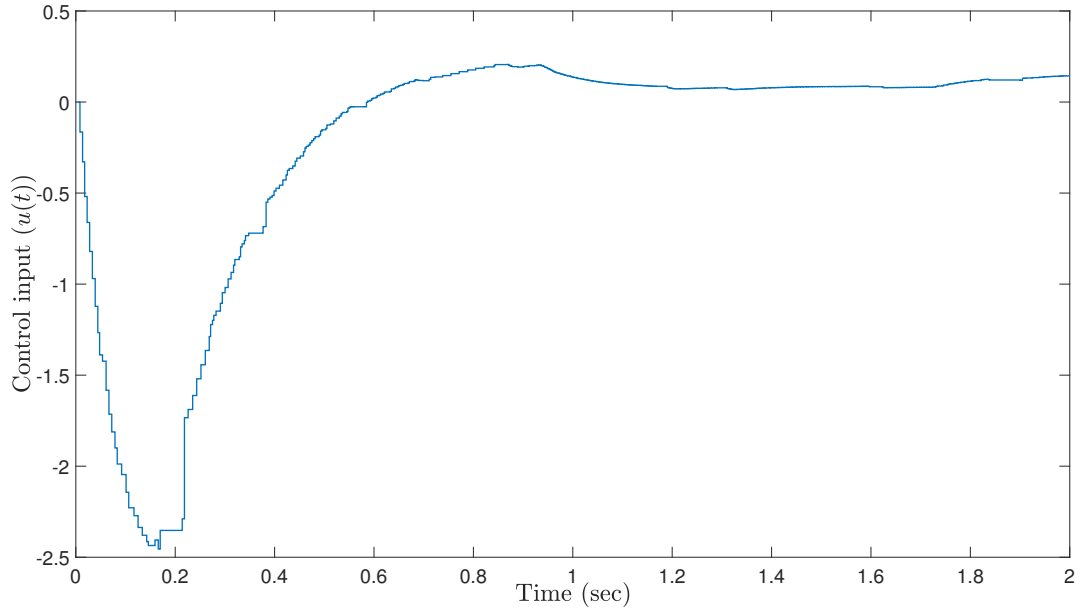

FIGURE 4.7: Response of control input $(u(t))$ illustrating characterization of FSDoS.

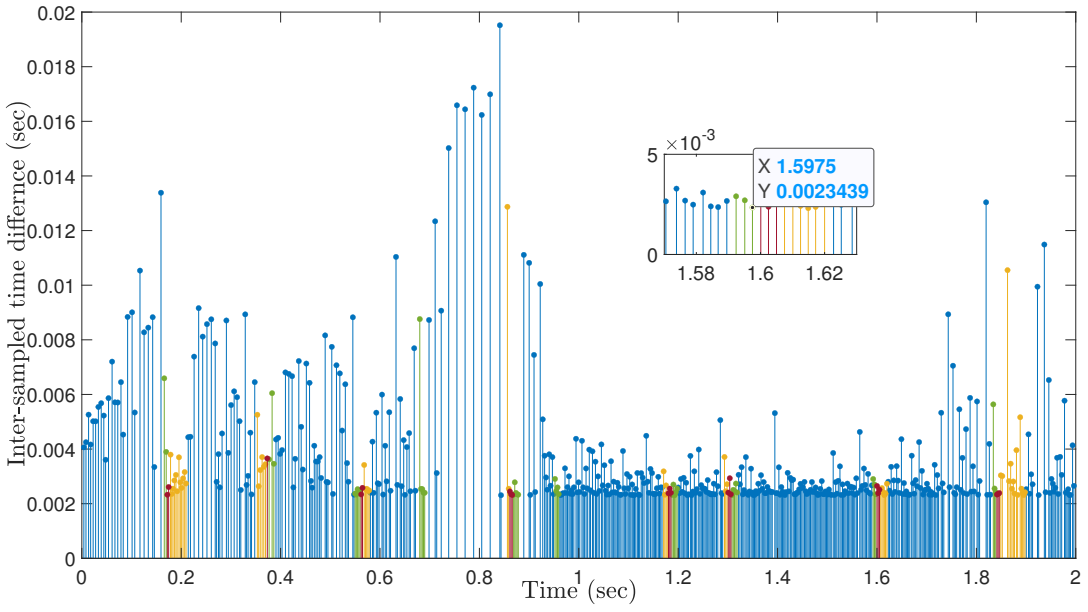

FIGURE 4.8: Data update instants for ETM illustrating characterization of FSDoS. Blue sticks indicate successful data updates on both sides. Green sticks represent data updates only between the controller and actuator, due to FSDoS on the measurement side (Ω_m). Yellow sticks denote data updates only between the sensors and controller, due to FSDoS on the controller side (Ω_c). Red sticks indicate failed control attempts caused by FSDoS on both sides$(\Omega_m \cap \Omega_c)$.

$L_1 = \begin{bmatrix} 4.356739143438354 \\ 4.103253033908143 \end{bmatrix}, L_2 = \begin{bmatrix} 1.892770640292722 \\ 2.050693085341698 \end{bmatrix}, \psi_1 = 0.001000000002368, \psi_2 = 0.00100000000003, \varepsilon_{1_1} = 9.512777137119125 \times 10^3, \varepsilon_{2_1} = 9.790175326489278 \times 10^3, \varepsilon_{1_2} = 9.452902117679011 \times 10^3, \varepsilon_{2_2} = 9.448310009192484 \times 10^3, \zeta_{1_1} = 0.004999804673599$, and $\zeta_{1_2} = 0.006867501782396$. Hence, $\tau_D > 0.977742153669935$. Also, from optimization step 3, $\gamma_{1_1} = 0.006399236932393, \gamma_{1_2} = 0.008984373226072, \gamma_{2_1} = 0.022287991043270, \gamma_{2_2} = 0.020569064642907, \gamma_{3_1} = 0.052426746790196$, and $\gamma_{3_2} = 0.029180904207728$. Hence, we calculate $\omega_{1_1}/(\omega_{1_1} + \omega_{2_1}) = 0.013621950374163$ and $\omega_{1_2}/(\omega_{1_2} + \omega_{2_2}) = 0.033831733610201$ is obtained. Therefore, the average FSDoS the system can handle $\sim 2.5\%$. From Lemma 3.10, $\underline{\Delta} = 0.002309426565894$ is obtained. The maximum allowable $\varkappa$ is 0.997638623143258 considering $\tau_D = 0.978$. So maximum allowable MCDoS changing frequency is $l(0, 0.5) \approx 1.5, l(0, 1) \approx 2, l(0, 1.5) \approx 2.5$, and $l(0, 2) \approx 3$. So $0 - 0.5$s observer changes its switching mode 1 time, $0 - 1$s observer changes its switching mode 2 times, and $0 - 2$s observer changes its switching mode 3 times. The observer changes its switching mode at 0.17625s, 0.93s, and 1.72s in Figure 4.4. An FSDoS is introduced at a rate of 2.5%, meaning that every 0.25s, FSDoS is present for 0.00625s. If an FSDoS attack occurs asynchronously in StC and CtA channels, the permissible limits of Ω_m and Ω_c under the asynchronous triggering policy mentioned in Section 4.5 have not yet been characterized. In this situation, the system is assumed to tolerate up to 2.5% of the total time when control update attempts fail on both sides simultaneously, represented as $\Omega_m \cap \Omega_c$. In Figure 4.3, all the DoS types and their span are mentioned. In Figures 4.5, 4.6, and 4.7, plant states response $(x_p(t))$, switched observer error response $(\tilde{x}(t))$, and control input $(u(t))$ responses are shown, respectively. Data update instants for the asynchronous triggering mechanism are shown in Figure 4.8, where it is shown that the minimum inter-execution time $\underline{\Delta} \approx 0.0023$.

4.7 Chapter summary

This chapter provided a comprehensive characterization of FSDoS, complementing the previous work on MCDoS. To formally define FSDoS behaviour, two key assumptions

were introduced to constrain its frequency and duration. Analytical bounds for these parameters were then derived to mitigate the impact of FSDoS on system performance.

With the integration of a switched observer, the overall system exhibits behaviour analogous to a switched system. Analyzing the stability of this system under the combined influence of MCDoS and FSDoS, each governed by distinct assumptions, posed significant challenges, which were systematically addressed in this work. To ensure resilience under FSDoS, a resilient ETM was proposed that accounts for the characterized bounds on both the frequency and duration of FSDoS. The parameters of the switched observer and ETM were designed optimally to achieve resilience against the maximum allowable MCDoS changing frequency, as well as the maximum frequency and duration of FSDoS. Furthermore, asynchronous triggering policies were introduced to handle cases where FSDoS events affect the StC and CtA paths at different times.

It is worth noting that in this chapter, the parameter q was set to 0.005, whereas in the previous chapter it was chosen as 10^{-4}. This change reflects a shift in objective; while the previous chapter focused solely on maximizing the MCDoS changing frequency, this chapter aimed to simultaneously maximize both MCDoS and FSDoS characteristics. As a result, the maximum MCDoS changing frequency achieved here is lower than in the previous chapter, a trade-off necessary to accommodate the more demanding FSDoS resilience requirements.

Chapter 5

Integration of optimal dynamic event-triggered mechanism against multi-channel denial-of-service

5.1 Introduction

In this chapter, the conventional Static ETM (SETM) employed in previous chapters is replaced with a Dynamic ETM (DETM). The DETM incorporates an internal dynamic variable, which underlies its designation. As observed by Girard [147], DETM generally leads to fewer triggering instants compared to SETM, thereby substantially reducing control costs. Here, DETM is utilized as a key component of a resilient control framework aimed at mitigating the effects of DoS on both the StC and CtA communication channels within a multi-sensor system architecture.

5.2 Problem formulation

In this chapter, the switched observer architecture introduced in Chapter 3 is adopted as the foundation for state estimation. Building upon this foundation, a DETM is developed

to enhance system resilience against DoS attacks on both sides of the control architecture within a multi-sensor framework. The DETM is specifically designed to reduce communication and control overhead while maintaining resilient system performance under adversarial conditions. The DETM architecture adopted from the existing literature is refined to enable resilience against the maximum MCDoS changing frequency.

To ensure optimal performance, an optimization algorithm based on LMIs is proposed to simultaneously design the parameters of the switched observer and DETM. The goal is to maximize the resilience of the system against the highest admissible MCDoS changing frequency while preserving closed-loop stability. In addition to ensuring system stability and performance, the minimum inter-execution time for DETM is analytically computed to avoid Zeno behaviour, guaranteeing a strictly positive time between consecutive triggering events. Moreover, in the absence of FSDoS, the maximum inter-execution time is derived, which helps bound the triggering interval from above and aids in control scheduling and communication planning.

Finally, building upon this framework, a novel resilient control strategy is developed to handle both MCDoS and FSDoS simultaneously. This strategy combines the DETM, switched observer, and the derived timing bounds to form a comprehensive solution for ensuring system performance and resilience in the face of sophisticated networked attacks.

5.3 Stability analysis of observer-based DETM under multi-channel DoS

5.3.1 Control architecture

Consider the LTI system with disturbance as defined in (2.1) and (3.1). To estimate the full state vector under the influence of MCDoS, the switched observer framework introduced in (3.7) is adopted. The control input is designed according to the control law given in (3.11). The structures of MCDoS and FSDoS follow the framework described in

Chapter 3, Subsection 3.3.2. The error between the estimated and actual state available to the controller is denoted in (3.13), while the internal observer state error is defined in (3.14). The resulting closed-loop dynamics of the switched-observer-based control system are represented in (3.15).

To improve communication efficiency and reduce the frequency of control updates, the SETM is replaced with a DETM. The DETM introduces an internal dynamic variable and is defined by the boundedness inequality

$$\xi_\sigma^\top(t)\xi_\sigma(t) + \xi_e^\top(t)\xi_e(t) \leq \frac{1}{\theta}\eta(t) + \psi_1\left(y_\sigma^\top(t)y_\sigma(t) + \|w_t\|_\infty^2\right) + \psi_2 x_e^\top(t)x_e(t) \tag{5.1}$$

where $\eta(t)$ is an internal dynamic variable defined by

$$\dot{\eta}(t) = \begin{cases} -\frac{\lambda}{\kappa}\eta(t) & \text{if } t \in \Omega(0,t), \\ \rho_{1_\sigma} & \text{otherwise,} \end{cases} \tag{5.2}$$

where

$$\rho_{1_\sigma}(t) := \frac{1}{\kappa}\Big[-\lambda\eta(t) - \xi_\sigma^\top(t)\xi_\sigma(t) - \xi_e^\top(t)\xi_e(t) + \psi_1\left(y_\sigma^\top(t)y_\sigma(t) + \|w_t\|_\infty^2\right) + \psi_2 x_e^\top(t)x_e(t)\Big], \tag{5.3}$$

$\forall t \in [t_k, t_{k+1})$, where $\{\lambda, \kappa\} \in \mathbb{R}_{>0}$, $\{\theta, \psi_1, \psi_2\} \in \mathbb{R}_{\geq 0}$, and σ follows (3.8). When (5.1) is violated, the $k+1$th task will be executed. The dynamics of $\eta(t)$ are chosen as in (5.2) to ensure that $\eta(t)$ remains positive for any non-negative initial condition $\eta(0)$, even in the presence of FSDoS. This aspect is discussed in detail later. The observer-based DETM is shown in Figure 5.1.

5.3.2 ISS for DETM under MCDoS

To show the ISS of the closed loop system with DETM, we consider the following candidate Lyapunov function $W_\sigma : \mathbb{R}^{2n_p} \times \mathbb{R}_{\geq 0} \to \mathbb{R}_{\geq 0}$ for the argument of the dynamic system given

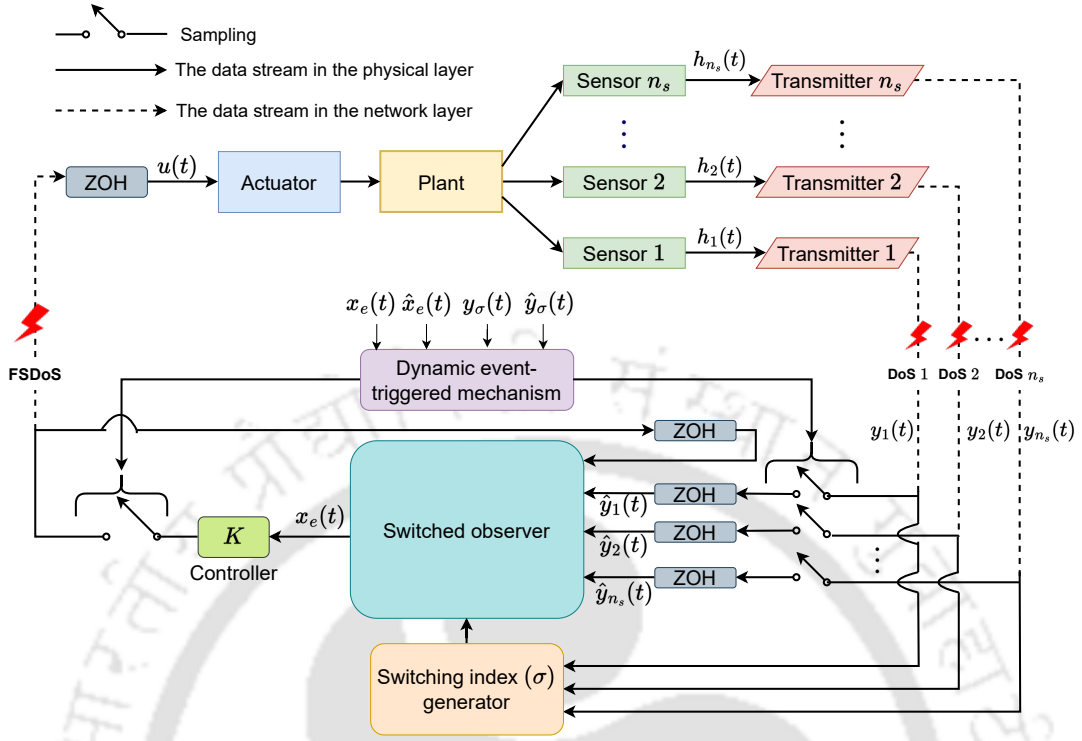

FIGURE 5.1: Block diagram of the closed-loop system with switched observer-based DETM control architecture for multiple transmission channels under DoS.

by (3.15) and (5.2)

$$W_\sigma(x(t),\eta(t)) = V_\sigma(x(t)) + \kappa\eta(t). \tag{5.4}$$

It is clear that $W_\sigma(x(t),\eta(t))$ is positive definite and radially unbounded if $\eta(t) \geq 0$. We prove later in Lemma 5.5 that $\eta(t) \geq 0$ if $\eta(0) \geq 0$. Furthermore, $\forall(x(t),\eta(t)) \in \mathbb{R}^{2n_p} \times \mathbb{R}_{\geq 0} \to \mathbb{R}_{\geq 0}$, we have $W_\sigma(x(t),\eta(t)) \geq V_\sigma(x(t))$. Also, $\forall t \in \mathbb{R}_{\geq 0}$, we have

$$\frac{d}{dt}W_\sigma(x(t),\eta(t),\xi_\sigma(t),\xi_e(t)) = \frac{d}{dt}V_\sigma(x(t),\xi_\sigma(t),\xi_e(t)) + \kappa\dot{\eta}(t), \tag{5.5}$$

where the upper bound of $\dot{V}_\sigma(x(t),\xi_\sigma(t),\xi_e(t))$ is mentioned in (3.23). By using the expression of (5.2), we get

$$\frac{d}{dt}W_\sigma(x(t),\eta(t)) = \frac{d}{dt}V_\sigma(x(t)) - \lambda\eta(t), \tag{5.6}$$

in the absence of FSDoS, where the upper bound of $\dot{V}_\sigma(x(t))$ is mentioned in (3.25).

Theorem 5.1. *In addition to the control law (3.11), consider the control system (3.15) with process dynamics (2.1) and (3.1), where K is such that $A-BK$ is Hurwitz. Consider restricted sampling rate with $\psi_1, \psi_2, \eta(0), \lambda, \kappa$, and θ which satisfy DETM (5.1), (5.2) and switched observer (3.7) with observer gain L_σ, which ensure the LMIs by*

$$\Gamma_{7_\sigma} := diag\{\Gamma_{2_\sigma}, \lambda\} > 0, \tag{5.7}$$

for $\{P_{p_\sigma}, P_{e_\sigma}\} > 0, \{\lambda, \psi_1, \psi_2, \varepsilon_{1_\sigma}, \varepsilon_{2_\sigma}\} \in \mathbb{R}_{>0}, H_\sigma \in \mathbb{R}^{n_p \times n_{h_\sigma}}, \forall \sigma \in \{1, \cdots, n_s\}$, where Γ_{2_σ} is mentioned in (3.28), and any MCDoS frequency that meets Assumption 3.1 and has arbitrary $\tau_D, \varkappa$ such that $\tau_{D_{detm}}$ and $\varkappa_{detm}$ satisfy

$$\tau_{D_{detm}} > \max\left\{\overline{\Delta}_{detm}, \max_{\forall \sigma \in \{1,\cdots,n_s\}} \frac{\max\{\overline{\alpha}_{p_\sigma}, \overline{\alpha}_{e_\sigma}, \kappa\}}{\zeta_{2_\sigma}} \ln\left\{\frac{\max\{\overline{\alpha}_{p_\sigma}, \overline{\alpha}_{e_\sigma}, \kappa\}}{\min\{\underline{\alpha}_{p_\sigma}, \underline{\alpha}_{e_\sigma}, \kappa\}}\right\}\right\}, \tag{5.8}$$

and

$$\varkappa_{detm} \leq 1 - \frac{\overline{\Delta}_{detm}}{\tau_{D_{detm}}}, \tag{5.9}$$

respectively, where $\underline{\alpha}_{p_\sigma}$ and $\overline{\alpha}_{p_\sigma}, \underline{\alpha}_{e_\sigma}$, and $\overline{\alpha}_{e_\sigma}$ are mentioned in (3.41), and (3.42), respectively,

$$\zeta_{2_\sigma} := \lambda_m(\Gamma_{7_\sigma}), \tag{5.10}$$

and $\overline{\Delta}_{detm}$ is the maximum inter-execution time for DETM. Then the system (3.15) is ISS.

Proof. From (5.6), we can write

$$\frac{d}{dt}W_\sigma(x(t), \eta(t)) \leq -X^\top(t)\Gamma_{8_\sigma}X(t) + (\varepsilon_{1_\sigma} + \varepsilon_{2_\sigma} + \psi_1)f^2(t) \tag{5.11}$$

where $\Gamma_{8_\sigma} := \text{diag}\{\Gamma_{1_\sigma}, \lambda\}$ and

$$X(t) := \begin{bmatrix} x^\top(t) & \sqrt{\eta(t)} \end{bmatrix}^\top. \tag{5.12}$$

By using Schur complement [158] in Γ_{8_σ} we get (5.7). From Theorem 5.1, we get that $\Gamma_{7_\sigma} > 0$. It is obvious because $\Gamma_{2_\sigma} > 0$ from Theorem 3.5, and $\lambda > 0$. $\Gamma_{8_\sigma} > 0$ because $\Gamma_{7_\sigma} > 0$ is the LMI form of $\Gamma_{8_\sigma} > 0$. From (5.11), we can write

$$\frac{d}{dt}W_\sigma(X(t)) \leq -\zeta_{2_\sigma}\|X(t)\|^2 + (\varepsilon_{1_\sigma} + \varepsilon_{2_\sigma} + \psi_1)d^2(t), \tag{5.13}$$

$d(t)$ is mentioned in (3.27). Also, the Lyapunov function in (5.6) can be rewritten in the following form

$$\underline{\alpha}_{p_\sigma}\|x_p(t)\|^2 + \underline{\alpha}_{e_\sigma}\|\tilde{x}(t)\|^2 + \kappa\eta(t) \leq W_\sigma(x_p(t), \tilde{x}(t), \eta(t)) \leq \overline{\alpha}_{p_\sigma}\|x_p(t)\|^2 + \overline{\alpha}_{e_\sigma}\|\tilde{x}(t)\|^2 + \kappa\eta(t). \tag{5.14}$$

From (5.11), the succeeding equation can be written as

$$\frac{d}{dt}W_\sigma(X(t)) \leq -\omega_{3_\sigma}W_\sigma(X(t)) + (\varepsilon_{1_\sigma} + \varepsilon_{2_\sigma} + \psi_1)d^2(t), \tag{5.15}$$

where

$$\omega_{3_\sigma} := \frac{\zeta_{2_\sigma}}{\max\{\overline{\alpha}_{s_\sigma}, \overline{\alpha}_{e_\sigma}, \kappa\}}. \tag{5.16}$$

Hence, from the comparison lemma, we get

$$W_\sigma(X(t)) \leq e^{-\omega_{3_\sigma}\left(t-\iota_{g(t)}\right)}W_\sigma(X(\iota^+_{g(t)})) + \nu_{4_\sigma}\|w_t\|^2_\infty, \tag{5.17}$$

in the interval $[\iota_{g(t)}, t]$, where

$$\nu_{4_\sigma} := \frac{\varepsilon_{1_\sigma} + \varepsilon_{2_\sigma} + \psi_1}{\omega_{3_\sigma}}. \tag{5.18}$$

From (5.4), we can say $W_\sigma(x(t), \eta(t))$ is the scaled version of the Lyapunov function of $V_\sigma(x(t))$ with the scaled term $\kappa\eta(t)$. We can also apply Lemma 3.6 in (5.17) by using the

scaled term κ. Applying Lemma 3.6, in (5.17), we get

$$\|X(t)\|^2 \leq \frac{\overline{\alpha}_{2_{\sigma(\iota^+_{g(t)})}} \cdots \overline{\alpha}_{2_{\sigma(\iota^+_0)}}}{\underline{\alpha}_{2_{\sigma(\iota^+_{g(t)})}} \cdots \underline{\alpha}_{2_{\sigma(\iota^+_0)}}} e^{-\left(\sum_{i=1}^{n_s} \omega_{3_i} |\mathcal{O}_i(\iota_0,t)|\right)} \|X(\iota_0)\|^2 + \left[\frac{\nu_{4_{\sigma(\iota^+_{g(t)})}}}{\underline{\alpha}_{2_{\sigma(\iota^+_{g(t)})}}} + \sum_{\substack{l\in\mathbb{N};\\ 0\leq \iota_{g(t)-l}\leq t}} \left\{ \frac{\nu_{4_{\sigma(\iota^+_{g(t)-l})}}}{\underline{\alpha}_{2_{\sigma(\iota^+_{g(t)})}}} \prod_{\substack{q\in\mathbb{N}_0;\\ \iota_{g(t)-l}<\iota_{g(t)-q}\leq t}} \left(\frac{\overline{\alpha}_{2_{\sigma(\iota^+_{g(t)-q})}}}{\underline{\alpha}_{2_{\sigma(\iota^+_{g(t)-(q+1)})}}} \right) e^{-\left(\sum_{i=1}^{n_s} \omega_{3_i} |\mathcal{O}_i(\iota_{g(t)-(l-1)},t)|\right)} \right\} \right] \|w_t\|^2_\infty, \tag{5.19}$$

where $\underline{\alpha}_{2_\sigma} := \min\{\underline{\alpha}_{p_\sigma}, \underline{\alpha}_{e_\sigma}, \kappa\}$ and $\overline{\alpha}_{2_\sigma} := \max\{\overline{\alpha}_{p_\sigma}, \overline{\alpha}_{e_\sigma}, \kappa\}$, and $\iota_0 = 0$. Following Lemma 3.7 and 3.8, one can argue that the series associated with $\|X(\iota_0)\|^2$ and the sum term associated with $\|w_t\|^2_\infty$ are convergent in nature followed by $\tau_{D_{\text{detm}}}$ mentioned in (5.8). One should note that $\tau_{D_{\text{detm}}}$ is obtained by scaling the value of τ_D mentioned in (3.32) using the parameter κ. Every convergent series is bounded. Hence, the summation term in (5.19) is bounded. Therefore, comparing (5.19) with (3.20), (3.15) is ISS. ■

Remark 5.2. The parameter κ is introduced in this work, whereas previous literature considered its value as 1. Using 1 instead of κ would replace all instances of κ in (5.8) with 1. In such a case, minimizing $\tau_{D_{\text{detm}}}$ in Section 5.4 would not be feasible due to the fixed value of 1. In contrast, κ offers greater flexibility, allowing the design of an optimal value to minimize $\tau_{D_{\text{detm}}}$ and enhance system resilience against the maximum MCDoS changing frequency. In (5.8), $\tau_{D_{\text{detm}}}$ is scaled by κ from τ_D in (3.32), hence the term scaling parameter.

Unlike the lower bound of τ_D and $\varkappa$ presented in (3.33), the modified resilient control logic introduced in Section 5.6 uses $\overline{\Delta}$ instead of $\underline{\Delta}$ as the default inter-execution time in the absence of FSDoS. This differs from the original resilient control logic described in Section 3.7, where $\underline{\Delta}$ was used as the default inter-execution time regardless of FSDoS presence. As a result of this modification, the allowable lower bound of τ_D and upper bound of $\varkappa$ under the SETM are also altered. The updated lower bound of τ_D and upper

bound for $\varkappa$ for SETM are

$$\tau_{D_{\text{setm}}} \geq \max\left\{\overline{\Delta}_{\text{setm}}, \max_{\forall\sigma\in\{1,\cdots,n_s\}} \frac{\max\{\lambda_M(P_{p_\sigma}), \lambda_M(P_{e_\sigma})\}}{\lambda_m(\Gamma_{2_\sigma})} \ln\left\{\frac{\max\{\lambda_M(P_{p_\sigma}), \lambda_M(P_{e_\sigma})\}}{\min\{\lambda_m(P_{p_\sigma}), \lambda_m(P_{e_\sigma})\}}\right\}\right\} \tag{5.20}$$

$$\varkappa_{\text{setm}} \leq 1 - \frac{\overline{\Delta}_{\text{setm}}}{\tau_D}, \tag{5.21}$$

where $\overline{\Delta}_{\text{setm}}$ is the maximum inter-execution time for SETM mentioned in later in (5.42).

5.3.3 Choice of parameters

The proposed DETM has several design parameters such as $\lambda, \eta_0, \psi_1, \psi_2, \kappa$, and θ. We put forward the next few results towards an appropriate selection of these parameters.

5.3.3.1 Minimum inter-execution time

Avoiding Zeno behaviour is an important phenomenon in the ETM mechanism. To avoid this, we first have to set up a minimum inter-execution time.

Lemma 5.3. *Let $\lambda \in \mathbb{R}_{>0}$ and $\{\eta_0, \psi_1, \psi_2, \kappa, \theta\} \in \mathbb{R}_{\geq 0}$. Then for any initial condition $x(0) \in \mathbb{R}^{2n_p}$, and $\forall t \in \Upsilon(0,t)$, the sequence $\{t_k\}_{k\in\mathbb{N}}$ defined by DETM (5.1) satisfies (2.16) where $\underline{\Delta}$ satisfies (3.76) and $\underline{\Delta}_\sigma > 0$ is given by the following*

a. If $\|\mathcal{G}_\sigma\| + \|C_\sigma\| \leq \frac{\lambda}{2\kappa}$, $\underline{\Delta}_\sigma$ satisfies (3.77).

b. If $\|\mathcal{G}_\sigma\| + \|C_\sigma\| > \frac{\lambda}{2\kappa}$ and $\theta \leq \frac{1}{2\kappa(\|\mathcal{G}_\sigma\|+\|C_\sigma\|)-\lambda}$,

$$\underline{\Delta}_\sigma = \int_0^1 \frac{1}{\mathcal{I}_\sigma(s) + \left(\|\mathcal{G}_\sigma\| + \|C_\sigma\| - \frac{\lambda}{2\kappa}\right)(s^3 - s)}\, ds. \tag{5.22}$$

c. If $\|\mathcal{G}_\sigma\| + \|C_\sigma\| > \frac{\lambda}{2\kappa}$ *and* $\theta > \frac{1}{2\kappa(\|\mathcal{G}_\sigma\|+\|C_\sigma\|)-\lambda}$,

$$\underline{\Delta}_\sigma = \int_0^1 \frac{1}{\mathcal{I}_\sigma(s) + \frac{1}{2\theta\kappa}(s^3 - s)}\, ds. \tag{5.23}$$

where $\mathcal{I}_\sigma(s), \mathcal{G}_\sigma$, *and* $\mathcal{H}_\sigma$ *are mentioned in* (3.78), (3.80), *and* (3.81), *respectively.*

Proof. Lemma 3.10 contains the proof of (3.77). The proofs of (5.22) and (5.23) are given subsequently. If

$$\|e_\sigma(t)\| \leq \sqrt{\frac{1}{\theta}\eta(t) + \psi\left(\|x_\sigma(t)\|^2 + \|w_t\|_\infty^2\right)}, \tag{5.24}$$

then (5.1) is true where $x_\sigma(t), e_\sigma(t)$, and ψ are mentioned in (3.84), (3.85), and (3.79) respectively. Thus, it obeys a lower bound on the inter-execution time given by the time it takes for the function

$$\phi_{2_\sigma}(t) \coloneqq \frac{\sqrt{\theta}\|e_\sigma(t)\|}{\sqrt{\eta(t) + \theta\psi(\|x_\sigma(t)\|^2 + \|w_t\|_\infty^2)}} \tag{5.25}$$

to go from 0 to 1. We have

$$\dot{\phi}_{2_\sigma}(t) = \frac{\sqrt{\theta}e_\sigma^\top(t)\dot{e}_\sigma(t)}{\|e_\sigma(t)\|\sqrt{\eta(t) + \theta\psi\left(\|x_\sigma(t)\|^2 + \|w_t\|_\infty^2\right)}} - \frac{\sqrt{\theta}\|e_\sigma(t)\|}{2\left\{\eta(t) + \theta\psi\left(\|x_\sigma(t)\|^2 + \|w_t\|_\infty^2\right)\right\}^{\frac{3}{2}}}$$
$$\left(\dot{\eta}(t) + 2\theta\psi x_\sigma^\top(t)\dot{x}_\sigma(t)\right). \tag{5.26}$$

From (5.2), we can write

$$\dot{\eta}(t) \geq \frac{1}{\kappa}\left(-\lambda\eta(t) + \psi\|x_\sigma(t)\|^2 + \psi\|w_t\|_\infty^2 - \|e_\sigma(t)\|^2\right), \tag{5.27}$$

$\forall t \in \Upsilon(0,t)$, where ψ is mentioned in (3.79). After considering (3.90), the bound of $\|\dot{x}_\sigma(t)\|$ in (3.86), and the bound of $\dot{\eta}(t)$ in (5.27), it follows

$$\begin{aligned}\dot{\phi}_{2_\sigma}(t) \leq & \frac{\sqrt{\theta}}{\sqrt{\eta(t)+\theta\psi\left(\|x_\sigma(t)\|^2+\|w_t\|_\infty^2\right)}}\left(\|\mathcal{G}_\sigma\|\|x_\sigma(t)\|+\|\mathcal{H}_\sigma\|\|e_\sigma(t)\|+\|C_\sigma\|\|w_t\|_\infty\right) \\ & + \frac{\sqrt{\theta}\|e_\sigma(t)\|}{2\left\{\eta(t)+\theta\psi\left(\|x_\sigma(t)\|^2+\|w_t\|_\infty^2\right)\right\}^{\frac{3}{2}}}\left\{\frac{1}{\kappa}\left(\lambda\eta(t)-\psi\|x_\sigma(t)\|^2-\psi\|w_t\|_\infty^2+\|e_\sigma(t)\|^2\right)\right. \\ & \left.+2\theta\psi\|\mathcal{G}_\sigma\|\|x_\sigma(t)\|^2+2\theta\psi\|\mathcal{H}_\sigma\|\|x_\sigma(t)\|\|e_\sigma(t)\|+2\theta\psi\|C_\sigma\|\|x_\sigma(t)\|\|w_t\|_\infty\right\} \end{aligned} \tag{5.28}$$

By recognising the fact that $\|x(t)\| \geq 0, \|w_t\|_\infty \geq 0$, and $\eta(t) \geq 0$, we can write

$$\begin{aligned}\dot{\phi}_{2_\sigma}(t) \leq & \frac{1}{\sqrt{\psi}}\left(\|\mathcal{G}_\sigma\|+\|C_\sigma\|\right)+\left(\|\mathcal{H}_\sigma\|+\frac{\lambda}{2\kappa}\right)\phi_{2_\sigma}(t)+\sqrt{\psi}\|\mathcal{H}_\sigma\|\phi_{2_\sigma}^2(t)+\frac{1}{2\theta\kappa}\phi_{2_\sigma}^3(t) \\ & +\left\{-\lambda-\frac{1}{\theta}+2\kappa\left(\|\mathcal{G}_\sigma\|+\|C_\sigma\|\right)\right\}\frac{\theta\psi\left(\|x_\sigma(t)\|^2+\|w_t\|_\infty^2\right)}{2\kappa\left\{\eta(t)+\theta\psi\left(\|x_\sigma(t)\|^2+\|w_t\|_\infty^2\right)\right\}}\phi_{2_\sigma}(t) \end{aligned} \tag{5.29}$$

1. If $-\lambda-\frac{1}{\theta}+2\kappa\left(\|\mathcal{G}_\sigma\|+\|C_\sigma\|\right) \leq 0$, then $\theta \in \left[0, \frac{1}{2\kappa(\|\mathcal{G}_\sigma\|+\|C_\sigma\|)-\lambda}\right]$ and $\|\mathcal{G}_\sigma\|+\|C_\sigma\| > \frac{\lambda}{2\kappa}$. In this scenario

$$\dot{\phi}_{2_\sigma}(t) \leq \frac{1}{\sqrt{\psi}}\left(\|\mathcal{G}_\sigma\|+\|C_\sigma\|\right)+\left(\|\mathcal{H}_\sigma\|+\frac{\lambda}{2\kappa}\right)\phi_{2_\sigma}(t)+\sqrt{\psi}\|\mathcal{H}_\sigma\|\phi_{2_\sigma}^2(t)+\frac{1}{2\theta\kappa}\phi_{2_\sigma}^3(t). \tag{5.30}$$

For $\theta = \frac{1}{2\kappa(\|\mathcal{G}_\sigma\|+\|C_\sigma\|)-\lambda}$, we get

$$\begin{aligned}\dot{\phi}_{2_\sigma}(t) \leq & \frac{1}{\sqrt{\psi}}\left(\|\mathcal{G}_\sigma\|+\|C_\sigma\|\right)+\left(\|\mathcal{G}_\sigma\|+\|\mathcal{H}_\sigma\|+\|C_\sigma\|\right)\phi_{2_\sigma}(t)+\sqrt{\psi}\|\mathcal{H}_\sigma\|\phi_{2_\sigma}^2(t) \\ & +\left(\|\mathcal{G}_\sigma\|+\|C_\sigma\|-\frac{\lambda}{2\kappa}\right)\left(\phi_{2_\sigma}^3(t)-\phi_{2_\sigma}(t)\right). \end{aligned} \tag{5.31}$$

Thus, the comparison lemma for differential inequalities yields the result of (5.22).

2. If $-\lambda - \frac{1}{\theta} + 2\kappa\left(\|\mathcal{G}_\sigma\| + \|C_\sigma\|\right) > 0$, then $\theta > \frac{1}{2\kappa(\|\mathcal{G}_\sigma\|+\|C_\sigma\|)-\lambda}$ and $\|\mathcal{G}_\sigma\| + \|C_\sigma\| > \frac{\lambda}{2\kappa}$. Hence we can write from (5.28) by observing that $\eta(t) \geq 0$,

$$\dot{\phi}_{2_\sigma}(t) \leq \frac{1}{\sqrt{\psi}}\left(\|\mathcal{G}_\sigma\| + \|C_\sigma\|\right) + \left(\|\mathcal{H}_\sigma\| + \frac{\lambda}{2\kappa}\right)\phi_{2_\sigma}(t) + \sqrt{\psi}\phi^2_{2_\sigma}(t) + \frac{1}{2\theta\kappa}\phi^3_{2_\sigma}(t)$$
$$+ \frac{1}{2\kappa}\left\{-\lambda - \frac{1}{\theta} + 2\kappa\left(\|\mathcal{G}_\sigma\| + \|C_\sigma\|\right)\right\}\phi_{2_\sigma}(t). \tag{5.32}$$

In a similar fashion, applying the comparison Lemma in (5.32), we get the result of (5.23).

■

Remark 5.4. The lower bound (3.77) is exactly the same as the lower bound on minimum inter-execution times for the SETM given by (3.17) in the first case. In this scenario, [147] gives an intuitive interpretation that if $\frac{\lambda}{2\kappa} \geq \|\mathcal{G}_\sigma\| + \|C_\sigma\|$ then filter (5.2) is too fast, that it doesn't guarantee a large minimum inter-execution time than SETM. Hence, to get a larger inter-execution time λ should be kept lower than $2\kappa\left(\|\mathcal{G}_\sigma\| + \|C_\sigma\|\right)$.

Lemma 5.5. *Let* (4.7) *holds,* $\theta \in \mathbb{R}_{\geq 0}, \eta(0) = 0, \lambda = \max_{\forall\sigma\in\{1,\cdots,n_s\}}\{\zeta_{1_\sigma}\}$, *and*

$$\max_{\forall\sigma\in\{1,\cdots,n_s\}}\{\underline{\alpha}_{p_\sigma}, \underline{\alpha}_{e_\sigma}\} \leq \kappa \leq \min_{\forall\sigma\in\{1,\cdots,n_s\}}\{\overline{\alpha}_{p_\sigma}, \overline{\alpha}_{e_\sigma}\}, \tag{5.33}$$

where $\zeta_{1_\sigma}, \overline{\alpha}_{p_\sigma}$, *and* $\overline{\alpha}_{e_\sigma}$ *are mentioned in* (3.39), (3.41), *and* (3.42), *respectively. Then for all initial conditions* $x(0)$, (3.48) *is true.*

Proof. Observing that $\lambda = \max_{\forall\sigma\in\{1,\cdots,n_s\}}\{\zeta_{1_\sigma}\}$, we can say $\zeta_{1_\sigma} = \zeta_{2_\sigma}$. Hence, $\omega_{1_\sigma} = \omega_{3_\sigma}, \nu_{1_\sigma} = \nu_{2_\sigma}, \overline{\alpha}_\sigma = \overline{\alpha}_{2_\sigma}$, and $\underline{\alpha}_\sigma = \underline{\alpha}_{2_\sigma}$ if (5.33) is true. From (5.1), we can say if $\theta = 0$, then $\eta(t) \geq 0$. If $\theta \neq 0$, then we can write from (5.1),

$$-\xi^\top_\sigma(t)\xi_\sigma(t) - \xi^\top_e(t)\xi_e(t) + \psi_1\left(y^\top_\sigma(t)y_\sigma(t) + \|w_t\|^2_\infty\right) + \psi_2 x^\top_e(t)x_e(t) \geq -\frac{1}{\theta}\eta(t). \tag{5.34}$$

Therefore, we get from (5.2), $\dot{\eta}(t) \geq \frac{1}{\kappa}\left(-\lambda\eta(t) - \frac{1}{\theta}\eta(t)\right)$, if $t \in \Upsilon(0,t)$, by using (5.34). From comparison Lemma, we can say $\eta(t) \geq 0$ if $\eta(0) \geq 0$. In other cases, when $t \in \Omega(0,t)$, we get $\dot{\eta}(t) = -\left(\lambda/\kappa\right)\eta(t)$. Then the solution is $\eta(t) = \exp\{-(\lambda/\kappa)t\}\eta(0)$. Therefore $\eta(t) \geq 0$ subject to $\eta(0) \geq 0$. Now we can say $\|x(t)\| \leq \|X(t)\|$ because $\eta(t) \geq 0, \|X(0)\| =$

$\|x(0)\|$ and $\eta(0) = 0$. In this scenario, the RHS of (3.48) and (5.19) are equal. Hence (3.48) holds. ■

Remark 5.6. Lemma 5.5 provides bounds on the parameters λ and κ, as well as on the initial value $\eta(0)$. The optimal values of λ and κ are subsequently determined by solving an optimization problem aimed at ensuring system resilience against the maximum MCDoS changing frequency.

5.4 Optimization problem

An algorithm to minimise $\tau_{D_{\text{detm}}}$ is given in this section. The lower bound of $\tau_{D_{\text{detm}}}$ in (5.8) is to be considered as the cost function. Minimising the cost function also minimises the value of $\tau_{D_{\text{detm}}}$. Therefore, the cost function is

$$\tilde{J} = \max_{\forall \sigma \in \{1,\cdots,n_s\}} \frac{\max\{\overline{\alpha}_{p_\sigma}, \overline{\alpha}_{e_\sigma}, \kappa\}}{\zeta_{2_\sigma}} \ln \left\{ \frac{\max\{\overline{\alpha}_{p_\sigma}, \overline{\alpha}_{e_\sigma}, \kappa\}}{\min\{\underline{\alpha}_{p_\sigma}, \underline{\alpha}_{e_\sigma}, \kappa\}} \right\}, \tag{5.35}$$

where $\underline{\alpha}_{p_\sigma}, \overline{\alpha}_{p_\sigma}, \underline{\alpha}_{e_\sigma}, \overline{\alpha}_{e_\sigma}$ are mentioned in (3.41) and (3.42), respectively, ζ_{2_σ} and κ are mentioned in (5.10) and (5.2), respectively. Hence, the optimization problem is to minimize $\tilde{J}$ subject to $\underline{\alpha}_{p_\sigma} I \leq P_{p_\sigma} \leq \overline{\alpha}_{p_\sigma} I, \underline{\alpha}_{e_\sigma} I \leq P_{e_\sigma} \leq \overline{\alpha}_{e_\sigma} I, \Gamma_{7_\sigma} \geq \zeta_{2_\sigma} I, \lambda = \max_{\forall \sigma \in \{1,\cdots,n_s\}} \zeta_{2_\sigma}, \max_{\forall \sigma \in \{1,\cdots,n_s\}} \{\underline{\alpha}_{p_\sigma}, \underline{\alpha}_{e_\sigma}\} \leq \kappa \leq \min_{\forall \sigma \in \{1,\cdots,n_s\}} \{\overline{\alpha}_{p_\sigma}, \overline{\alpha}_{e_\sigma}\}, \{\underline{\alpha}_{p_\sigma}, \underline{\alpha}_{e_\sigma}, \psi_1, \psi_2, \varepsilon_{1_\sigma}, \varepsilon_{2_\sigma}\} > 0$ and $H_\sigma \in \mathbb{R}^{n_p \times n_{h_\sigma}}$. In this case, the cost function is non-convex. This NCO finds the optimal value of $\tilde{J}$ by solving LMIs present in constraints. Nevertheless, there isn't an optimization technique that can solve LMIs besides NCO. The same 2−step process described in Section 3.6 of Chapter 3 is employed to minimize $\tilde{J}$, converting the NCO into a CO to solve the problem.

Step 1 The first cost function is

$$J_\sigma := \max\{\overline{\alpha}_{p_\sigma}, \overline{\alpha}_{e_\sigma}, \kappa\} - \min\{\underline{\alpha}_{p_\sigma}, \underline{\alpha}_{e_\sigma}, \kappa\} \geq 0. \tag{5.36}$$

Minimize J_σ subject to $\underline{\alpha}_{p_\sigma} I \leq P_{p_\sigma} \leq \overline{\alpha}_{p_\sigma} I, \underline{\alpha}_{e_\sigma} I \leq P_{e_\sigma} \leq \overline{\alpha}_{e_\sigma} I, \lambda = \zeta_{2_\sigma}, \{\underline{\alpha}_{p_\sigma}, \underline{\alpha}_{e_\sigma}\} \leq \kappa \leq \{\overline{\alpha}_{p_\sigma}, \overline{\alpha}_{e_\sigma}\}, \{\underline{\alpha}_{p_\sigma}, \underline{\alpha}_{e_\sigma}, \psi_1, \psi_2, \varepsilon_{1_\sigma}, \varepsilon_{2_\sigma}\} > 0, \Gamma_{7_\sigma} \geq qI$, and $H_\sigma \in \mathbb{R}^{n_p \times n_{y\sigma}}$ is the first CO problem.

Step 2 From (5.36), we can write

$$J_\sigma = \max \Big\{ \overline{\alpha}_{p_\sigma} - \underline{\alpha}_{p_\sigma}, \overline{\alpha}_{p_\sigma} - \underline{\alpha}_{e_\sigma}, \overline{\alpha}_{p_\sigma} - \kappa, \overline{\alpha}_{e_\sigma} - \underline{\alpha}_{p_\sigma}, \overline{\alpha}_{e_\sigma} - \underline{\alpha}_{e_\sigma}, \overline{\alpha}_{e_\sigma} - \kappa, \kappa - \underline{\alpha}_{p_\sigma}, \kappa - \underline{\alpha}_{e_\sigma} \Big\}. \tag{5.37}$$

From (5.37), we reached to the conclusion that $\overline{\alpha}_{p_\sigma} - \underline{\alpha}_{p_\sigma}, \overline{\alpha}_{p_\sigma} - \underline{\alpha}_{e_\sigma}, \overline{\alpha}_{p_\sigma} - \kappa, \overline{\alpha}_{e_\sigma} - \underline{\alpha}_{p_\sigma}, \overline{\alpha}_{e_\sigma} - \underline{\alpha}_{e_\sigma}, \overline{\alpha}_{e_\sigma} - \kappa, \kappa - \underline{\alpha}_{p_\sigma}$, and $\kappa - \underline{\alpha}_{e_\sigma}$ are bounded from above by J_σ. The second cost function is

$$J \coloneqq \min_{\forall \sigma \in \{1, \cdots, n_s\}} \zeta_{2_\sigma}. \tag{5.38}$$

It is possible to maximize all values of $\zeta_{2_\sigma}, \forall \sigma \in \{1, \cdots, n_s\}$ by maximizing the minimum value of ζ_{2_σ}. Therefore, maximize J subject to $\Gamma_{7_\sigma} \geq \zeta_{2_\sigma} I, \underline{\alpha}_{p_\sigma} I \leq P_{p_\sigma} \leq \overline{\alpha}_{p_\sigma} I, \underline{\alpha}_{e_\sigma} I \leq P_{e_\sigma} \leq \overline{\alpha}_{e_\sigma} I, \{\overline{\alpha}_{p_\sigma} - \underline{\alpha}_{p_\sigma}, \overline{\alpha}_{p_\sigma} - \underline{\alpha}_{e_\sigma}, \overline{\alpha}_{p_\sigma} - \kappa, \overline{\alpha}_{e_\sigma} - \underline{\alpha}_{p_\sigma}, \overline{\alpha}_{e_\sigma} - \underline{\alpha}_{e_\sigma}, \overline{\alpha}_{e_\sigma} - \kappa, \kappa - \underline{\alpha}_{p_\sigma}, \kappa - \underline{\alpha}_{e_\sigma}\} \leq J_\sigma, \lambda \leq \zeta_{2_\sigma}, \{\underline{\alpha}_{p_\sigma}, \underline{\alpha}_{e_\sigma}\} \leq \kappa \leq \{\overline{\alpha}_{p_\sigma}, \overline{\alpha}_{e_\sigma}\}, \{\psi_1, \psi_2, \varepsilon_{1_\sigma}, \varepsilon_{2_\sigma}\} > 0$, and $H_\sigma \in \mathbb{R}^{n_p \times n_{h\sigma}}$ is the second CO problem.

However, optimizing J_σ and J does not guarantee the optimization of $\tilde{J}$. Γ_{7_σ} in step 1 is a sensitive parameter and must satisfy $\Gamma_{7_\sigma} \geq qI$, where q is a positive scalar. The choice of q also influences the optimization of $\tilde{J}$. In Chapters 3 and 4, q was chosen manually. Here, Algorithm 5.1 is developed to determine a suitable q and compute $P_{p_\sigma}, P_{e_\sigma}, \lambda, \kappa, \psi_1, \psi_2, \varepsilon_{1_\sigma}, \varepsilon_{2_\sigma}$, and H_σ, ultimately yielding the optimal $\tilde{J}$. Since this is a nonlinear optimization problem, the results depend on the initial value of q.

Algorithm 5.1 Minimizing $\tau_{D_{\text{detm}}}$

Inputs: A, B, C_σ, K, q
Outputs: $q_{\text{final}}, P_{p_\sigma}, P_{e_\sigma}, \lambda, \kappa, \psi_1, \psi_2, \varepsilon_{1_\sigma}, \varepsilon_{2_\sigma}, \Gamma_{7_\sigma}, H_\sigma$
Function optimizationCVX(A, B, C_σ, K, q_1)
Start a for loop for $\sigma = 1$ to n_s.
Begin CVX with CVX solver Sedumi
$J_\sigma := \max\{\overline{\alpha}_{p_\sigma}, \overline{\alpha}_{e_\sigma}, \kappa\} - \min\{\underline{\alpha}_{p_\sigma}, \underline{\alpha}_{e_\sigma}, \kappa\}$
Minimize J_σ
Subject to $\underline{\alpha}_{p_\sigma} I \leq P_{p_\sigma} \leq \overline{\alpha}_{p_\sigma} I$, $\underline{\alpha}_{e_\sigma} I \leq P_{e_\sigma} \leq \overline{\alpha}_{e_\sigma} I$, $\{\underline{\alpha}_{p_\sigma}, \underline{\alpha}_{e_\sigma}, \psi_1, \psi_2, \varepsilon_{1_\sigma}, \varepsilon_{2_\sigma}\} \geq 0.001, \Gamma_{7_\sigma} \geq q_1 I$, $\lambda = \zeta_{2_\sigma}, \{\underline{\alpha}_{p_\sigma}, \underline{\alpha}_{e_\sigma}\} \leq \kappa \leq \{\overline{\alpha}_{p_\sigma}, \overline{\alpha}_{e_\sigma}\}$.
End CVX.
End for loop.
Begin CVX with CVX solver Sedumi
$J := \min_{\forall \sigma \in \{1,\cdots,n_s\}} \zeta_{2_\sigma}$
Maximize J
Subject to $\Gamma_{7_\sigma} \geq \zeta_{2_\sigma} I, \underline{\alpha}_{p_\sigma} I \leq P_{p_\sigma} \leq \overline{\alpha}_{p_\sigma} I, \underline{\alpha}_{e_\sigma} I \leq P_{e_\sigma} \leq \overline{\alpha}_{e_\sigma} I, \{\overline{\alpha}_{p_\sigma} - \underline{\alpha}_{p_\sigma}, \overline{\alpha}_{p_\sigma} - \underline{\alpha}_{e_\sigma}, \overline{\alpha}_{p_\sigma} - \kappa, \overline{\alpha}_{e_\sigma} - \underline{\alpha}_{p_\sigma}, \overline{\alpha}_{e_\sigma} - \underline{\alpha}_{e_\sigma}, \overline{\alpha}_{e_\sigma} - \kappa, \varphi - \underline{\alpha}_{p_\sigma}, \kappa - \underline{\alpha}_{e_\sigma}\} \leq J_\sigma, \lambda \leq \zeta_{2_\sigma}, \{\underline{\alpha}_{p_\sigma}, \underline{\alpha}_{e_\sigma}\} \leq \kappa \leq \{\overline{\alpha}_{p_\sigma}, \overline{\alpha}_{e_\sigma}\}, \{\underline{\alpha}_{p_\sigma}, \underline{\alpha}_{e_\sigma}, \psi_1, \psi_2, \varepsilon_{1_\sigma}, \varepsilon_{2_\sigma}\} \geq 0.001$.
End CVX.
Return $P_{p_\sigma}, P_{e_\sigma}, \lambda, \kappa, \psi_1, \psi_2, \varepsilon_{1_\sigma}, \varepsilon_{2_\sigma}, \Gamma_{7_\sigma}, H_\sigma$
end function
$q_2 \leftarrow q$
$q_3 \leftarrow [\ ]$
$r_1 \leftarrow \infty$
$r_2 \leftarrow \infty$
$r_3 \leftarrow \infty$
$r_4 \leftarrow \infty$
while $(r_1 \leq r_2)$ **do**
$P_{p_\sigma}, P_{e_\sigma}, \lambda, \kappa, \psi_1, \psi_2, \varepsilon_{1_\sigma}, \varepsilon_{2_\sigma}, \Gamma_{7_\sigma}, H_\sigma \leftarrow$ optimizationCVX(A, B, C_σ, K, q_2)
Compute $\tilde{J}$
$r_2 \leftarrow r_1$
$r_1 \leftarrow \tilde{J}$
$q_4 \leftarrow q_3$
$q_3 \leftarrow q_2$
$q_2 \leftarrow q_2 + 10^{-4}$
end while
while $(r_3 \leq r_4)$ **do**
if $q \leq 0$ **then**
break
end if
$q_5 \leftarrow q$
$q \leftarrow q - 10^{-4}$
$P_{p_\sigma}, P_{e_\sigma}, \lambda, \kappa, \psi_1, \psi_2, \varepsilon_{1_\sigma}, \varepsilon_{2_\sigma}, \Gamma_{3_\sigma}, H_\sigma \leftarrow$ optimizationCVX(A, B, C_σ, K, q)
Compute $\tilde{J}$
$r_4 \leftarrow r_3$
$r_3 \leftarrow \tilde{J}$
end while
if $r_4 \leq r_2$ **then**
$q_{\text{final}} \leftarrow q_5$
$\tilde{J} \leftarrow r_4$
else
$q_{\text{final}} \leftarrow q_4$
$\tilde{J} \leftarrow r_2$
end if
Compute $P_{p_\sigma}, P_{e_\sigma}, \lambda, \kappa, \psi_1, \psi_2, \varepsilon_{1_\sigma}, \varepsilon_{2_\sigma}, H_\sigma$ corresponds to q_{final}.

5.5 Upper bound of inter-sampling rate

In Lemma 3.10 and 5.3, the lower inter-execution time is calculated for SETM and DETM, respectively. Now, the problem boils down to finding the upper inter-execution time. Given a square matrix R, let

$$\|R\|_{\mathcal{L}} \coloneqq \max\left\{\lambda : \lambda \in \text{spectrum}\left\{\frac{R+R^{\top}}{2}\right\}\right\} \tag{5.39}$$

denote the logarithmic norm of R [160].

Lemma 5.7. *Assume the identical notation seen in Theorem 3.5. Any control update rule without FSDoS that has inter-execution time for a specific σ value less than or equal to*

$$\overline{\Delta}_{\sigma_{setm}} \coloneqq \frac{1}{\max\{\|\mathcal{G}_\sigma\|, \|C_\sigma\|\}}\left(\frac{\sqrt{\psi}}{\sqrt{\psi}+2}\right), \tag{5.40}$$

when $\|\mathcal{F}_\sigma\|_{\mathcal{L}} \leq 0$, and

$$\overline{\Delta}_{\sigma_{setm}} \coloneqq \frac{1}{\|\mathcal{F}_\sigma\|_{\mathcal{L}}} \ln\left[\left(\frac{\sqrt{\psi}}{\sqrt{\psi}+2}\right)\frac{1}{\max\{\|\mathcal{G}_\sigma\|, \|C_\sigma\|\}}\|\mathcal{F}_\sigma\|_{\mathcal{L}}+1\right], \tag{5.41}$$

when $\|\mathcal{F}_\sigma\|_{\mathcal{L}} > 0$, satisfies SETM condition (3.17). In the absence of FSDoS, all the inter-execution times $\forall\sigma$ become less than or equal to

$$\overline{\Delta}_{setm} \coloneqq \max_{\forall\sigma\in\{1,\cdots,n_s\}} \overline{\Delta}_{\sigma_{setm}}. \tag{5.42}$$

Proof. Any attempt at a control update is successful when there is no FSDoS. Thus, in accordance with (3.13), (3.14), and (3.85), the dynamics of $e_\sigma(t)$ satisfies

$$\dot{e}_\sigma(t) = \mathcal{F}_\sigma e_\sigma(t) - \mathcal{G}_\sigma x_\sigma(t_k) - \begin{bmatrix} C_\sigma^{\top} & 0 \end{bmatrix}^{\top} w(t), \tag{5.43}$$

$\forall t \in [t_k, t_{k+1})$ and $\forall k \in \mathbb{N}_0$, where

$$\mathcal{F}_\sigma \coloneqq \begin{bmatrix} C_\sigma A C_\sigma^{\dagger} & 0 \\ 0 & A - L_\sigma C_\sigma \end{bmatrix}, \tag{5.44}$$

$\mathcal{G}_\sigma$ is mentioned in (3.80), $e_\sigma(t_k) = 0$, and $x_\sigma(t)$ is mentioned in (3.84). Recall that $\|e^{\mathcal{F}_\sigma t}\| \leq e^{\|\mathcal{F}_\sigma\|_{\mathcal{L}} t}, \forall t \in \mathbb{R}_{\geq 0}$. With this attribute, we subsequently have

$$\|e_\sigma(t)\| \leq \delta_{1_\sigma} \int_{t_k}^{t} e^{\|\mathcal{F}_\sigma\|_{\mathcal{L}}(t-s)} \left[\|x_\sigma(t_k)\| + \|w(s)\|\right] ds \tag{5.45}$$

$\forall t \in [t_k, t_{k+1})$ and $\forall k \in \mathbb{N}_0$, where $\delta_{1_\sigma} \coloneqq \max\{\|\mathcal{G}_\sigma\|, \|C_\sigma\|\}$. Let $b_\sigma(t-t_k) \coloneqq \int_{t_k}^{t} e^{\|\mathcal{F}_\sigma\|_{\mathcal{L}}(t-s)} ds$. Taking advantage of the fact that $x_\sigma(t_k) = e_\sigma(t) + x_\sigma(t)$, we obtain

$$\|e_\sigma(t)\| \leq \delta_{1_\sigma} b_\sigma(t-t_k)\|e_\sigma(t)\| + \delta_{1_\sigma} b_\sigma(t-t_k)(\|x_\sigma(t)\| + \|w_t\|_\infty). \tag{5.46}$$

Note that $b_\sigma(0) = 0$ and $b_\sigma(t-t_k)$ increase monotonically with t. For any positive real Δ, we have

$$b_\sigma(\Delta) \leq \frac{1}{\delta_{1_\sigma}} \frac{\sqrt{\psi}}{\sqrt{\psi}+2}. \tag{5.47}$$

If $\Delta_k \leq \Delta$, then any control update rule will fulfil

$$\|e_\sigma(t)\| \leq \frac{\sqrt{\psi}}{2} \left(\|x_\sigma(t)\| + \|w_t\|_\infty\right), \tag{5.48}$$

which eventually will satisfy (3.17), $\forall t \in \mathbb{R}_{\geq 0}$. We obtain an explicit expression for Δ to wrap up the proof. Let first $\|\mathcal{F}_\sigma\|_{\mathcal{L}} \leq 0$. In this case, $b_\sigma(\Delta) \leq \Delta$, so that (5.40) produces the intended outcome. If $\|\mathcal{F}_\sigma\|_{\mathcal{L}} > 0$, we have

$$b_\sigma(\Delta) = \frac{1}{\|\mathcal{F}_\sigma\|_{\mathcal{L}}} \left(e^{\|\mathcal{F}_\sigma\|_{\mathcal{L}}\Delta} - 1\right) \tag{5.49}$$

and (5.41) yields the desired result. For all the values of σ, (5.42) is the upper limit of the inter-execution time. ■

Lemma 5.8. *Assume the identical notation seen in Theorem 5.1. Any control update rule without FSDoS that has inter-execution times for a specific σ value less than or equal to*

$$\overline{\Delta}_{\sigma_{detm}} \coloneqq \frac{1}{\max\{\|\mathcal{G}_\sigma\|, \|C_\sigma\|\}} \left(\frac{\sqrt{\psi}}{\sqrt{\psi}+\sqrt{3}}\right), \tag{5.50}$$

when $\|\mathcal{F}_\sigma\|_{\mathcal{L}} \leq 0$, *and*

$$\overline{\Delta}_{\sigma_{detm}} := \frac{1}{\|\mathcal{F}_\sigma\|_{\mathcal{L}}} \ln \left[\left(\frac{\sqrt{\psi}}{\sqrt{\psi}+\sqrt{3}} \right) \frac{1}{\max\{\|\mathcal{G}_\sigma\|, \|C_\sigma\|\}} \|\mathcal{F}_\sigma\|_{\mathcal{L}} + 1 \right] \tag{5.51}$$

when $\|\mathcal{F}_\sigma\|_{\mathcal{L}} > 0$, *satisfies DETM condition* (5.1). *In the absence of FSDoS, all the inter-execution times become less than or equal to*

$$\overline{\Delta}_{detm} := \max_{\forall \sigma \in \{1,\cdots,n_s\}} \overline{\Delta}_{\sigma_{detm}}, \tag{5.52}$$

for all σ.

Proof. From (5.46), we can write,

$$\sqrt{\psi}\|e_\sigma(t)\| \leq \sqrt{\psi}\delta_{1_\sigma} b_\sigma(t-t_k)\|e_\sigma(t)\| + \delta_{1_\sigma} b_\sigma(t-t_k)\left(\frac{1}{\sqrt{\theta}}\sqrt{\eta(t)} + \sqrt{\psi}\|x_\sigma(t)\| + \sqrt{\psi}\|w_t\|_\infty \right). \tag{5.53}$$

Like the proof of Lemma 5.7, in this case also $b_\sigma(0) = 0$ and $b_\sigma(t-t_k)$ is monotonically increasing with t. Similarly, for any positive real Δ, we can express it as

$$b_\sigma(\Delta) \leq \frac{1}{\delta_{1_\sigma}} \frac{\sqrt{\psi}}{\sqrt{\psi}+\sqrt{3}}. \tag{5.54}$$

If $\Delta_k \leq \Delta$, then any control update rule will fulfil

$$\|e_\sigma(t)\| \leq \frac{1}{\sqrt{3\theta}}\sqrt{\eta(t)} + \sqrt{\frac{\psi}{3}}\|x_\sigma(t)\| + \sqrt{\frac{\psi}{3}}\|w_t\|_\infty, \tag{5.55}$$

which eventually will satisfy (5.24) and (5.1), $\forall t \in \mathbb{R}_{\geq 0}$. The rest of the proof is similar to Lemma 5.7. ■

5.6 Modified resilient control logic

The direct implementation of the SETM in (3.17) and the DETM in (5.1) and (5.2) is not feasible due to their dependence on the supremum norm of the disturbance w. Fundamentally, the event-based control logic in (3.17) and (5.1) can be reformulated to eliminate the need for the supremum norm of the disturbance. By omitting the disturbance, we have (3.99) from (3.17),

$$\xi_\sigma^\top(t)\xi_\sigma(t) + \xi_e^\top(t)\xi_e(t) = \frac{1}{\theta}\eta(t) + \psi_1 y_\sigma^\top(t)y_\sigma(t) + \psi_2 x_e^\top(t)x_e(t) \tag{5.56}$$

from (5.1), and

$$\dot{\eta}(t) = \begin{cases} -\frac{\lambda}{\kappa}\eta(t) & \text{if } t \in \Omega(0,t), \\ \rho_{2_\sigma}(t) & \text{otherwise,} \end{cases} \tag{5.57}$$

where

$$\rho_{2_\sigma}(t) \coloneqq \frac{1}{\kappa}\left[-\lambda\eta(t) - \xi_\sigma^\top(t)\xi_\sigma(t) - \xi_e^\top(t)\xi_e(t) + \psi_1 y_\sigma^\top(t)y_\sigma(t) + \psi_2 x_e^\top(t)x_e(t)\right] \tag{5.58}$$

from (5.2). Omitting the disturbance prevents the avoidance of Zeno behaviour. Therefore, a lower bound on the sampling rate must be imposed a priori. The lower bound of the sampling rate ($\underline{\Delta}$) is calculated for SETM and DETM in Lemma 3.10. Let

$$\varpi_{2_{\sigma_k}} \coloneqq \inf\Big\{t \in \mathbb{R}_{>t_k} : \xi_\sigma^\top(t^-)\xi_\sigma(t^-) + \xi_e^\top(t^-)\xi_e(t^-) \geq \frac{1}{\theta}\eta(t) + \psi_1 y_\sigma^\top(t)y_\sigma(t) + \psi_2 x_e^\top(t)x_e(t)\Big\} \tag{5.59}$$

$\forall k \in \mathbb{N}_0$ and $\forall \sigma \in \{1, \cdots, n_s\}$, where $\eta(t)$ follows the dynamics of (5.57).

Proposition 5.9. *Let $\underline{\Delta}$ be the positive constant which follows (3.76) and (3.77) as in Lemma 3.10 and $\overline{\Delta}_{setm}$ be the positive constant which follows (5.42) in Lemma 5.7. Then*

the sequence $\{t_k\}_{k\in\mathbb{N}_0}$ *for SETM is formally defined by*

$$t_{k+1} = \begin{cases} t_k + \underline{\Delta}, & \text{if } t_k \in \Omega(0,t) \wedge \varpi_{1_{\sigma_k}} \leq t_k + \underline{\Delta}, \\ t_k + \overline{\Delta}_{setm}, & \text{if } t_k \in \Upsilon(0,t) \wedge \varpi_{1_{\sigma_k}} \leq t_k + \overline{\Delta}_{setm}, \\ \varpi_{1_{\sigma_k}}, & \text{otherwise}, \end{cases} \tag{5.60}$$

where $\varpi_{1_{\sigma_k}}$ *is mentioned in* (3.100).

Proof. The inter-sampling related to (5.60) is equivalent to $\varpi_{1_{\sigma_k}} - t_k, \underline{\Delta}$, or $\overline{\Delta}_{\text{setm}}$. By (5.60), $t_{k+1} = \varpi_{1_{\sigma_k}}$ only if $\varpi_{1_{\sigma_k}} \geq t_k + \underline{\Delta}$ when FSDoS is present in the system ($t_k \in \Omega(0,t)$) and $\varpi_{1_{\sigma_k}} \geq t_k + \overline{\Delta}_{\text{setm}}$ when FSDoS is not present in the system ($t_k \in \Upsilon(0,t)$). We know the fact that $\underline{\Delta} \leq \overline{\Delta}_{\text{setm}}$. This is why we put the inter-sampling time $\underline{\Delta}$ in the presence of FSDoS when $\varpi_{1_{\sigma_k}} \leq t_k + \underline{\Delta}$. So that when FSDoS is lifted out, the control update will take place in a minimum time of less than $\underline{\Delta}$. When FSDoS is not present, the control update takes place at a minimum feasible time of $\overline{\Delta}_{\text{setm}}$. ■

Proposition 5.10. *Let* $\underline{\Delta}$ *be the positive constant which follows* (5.22) *or* (5.23) *depending on the value of* θ *and followed by* (3.76) *as in Lemma 3.10. Let* $\overline{\Delta}_{detm}$ *be the positive constant which follows* (5.52) *in Lemma 5.8. Then the sequence* $\{t_k\}_{k\in\mathbb{N}_0}$ *for DETM is formally defined by*

$$t_{k+1} = \begin{cases} t_k + \underline{\Delta}, & \text{if } t_k \in \Omega(0,t) \wedge \varpi_{2_{\sigma_k}} \leq t_k + \underline{\Delta}, \\ t_k + \overline{\Delta}_{detm}, & \text{if } t_k \in \Upsilon(0,t) \wedge \varpi_{2_{\sigma_k}} \leq t_k + \overline{\Delta}_{detm}, \\ \varpi_{2_{\sigma_k}}, & \text{otherwise}, \end{cases} \tag{5.61}$$

where $\varpi_{2_{\sigma_k}}$ *is mentioned in* (5.59).

Proof. Same as the Proposition 5.9. ■

From the following Lemma, we can say that DETM has a longer inter-execution time than SETM.

Lemma 5.11. *Let* $\{\theta, \psi_1, \psi_2, \eta(0)\} \in \mathbb{R}_{\geq 0}$, *let* $k \in \mathbb{N}_0, t_k \in \mathbb{R}_{\geq 0}, x(t_k) \in \mathbb{R}^{2n_p}$ *and* $\eta(t_k) \geq 0$, *let* t^s_{k+1} *be given by the rule* (3.101) *and* t^d_{k+1} *be given by the rule* (5.61), *then* $t^s_{k+1} \leq t^d_{k+1}$.

Proof. Let us assume that $t^s_{k+1} > t^d_{k+1}$. Then by (3.101), we have

$$\psi_1 y_\sigma^\top(t^d_{k+1}) y_\sigma(t^d_{k+1}) + \psi_2 x_e^\top(t^d_{k+1}) x_e(t^d_{k+1}) - \xi_\sigma^\top(t^{d-}_{k+1})\xi_\sigma(t^{d-}_{k+1}) - \xi_e^\top(t^{d-}_{k+1})\xi_e(t^{d-}_{k+1}) > 0. \tag{5.62}$$

We will now consider two different cases. If $\theta > 0$, then from (5.61), we must have

$$\begin{aligned}&\eta(t^d_{k+1}) + \theta[\psi_1 y_\sigma^\top(t^d_{k+1}) y_\sigma(t^d_{k+1}) + \psi_2 x_e^\top(t^d_{k+1}) x_e(t^d_{k+1}) - \xi_\sigma^\top(t^{d-}_{k+1})\xi_\sigma(t^{d-}_{k+1}) \\ &- \xi_e^\top(t^{d-}_{k+1})\xi_e(t^{d-}_{k+1})] \leq 0.\end{aligned} \tag{5.63}$$

From Lemma 5.5, we can say $\eta(t) \geq 0$. Hence $\psi_1 y_\sigma^\top(t^d_{k+1}) y_\sigma(t^d_{k+1}) + \psi_2 x_e^\top(t^d_{k+1})\, x_e(t^d_{k+1}) - \xi_\sigma^\top(t^{d-}_{k+1})\xi_\sigma(t^{d-}_{k+1}) - \xi_e^\top(t^{d-}_{k+1})\xi_e(t^{d-}_{k+1}) < 0$ when $\theta \in \mathbb{R}_{\geq 0}$. Hence, it contradicts (5.62). $\eta(t^{d-}_{k+1}) = 0$ is the result of the triggering condition, which is defined by (5.61) if $\theta = 0$ in addition to $\dot{\eta}(t^{d-}_{k+1}) \leq 0$. Then (5.57) gives

$$\begin{aligned}&\dot{\eta}(t^{d-}_{k+1}) = \psi_1 y_\sigma^\top(t^d_{k+1}) y_\sigma(t^d_{k+1}) + \psi_2 x_e^\top(t^d_{k+1}) x_e(t^d_{k+1}) - \xi_\sigma^\top(t^{d-}_{k+1})\xi_\sigma(t^{d-}_{k+1}) \\ &- \xi_e^\top(t^{d-}_{k+1})\xi_e(t^{d-}_{k+1}) \leq 0,\end{aligned} \tag{5.64}$$

which contradicts again (5.62). Hence, $t^s_{k+1} \leq t^d_{k+1}$. ■

5.7 Simulation result

The same system dynamics described in (3.105) are utilized to validate the proposed results. In this setup, $w_1(t)$ and $w_2(t)$ represent pseudo-random disturbances drawn from a standard normal distribution. Both states, $x_{p_1}(t)$ and $x_{p_2}(t)$, as defined in (3.105), are measurable and transmitted over two distinct communication channels. Under MCDoS Type 1, Channel 2 (transmitting the value of x_{p_2}) is compromised, whereas in the case of MCDoS Type 2, Channel 1 (transmitting the value of x_{p_1}) is targeted. The corresponding

output matrices for these scenarios are given in (3.103) and (3.104), respectively, with $\sigma \in \{1, 2\}$ denoting the active MCDoS type. The controller gain is $K = \begin{bmatrix} 0.4666 & 0.3245 \end{bmatrix}$, which makes $(A-BK)$ of (3.105) Hurwitz. The DETM proposed in (5.61) is implemented. Given $q = 0.01$, the final q_{final} obtained from Algorithm 5.1 is 10^{-4}. The other values we get from Algorithm 5.1 is

$$P_{p_1} = \begin{bmatrix} 0.008868464200688 & -0.000006399765749 \\ -0.000006399765749 & 0.008853717542715 \end{bmatrix},$$

$$P_{e_1} = \begin{bmatrix} 0.008859824695343 & -0.000010163678998 \\ -0.000010163678998 & 0.008863418281882 \end{bmatrix},$$

$$P_{p_2} = P_{e_2} = \begin{bmatrix} 0.008861430878248 & 0 \\ 0 & 0.008861430878248 \end{bmatrix},$$

$$L_1 = \begin{bmatrix} 38.7368 \\ 1.5908 \end{bmatrix}, L_2 = \begin{bmatrix} 18.4353 \\ 137.2598 \end{bmatrix}, \psi_1 = 0.001002, \psi_2 = 0.001, \quad \varepsilon_{1_1} = 5.6371 \times 10^3,$$

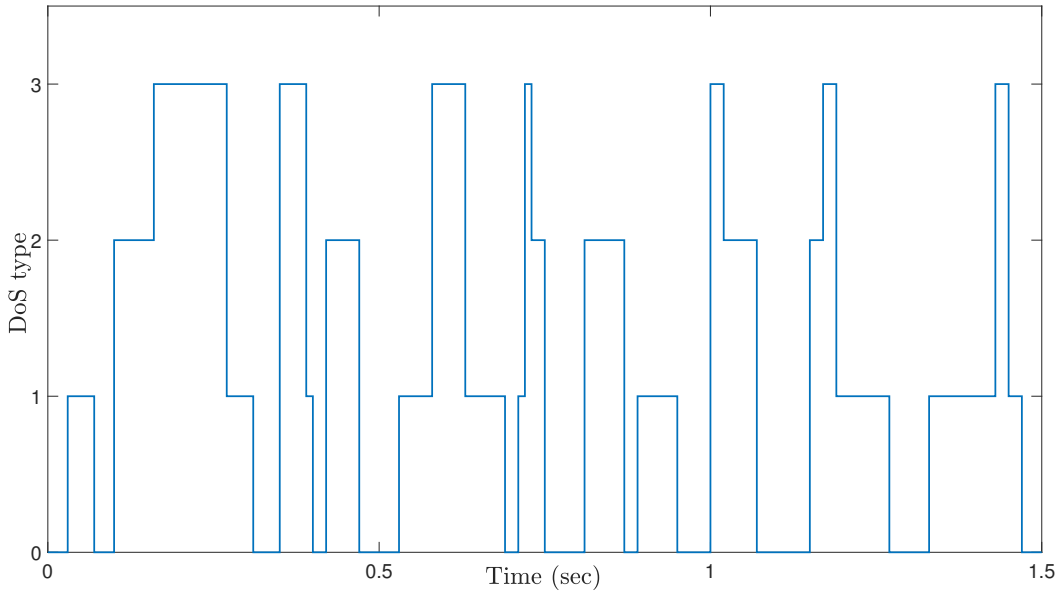

FIGURE 5.2: DoS scenarios for both SETM and DETM architecture. DoS type 0 indicates no attack, type 1 represents MCDoS type 1 (DoS affecting only channel 2), type 2 represents MCDoS type 2 (DoS affecting only channel 1), and type 3 corresponds to FSDoS affecting the system.

$\varepsilon_{2_1} = 5.7958 \times 10^3, \varepsilon_{1_2} = 5.607 \times 10^3, \varepsilon_{2_2} = 5.6068 \times 10^3, \lambda = 10^{-4}$, and $\kappa = 0.00886$.

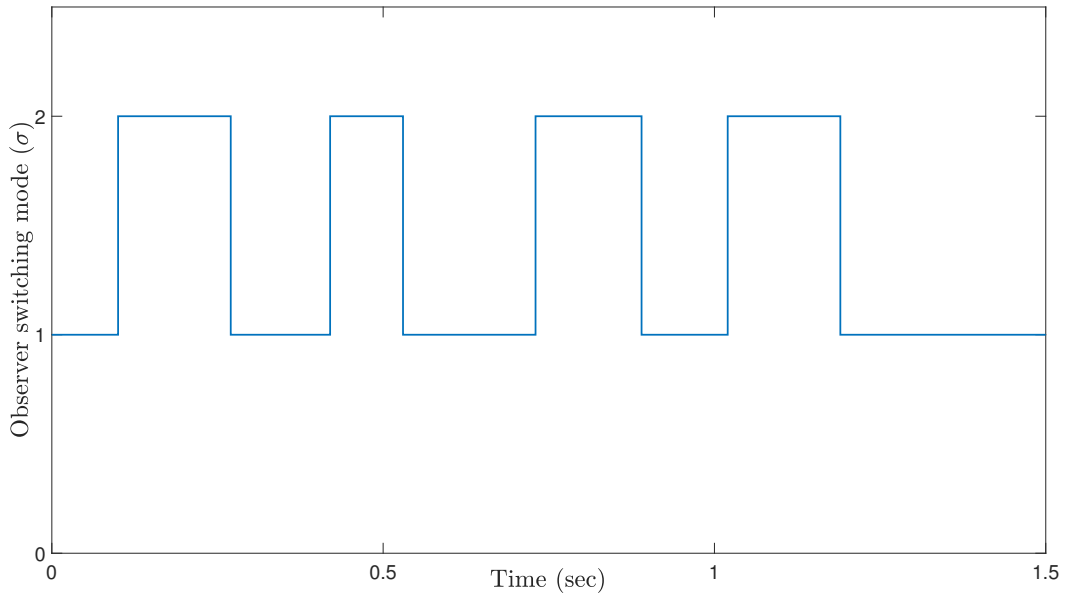

FIGURE 5.3: Real-time plot when observer treated it as an MCDoS frequency changing phenomenon according to the MCDoS type in Figure 5.2 and change its switching mode σ accordingly for illustrating SETM and DETM comparison. It follows $l(0, 1.5) = 8$, which implies the observer changes its switching mode 8 times within the interval of 0s to 1.5s.

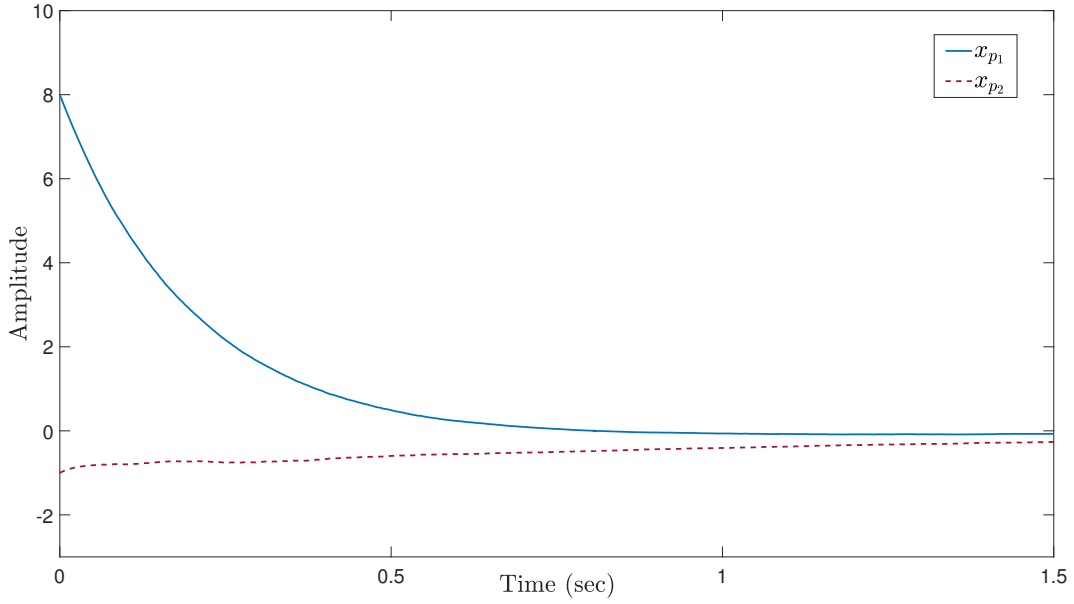

FIGURE 5.4: Plant state response ($x_p(t)$) for observer-based ETM of the system illustrating SETM and DETM comparison where the initial condition is $x_p(0) = (8, -1)$.

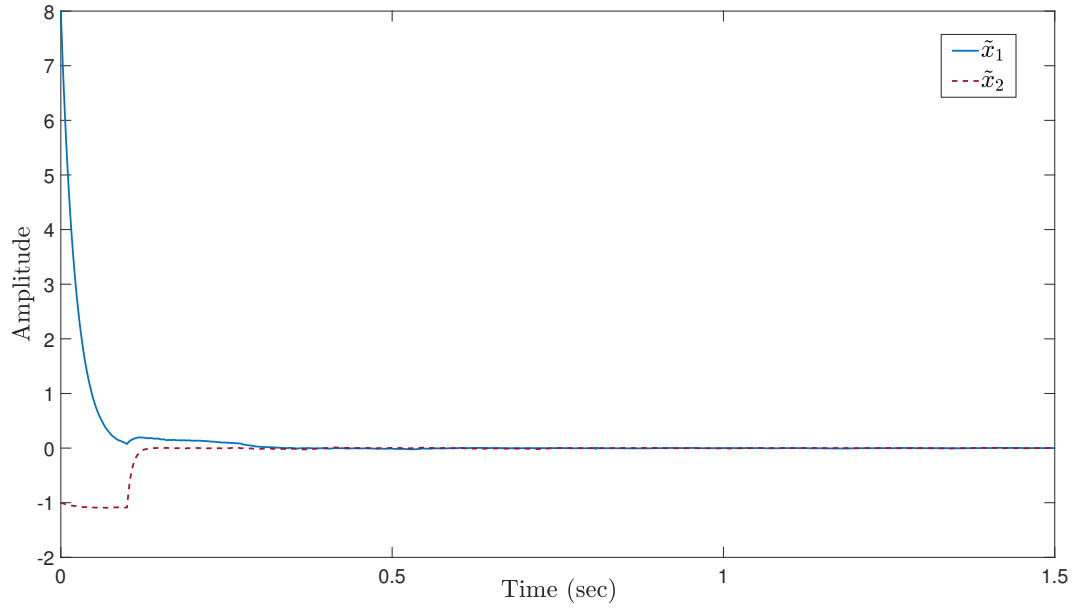

FIGURE 5.5: Observer error ($\tilde{x}(t) = x_p(t) - x_e(t)$) response for SETM illustrating SETM and DETM comparison where the initial condition is $x_p(0) = (8, -1)$ and $x_e(0) = (0, 0)$.

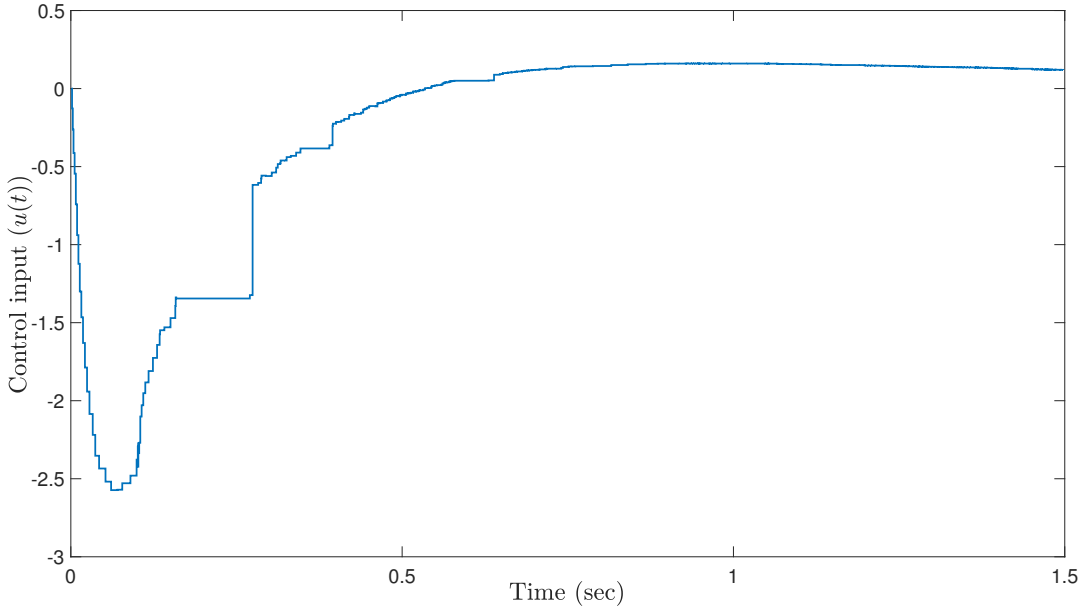

FIGURE 5.6: Control input ($u(t)$) response for SETM illustrating SETM and DETM comparison.

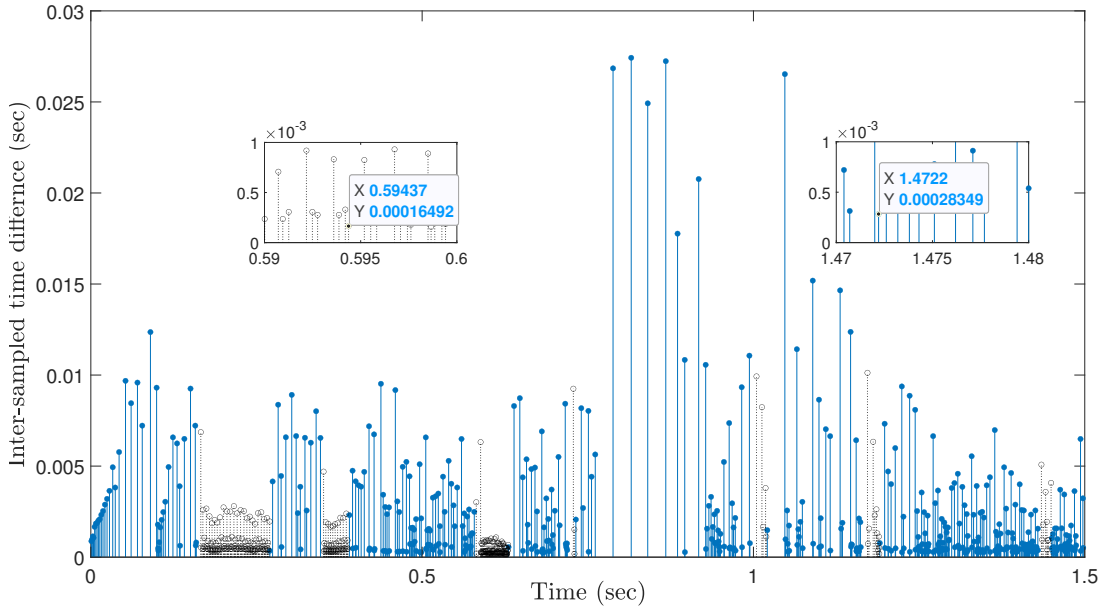

FIGURE 5.7: Control law update instants for SETM illustrating SETM and DETM comparison, where blue solid sticks are successful control law updates, and black dashed sticks are failed control attempts because of FSDoS.

From the LMIs Γ_{7_σ} in (5.7), $\zeta_{2_1} = 10^{-4}$ and $\zeta_{2_2} = 10^{-4}$. Hence, $\tau_{D_{\text{detm}}} > 0.2066$. In order to minimize $\tau_{D_{\text{detm}}}$, the controller parameters $L_1, L_2, \psi_1, \psi_2, \lambda$, and κ are designed by solving LMIs. Hence $L_1, L_2, \psi_1, \psi_2, \lambda$, and κ are optimal values. The value of θ is chosen as $\theta = \min_{\forall\sigma\in\{1,\cdots,n_s\}} 1/\{2\kappa(\|\mathcal{G}_\sigma\| + \|C_\sigma\|) - \lambda\} = 0.2846$. From (5.22) and (3.76), $\underline{\Delta} = 1.5726\times10^{-4}$. From (5.50), (5.51), and (5.52), $\overline{\Delta}_{\text{detm}} = 3.0622\times10^{-4}$ is obtained. The maximum permissible $\varkappa_{\text{detm}}$ value is 0.9997 for $\tau_{D_{\text{detm}}} = 0.21$, as obtained from (5.9). So the maximum permissible MCDoS changing frequency $l(0,1) \approx 6, l(0,1.5) \approx 8, l(0,2) \approx 10$ and so on.

For SETM, we have used the same parameter values, which we found for the DETM case, such as $K, L_1, L_2, \psi_1, \psi_2, P_{p_1}, P_{e_1}, P_{p_2}, P_{e_2}, \varepsilon_{1_1}, \varepsilon_{2_1}, \varepsilon_{1_2}$ and ε_{2_2}. Hence, we find $\tau_{D_{\text{setm}}} > 0.2066$ from (5.20), which is same as $\tau_{D_{\text{detm}}}$. This occurs due to the selection of the scaling parameters κ in accordance with Lemma 5.5, which ensures that $\tau_{D_{\text{setm}}}$ and $\tau_{D_{\text{detm}}}$ are almost identical. From (3.76) and (3.77), $\underline{\Delta} = 1.5605 \times 10^{-4}$. From (5.40), (5.41), and (5.42), $\overline{\Delta}_{\text{setm}} = 2.6583 \times 10^{-4}$ for SETM. Maximum allowable $\varkappa_{\text{setm}}$ value are 0.9997 calculated from (3.33) same as $\varkappa_{\text{detm}}$. In both SETM and DETM cases, DoS attacks are introduced in the same fashion (see Figure 5.2). The observer switching mode is shown

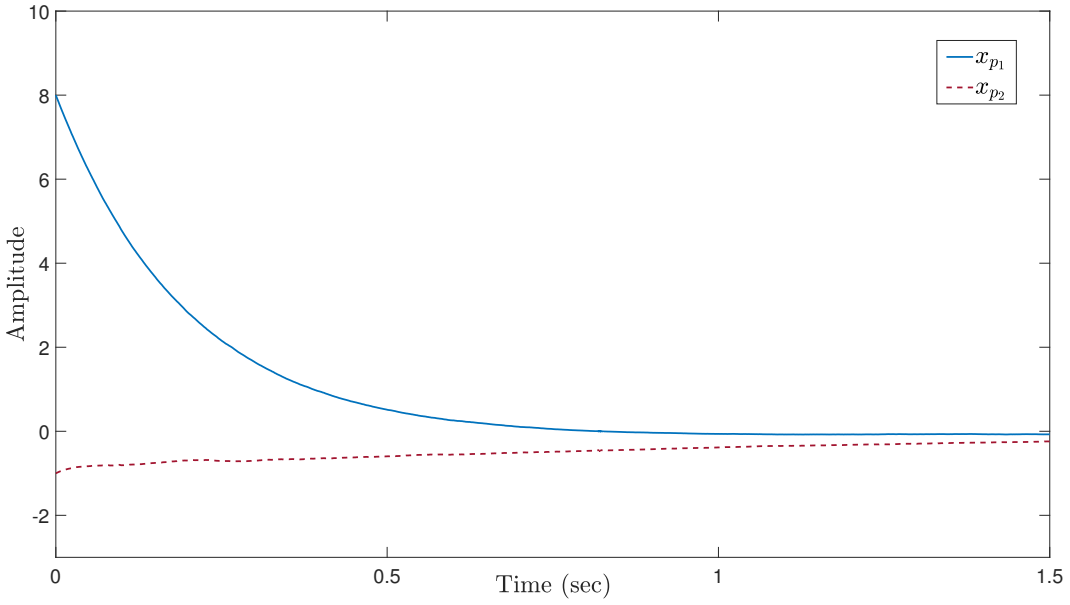

FIGURE 5.8: Plant state response for DETM illustrating SETM and DETM comparison where the initial condition is $x_p(0) = (8, -1)$.

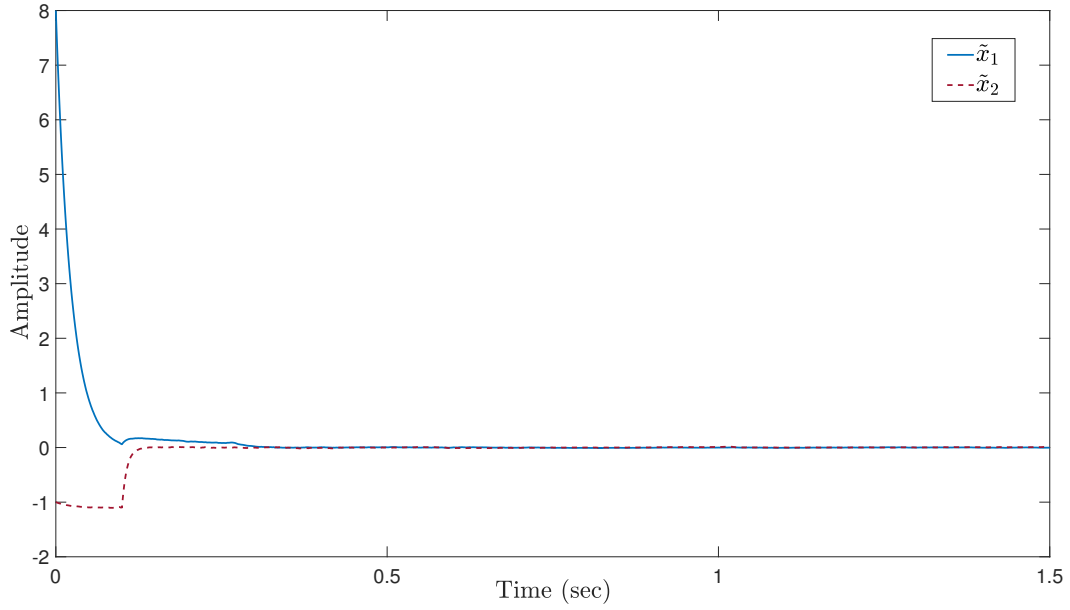

FIGURE 5.9: Observer error ($\tilde{x}(t) = x_s(t) - x_e(t)$) response for DETM illustrating SETM and DETM comparison where the initial condition is $x_p(0) = (8, -1)$ and $x_e(0) = (0, 0)$.

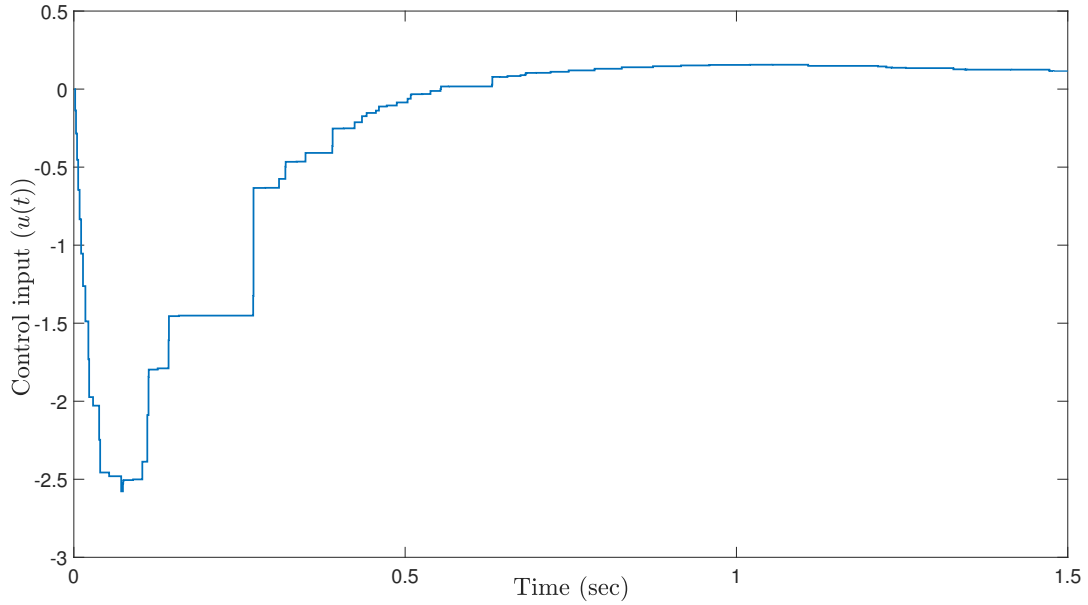

FIGURE 5.10: Control input ($u(t)$) response for DETM illustrating SETM and DETM comparison.

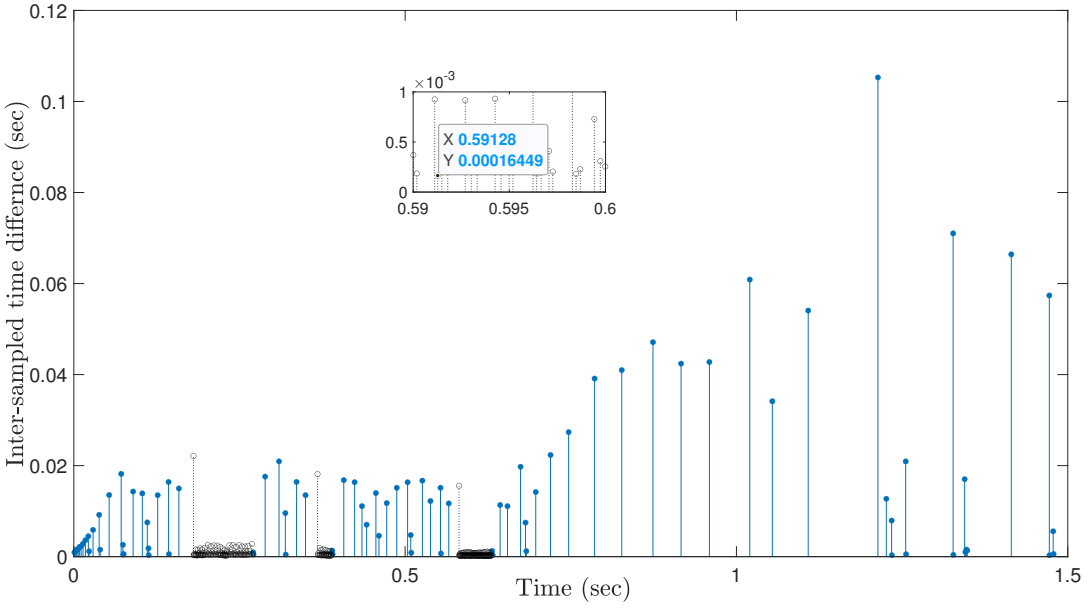

FIGURE 5.11: Control law update instants for DETM illustrating SETM and DETM comparison, where blue solid sticks are successful control law update instants and black dashed sticks are failed control attempts because of FSDoS.

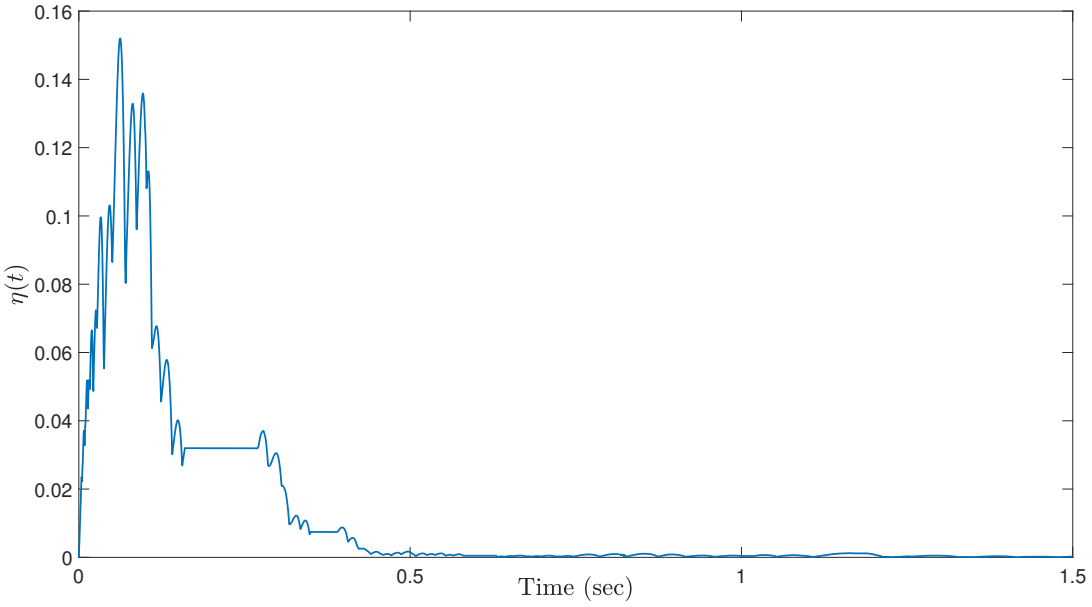

FIGURE 5.12: Response of $\eta(t)$ for DETM illustrating SETM and DETM comparison.

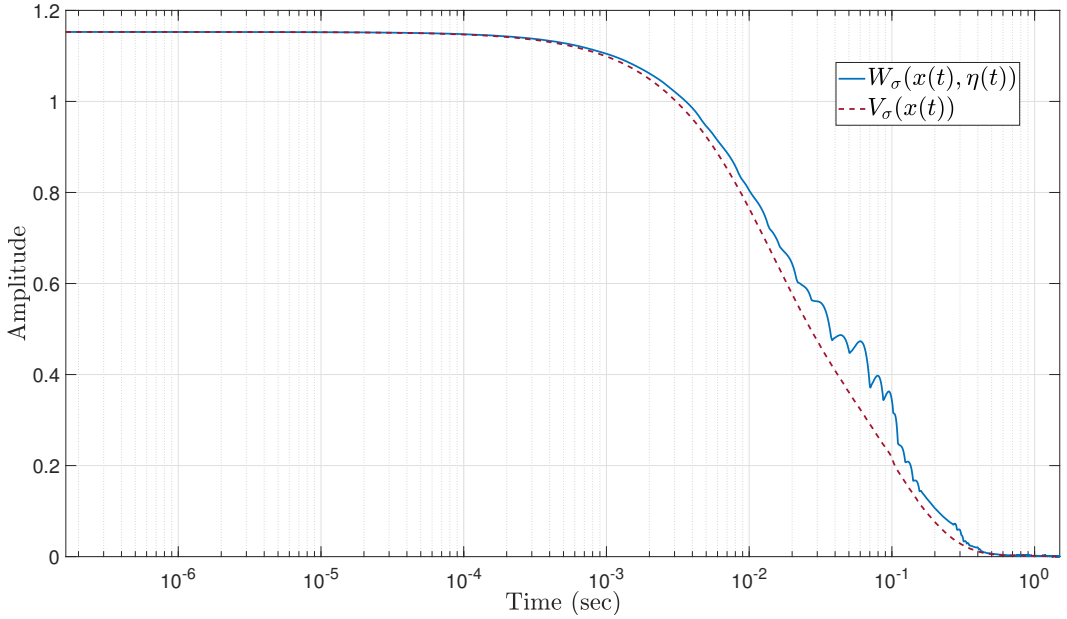

FIGURE 5.13: Response of Lyapunov function $V_\sigma(x(t))$ in (3.18) for SETM and $W_\sigma(x(t), \eta(t))$ in (5.4) for DETM illustrating SETM and DETM comparison where σ is varying between 1 and 2 according to Figure 5.3.

in Figure 5.3, where t = 0.1s, 0.27s, 0.42s, 0.53s, 0.73s, 0.89s, 1.02s, 1.17s, the observer detects it as an MCDoS frequency changing phenomenon and changes its switching mode. From Figure 5.3, it is also noticeable that the observer does not change its switching mode when the FSDoS condition (DoS type 3 in Figure 5.2) and no DoS condition (DoS type 1 in Figure 5.2) occur. The responses of the states of the plant, observer error, control law ($u(t)$) and control law triggering instants (t_k) for SETM are shown in Figures 5.4, 5.5, 5.6 and 5.7, respectively. Similarly, the responses of the plant states, observer errors, control law, and control law triggering instants for DETM are shown in Figures 5.8, 5.9, 5.10, and 5.11, respectively. $\eta(t)$ response is shown in Figure 5.12. In Lemma 5.5, it is proved that $\eta(t) \geq 0$. The simulation result validates the theoretical finding. In the presence of FSDoS $\eta(t) = \exp\{-(\lambda/\kappa)t\}\,\eta(0)$. The decay rate λ/κ is very low, approx 0.0113. Hence, the $\eta(t)$ graph is almost a flat line in the time of FSDoS, which is shown in Figure 5.12. In Figure 5.13, we show the Lyapunov function graph for SETM and DETM. The readers can notice that the Lyapunov function candidate for DETM ($W(x(t), \eta(t))$) is always greater than the Lyapunov function candidate for SETM ($V(x(t))$) because of non-negative $\eta(t)$ which is shown in Figure 5.12.

5.8 Chapter summary

This chapter presented a comparative analysis of SETM and DETM in a multiple-sensor framework, particularly under scenarios where both the StC and CtA communication links are affected by DoS. A theoretical comparison was developed and validated through simulations, demonstrating that DETM achieves significantly larger inter-execution times and fewer triggering instances than SETM, thereby reducing overall control costs.

A key contribution of this work is the introduction of a novel scaling parameter, κ, into the DETM structure. A suitable bound for κ was derived to ensure that the changing frequency of MCDoS remains comparable between SETM and DETM, thereby maintaining system stability. The DETM parameters and switched observer gains were optimally

designed using an LMI-based optimization algorithm, ensuring resilience against the maximum changing frequency of MCDoS.

Additionally, a modified Zeno-free resilient control strategy was proposed to address the presence of FSDoS, although the formal characterization of FSDoS was not undertaken in this chapter. Future research will focus on the characterization of FSDoS and the development of an optimal control strategy resilient to its maximum frequency and duration.

Chapter 6

Conclusion

6.1 Synthesis and closure

In this thesis, the resilient control problem for CPSs was investigated in a setting where both sides of the control structure, namely, the StC and CtA channels, are susceptible to DoS in a multi-sensor framework. This stands in contrast to the majority of prior research in the CPS literature, where DoS vulnerability was typically assumed to affect only the StC channels. By considering both StC and CtA channels as vulnerable, the problem formulation becomes not only significantly more complex but also more representative of real-world operational scenarios. Such a configuration introduces intricate interdependencies between attack patterns, communication delays, and control actions, rendering existing characterization results, developed for single-sensor or multi-sensor systems with DoS affecting only the StC channels, insufficient for the present problem. This gap in the literature provided the primary motivation to develop a comprehensive characterization of both MCDoS and FSDoS, enabling the formulation of robust control strategies tailored to these challenging conditions. The key contributions and findings of the thesis are briefly summarized below.

The first part of the thesis, presented in Chapter 3, focused on the characterization of MCDoS. While a system may remain stabilizable under MCDoS, its stability can be

compromised by frequent changes in the type of MCDoS, thereby necessitating a bound on its changing frequency rather than its duration. To achieve this characterization, a switched observer-based ETM architecture was adopted, and the minimum inter-execution time for such an architecture was derived. An LMI-based optimization framework was then developed to jointly design the ETM and switched observer parameters, ensuring resilience against the maximum permissible MCDoS changing frequency. Additionally, a Zeno-free resilient ETM strategy was proposed, removing dependency on the supremum norm of disturbances. The efficacy of the approach was validated through simulation results.

Chapter 4 addressed the characterization of FSDoS while retaining the core control architecture from Chapter 3. A rigorous ISS analysis was conducted to determine bounds on the frequency and duration of FSDoS, complementing the previously established bounds on MCDoS changing frequency. Building on this analysis, a multi-objective LMI-based optimization procedure was formulated to jointly design the switched observer and ETM gains such that the system could withstand the maximum allowable MCDoS changing frequency as well as the maximum frequency and duration of FSDoS. Furthermore, an asynchronous triggering policy was introduced to handle situations where FSDoS occurs in the StC and CtA channels at different times. The proposed method's performance was substantiated through detailed simulation studies.

Chapter 5 extended the analysis by replacing the conventional static ETM (SETM) with a novel DETM aimed at reducing the control cost. The DETM architecture incorporated a scaling parameter κ, a novel addition to the literature, purposefully designed to improve resilience against the maximum MCDoS changing frequency. The minimum inter-execution time for the switched observer-based DETM was derived, and an LMI-based optimization algorithm was developed to design both the switched observer and DETM parameters to maintain stability under maximum MCDoS changing conditions. A modified resilient control strategy was also formulated to prevent Zeno behavior. Comparative simulation results between SETM and DETM showed, both theoretically and experimentally, that DETM achieves the same level of resilience with fewer triggering instants, thereby reducing control effort and communication overhead.

Overall, this thesis makes a significant step forward in the study of resilient control for CPSs by tackling a problem formulation that had not previously been considered, both StC and CtA channels subject to DoS in a multi-sensor framework. The theoretical developments, optimization strategies, and simulation-based validations presented herein establish a foundation for future research that can further deepen the understanding of CPSs' resilience under more diverse and severe adversarial conditions. While the present work has primarily focused on MCDoS and FSDoS characterization, numerous avenues remain unexplored. It is anticipated that the methods and insights introduced in this thesis will serve as a springboard for the systems and control community to address even more complex real-world CPSs' resilience challenges in the years ahead. The following section outlines several promising directions for such future research.

6.2 Pathways for future investigation

There are several promising avenues through which the work presented in this thesis can be extended and investigated in greater depth. These directions span both theoretical developments and practical implementations, offering opportunities to advance the state of the art in resilient control for CPSs under DoS. The most notable future research possibilities are outlined below.

- *Joint optimization of controller, observer, and ETM parameters:* In this thesis, it has been demonstrated that a switched observer can be co-designed with either SETM parameters or DETM parameters. The state-feedback controller, however, was designed separately using the pole-placement technique. A compelling extension would be to integrate the design of the controller gain into the same LMI-based optimization framework used for the observer and ETM parameters. By jointly solving for the optimal control gain K, the optimal switched observer gains, and the optimal ETM parameters, it would be possible to achieve a unified design that maximizes system resilience against the worst-case MCDoS changing frequency as well as the maximum frequency and duration of FSDoS.

- *Characterization of asynchronous FSDoS:* Chapter 4 introduced an asynchronous triggering mechanism to handle FSDoS events occurring at different times in the StC channels and the CtA channel. However, the precise characterization of such asynchronous FSDoS patterns was not undertaken. As a result, it remains unclear how much independent FSDoS in the StC channels and CtA channel the system can tolerate. This presents an open research problem, namely, to rigorously characterize FSDoS when it appears asynchronously across both sides of the control structure and to develop corresponding resilient control strategies.

- *Implementation of resilient control for unknown system dynamics:* In this thesis, the system dynamics were assumed to be known. Future research may extend this work toward resilient control design for multiple transmission channels under DoS when the system dynamics are unknown. In such scenarios, a promising direction is to develop resilient control architectures based on data-driven methodologies. Data-driven control provides an effective framework for handling model uncertainties and unknown dynamics. In particular, the design of data-driven event-triggered controllers appears to be a promising approach for mitigating the effects of DoS attacks while efficiently utilizing limited communication resources.

- *Extension to nonlinear systems:* The present work is restricted to linear system models. Extending the analysis and control design to nonlinear systems subjected to DoS on both StC and CtA channels in a multi-sensor framework would be a challenging yet impactful direction. The primary difficulty lies in the design of both the controller and the switched observer, as the simple state-feedback controller and Luenberger switched observer employed here are inadequate for nonlinear dynamics. Nonlinear systems require robust, high-performance control and estimation schemes. Feedback linearization emerges as a promising approach, as it may be possible to co-design the feedback linearization observer gain and ETM parameters via LMI-based optimization to yield optimal gains for maximum resilience against MCDoS and FSDoS. Other advanced control architectures, such as SMC, MPC, backstepping, and quantitative feedback theory, also hold significant potential for addressing the resilience of nonlinear CPSs in the presence of DoS.

- *Experimental validation:* While this thesis provided extensive simulation-based evidence of the effectiveness of the proposed methods, experimental validation represents an essential next step to assess their practical viability. Physical testbeds such as magnetic levitation systems, coupled-tank systems, or twin-rotor MIMO systems could serve as suitable environments for implementing and evaluating the proposed control architectures. Such experiments would not only validate the theoretical findings but also reveal practical considerations such as sensor noise, unmodeled dynamics, actuator limitations, and hardware-induced delays.

Beyond these specific directions, this thesis has ventured into a largely unexplored domain by simultaneously considering DoS attacks on both sides of the control structure within a multi-sensor framework. This novel perspective significantly broadens the scope of resilient control research, as prior studies have almost exclusively examined DoS effects on one side of the control loop. By opening this new line of inquiry, the present work lays the groundwork for a rich set of future investigations that can push the boundaries of system resilience in adversarial environments. It is anticipated that the methods, problem formulations, and insights introduced herein will inspire further theoretical advancements and practical innovations in the years ahead.

Appendix A

A.1 Proof of Theorem 2.2

By substituting (2.12) into (2.15), the expression

$$\dot{V}(x_p(t)) \leq -\left(\lambda_m(Q) - 2\tilde{\psi}\|PBK\|\right)\|x_p(t)\|^2 + \left(2\lambda_M(P) + 2\tilde{\psi}\|PBK\|\right)\|x_p(t)\|d(t) \tag{A.1}$$

is obtained, where $d(t)$ is mentioned in (3.27). It is important to observe that the positive scalar term $(2\lambda_M(P) + \tilde{\psi}\|2PBK\|)/(\lambda_m(Q) - \tilde{\psi}\|2PBK\|)$, appears in the context of the inequality. By applying Young's inequality (refer to [161]), the bound

$$2\|x_p(t)\|d(t) \leq \frac{\lambda_m(Q) - 2\tilde{\psi}\|PBK\|}{2\lambda_M(P) + 2\tilde{\psi}\|PBK\|}\|x_p(t)\|^2 + \frac{2\lambda_M(P) + 2\tilde{\psi}\|PBK\|}{\lambda_m(Q) - 2\tilde{\psi}\|PBK\|}d^2(t) \tag{A.2}$$

holds. This leads to the inequality

$$\dot{V}(x_p(t)) \leq -\frac{\lambda_m(Q) - 2\tilde{\psi}\|PBK\|}{2}\|x_p(t)\|^2 + \frac{\left(2\lambda_M(P) + 2\tilde{\psi}\|PBK\|\right)^2}{2\left(\lambda_m(Q) - 2\tilde{\psi}\|PBK\|\right)}d^2(t) \tag{A.3}$$

$$\leq -\omega_1 V(x_p(t)) + \frac{\left(2\lambda_M(P) + 2\tilde{\psi}\|PBK\|\right)^2}{2\left(\lambda_m(Q) - 2\tilde{\psi}\|PBK\|\right)}d^2(t), \tag{A.4}$$

where the decay rate ω_1 is mentioned in (2.23). It should be noted that the essential supremum of d_t over any time horizon $t \in \mathbb{R}_{>0}$ satisfies $\|d_t\|_\infty = \|w_t\|_\infty$. Consequently,

by invoking standard comparison principles for differential inequalities, one obtains

$$V(x_p(t)) \leq e^{-\omega_1 t} V(x_p(0)) + \delta_1 \|w_t\|_\infty, \tag{A.5}$$

where

$$\delta_1 := \frac{(2\lambda_M(P) + 2\tilde{\psi}\|PBK\|)^2}{2\omega_1(\lambda_m(Q) - 2\tilde{\psi}\|PBK\|)}. \tag{A.6}$$

By utilizing the bound in (2.14), the estimate is derived as

$$\|x_p(t)\|^2 \leq \frac{\lambda_M(P)}{\lambda_m(P)} e^{-\omega_1 t} \|x_p(0)\|^2 + \frac{\delta_1}{\lambda_m(P)} \|w_t\|_\infty^2. \tag{A.7}$$

Finally, since the inequality $a^2 + b^2 \leq (a+b)^2$ holds for any non-negative real numbers a and b, the result can be refined as

$$\|x_p(t)\| \leq \sqrt{\frac{\lambda_M(P)}{\lambda_m(P)}} e^{-\frac{\omega_1}{2} t} \|x_p(0)\| + \sqrt{\frac{\delta_1}{\lambda_m(P)}} \|w_t\|_\infty, \tag{A.8}$$

which yields the desired result. ■

A.2 Proof of Lemma 2.3

From (2.11), it follows that

$$\|\dot{x}_p(t)\| \leq \|A - BK\| \|x_p(t)\| + \|BK\| \|\xi(t)\| + \|w_t\|_\infty. \tag{A.9}$$

Consequently, it obeys the lower bound on the inter-execution time given by the time it takes for the function

$$\phi(t) := \frac{\|\xi(t)\|}{\|x_p(t)\| + \|w_t\|_\infty} \tag{A.10}$$

to go from 0 to $\tilde{\psi}$ by following (2.12). Hence, the time derivative of $\phi(t)$ becomes

$$\dot{\phi}(t) = \frac{\xi^\top(t)\dot{\xi}(t)}{\|\xi(t)\|\left(\|x_p(t)\| + \|w_t\|_\infty\right)} - \frac{\|\xi(t)\|x_p^\top(t)\dot{x}_p(t)}{\|x_p(t)\|\left(\|x_p(t)\| + \|w_t\|_\infty\right)}. \tag{A.11}$$

By noting that $\dot{\xi}(t) = -\dot{x}_p(t)$ and using the bound on $\|\dot{x}_p(t)\|$ from (A.9), the inequality for the derivative of $\phi(t)$ is

$$\begin{aligned}
\dot{\phi}(t) &\leq \frac{1}{\|x_p(t)\| + \|w_t\|_\infty}\left(\|A - BK\|\|x_p(t)\| + \|BK\|\|\xi(t)\| + \|w_t\|_\infty\right) \\
&+ \frac{\|\xi(t)\|}{\left(\|x_p(t)\| + \|w_t\|_\infty\right)^2}\left(\|A - BK\|\|x_p(t)\| + \|BK\|\|\xi(t)\| + \|w_t\|_\infty\right) \\
&\leq \|A - BK\|\frac{\|x_p(t)\|}{\|x_p(t)\| + \|w_t\|_\infty} + \|BK\|\phi(t) + \frac{\|w_t\|_\infty}{\|x_p(t)\| + \|w_t\|_\infty} + \|A - BK\| \\
&\frac{\|x_p(t)\|}{\|x_p(t)\| + \|w_t\|_\infty}\phi(t) + \|BK\|\phi^2(t) + \frac{\|w_t\|_\infty}{\|x_p(t)\| + \|w_t\|_\infty}\phi(t).
\end{aligned} \tag{A.12}$$

Note that $\left\{\|x_p(t)\|/\sqrt{\|x_p(t)\|^2 + \|w_t\|_\infty^2}, \|w_t\|_\infty/\sqrt{\|x_p(t)\|^2 + \|w_t\|_\infty^2}\right\} \leq 1$ due to $\{\|x_p(t)\|, \|w_t\|_\infty\} \geq 0$. Hence,

$$\dot{\phi}(t) \leq \|A - BK\| + 1 + \left(\|A - BK\| + \|BK\| + 1\right)\phi(t) + \|BK\|\phi^2(t). \tag{A.13}$$

Thus, the comparison lemma for differential inequalities yields

$$\int_{t_k}^{t_{k+1}} dt \geq \int_0^{\tilde{\psi}} \frac{1}{\|A - BK\| + 1 + \left(\|A - BK\| + \|BK\| + 1\right)\phi(t) + \|BK\|\phi^2(t)}\, d\phi \tag{A.14}$$

By substituting ϕ with $s \coloneqq \phi/\tilde{\psi}$, the result in (2.18) is obtained. ■

A.3 Proof of Theorem 2.4

As outlined in Section 2.3, the key idea involves partitioning the time axis into segments where condition (2.12) can be satisfied, and segments where this condition may be violated due to the presence of DoS. The resulting closed-loop behavior is interpreted as a

switched system alternating between stable and unstable modes. To maintain clarity in presentation, the proof is structured into three distinct steps.

Step I. Decomposition of the time-axis into stable and unstable phases

This step focuses on identifying the time intervals over which condition (2.12) is satisfied, as well as those where it may not hold due to the influence of DoS. The system exhibits stable dynamics during the former and may follow unstable behavior during the latter. This temporal decomposition plays a crucial role in the Lyapunov-based analysis that follows and is formalized in what comes next.

Lemma A.1. *For any $\tau, t \in \mathbb{R}_{\geq 0}$ with $0 \leq \tau \leq t$, the interval $[\tau, t]$ can be partitioned into two disjoint subsets $\overline{\Lambda}(\tau, t)$ and $\overline{\Xi}(\tau, t)$. The set $\overline{\Lambda}(\tau, t)$ consists of all time intervals within $[\tau, t]$ where condition (2.12) holds, while $\overline{\Xi}(\tau, t)$ contains those where it is not guaranteed to hold. More precisely, there exist sequences of non-negative and positive real numbers $\{\varphi_m\}_{m\in\mathbb{N}}$ and $\{v_m\}_{m\in\mathbb{N}}$, respectively, such that*

$$\overline{\Xi}(\tau, t) \coloneqq \bigcup_{m\in\mathbb{N}} W_m \cap [\tau, t] \tag{A.15}$$

$$\overline{\Lambda}(\tau, t) \coloneqq \bigcup_{m\in\mathbb{N}} Y_{m-1} \cap [\tau, t] \tag{A.16}$$

where $\forall m \in \mathbb{N}$,

$$W_m \coloneqq \{\varphi_m\} \cup [\varphi_m, \varphi_m + v_m) \tag{A.17}$$

$$Y_m \coloneqq \{\varphi_m + v_m\} \cup [\varphi_m + v_m, \varphi_{m+1}) \tag{A.18}$$

and $\varphi_0 = v_0 \coloneqq 0$.

Proof. Let $\mathcal{S}_n \coloneqq \{k \in \mathbb{N}_0 : t_k \in D_n\}$ denote the set of integers related to a control update attempt occurring over $D_n, n \in \mathbb{N}$. Define

$$f_n \coloneqq \begin{cases} \tau_n, & \text{if } \mathcal{S}_n = \emptyset \\ t_{\sup\{k\in\mathbb{N}_0 : k\in\mathcal{S}_n\}} - d_n, & \text{otherwise,} \end{cases} \tag{A.19}$$

$$F_n \coloneqq \begin{cases} 0, & \text{if } \mathcal{S}_n = \emptyset \\ \Delta_{\sup\{k\in\mathbb{N}_0 : k\in\mathcal{S}_n\}}, & \text{otherwise.} \end{cases} \tag{A.20}$$

Thus,

$$\overline{D}_n \coloneqq \{d_n\} \cup [d_n, d_n + f_n + F_n) \tag{A.21}$$

denotes the nth time interval during which condition (2.12) may be violated. This interval incorporates both D_n and the associated actuation delay induced by the DoS attack. It is important to observe that $f_n + F_n \geq \tau_n, \forall n \in \mathbb{N}$. Additionally, the intervals $\overline{D}_n$ and $\overline{D}_{n+1}$ are not necessarily disjoint, since d_{n+1} may lie within $\overline{D}_n$. For analytical convenience, such overlapping intervals are treated as a single interval conforming to the structure of (A.17). To facilitate this, an auxiliary sequence $\{\varphi_m\}_{m\in\mathbb{N}}$ is introduced, recursively constructed from the sequence $\{d_n\}_{n\in\mathbb{N}}$ as follows:

$$\varphi_1 \coloneqq d_1, \tag{A.22}$$

$$\varphi_{m+1} \coloneqq \inf\{d_n > \varphi_m : d_n > d_{n-1} + f_{n-1} + F_{n-1}\}, \tag{A.23}$$

$\forall m \in \mathbb{N}$. For any $\{\tau, t\} \in \mathbb{R}_{\geq 0}$, the set $\overline{\Xi}(\tau, t)$ defined in (A.15) captures the union of all such subintervals within $[\tau, t]$ where condition (2.12) is not guaranteed to be satisfied due to the impact of DoS. Let Y_m be defined as in (A.18), and consider $\{\tau, t\} \in \mathbb{R}_{\geq 0}$. Define $\overline{\Lambda}(\tau, t)$ according to (A.16). Over the interval $[\tau, t]$, the sets $\overline{\Xi}(\tau, t)$ and $\overline{\Lambda}(\tau, t)$ form a partition, their union covers the entire interval $[\tau, t]$, and they are mutually disjoint. The set $\overline{\Lambda}(\tau, t)$ specifically consists of all subintervals within $[\tau, t]$ during which condition (2.12) remains valid. More precisely, by construction, each interval Y_m (for $m \in \mathbb{N}$) begins with a guaranteed successful control update at time $\varphi_m + v_m$, and no DoS event occurs

throughout Y_m. ■

Step II: Lyapunov function analysis

Consider the intervals $Y_m, m \in \mathbb{N}$, over which condition (2.12) is satisfied by construction. From inequality (A.5), it follows that

$$V(x_p(t)) \leq e^{-\omega_1(t-\varphi_m-v_m)} V(x_p(\varphi_m + v_m)) + \delta_1 \|w_t\|_\infty^2 \tag{A.24}$$

holds $\forall t \in Y_m$ and every $m \in \mathbb{N}$. Throughout this analysis, all constants are the same as those used in the proof of Theorem 2.2. Specifically, the constant δ_1 is given by (A.6), with $\tilde{\psi}$ defined in (2.17). Turning attention to the intervals W_m for $m \in \mathbb{N}$, where condition (2.12) may not hold, an estimate for the evolution of $V(x_p(t))$ over these intervals requires additional derivations. As an intermediate result, for each $m \in \mathbb{N}$ the inequality

$$\|\xi(t)\| \leq (1 + \tilde{\psi})\|x_p(\varphi_m)\| + \|x_p(t)\| + \tilde{\psi}\|w_t\|_\infty \tag{A.25}$$

can be established $\forall t \in W_m$. Recall that the error term $\xi(t)$ is defined as

$$\xi(t) = x_p(t_{k(\varphi_m)}) - x_p(t) \tag{A.26}$$

$\forall t \in W_m$, where $x_p(t_{k(\varphi_m)})$ denotes the process state at the last successful control update prior to or at time φ_m. In the special case where $\varphi_1 = 0$, the value $x_p(t_{k(\varphi_1)})$ is defined to be zero, making inequality (A.25) trivially valid. For the general case $\varphi_1 > 0$, it is observed that (2.12) remains valid over all $t \in Y_m$ due to the construction. Consequently, the continuity of $x_p(t)$ implies that

$$\|\xi(\varphi_m)\| \leq \tilde{\psi}\left(\|x_p(\varphi_m)\| + \|w_{\varphi_m}\|_\infty\right) \tag{A.27}$$

$\forall m \in \mathbb{N}$. Therefore,

$$\|x_p(t_{k(\varphi_m)}) - x(\varphi_m)\| \leq \tilde{\psi}\left(\|x_p(\varphi_m)\| + \|w_{\varphi_m}\|_\infty\right) \tag{A.28}$$

holds, and inequality (A.25) is obtained by invoking the triangle inequality. Substituting (A.25) into (2.15) yields

$$\begin{aligned}\dot{V}(x_p(t)) \leq &(2\|PBK\| - \lambda_m(Q))\,\|x_p(t)\|^2 + 2\|PBK\|(1+\tilde{\psi})\|x_p(t)\|\|x_p(\varphi_m)\| \\ &+ \left(2\lambda_M(P) + 2\tilde{\psi}\|PBK\|\right)\|x_p(t)\|d(t) \end{aligned} \tag{A.29}$$

where $d(t)$ is mentioned in (3.27). We then proceed as in the proof of Theorem 2.2. Using (A.2), simple calculations yield

$$\begin{aligned}\dot{V}(x_p(t)) \leq &2\|PBK\|(1-\tilde{\psi})\|x_p(t)\|^2 + 2\|PBK\|(1+\tilde{\psi})\|x_p(t)\|\|x_p(\varphi_m)\| \\ &+ \frac{\left(2\lambda_M(P) + 2\tilde{\psi}\|PBK\|\right)^2}{2\left(\lambda_m(Q) - 2\tilde{\psi}\|PBK\|\right)} d^2(t). \end{aligned} \tag{A.30}$$

Note that

$$\dot{V}(x_p(t)) \leq \omega_2 \max\{V(x_p(t)), V(x_p(\varphi_m))\} + \frac{\left(2\lambda_M(P) + 2\tilde{\psi}\|PBK\|\right)^2}{2\left(\lambda_m(Q) - 2\tilde{\psi}\|PBK\|\right)} d^2(t), \tag{A.31}$$

where ω_2 is mentioned in (2.24). Since $\|d_t\|_\infty = \|w_t\|_\infty, \forall t \in \mathbb{R}_{\geq 0}$, it follows that

$$V(x_p(t)) \leq e^{\omega_2(t-\varphi_m)} V(x_p(\varphi_m)) + \delta_2 e^{\omega_2(t-\varphi_m)} \|w_t\|_\infty^2 \tag{A.32}$$

for every $t \in W_m$, with

$$\delta_2 := \frac{(2\lambda_M(P) + 2\tilde{\psi}\|PBK\|)^2}{2\omega_2(\lambda_m(Q) - 2\tilde{\psi}\|PBK\|)}. \tag{A.33}$$

By combining (A.24) and (A.32), the following result is obtained.

Lemma A.2. *For any $t \in \mathbb{R}_{\geq 0}$, the Lyapunov function satisfies*

$$V(x_p(t)) \leq e^{-\omega_1|\overline{\Lambda}(0,t)|} e^{\omega_2|\overline{\Xi}(0,t)|} V(x_p(0)) + \delta_3 \left[1 + 2\sum_{\substack{m\in\mathbb{N};\\ \varphi_m \leq t}} e^{-\omega_1|\overline{\Lambda}(\varphi_m+\upsilon_m,t)|} e^{\omega_2|\overline{\Xi}(\varphi_m,t)|}\right] \|w_t\|_\infty^2, \tag{A.34}$$

with $\delta_3 := \max\{\delta_1, \delta_2\}$. *From this point onward, following the definition in* (A.16), *it is assumed that* $|\overline{\Lambda}(\varphi_m + v_m, t)| = 0$ *whenever* $t < \varphi_m + v_m$.

Proof. An induction approach is applied. To begin, consider the interval $Y_0 = [0, \varphi_1]$. If $\varphi_1 = 0$, the statement is immediately satisfied. For the case $\varphi_1 > 0$, within Y_0 the Lyapunov function satisfies (A.24). Expression (A.34) is then obtained by observing that $|\overline{\Lambda}(0,t)| = t$ and $|\overline{\Xi}(0,t)| = 0, \forall t \in Y_0$, while the summation term in (A.34) vanishes.

Suppose that (A.34) is valid over the interval $[0, \varphi_q]$, for some $q \in \mathbb{N}$. From this assumption, and using the continuity of $V(x_p(t))$ it follows that

$$\begin{aligned} V(x_p(\varphi_q)) \leq & e^{-\omega_1|\overline{\Lambda}(0,\varphi_q)|}e^{\omega_2|\overline{\Xi}(0,\varphi_q)|}V(x_p(0)) \\ & + \delta_3\left[1 + 2\sum_{\substack{m\in\mathbb{N};\\ \varphi_m\leq\varphi_q}} e^{-\omega_1|\overline{\Lambda}(\varphi_m+v_m,\varphi_q)|}e^{\omega_2|\overline{\Xi}(\varphi_m,\varphi_q)|}\right]\|w_{\varphi_q}\|_\infty^2. \end{aligned} \tag{A.35}$$

Next, consider the interval W_q. Within W_q, the Lyapunov function satisfies (A.32), leading to

$$V(x_p(t)) \leq e^{\omega_2(t-\varphi_q)}V(\varphi_q) + \delta_3 e^{\omega_2(t-\varphi_q)}\|w_t\|_\infty^2. \tag{A.36}$$

Notice that $t - \varphi_q = |\overline{\Xi}(\varphi_q, t)|, \forall t \in W_q$. Hence,

$$\left|\overline{\Xi}(0,t)\right| = t - \varphi_q + \left|\overline{\Xi}(0,\varphi_q)\right| \tag{A.37}$$

$$\left|\overline{\Lambda}(0,t)\right| = \left|\overline{\Lambda}(0,\varphi_q)\right| \tag{A.38}$$

$\forall t \in W_q$. By multiplying $\exp\{\omega_2(t-\varphi_q)\}$ with the first term on the right-hand side (RHS) of (A.35), we obtain the first term on the RHS of (A.34). Similarly, multiplying $\exp\{\omega_2(t-\varphi_q)\}$ with the summation term in (A.35) yields

$$e^{\omega_2(t-\varphi_q)}\sum_{\substack{m\in\mathbb{N};\\ \varphi_m<\varphi_q}} e^{-\omega_1\left|\overline{\Lambda}(\varphi_m+v_m,\varphi_q)\right|}e^{\omega_2\left|\overline{\Xi}(\varphi_m,\varphi_q)\right|} = \sum_{\substack{m\in\mathbb{N};\\ \varphi_m<\varphi_q}} e^{-\omega_1\left|\overline{\Lambda}(\varphi_m+v_m,t)\right|}e^{\omega_2\left|\overline{\Xi}(\varphi_m,t)\right|} \tag{A.39}$$

for every $t \in W_q$, since $\left|\overline{\Lambda}(\varphi_m + v_m, \varphi_q)\right| = \left|\overline{\Lambda}(\varphi_m + v_m, t)\right|$ and $t - \varphi_q + \left|\overline{\Xi}(\varphi_m, \varphi_q)\right| = \left|\overline{\Xi}(\varphi_m, t)\right|$ hold in this interval. Consequently, the factor associated with the disturbance term can be rewritten as

$$2\delta_3 e^{\omega_2(t-\varphi_q)} + 2\delta_3 \sum_{\substack{m\in\mathbb{N};\\ \varphi_m<\varphi_q}} e^{-\omega_1\left|\overline{\Lambda}(\varphi_m+v_m,t)\right|} e^{\omega_2\left|\overline{\Xi}(\varphi_m,t)\right|} = 2\delta_3 \sum_{\substack{m\in\mathbb{N};\\ \varphi_m<\varphi_q}} e^{-\omega_1\left|\overline{\Lambda}(\varphi_m+v_m,t)\right|} e^{\omega_2\left|\overline{\Xi}(\varphi_m,t)\right|}$$
$$= 2\delta_3 \sum_{\substack{m\in\mathbb{N};\\ \varphi_m\le t}} e^{-\omega_1\left|\overline{\Lambda}(\varphi_m+v_m,t)\right|} e^{\omega_2|\overline{\Xi}(\varphi_m,t)|} \tag{A.40}$$

where the first equality uses $\left|\overline{\Lambda}(\varphi_q + v_q, t)\right| = 0$ and $t - \varphi_q = \left|\overline{\Xi}(\varphi_q, t)\right|, \forall t \in W_q$, while the second equality follows because the condition $\varphi_m \le \varphi_q$ is equivalent to $\varphi_m \le t$ over the set W_q. Therefore, relation (A.34) remains valid $\forall t \in [0, \varphi_q + v_q]$.

Consider now the interval Y_q. Within Y_q, the Lyapunov function satisfies the inequality

$$V(x_p(t)) \le e^{-\omega_1(t-\varphi_q-v_q)} e^{\omega_2 v_q} V\left(x(\varphi_q)\right) + \delta_3\left[1 + e^{-\omega_1(t-\varphi_q-v_q)} e^{\omega_2 v_q}\right] \|w_t\|_\infty^2, \tag{A.41}$$

$\forall t \in Y_q$, where $V(x_p(\varphi_q))$ is given by (A.35). From this inequality, it follows that condition (A.34) remains valid. In particular, note that $t - \varphi_q - v_q = \left|\overline{\Lambda}(\varphi_q + v_q, t)\right|$ and $\left|\overline{\Lambda}(0, \varphi_q)\right| = \overline{\Lambda}(0, \varphi_q + v_q)$. Thus, it is obtained that

$$\left|\overline{\Lambda}(0, t)\right| = t - \varphi_q - v_q + \left|\overline{\Lambda}(0, \varphi_q)\right|, \tag{A.42}$$

$\forall t \in Y_q$. Furthermore, since $v_q = \left|\overline{\Xi}(\varphi_q, \varphi_q + v_q)\right|$ and $\left|\overline{\Xi}(\varphi_q + v_q, t)\right| = 0$, it follows that

$$\left|\overline{\Xi}(0, t)\right| = v_q + \left|\overline{\Xi}(0, \varphi_q)\right|, \tag{A.43}$$

$\forall t \in Y_q$. Hence, multiplying $e^{-\omega_1(t-\varphi_q-v_q)} e^{\omega_2 v_q}$ by the first term on the right-hand side of (A.35) produces the first term on the right-hand side of (A.34). Furthermore, multiplying

$e^{-\omega_1(t-\varphi_q-v_q)}e^{\omega_2 v_q}$ by the summation term in (A.35) yields

$$e^{-\omega_1(t-\varphi_q-v_q)}e^{\omega_2 v_q}\sum_{\substack{m\in\mathbb{N};\\ \varphi_m<\varphi_q}} e^{-\omega_1\left|\overline{\Lambda}(\varphi_m+v_m,\varphi_q)\right|}e^{\omega_2\left|\overline{\Xi}(\varphi_m,\varphi_q)\right|} = \sum_{\substack{m\in\mathbb{N};\\ \varphi_m<\varphi_q}} e^{-\omega_1\left|\overline{\Lambda}(\varphi_m+v_m,t)\right|}e^{\omega_2\left|\overline{\Xi}(\varphi_m,t)\right|}. \tag{A.44}$$

Consequently, the coefficient multiplying the disturbance term can be reformulated as

$$\begin{aligned}&\delta_3\left[1+2e^{-\omega_1(t-\varphi_q-v_q)}e^{\omega_2 v_q}\right]+2\delta_3\sum_{\substack{m\in\mathbb{N};\\ \varphi_m<\varphi_q}} e^{-\omega_1\left|\overline{\Lambda}(\varphi_m+v_m,t)\right|}e^{\omega_2\left|\overline{\Xi}(\varphi_m,t)\right|}\\ &=2\delta_3\sum_{\substack{m\in\mathbb{N};\\ \varphi_m<\varphi_q}} e^{-\omega_1\left|\overline{\Lambda}(\varphi_m+v_m,t)\right|}e^{\omega_2\left|\overline{\Xi}(\varphi_m,t)\right|}=2\delta_3\sum_{\substack{m\in\mathbb{N}\\ \varphi_m\le t}} e^{-\omega_1\left|\overline{\Lambda}(\varphi_m+v_m,t)\right|}e^{\omega_2\left|\overline{\Xi}(\xi_m,t)\right|}.\end{aligned} \tag{A.45}$$

In the last step, the second equality holds because, $\forall t\in Y_q$, the condition $\varphi_m\le\varphi_q$ is equivalent to $\varphi_m\le t$. Therefore, (A.34) remains valid $\forall t\in[0,\varphi_{q+1}]$, which concludes the proof. ■

Step III: Constraints on DoS attack occurrence and persistence

To complete the proof of Theorem 2.4, it remains to establish a bound for the summation term in (A.34). The following result holds.

Lemma A.3. *Suppose Assumptions 2.1 and 2.2 hold, and condition (2.22) is satisfied. Then, $\forall t\in\mathbb{R}_{\ge 0}$, the sum*

$$\sum_{\substack{m\in\mathbb{N};\\ \varphi_m\le t}} e^{-\omega_1\left|\overline{\Lambda}(\varphi_m+v_m,t)\right|},e^{\omega_2\left|\overline{\Xi}(\varphi_m,t)\right|} \tag{A.46}$$

admits the upper bound

$$e^{(\omega_1+\omega_2)\zeta_\star}\frac{e^{\beta_\star\tau_F\varrho}}{1-e^{-\beta_\star\tau_F}}. \tag{A.47}$$

Here, the constants

$$\zeta_\star \coloneqq \zeta + (1+\varrho)\underline{\Delta}, \tag{A.48}$$

$$\beta_\star \coloneqq \omega_1 - (\omega_1+\omega_2)\left(\frac{1}{T}+\frac{\underline{\Delta}}{\tau_F}\right), \tag{A.49}$$

ω_1 and ω_2 are mentioned in (2.23) and (2.24), respectively, ϱ, τ_F are mentioned in (2.20), and ζ, T are mentioned in (2.21).

Proof. Observe that

$$\left|\overline{\Xi}(\tau,t)\right| \leq \left|\overline{\Xi}(\tau,t)\right| + (1+n(\tau,t))\,\underline{\Delta}, \tag{A.50}$$

$\forall \tau, t \in \mathbb{R}_{\geq 0}$ with $t \geq \tau$. In other words, $\left|\overline{\Xi}(\tau,t)\right|$ can be bounded by the total duration of the DoS over the interval $[\tau,t]$, together with the maximum actuation delay $\underline{\Delta}$, which may occur once at the start of $[\tau,t]$ due to a preceding DoS event, plus $n(\tau,t)$ additional occurrences. Here, $n(\tau,t)$ denotes the number of on/off transitions of DoS within $[\tau,t]$. Under Assumptions 2.1 and 2.2, it follows that

$$\left|\bar{\Xi}(\tau,t)\right| \leq \zeta + \frac{t-\tau}{T} + \left(1+\varrho+\frac{t-\tau}{\tau_F}\right)\underline{\Delta} =: \zeta_\star + \frac{t-\tau}{T_\star}, \tag{A.51}$$

where

$$T_\star \coloneqq \frac{T\tau_F}{\underline{\Delta}T+\tau_F} \tag{A.52}$$

and $\zeta_\star$ is mentioned in (A.48). From the above inequality, it holds that

$$\left|\bar{\Xi}(\varphi_m,t)\right| \leq \zeta_\star + \frac{t-\varphi_m}{T_\star}, \tag{A.53}$$

$\forall t \in \mathbb{R}_{\geq 0}$ and $m \in \mathbb{N}$. Consider next the term $\left|\overline{\Lambda}(\varphi_m+v_m,t)\right|$. It follows that

$$\left|\bar{\Lambda}(\zeta_m+v_m,t)\right| = t - \zeta_m - \left|\bar{\Xi}(\zeta_m,t)\right|, \tag{A.54}$$

$\forall t \in \mathbb{R}_{\geq \varphi_m}$ and $m \in \mathbb{N}$. To verify (A.54), first consider $t \in W_m$. For all $t \in W_m$, the relation $\left|\overline{\Xi}(\varphi_m, t)\right| = t - \varphi_m$ holds, which implies (A.54) because, by definition, $\left|\overline{\Lambda}(\varphi_m + v_m, t)\right| = 0$ whenever $t < \varphi_m + v_m$. For all $t \in \mathbb{R}_{\geq \varphi_m + v_m}$, it holds that

$$\left|\overline{\Lambda}(\varphi_m + v_m, t)\right| = t - \varphi_m - v_m - \left|\bar{\Lambda}(\varphi_m, t)\right| = t - \varphi_m - \left|\overline{\Xi}(\varphi_m, t)\right|, \tag{A.55}$$

where the second equality follows since

$$\left|\overline{\Xi}(\varphi_m + v_m, t)\right| = \left|\overline{\Xi}(\varphi_m, t)\right| - \left|\overline{\Xi}(\varphi_m, \varphi_m + v_m)\right| = \left|\overline{\Xi}(\varphi_m, t)\right| - v_m. \tag{A.56}$$

Therefore, $\forall t \in \mathbb{R}_{\geq \varphi_m + v_m}$ and $m \in \mathbb{N}$,

$$\begin{aligned} \sum_{\substack{m \in \mathbb{N}; \\ \varphi_m \leq t}} e^{-\omega_1 \left|\overline{\Lambda}(\varphi_m + v_m, t)\right|} e^{\omega_2 \left|\overline{\Xi}(\varphi_m, t)\right|} &\leq e^{(\omega_1 + \omega_2)\zeta_\star} \sum_{\substack{m \in \mathbb{N}; \\ \varphi_m \leq t}} e^{\{\omega_1 - (\omega_1 + \omega_2)/T_*\}(t - \varphi_m)} \\ &= e^{(\omega_1 + \omega_2)\zeta_\star} \sum_{\substack{m \in \mathbb{N}; \\ \varphi_m \leq t}} e^{-\beta_\star (t - \varphi_m)}, \end{aligned} \tag{A.57}$$

where $\beta_\star$ is mentioned in (A.49). Under condition (4.5), it follows that $\beta_\star > 0$. Furthermore, from Assumption 2.1,

$$t - \varphi_m \geq \tau_F n(\varphi_m, t) - \tau_F \varrho \tag{A.58}$$

holds. From this inequality, one can deduce that

$$\sum_{\substack{m \in \mathbb{N}; \\ \varphi_m \leq t}} e^{-\beta_\star (t - \varphi_m)} \leq e^{\beta_\star \tau_F \varrho} \sum_{\substack{m \in \mathbb{N}; \\ \varphi_m \leq t}} e^{-\beta_\star \tau_F n(\varphi_m, t)}. \tag{A.59}$$

Define the function $m(t)$ as

$$m(t) := \begin{cases} 0, & \text{if } t < \varphi_1, \\ \sup\{m \in \mathbb{N} : \varphi_m \leq t\}, & \text{otherwise.} \end{cases} \tag{A.60}$$

This leads to

$$\sum_{\substack{m\in\mathbb{N}\\ \varphi_m\le t}} e^{-\beta_\star\tau_F n(\varphi_m,t)} = \sum_{m=1}^{m(t)} e^{-\beta_\star\tau_F n(\varphi_m,t)}. \tag{A.61}$$

Since

$$n(\varphi_m,t) \ge m(t)-m, \tag{A.62}$$

then,

$$\sum_{m=1}^{m(t)} e^{-\beta_\star\tau_F n(\varphi_m,t)} = \sum_{m=1}^{m(t)} e^{-\beta_\star\tau_F (m(t)-m)} = \sum_{m=1}^{m(t)} e^{-\beta_\star\tau_F m} \le \frac{1}{1-e^{-\beta_\star\tau_F}}. \tag{A.63}$$

Combining relations (A.57), (A.59), (A.61), and (A.63) leads to the required bound in (A.47). ■

The proof of Theorem 2.4 can now be completed. First, note that the first term on the right-hand side of (A.34) is bounded by

$$e^{\zeta_\star(\omega_1+\omega_2)} e^{-(\omega_1-\frac{\omega_1+\omega_2}{T_\star})t} V\left(x_p(0)\right), \tag{A.64}$$

where the equality $\left|\overline{\Lambda}(0,t)\right| = t - \left|\overline{\Xi}(0,t)\right|$ and inequality (A.51) have been used. Recall that $\beta_\star$ is defined in (A.49). From (A.34) and (A.47), it follows that the Lyapunov function $V(x_p(t))$ evaluated along any trajectory $x_p(t)$ satisfies

$$V(x_p(t)) \le e^{\zeta_\star(\omega_1+\omega_2)} e^{-\beta_\star t} V(x_p(0)) + \delta_3 \left[1 + 2e^{\zeta_\star(\omega_1+\omega_2)} \frac{e^{\beta_\star\tau_F\varrho}}{1-e^{-\beta_\star\tau_F}}\right] \|w_t\|_\infty^2. \tag{A.65}$$

Introducing $\delta_\star := \delta_3/\lambda_m(P)$ yields

$$\|x_p(t)\| \le \sqrt{\frac{\lambda_M(P)}{\lambda_m(P)}}\, e^{\frac{\zeta_\star(\omega_1+\omega_2)}{2}} e^{-\frac{\beta_\star t}{2}} \|x_p(0)\| + \sqrt{\delta_* \left[1 + 2e^{\zeta_\star(\omega_1+\omega_2)} \frac{e^{\beta_\star\tau_F\varrho}}{1-e^{-\beta_\star\tau_F}}\right]} \|w_t\|_\infty. \tag{A.66}$$

Here, $\delta_\star$ is a positive constant independent of both the initial state and the disturbance w. Since $\underline{\Delta}$ is positive, $\zeta_\star$ in (A.48) and $\beta_\star$ in (A.49) are independent of the initial condition and w. Therefore, ISS in Theorem 2.4 is established. ■

Publication from the thesis

Journal publication

- A. Basu and I. Kar, "Characterization of multi-channel denial-of-service," *European Journal of Control,* vol. 78, p. 101001, 2024.
- A. Basu and I. Kar, "Characterization of full-scale denial-of-service," *International Journal of Control*, pp. 1 – 32, 2025.
- A. Basu and I. Kar, "Switched observer-based optimal dynamic event-triggered control for multiple transmission channels under denial-of-service," *International Journal of Systems Science*, pp. 1 – 32, 2025.

Conference publication

- A. Basu and I. Kar, "Observer-based input-to-state stabilizing control for multiple transmission channels under denial-of-service," In 2022 *Eighth Indian Control Conference (ICC)* pp. 73 – 78, IEEE, 2022.

Bibliography

[1] V. Gunes, S. Peter, T. Givargis, and F. Vahid, "A survey on concepts, applications, and challenges in cyber-physical systems," *KSII Transactions on Internet and Information Systems (TIIS)*, vol. 8, no. 12, pp. 4242–4268, 2014.

[2] W. Wolf, "Cyber-physical systems," *Computer*, vol. 42, no. 03, pp. 88–89, 2009.

[3] E. A. Lee, "The past, present and future of cyber-physical systems: A focus on models," *Sensors*, vol. 15, no. 3, pp. 4837–4869, 2015.

[4] R. Poovendran, K. Sampigethaya, S. K. S. Gupta, I. Lee, K. V. Prasad, D. Corman, and J. L. Paunicka, "Special issue on cyber-physical systems [scanning the issue]," *Proceedings of the IEEE*, vol. 100, no. 1, pp. 6–12, 2011.

[5] N. Niu, L. Da Xu, and Z. Bi, "Enterprise information systems architecture-Analysis and evaluation," *IEEE Transactions on Industrial Informatics*, vol. 9, no. 4, pp. 2147–2154, 2013.

[6] I. Horváth, "Designing next-generation cyber-physical systems: Why is it an issue?," *Journal of Integrated Design and Process Science*, vol. 26, no. 3-4, pp. 317–349, 2023.

[7] S. I. Caramihai and I. Dumitrache, "Agricultural enterprise as a complex system: A cyber physical systems approach," in *2015 20th International Conference on Control Systems and Computer Science*, pp. 659–664, IEEE, 2015.

[8] P. O. Dusadeerungsikul, S. Y. Nof, A. Bechar, and Y. Tao, "Collaborative control protocol for agricultural cyber-physical system," *Procedia Manufacturing*, vol. 39, pp. 235–242, 2019.

[9] A. Y. Saber and G. K. Venayagamoorthy, "Efficient utilization of renewable energy sources by gridable vehicles in cyber-physical energy systems," *IEEE Systems Journal*, vol. 4, no. 3, pp. 285–294, 2010.

[10] L. Shi, Q. Dai, and Y. Ni, "Cyber–physical interactions in power systems: A review of models, methods, and applications," *Electric Power Systems Research*, vol. 163, pp. 396–412, 2018.

[11] A. Saad, S. Faddel, and O. Mohammed, "IoT-based digital twin for energy cyber-physical systems: design and implementation," *Energies*, vol. 13, no. 18, p. 4762, 2020.

[12] R. V. Yohanandhan, R. M. Elavarasan, P. Manoharan, and L. Mihet-Popa, "Cyber-physical power system (CPPS): A review on modeling, simulation, and analysis with cyber security applications," *IEEE Access*, vol. 8, pp. 151019–151064, 2020.

[13] X. Chen, M. A. Eder, A. Shihavuddin, and D. Zheng, "A human-cyber-physical system toward intelligent wind turbine operation and maintenance," *Sustainability*, vol. 13, no. 2, p. 561, 2021.

[14] A. Selmani, H. Oubehar, M. Outanoute, A. Ed-Dahhak, M. Guerbaoui, A. Lachhab, and B. Bouchikhi, "Agricultural cyber-physical system enabled for remote management of solar-powered precision irrigation," *Biosystems Engineering*, vol. 177, pp. 18–30, 2019.

[15] S. A. Haque, S. M. Aziz, and M. Rahman, "Review of cyber-physical system in healthcare," *International Journal of Distributed Sensor Networks*, vol. 10, no. 4, p. 217415, 2014.

[16] A. A. AlZubi, M. Al-Maitah, and A. Alarifi, "Cyber-attack detection in healthcare using cyber-physical system and machine learning techniques," *Soft Computing*, vol. 25, no. 18, pp. 12319–12332, 2021.

[17] C. Shan, J. Zhao, W. Zhao, T. Zhang, B. Du, and Z. Yuan, "Magnetic-Actuated cyber-physical system for interventional surgery," *Human-centric Computing and Information Sciences*, vol. 12, p. 37, 2022.

[18] Y. Van Tendeloo and H. Vangheluwe, "Teaching the fundamentals of the modelling of cyber-physical systems," in *2016 Symposium on Theory of Modeling and Simulation (TMS-DEVS)*, pp. 1–8, IEEE, 2016.

[19] H. S. Kang, J. Y. Lee, S. Choi, H. Kim, J. H. Park, J. Y. Son, B. H. Kim, and S. D. Noh, "Smart manufacturing: past research, present findings, and future directions," *International Journal of Precision Engineering and Manufacturing-Green Technology*, vol. 3, pp. 111–128, 2016.

[20] X. Yao, J. Zhou, Y. Lin, Y. Li, H. Yu, and Y. Liu, "Smart manufacturing based on cyber-physical systems and beyond," *Journal of Intelligent Manufacturing*, vol. 30, pp. 2805–2817, 2019.

[21] Y. H. Son, K. T. Park, D. Lee, S. W. Jeon, and S. Do Noh, "Digital twin–based cyber-physical system for automotive body production lines," *The International Journal of Advanced Manufacturing Technology*, vol. 115, pp. 291–310, 2021.

[22] Y. Zhao, Z. Liu, and W. S. Wong, "Resilient platoon control of vehicular cyber physical systems under DoS attacks and multiple disturbances," *IEEE Transactions on Intelligent Transportation Systems*, vol. 23, no. 8, pp. 10945–10956, 2021.

[23] Y.-J. Shin, L. Liu, S. Hyun, and D.-H. Bae, "Platooning legos: An open physical exemplar for engineering self-adaptive cyber-physical systems-of-systems," in *2021 International Symposium on Software Engineering for Adaptive and Self-Managing Systems (SEAMS)*, pp. 231–237, IEEE, 2021.

[24] H. Zhu, Y. Zhou, X. Luo, and H. Zhou, "Joint control of power, beamwidth, and spacing for platoon-based vehicular cyber-physical systems," *IEEE Transactions on Vehicular Technology*, vol. 71, no. 8, pp. 8615–8629, 2022.

[25] D. Pan, D. Ding, X. Ge, Q.-L. Han, and X.-M. Zhang, "Privacy-preserving platooning control of vehicular cyber–physical systems with saturated inputs," *IEEE Transactions on Systems, Man, and Cybernetics: Systems*, vol. 53, no. 4, pp. 2083–2097, 2022.

[26] S. Sierla, B. M. O'Halloran, T. Karhela, N. Papakonstantinou, and I. Y. Tumer, "Common cause failure analysis of cyber–physical systems situated in constructed environments," *Research in Engineering Design*, vol. 24, pp. 375–394, 2013.

[27] G. Tanganelli, L. Cassano, A. Miele, and C. Vallati, "A methodology for the design and deployment of distributed cyber–physical systems for smart environments," *Future Generation Computer Systems*, vol. 109, pp. 420–430, 2020.

[28] R. Taormina, S. Galelli, N. O. Tippenhauer, E. Salomons, and A. Ostfeld, "Characterizing cyber-physical attacks on water distribution systems," *Journal of Water Resources Planning and Management*, vol. 143, no. 5, p. 04017009, 2017.

[29] D. Petriu, C. Shousha, and A. Jalnapurkar, "Architecture-based performance analysis applied to a telecommunication system," *IEEE Transactions on Software Engineering*, vol. 26, no. 11, pp. 1049–1065, 2000.

[30] G. Loukas, *Cyber-Physical Attacks: A Growing Invisible Threat*. Butterworth-Heinemann, 2015.

[31] A. D'Innocenzo, F. Smarra, and M. D. Di Benedetto, "Resilient stabilization of multi-hop control networks subject to malicious attacks," *Automatica*, vol. 71, pp. 1–9, 2016.

[32] J. Slay and M. Miller, "Lessons learned from the maroochy water breach," in *International Conference on Critical Infrastructure Protection*, pp. 73–82, Springer, 2007.

[33] S. Kuvshinkova, "Sql slammer worm lessons learned for consideration by the electricity sector," *North American Electric Reliability Council*, vol. 1, no. 2, p. 5, 2003.

[34] S. Karnouskos, "Stuxnet worm impact on industrial cyber-physical system security," in *IECON 2011-37th Annual Conference of the IEEE Industrial Electronics Society*, pp. 4490–4494, IEEE, 2011.

[35] J. P. Farwell and R. Rohozinski, "Stuxnet and the future of cyber war," *Survival*, vol. 53, no. 1, pp. 23–40, 2011.

[36] T. Halder, "A comprehensive survey of grid failure in India," in *2013 International Conference on Power, Energy and Control (ICPEC)*, pp. 704–709, IEEE, 2013.

[37] J. P. Conti, "The day the samba stopped [power blackouts]," *Engineering & Technology*, vol. 5, no. 4, pp. 46–47, 2010.

[38] F. Pasqualetti, F. Dörfler, and F. Bullo, "Attack detection and identification in cyber-physical systems," *IEEE Transactions on Automatic Control*, vol. 58, no. 11, pp. 2715–2729, 2013.

[39] D. Wang, Z. Wang, B. Shen, F. E. Alsaadi, and T. Hayat, "Recent advances on filtering and control for cyber-physical systems under security and resource constraints," *Journal of the Franklin Institute*, vol. 353, no. 11, pp. 2451–2466, 2016.

[40] D. Ding, Z. Wang, Q.-L. Han, and G. Wei, "Security control for discrete-time stochastic nonlinear systems subject to deception attacks," *IEEE Transactions on Systems, Man, and Cybernetics: Systems*, vol. 48, no. 5, pp. 779–789, 2016.

[41] M. Ramadan and F. Abdollahi, "An active approach for isolating replay attack from sensor faults," *European Journal of Control*, vol. 69, p. 100725, 2023.

[42] A. D. Wood and J. A. Stankovic, "Denial of service in sensor networks," *Computer*, vol. 35, no. 10, pp. 54–62, 2002.

[43] Y. Xia, W. Yang, and Z. Zhao, "Consensus-based filtering under false data injection attacks," *European Journal of Control*, vol. 48, pp. 3–8, 2019.

[44] W. Tu, J. Dong, and D. Zhai, "Optimal $\epsilon-$stealthy attack in cyber-physical systems," *Journal of the Franklin Institute*, vol. 358, no. 1, pp. 151–171, 2021.

[45] A. O. de Sá, L. F. R. da Costa Carmo, and R. C. Machado, "Covert attacks in cyber-physical control systems," *IEEE Transactions on Industrial Informatics*, vol. 13, no. 4, pp. 1641–1651, 2017.

[46] S. Amin, A. A. Cárdenas, and S. S. Sastry, "Safe and secure networked control systems under denial-of-service attacks," in *International Workshop on Hybrid Systems: Computation and Control*, pp. 31–45, Springer, 2009.

[47] H. S. Foroush and S. Martinez, "On multi-input controllable linear systems under unknown periodic dos jamming attacks," in *2013 Proceedings of the Conference on Control and its Applications*, pp. 222–229, SIAM, 2013.

[48] C. De Persis and P. Tesi, "Input-to-state stabilizing control under denial-of-service," *IEEE Transactions on Automatic Control*, vol. 60, no. 11, pp. 2930–2944, 2015.

[49] C. De Persis and P. Tesi, "On resilient control of nonlinear systems under denial-of-service," in *53rd IEEE Conference on Decision and Control*, pp. 5254–5259, IEEE, 2014.

[50] C. De Persis and P. Tesi, "Networked control of nonlinear systems under denial-of-service," *Systems & Control Letters*, vol. 96, pp. 124–131, 2016.

[51] V. Dolk, P. Tesi, C. De Persis, and W. Heemels, "Event-triggered control systems under denial-of-service attacks," *IEEE Transactions on Control of Network Systems*, vol. 4, no. 1, pp. 93–105, 2016.

[52] S. Feng and P. Tesi, "Resilient control under denial-of-service: Robust design," *Automatica*, vol. 79, pp. 42–51, 2017.

[53] S. Feng and P. Tesi, "Networked control systems under denial-of-service: Co-located vs. remote architectures," *Systems & Control Letters*, vol. 108, pp. 40–47, 2017.

[54] S. Feng, A. Cetinkaya, H. Ishii, P. Tesi, and C. De Persis, "Resilient quantized control under denial-of-service: variable bit rate quantization," *Automatica*, vol. 141, p. 110302, 2022.

[55] Y. Tang, D. Zhang, D. W. Ho, W. Yang, and B. Wang, "Event-based tracking control of mobile robot with denial-of-service attacks," *IEEE Transactions on Systems, Man, and Cybernetics: Systems*, vol. 50, no. 9, pp. 3300–3310, 2018.

[56] H. Yuan, Y. Xia, H. Yang, and Y. Yuan, "Resilient control for wireless networked control systems under DoS attack via a hierarchical game," *International Journal of Robust and Nonlinear Control*, vol. 28, no. 15, pp. 4604–4623, 2018.

[57] Y.-C. Sun and G.-H. Yang, "Event-triggered resilient control for cyber-physical systems under asynchronous DoS attacks," *Information Sciences*, vol. 465, pp. 340–352, 2018.

[58] Y.-C. Sun and G.-H. Yang, "Periodic event-triggered resilient control for cyber-physical systems under denial-of-service attacks," *Journal of the Franklin Institute*, vol. 355, no. 13, pp. 5613–5631, 2018.

[59] Y.-C. Sun and G.-H. Yang, "Robust event-triggered model predictive control for cyber-physical systems under denial-of-service attacks," *International Journal of Robust and Nonlinear Control*, vol. 29, no. 14, pp. 4797–4811, 2019.

[60] Y.-C. Sun and G.-H. Yang, "Event-triggered remote state estimation for cyber-physical systems under malicious DoS attacks," *Information Sciences*, vol. 602, pp. 43–56, 2022.

[61] Y. Zhu, F. Yang, C. Li, Y. Zhang, and Q.-L. Han, "Strong $\gamma_c - \gamma_{cl}$ H_∞ stabilization for networked control systems under denial of service attacks," *Journal of the Franklin Institute*, vol. 356, no. 5, pp. 2723–2741, 2019.

[62] S. Hu, D. Yue, Q.-L. Han, X. Xie, X. Chen, and C. Dou, "Observer-based event-triggered control for networked linear systems subject to denial-of-service attacks," *IEEE Transactions on Cybernetics*, vol. 50, no. 5, pp. 1952–1964, 2019.

[63] W. Chen, D. Ding, H. Dong, and G. Wei, "Distributed resilient filtering for power systems subject to denial-of-service attacks," *IEEE Transactions on Systems, Man, and Cybernetics: Systems*, vol. 49, no. 8, pp. 1688–1697, 2019.

[64] M. Wang and B. Xu, "Observer-based guaranteed cost control of cyber-physical systems under dos jamming attacks," *European Journal of Control*, vol. 48, pp. 21–29, 2019.

[65] X. Chen, Y. Wang, and S. Hu, "Event-triggered quantized H_∞ control for networked control systems in the presence of denial-of-service jamming attacks," *Nonlinear Analysis: Hybrid Systems*, vol. 33, pp. 265–281, 2019.

[66] C. Wu, L. Wu, J. Liu, and Z.-P. Jiang, "Active defense-based resilient sliding mode control under denial-of-service attacks," *IEEE Transactions on Information Forensics and Security*, vol. 15, pp. 237–249, 2019.

[67] H. Zhao, Y. Niu, and J. Zhao, "Event-triggered sliding mode control of uncertain switched systems under denial-of-service attacks," *Journal of the Franklin Institute*, vol. 356, no. 18, pp. 11414–11433, 2019.

[68] H. Sun, C. Peng, Y. Wang, and Y.-C. Tian, "Output-based resilient event-triggered control for networked control systems under denial of service attacks," *IET Control Theory & Applications*, vol. 13, no. 16, pp. 2521–2528, 2019.

[69] H. Sun, C. Peng, W. Zhang, T. Yang, and Z. Wang, "Security-based resilient event-triggered control of networked control systems under denial of service attacks," *Journal of the Franklin Institute*, vol. 356, no. 17, pp. 10277–10295, 2019.

[70] S. Hu, D. Yue, X. Chen, Z. Cheng, and X. Xie, "Resilient H_∞ filtering for event-triggered networked systems under nonperiodic DoS jamming attacks," *IEEE Transactions on Systems, Man, and Cybernetics: Systems*, vol. 51, no. 3, pp. 1392–1403, 2019.

[71] J. Zhang, J. Sun, and C. Zhang, "Stochastic game in linear quadratic Gaussian control for wireless networked control systems under DoS attacks," *IEEE Transactions on Systems, Man, and Cybernetics: Systems*, vol. 52, no. 2, pp. 902–910, 2020.

[72] N. Zhao, P. Shi, W. Xing, and J. Chambers, "Observer-based event-triggered approach for stochastic networked control systems under denial of service attacks," *IEEE Transactions on Control of Network Systems*, vol. 8, no. 1, pp. 158–167, 2020.

[73] P. S. Pessim and M. J. Lacerda, "State-feedback control for cyber-physical LPV systems under DoS attacks," *IEEE Control Systems Letters*, vol. 5, no. 3, pp. 1043–1048, 2020.

[74] P. S. Pessim and M. J. Lacerda, "On the robustness of cyber-physical LPV systems under DoS attacks," *Journal of the Franklin Institute*, vol. 359, no. 2, pp. 677–696, 2022.

[75] S. Liu, S. Li, and B. Xu, "Event-triggered resilient control for cyber-physical system under denial-of-service attacks," *International Journal of Control*, vol. 93, no. 8, pp. 1907–1919, 2020.

[76] R. Ma, P. Shi, and L. Wu, "Dissipativity-based sliding-mode control of cyber-physical systems under denial-of-service attacks," *IEEE Transactions on Cybernetics*, vol. 51, no. 5, pp. 2306–2318, 2020.

[77] R. Ma, P. Shi, Z. Wang, and L. Wu, "Resilient filtering for cyber-physical systems under denial-of-service attacks," *International Journal of Robust and Nonlinear Control*, vol. 30, no. 5, pp. 1754–1769, 2020.

[78] R. Ma, P. Shi, and L. Wu, "Active resilient control for two-dimensional systems under denial-of-service attacks," *International Journal of Robust and Nonlinear Control*, vol. 31, no. 3, pp. 759–771, 2021.

[79] N. Zhao, P. Shi, and W. Xing, "Dynamic event-triggered approach for networked control systems under denial of service attacks," *International Journal of Robust and Nonlinear Control*, vol. 31, no. 5, pp. 1774–1795, 2021.

[80] Y. Qi, N. Xing, J. Fu, and W. Guan, "Adaptive dynamic optimal control for triggered networked switched systems under dual-ended denial-of-service attacks," *International Journal of Robust and Nonlinear Control*, vol. 31, no. 9, pp. 4397–4415, 2021.

[81] T. Li, B. Chen, L. Yu, and W.-A. Zhang, "Active security control approach against DoS attacks in cyber-physical systems," *IEEE Transactions on Automatic Control*, vol. 66, no. 9, pp. 4303–4310, 2021.

[82] L. Zhang, Y. Chen, and M. Li, "Resilient predictive control for cyber–physical systems under denial-of-service attacks," *IEEE Transactions on Circuits and Systems II: Express Briefs*, vol. 69, no. 1, pp. 144–148, 2021.

[83] Z. Zhang, Y. Niu, and H. Zhao, "Secure sliding mode control of interval type-2 fuzzy systems against intermittent denial-of-service attacks," *International Journal of Robust and Nonlinear Control*, vol. 31, no. 6, pp. 1866–1884, 2021.

[84] R. Kato, A. Cetinkaya, and H. Ishii, "Linearization-based quantized stabilization of nonlinear systems under DoS attacks," *IEEE Transactions on Automatic Control*, vol. 67, no. 12, pp. 6826–6833, 2021.

[85] M. Sathishkumar and Y.-C. Liu, "Resilient adaptive event-triggered dissipative control for networked control systems with DoS attacks," *International Journal of Systems Science*, vol. 53, no. 7, pp. 1562–1578, 2022.

[86] Y. Zhou and X.-H. Chang, "Event-triggered quantized $\mathfrak{L}_2 - \mathfrak{L}_\infty$ filtering for neural networks under denial-of-service attacks," *International Journal of Robust and Nonlinear Control*, vol. 32, no. 10, pp. 5897–5918, 2022.

[87] J. Fu, Y. Qi, N. Xing, and Y. Li, "A new switching law for event-triggered switched systems under DoS attacks," *Automatica*, vol. 142, p. 110373, 2022.

[88] H. Gao, H. Zhang, K. Shi, and K. Zhou, "Event-triggered finite-time guaranteed cost control for networked Takagi-Sugeno (T-S) fuzzy switched systems under denial of service attacks," *International Journal of Robust and Nonlinear Control*, vol. 32, no. 9, pp. 5764–5775, 2022.

[89] A. Basit, M. Tufail, M. Rehan, M. Riaz, and I. Ahmed, "Distributed state and unknown input estimation under denial-of-service attacks: A dynamic event-triggered approach," *IEEE Transactions on Circuits and Systems II: Express Briefs*, vol. 70, no. 6, pp. 2266–2270, 2022.

[90] W. Liu, J. Sun, G. Wang, F. Bullo, and J. Chen, "Data-driven resilient predictive control under denial-of-service," *IEEE Transactions on Automatic Control*, vol. 68, no. 8, pp. 4722–4737, 2022.

[91] J. Yan, Y. Xia, X. Wang, and X. Feng, "Quantized stabilization of switched systems with partly unstabilizable subsystems and denial-of-service attacks," *International Journal of Robust and Nonlinear Control*, vol. 32, no. 8, pp. 4574–4593, 2022.

[92] Y.-W. Wang, Z.-H. Zeng, X.-K. Liu, and Z.-W. Liu, "Input-to-state stability of switched linear systems with unstabilizable modes under DoS attacks," *Automatica*, vol. 146, p. 110607, 2022.

[93] M. Shi, S. Feng, and H. Ishii, "Quantized state feedback stabilization of nonlinear systems under Denial-of-Service," *Automatica*, vol. 139, p. 110180, 2022.

[94] X. Wang, D. Ding, X. Ge, and Q.-L. Han, "Neural-network-based control for discrete-time nonlinear systems with denial-of-service attack: The adaptive event-triggered case," *International Journal of Robust and Nonlinear Control*, vol. 32, no. 5, pp. 2760–2779, 2022.

[95] W. Gao, C. Deng, Y. Jiang, and Z.-P. Jiang, "Resilient reinforcement learning and robust output regulation under denial-of-service attacks," *Automatica*, vol. 142, p. 110366, 2022.

[96] W. Gao, Z.-P. Jiang, and T. Chai, "Resilient control under denial-of-service and uncertainty: An adaptive dynamic programming approach," *IEEE Transactions on Automatic Control*, 2025.

[97] K. Chatterjee, V. K. Singh, P. Prasun, S. Kamal, S. Ghosh, and T. N. Dinh, "Fixed-time event-triggered control under denial-of-service attacks," *European Journal of Control*, vol. 69, p. 100765, 2023.

[98] R. Gao, J. Huang, X. Su, and L. Zhao, "Adaptive control of strict-feedback nonlinear systems under denial-of-service: A synthetic analysis," *IEEE Transactions on Information Forensics and Security*, vol. 19, pp. 2315–2327, 2023.

[99] A.-W. A. Saif, S. El-Ferik, and S. M. Elkhider, "Robust stabilization of linear time-delay systems under denial-of-service attacks," *Sensors*, vol. 23, no. 13, p. 5773, 2023.

[100] B.-C. Zheng, Y. Zhao, Y. Zhu, and T. Li, "Sliding-mode control under denial-of-service attacks: An event-triggered quantized state feedback approach," *IEEE Transactions on Circuits and Systems II: Express Briefs*, vol. 70, no. 8, pp. 2949–2953, 2023.

[101] Y. Ji, Y. Song, J. Liu, Q. Gao, and Z. Chen, "Small-gain-based adaptive secure control of switched cyber-physical systems with denial-of-service attacks," *IEEE Transactions on Industrial Informatics*, vol. 20, no. 3, pp. 3092–3103, 2023.

[102] H. Li, H. Gao, Z. Zuo, and J. Liu, "Security control based on variable-step predictive approach for networked control system with denial-of-service attacks," *International Journal of Robust and Nonlinear Control*, vol. 33, no. 14, pp. 8475–8489, 2023.

[103] X. Liu, F. Deng, P. Zeng, X. Gao, and X. Zhao, "Sampled-data resilient control for stochastic nonlinear CPSs under DoS attacks," *International Journal of Systems Science*, vol. 54, no. 5, pp. 1165–1171, 2023.

[104] J. Lu and D. E. Quevedo, "A jointly optimal design of control and scheduling in networked systems under denial-of-service attacks," *Automatica*, vol. 148, p. 110774, 2023.

[105] P. H. S. Coutinho, I. Bessa, P. S. Pessim, and R. M. Palhares, "A switching approach to event-triggered control systems under denial-of-service attacks," *Nonlinear Analysis: Hybrid Systems*, vol. 50, p. 101383, 2023.

[106] H. Qu and J. Zhao, "Event-triggered H_∞ control for switched interval type−2 fuzzy systems under denial-of-service," *International Journal of Robust and Nonlinear Control*, vol. 33, no. 3, pp. 2219–2237, 2023.

[107] R. Zhao, Z. Zuo, Y. Wang, and W. Zhang, "Active control strategy for switched systems against asynchronous DoS attacks," *Automatica*, vol. 148, p. 110765, 2023.

[108] H. Ren, G. Zong, X. Qian, W. Yue, and K. Shi, "Hybrid event-based asynchronous finite-time control for cyber-physical switched systems under denial-of-service attacks," *Journal of the Franklin Institute*, vol. 360, no. 2, pp. 1036–1057, 2023.

[109] Y. Liu and Q. Ling, "Event-triggered stabilization of linear systems under quantization and denial-of-service attacks," *International Journal of Robust and Nonlinear Control*, vol. 34, no. 2, pp. 1196–1216, 2024.

[110] C. Wang, W. Xie, J. Gao, P. Wu, and P. X. Liu, "Adaptive event-based dynamic output feedback control for unmanned marine vehicle systems under denial-of-service attack," *Electronics*, vol. 13, no. 3, p. 515, 2024.

[111] J. Xie, Y. Zhang, and D. Yang, "Event-triggered control for networked switched systems with unstabilizable subsystems subject to mode-dependent denial-of-service attacks," *Nonlinear Dynamics*, vol. 112, pp. 1–17, 2024.

[112] S. Shen, C. Zhang, R. Chai, L. Dai, S. Chai, and Y. Xia, "Stabilizing nonlinear model predictive control under denial-of-service attack via dynamic samples selection," *Automatica*, vol. 164, p. 111591, 2024.

[113] A. Sharafian, I. Ullah, S. K. Singh, A. Ali, H. Khan, and X. Bai, "Adaptive fuzzy backstepping secure control for incommensurate fractional order cyber–physical power systems under intermittent denial of service attacks," *Chaos, Solitons & Fractals*, vol. 186, p. 115288, 2024.

[114] S. Dong, E. Liu, B. Wang, M. Liu, and G. Chen, "Adaptive neural network-based security asynchronous control for uncertain Markov jump power systems with dead zone under DoS attack," *International Journal of Robust and Nonlinear Control*, vol. 34, no. 13, pp. 8902–8918, 2024.

[115] L. Yin, L. Xu, H. Zhu, Y. Zhu, and C. Wu, "Input-output data based tracking control under DoS attacks," *International Journal of Control*, vol. 97, no. 7, pp. 1627–1637, 2024.

[116] J. Wei, R. Jia, Y. Song, F. Jing, and J. Guo, "Binary observation-based FIR system identification under sequence denial of service attacks," *International Journal of Robust and Nonlinear Control*, vol. 34, no. 5, pp. 3442–3463, 2024.

[117] A. Fu, Y. Zhang, and J. Qiao, "Dynamic switched periodic event-triggered control systems under denial-of-service attacks," *International Journal of Robust and Nonlinear Control*, vol. 34, no. 5, pp. 3109–3125, 2024.

[118] G. Wang, F. Li, J. Xia, H. Shen, and J. Wang, "Hidden Markov model-based $\mathcal{H}_\infty$ control for singular Markov jump systems under denial of service attacks," *International Journal of Robust and Nonlinear Control*, vol. 34, no. 6, pp. 4310–4324, 2024.

[119] L. Qiu, R. Chen, S. Lin, X. Liu, and M. Najariyan, "Constrained model predictive control for networked jump systems under denial-of-service attacks and time delays," *International Journal of Robust and Nonlinear Control*, vol. 34, no. 15, pp. 10513–10531, 2024.

[120] X. Tian, C. Wang, Z. Xiang, and X. Wang, "Event-triggered control for a class of switched linear systems with actuator saturation and denial-of-service attacks," *Journal of the Franklin Institute*, vol. 361, no. 17, p. 107097, 2024.

[121] C. Tan, T. Ding, Z. Chen, and H. Sun, "Event-triggered fault detector design in networked fuzzy control systems under denial-of-service attacks," *International Journal of Robust and Nonlinear Control*, vol. 34, no. 15, pp. 10494–10512, 2024.

[122] X. Du, G. Liu, H. Zhang, J. H. Park, and X. Liu, "Security load frequency control of networked power systems via Round-Robin protocol under denial of service attacks," *Journal of the Franklin Institute*, vol. 361, no. 16, p. 107155, 2024.

[123] T. Zhou, Q. Wang, H. Li, Y. Du, and G. Yue, "Asynchronous encoder-based event-triggered control of nonlinear networked control system under DoS attacks," *Journal of the Franklin Institute*, vol. 361, no. 16, p. 107180, 2024.

[124] Q. Meng, A. Kasis, H. Yang, and M. M. Polycarpou, "Secure state estimation of networked switched systems under denial-of-service attacks," *European Journal of Control*, vol. 80, p. 101037, 2024.

[125] Z. Yang, X. Dai, L. Fang, J. Zhou, and Z. Yan, "Safe event-triggered control of unmanned surface vehicles with Gaussian process: Resilience in denial of service attacks and uncertain dynamics," *Engineering Applications of Artificial Intelligence*, p. 110776, 2025.

[126] C. Wang, X. Fan, and Y. Fu, "Aperiodic sampled-data-based resilient control for a class of switched nonlinear systems against denial-of-service attacks," *International Journal of Robust and Nonlinear Control*, 2025.

[127] L. An, C. Zhao, and L. Zhang, "Resilient adaptive backstepping tracking control of nonlinear systems without a priori knowledge of DoS attacks," *Automatica*, vol. 174, p. 112119, 2025.

[128] L. Zou, X. Liu, J. Wang, and Y. Chen, "Robust adaptive rapid exponential stabilization for a class of nonlinear cyber-physical systems under denial-of-service attacks," *International Journal of Robust and Nonlinear Control*, 2025.

[129] S. Roy, A. K. Chaudhary, D. Guha, and R. Negi, "Adaptive event-triggered finite-time control of affine cyber-physical systems under denial-of-service (DoS) and deception attacks," *International Journal of Robust and Nonlinear Control*, 2025.

[130] L. Qiu, L. Dong, Z. Shao, and S. Zhou, "Dynamic event-triggered predictive control strategy for networked semi-Markov jump systems," *Systems & Control Letters*, vol. 196, p. 105986, 2025.

[131] Y. Chen, G. Wen, A. Rahmani, Z. Peng, J. Jiang, and T. Huang, "Resilient stepped transmission and control for nonlinear systems against DoS attacks," *Automatica*, vol. 172, p. 111990, 2025.

[132] A.-Y. Lu and G.-H. Yang, "Input-to-state stabilizing control for cyber-physical systems with multiple transmission channels under denial of service," *IEEE Transactions on Automatic Control*, vol. 63, no. 6, pp. 1813–1820, 2017.

[133] A.-Y. Lu and G.-H. Yang, "Resilient observer-based control for cyber-physical systems with multiple transmission channels under denial-of-service," *IEEE Transactions on Cybernetics*, vol. 50, no. 11, pp. 4796–4807, 2019.

[134] A.-Y. Lu and G.-H. Yang, "Observer-based control for cyber-physical systems under denial-of-service with a decentralized event-triggered scheme," *IEEE Transactions on Cybernetics*, vol. 50, no. 12, pp. 4886–4895, 2019.

[135] Z. Gu, C. K. Ahn, D. Yue, and X. Xie, "Event-triggered H_∞ filtering for T–S fuzzy-model-based nonlinear networked systems with multisensors against DoS attacks," *IEEE Transactions on Cybernetics*, vol. 52, no. 6, pp. 5311–5321, 2020.

[136] G. Wu, G.-H. Yang, and H. Wang, "ISS control synthesis of T–S fuzzy systems with multiple transmission channels under denial of service," *Journal of the Franklin Institute*, vol. 358, no. 6, pp. 3010–3032, 2021.

[137] L. Ma, Y. Zhang, C. Yang, and L. Zhou, "Security control for two-time-scale cyber physical systems with multiple transmission channels under DoS attacks: The input-to-state stability," *Journal of the Franklin Institute*, vol. 358, no. 12, pp. 6309–6325, 2021.

[138] J. Li, Y. Liu, J. Yu, and A. Luque, "Resilient sliding mode control for a class of cyber-physical systems with multiple transmission channels under denial-of-service attacks," *Journal of the Franklin Institute*, vol. 359, no. 11, pp. 5302–5321, 2022.

[139] R. Gao and G.-H. Yang, "Sampled-data distributed state estimation with multiple transmission channels under denial-of-service attacks," *Applied Mathematics and Computation*, vol. 429, p. 127229, 2022.

[140] K. Zhang, H. Wang, G. Wu, and Z. Zhipeng, "Resilient control for TS fuzzy systems with multiple transmission channels under asynchronous denial-of-Service attacks," *Journal of the Franklin Institute*, vol. 360, no. 3, pp. 2215–2233, 2023.

[141] Y.-P. Sun, G.-H. Yang, and G. M. Dimirovski, "Dynamic event-triggered control for multi-channel cyber–physical systems under denial-of-service attacks," *Journal of the Franklin Institute*, vol. 361, no. 11, p. 106933, 2024.

[142] A. Tahoun and M. Arafa, "Secure control design for nonlinear cyber-physical systems under DoS, replay, and deception cyber-attacks with multiple transmission channels," *ISA Transactions*, vol. 128, pp. 294–308, 2022.

[143] P. Tabuada, "Event-triggered real-time scheduling of stabilizing control tasks," *IEEE Transactions on Automatic Control*, vol. 52, no. 9, pp. 1680–1685, 2007.

[144] J. Lunze and D. Lehmann, "A state-feedback approach to event-based control," *Automatica*, vol. 46, no. 1, pp. 211–215, 2010.

[145] D. P. Borgers and W. M. H. Heemels, "Event-separation properties of event-triggered control systems," *IEEE Transactions on Automatic Control*, vol. 59, no. 10, pp. 2644–2656, 2014.

[146] X.-M. Zhang, Q.-L. Han, and B.-L. Zhang, "An overview and deep investigation on sampled-data-based event-triggered control and filtering for networked systems," *IEEE Transactions on Industrial Informatics*, vol. 13, no. 1, pp. 4–16, 2016.

[147] A. Girard, "Dynamic triggering mechanisms for event-triggered control," *IEEE Transactions on Automatic Control*, vol. 60, no. 7, pp. 1992–1997, 2014.

[148] D. Liu and G.-H. Yang, "Dynamic event-triggered control for linear time-invariant systems with-gain performance," *International Journal of Robust and Nonlinear Control*, vol. 29, no. 2, pp. 507–518, 2019.

[149] K.-Z. Liu, A. R. Teel, X.-M. Sun, and X.-F. Wang, "Model-based dynamic event-triggered control for systems with uncertainty: A hybrid system approach," *IEEE Transactions on Automatic Control*, vol. 66, no. 1, pp. 444–451, 2020.

[150] F. J. Bejarano and A. Pisano, "Switched observers for switched linear systems with unknown inputs," *IEEE Transactions on Automatic Control*, vol. 56, no. 3, pp. 681–686, 2010.

[151] A. Tanwani, H. Shim, and D. Liberzon, "Observability for switched linear systems: characterization and observer design," *IEEE Transactions on Automatic Control*, vol. 58, no. 4, pp. 891–904, 2012.

[152] G. C. Walsh, H. Ye, and L. G. Bushnell, "Stability analysis of networked control systems," *IEEE Transactions on Control Systems Technology*, vol. 10, no. 3, pp. 438–446, 2002.

[153] J. P. Hespanha and A. S. Morse, "Stability of switched systems with average dwell-time," in *Proceedings of the 38th IEEE Conference on Decision and Control (Cat. No. 99CH36304)*, vol. 3, pp. 2655–2660, IEEE, 1999.

[154] W. Xu, K. Ma, W. Trappe, and Y. Zhang, "Jamming sensor networks: attack and defense strategies," *IEEE Network*, vol. 20, no. 3, pp. 41–47, 2006.

[155] P. Tague, M. Li, and R. Poovendran, "Mitigation of control channel jamming under node capture attacks," *IEEE Transactions on Mobile Computing*, vol. 8, no. 9, pp. 1221–1234, 2009.

[156] B. DeBruhl and P. Tague, "Digital filter design for jamming mitigation in 802.15. 4 communication," in *2011 Proceedings of 20th International Conference on Computer Communications and Networks (ICCCN)*, pp. 1–6, IEEE, 2011.

[157] E. D. Sontag, "Input to state stability: basic concepts and results," in *Nonlinear and Optimal Control Theory*, pp. 163–220, Springer, 2008.

[158] S. Boyd, L. El Ghaoui, E. Feron, and V. Balakrishnan, *Linear matrix inequalities in system and control theory*. SIAM, 1994.

[159] M. A. Ahmad and P. Rai, "Speed control of a DC motor using Controllers," *Automation, Control and Intelligent Systems*, vol. 2, no. 6-1, pp. 1–9, 2014.

[160] T. Ström, "On logarithmic norms," *SIAM Journal on Numerical Analysis*, vol. 12, no. 5, pp. 741–753, 1975.

[161] G. H. Hardy, J. E. Littlewood, G. Pólya, G. Pólya, D. Littlewood, *et al.*, *Inequalities*. Cambridge University Press, 1952.